UNIVERSITY OF CALIFORNIA SAN DIEGO

SAN DIEGO STATE UNIVERSITY

A variable kinematic model for large deflection of functionally graded variable-stiffness composite laminates

A dissertation submitted in partial satisfaction of the
requirements for the degree Doctor of Philosophy

in

Engineering Sciences (Structural Engineering)

by

Enrico Santarpia

Committee in charge:

University of California San Diego

Professor Jiun-Shyan Chen, Chair
Professor Philip Gill
Professor Hyonny Kim
Professor Quiang Zhu

San Diego State University

Professor Luciano Demasi, Co-chair
Professor Antonio Palacios

2020

The Dissertation of Enrico Santarpia is approved, and it is acceptable in quality and form for publication on microfilm and electronically:

_____

_____

_____

_____

_____

_____

Co-Chair

_____

Chair

University of California San Diego

San Diego State University

2020

TABLE OF CONTENTS

LIST OF FIGURES

LIST OF TABLES

ACKNOWLEDGEMENTS

Chapter 1, in part, is a reprint of the material as it appears in *Computational Architecture Based on Murakami's Zig-Zag function for the Geometrically Nonlinear Analysis of Variable Angle Tow Laminates*, AIAA Scitech Forum, Orlando, Florida, January 2020. Santarpia, Enrico; Demasi, Luciano. The dissertation author was the primary investigator and author of this paper.

Chapter 3, in part, is a reprint of the material as it appears in *Large displacement models for composites based on Murakami's Zig-Zag Function, Green-Lagrange Strain Tensor, and Generalized Unified Formulation* in Thin Walled Structure 2020. Santarpia, Enrico; Demasi, Luciano. The dissertation author was the primary investigator and author of this paper.

Chapter 5, in part, is a reprint of the material as it appears in *"Computational Architecture Based on Murakami's Zig-Zag function for the Geometrically Nonlinear Analysis of Variable Angle Tow Laminates"*, AIAA Scitech Forum, Orlando, Florida, January 2020 and co-authored by Luciano Demasi. The author of this dissertation is the primary investigator and author of this paper.

Chapter 6, in part, is a reprint of the material as it appears in *Large displacement models for composites based on Murakami's Zig-Zag Function, Green-Lagrange Strain Tensor, and Generalized Unified Formulation* in Thin Walled Structure 2020. Santarpia, Enrico; Demasi, Luciano. The dissertation author was the primary investigator and author of this paper.

Chapter 6, in part, is a reprint of the material as it appears in *Computational Architecture Based on Murakami's Zig-Zag function for the Geometrically Nonlinear Analysis of Variable Angle Tow Laminates*, AIAA Scitech Forum, Orlando, Florida, January 2020. Santarpia, Enrico; Demasi, Luciano. The dissertation author was the primary investigator and author of this paper.

VITA

2010 Bachelor of Science in Aerospace Engineering, University of Pisa, Italy

2013 Master of Science in Space Engineering, University of Pisa, Italy

2014 Research assistant, San Diego State University, San Diego, USA

2020 Doctor of Philosophy in Engineering Sciences (Structural Engineering), University of California San Diego, San Diego State University, San Diego, USA.

PUBLICATIONS

Journal Papers

E. Santarpia, L. Demasi "Large Displacement Models for Composite Based on Murakami's Zig-Zag Function, Green-Lagrange Strain Tensor, and Generalized Unified Formulation", Thin-Walled Structures, Vol. 150, May 2020

L. Demasi, A. Palazzotto, **E. Santarpia** "Starred Polyhedral Shell Reinforced with Internal Pockets Considering an Internal Vacuum", Journal of Engineering Mechanics, Vol 145, No. 9, 2019

L. Demasi, **E. Santarpia** "Functional Reconstitution of Reissner's Mixed Variational Theorem for Finite Element Applications", AIAA Journal, Vol.57, No. 1, pp. 1-14, 2019

L. Demasi, G. Biagini, F. Vannucci, **E. Santarpia**, R.Cavallaro "Equivalent Single Layer, Zig-Zag, and Layer Wise Theories for Variable Angle Tow Composites Based on the Generalized Unified Formulation", Composite Structures, Vol. 177, No. 1, pp. 54-79, 2017

L. Demasi, **E. Santarpia**, A. Dipace, R. Cavallaro, R. E. Gordnier "Aerodynamic and Structural Studies of a Flapping Wing in Forward Flight", AIAA Journal, Vol.54, No. 9, pp. 2768-2781, 2016

L. Demasi, Y. Ashenafi, R. Cavallaro, **E. Santarpia** "Generalized Unified Formulation shell element for functionally graded Variable-Stiffness Composite Laminates and aeroelastic applications", Composite Structures, Vol. 131, No. 1, pp. 501-515, 2015

Conference Papers

V. Hong, **E. Santarpia**, L. Demasi, "Reissner's Mixed Variational Theorem and Energy Reconstitution for Triangular Elements", AIAA Scitech Forum, Orlando, Florida, January 2020

E. Santarpia, L. Demasi, "Computational Architecture Based on Murakami's Zig-Zag function for the Geometrically Nonlinear Analysis of Variable Angle Tow Laminates", AIAA Scitech Forum, Orlando, Florida, January 2020

E. Santarpia, L. Demasi, N.T. Nguyen, "Aerodynamic analysis of a Flapping Transitional Configuration", AIAA Aviation Forum, Dallas, Texas, June 2019

L. Demasi, **E. Santarpia**, R. Cavallaro, "Functional Reconstitution of Reissner Mixed Variational Theorem for Effective Finite Element Implementations", 60th AIAA/ASME/ASCE/AHS/ASC Structures, Structural Dynamics & Materials Conference, San Diego, California, January 2019

L. Demasi, G. Biagini, F. Vannucci, **E. Santarpia**, R. Cavallaro "Zig-Zag and Layer Wise Models for Variable-Stiffness Composite Laminates Based on the Generalized Unified Formulation", 58th AIAA/ASME/ASCE/AHS/ASC Structures, Structural Dynamics & Materials Conference, Grapevine, Texas, January 2017

L. Demasi, Y. Ashenafi, R. Cavallaro, **E. Santarpia** "Generalized Unified Formulation Shell Element for Functionally Graded Variable-Stiffness Composite Laminates and Aeroelastic Applications", 56th AIAA/ASME/ASCE/AHS/ASC Structures, Structural Dynamics & Materials Conference, Kissimmee, Florida, January 2015

L. Demasi, R. E. Gordnier, **E. Santarpia**, A. Dipace "High-fidelity Simulations of a Flexible Flapping Wing in Forward Flight", 54th AIAA/ASME/ASCE/AHS/ASC Structures, Structural Dynamics & Materials Conference, Boston, Massachusetts, April 2013.

ABSTRACT OF THE DISSERTATION

A variable kinematic model for large deflection of functionally graded variable-stiffness composite laminates

by

Enrico Santarpia

Doctor of Philosophy in Engineering Sciences (Structural Engineering)

University of California San Diego, 2020

San Diego State University, 2020

Professor Jyun-Shyan Chen, Chair

Professor Luciano Demasi, Co-Chair

Composite materials play an important role in the aerospace industry. They are increasingly used in primary structures, and recent manufacturing technology advancements are making Variable Angle Tow (VAT) composites a valuable option for the design of innovative airplanes. One of the challenges of the future of aviation is to have aerodynamically efficient configurations, which often result in very flexible structures. Thus, the large deformation analysis of VAT composites is a necessary phase of the design. A difficulty is often represented by the higher degree of anisotropy of these structures, which needs to be taken into account with the necessary computational flexibility and without a compromise on the accuracy of the evaluations, especially on the determination of stress levels.

This dissertation introduces a finite-element based computational framework for the variable-kinematic analysis of geometrically nonlinear variable-stiffness composite laminates. A unified approach allows the analyst to master a virtually infinite number of types of elements. They are based on a compact writing of the equations of motion so that each layer can be independently modeled with an axiomatic

approach, or effective equivalent single layer models, able to correctly take into account the zig-zag form of the displacements, can be used. In particular, formulations originally developed for linear classical composites, are now introduced for the large displacement analysis of VAT laminates. The accurate prediction of transverse stresses is achieved by a quasi-3D recovery procedure originally proposed and based on integration of the Second-Piola Kirchhoff Stress Tensor. It is demonstrated that the level of accuracy is comparable to the more computationally demanding three-dimensional finite element approaches.

Chapter 1

Introduction

1.1 Motivation

Composite materials are widespread in aerospace applications due to their design flexibility and capacity to form lightweight structures. They are commonly employed as laminates with straight fibers oriented at a specific angle in each layer, Constant Stiffness Composite Laminate (CSCL). Recent advancement in the manufacturing techniques allows the use of Variable Angle Tow (VAT) laminates [1–4]. The latter are attractive because of the removal of the straight fibers constraint, dramatically increasing the design space. Thus, more efficient structures can be achieved. Initial studies on VAT structures were done for their ability to redistribute loads. For instance, a reduction of the stress concentration in the presence of holes was observed [5]. One of the main issues of thin-walled structure is buckling. VAT laminates proved to be able to increase the buckling load [6, 7] and improve the post-buckling behaviour [8, 9]. Recently, it was shown the possibility to use VAT composites for primary structures like a wingbox [4] and how an improvement in postbuckling behaviour can be obtained with respect to CSCL [10]. VAT composites can also be used to improve the dynamic response of wing structures. The fiber orientation can be optimized to increase certain frequency (e.g. bending and torsion) without affecting others [11]. Few studies have been done to asses the advantage of VAT laminates to control aeroelastic instability and more needs to be done. Studies on one- and two-dimensional wing models coupled with unsteady strip theory aerodynamics [12, 13] showed an increase of both divergence and flutter speeds. An increase of flutter speed compared to straight fiber was also found in case of a symmetric stacking sequence plate with supersonic flow [14]. A mass minimization problem conducted on a high aspect ratio Common Research Model concluded that under aeroelastic stress and flutter constraints the curvilinear fibers as well as using curvilinear stiffeners can reduce the mass up to 11% relative to un-steered composites [15]. Other studies show that VAT laminates potentially can increase

the flutter speed of a plate in supersonic flows but their effect was strongly dependent on the boundary conditions [16].

As shown in this brief review, VAT composite are promising. However, their analysis in a multi-disciplinary design and optimization framework requires a higher computational cost than CSCL. Thus, it becomes essential to have a fast and accurate model at the same time. The finite element method (FEM) proved to be a useful tool for structural analysis. It is based on the subdivision of the domain in elements. They can be one-, two- or three-dimensional based on the particular geometry to be analyzed. In practical applications, composite laminates are produced as plates and two-dimensional elements can often accurately describe these three-dimensional continuous structures. A-priori assumptions (axiomatic theories) of the variation of field variables (e.g. displacements) along the thickness are adopted. Simpler and computationally cheaper axiomatic theories can capture the global behavior of the structure, but they can fail to provide an accurate stress representation. This is especially true for thicker laminates with strong anisotropy. The correct evaluation of the stress field is of fundamental importance to successfully apply the failure criteria [17]. An erroneous estimation can cause safety issues. In these situations it becomes necessary the adoption of high-order theories or even three-dimensional elements. Many authors have dealt with the problem to reduce the computational burden associated with composite laminates. Some are based on the use of a combination of different methods (global-local methods) and others are based on post-processing operations to recover the actual stress field in specific areas [18–21].

1.2 Contribution of the present study

The objective of this study is to develop a flexible computational tool for geometrically nonlinear static and dynamic analysis of composite laminates. The focus is on the accurate evaluation of the stress field in the area of interest at low computational cost. This tool is based on the Generalized Unified Formulation (GUF) [22] originally proposed for linear composite structures. GUF provides the flexibility to model each spatial direction independently using several axiomatic models, like Equivalent Single Layer (ESL) and layer-wise (LW) [23] ones. It has been extensively validated for linear analysis of CSCL [24–26] and VAT [27–29] composites. When applied to FEM, it generates polymorphic elements giving the user a virtually infinite element library. Different elements can be used and compared, giving the opportunity of finding the more cost effective modeling strategy for a particular application. Among all theories, particular attention is given to the Zig-Zag theory [30–33] based on the Murakami's Zig-Zag function (MZZF) [34]. It will be demonstrated for the first time in this dissertation that MZZF is an effective alternative to the more expensive LW theory also in nonlinear analysis. This is especially true if used in conjunction with a

dedicated stress recovery procedure. For this purpose a post-processing procedure based on the thickness integration of the nonlinear equilibrium equations is developed to further enhance the stress accuracy of computationally cheaper elements. It is also shown how all elements can be used simultaneously through the use of a penalty formulation, making it a viable tool for global-local analysis.

The original contributions of this work are summarized below.

- The Generalized Unified Formulation is applied to the geometrically nonlinear static analysis of CSCL and VAT laminates. The expressions of the kernels (formally invariant scalars and building block of the notation) are derived for the first time for a total Lagrangian finite element formulation.
- The algorithm is further extended to dynamic analysis. Additional kernels expression are derived for the inertial terms (mass matrix).
- The study of flapping wing systems and blades for wind and marine application can be more convenient done in a frame of reference attached to the body. The nonlinear dynamic governing equation are derived for a non-inertial reference system and the kernels associated with the additional terms (apparent forces, dynamic stiffness matrix, gyroscopic damping matrix) are derived.
- Development of a point-wise stress recovery procedure for nonlinear analysis of VAT composites. The method retains all the nonlinear terms of the governing equation written in terms of Second Piola-Kirchhoff stress tensor.
- The effectiveness of Murakami's Zig-Zag Function for the geometrical nonlinear analysis of VAT structures is presented for the first time. Results are compared with commercial codes or test cases found in literature.

1.3 Outline

The dissertation is organized as follows:

- Chapter 2 is subdivided in three sections. First, the most commonly adopted displacement based axiomatic theories are listed. Then, it is presented a literature review of the algorithms developed to mitigate the additional computational cost that composites and laminates typically introduce in a finite element analysis. The additional cost often is due to a complex three-dimensional stress field that has to be accurately modeled to correctly apply failure criteria. Many of these algorithms are based on the simultaneous usage of different axiomatic theories. Finally, the concepts of compact

notation, unified formulation and invariant kernels are introduced. The main characteristics of GUF are explained together with its implementation in a finite element framework.

- In Chapter 3 GUF is extended to the geometrically nonlinear static analysis of laminates. Novel expressions of the nonlinear invariant kernels are derived using a total Lagrangian formulation.

- Chapter 4 further extends the nonlinear finite element analysis to dynamic problems. The kernels of the mass matrix are obtained. With in mind a possible application on the analysis of flapping wings and wind turbines, the formulation is also presented by using a frame of reference attached to the body. With this intent, the weak form is rewritten in a non-inertial reference frame. Additional contributions to the stiffness and damping matrix are obtained and the associated kernels derived for the first time.

- Chapter 5 illustrates the variable angle tow modeling in the finite element formulation. This is done as preparatory step for developing a stress recovery procedure for the large displacements and rotations analysis of generic composite laminates.

- In Chapter 6 the tools introduced in the previous chapters are validated against data from literature and commercial codes. The capability to have an infinite library of elements allows one to compare different models. In particular, it is shown how Murakami's Zig-Zag function can be successfully used also in nonlinear analysis to improve the accuracy of ESL theories in term of transverse stresses. It is shown that an accuracy comparable with LW theories is achieved. In addition, it is shown the effectiveness of GUF in reducing the computational cost using high-order axiomatic theories only in the area of interest.

1.4 Acknowledgments

Chapter 1 is in part a reprint of:

- "*Computational Architecture Based on Murakami's Zig-Zag function for the Geometrically Nonlinear Analysis of Variable Angle Tow Laminates*", AIAA Scitech Forum, Orlando, Florida, January 2020 and co-authored by Luciano Demasi. The author of this dissertation is the primary investigator and author of this paper.

Chapter 2

Multi-model analysis and Unified Formulation

In this chapter the most common axiomatic models for composite multilayered structures are described. Follows a brief survey of algorithms used to minimize the computational cost that such composites require in a Finite Element Analysis. Most of them are based on the usage of different element types (multi-models) in different areas of the structure. Finally, the concept of unified formulation is introduced together with a description of its practical implementation in a Finite Element framework. It is shown how the particular form of the unified formulation used in this dissertation allows for simultaneous use of several axiomatic models, making it a useful tool for multi-model analysis.

2.1 Axiomatic models

The most common methods for the structural analysis of composite laminates are based on the so called axiomatic models. These methods rely on hypotheses on the shape of the solution without an a-priori knowledge . Their accuracy is tested only a posteriori. These assumptions allow to reduce the three-dimensional continuum elasticity problem to a two-dimensional one. They define how the field variables (e.g. displacements) vary along the thickness of the plate (linearly, parabolic, or other type of description). There are two main classes of axiomatic models: the Equivalent Single Layer (ESL) and the Layer-Wise (LW) ones. The former hypothesizes the structure as a single lamina with smeared material property, whereas the latter treats each layer independently. The ESL models are computationally inexpensive, but are not accurate for thicker plates or when a strong anisotropy is present. Moreover, they do not provide a correct evaluation of the transverse stresses. On the contrary, LW models are more accurate, but expensive, especially when the

number of layer increases. They resemble the original three-dimensional modeling so that they are referred as quasi-3D models.

Consider a planar composite panel assumed to be on the x-y plane and the thickness is along the vertical z direction (Fig. 2.1).

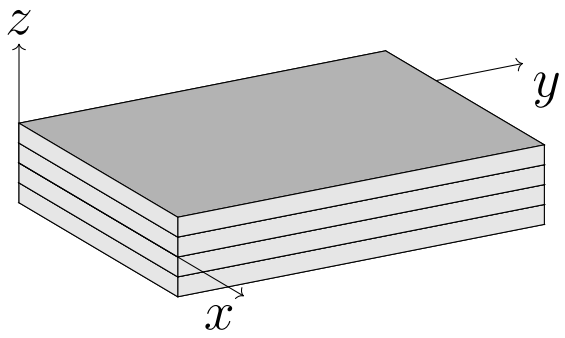

Figure 2.1: Plate geometry and reference system

The layers are numbered from bottom to top and k indicates the identity of a generic layer (Fig. 2.2).

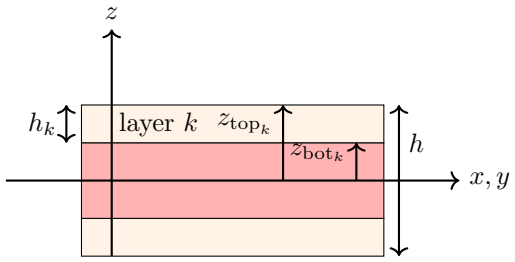

Figure 2.2: Thickness coordinate of a generic layer.

A list of the most common axiomatic model is presented. Then in the next sections it will be shown how all these models can be included in one through the use of an unified formulation.

2.1.1 Equivalent Single Layer theories

The displacements variables are expresses as a Taylor expansion along the thickness direction from the middle of the plate (z=0). The most general form is:

$$\begin{aligned} u_x(x,y,z) &= \sum_{i=0}^{n_x} z^i \phi_{x_i}(x,y) \\ u_y(x,y,z) &= \sum_{i=0}^{n_y} z^i \phi_{y_i}(x,y) \\ u_z(x,y,z) &= \sum_{i=0}^{n_z} z^i \phi_{z_i}(x,y) \end{aligned} \tag{2.1}$$

where ϕ_{x_i}, ϕ_{y_i}, ϕ_{z_i} are the unknown coefficients that have to be found. n_x, n_y, n_z are the orders of the expansion for each coordinate direction. Depending on the number of terms retained, different theories can be generated (see Fig. 2.3).

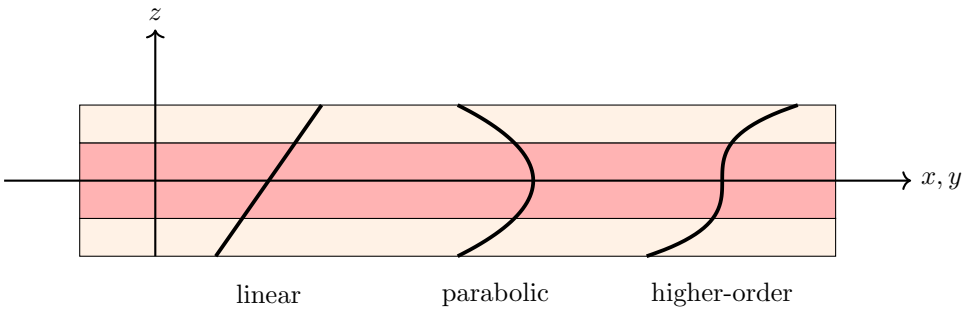

Figure 2.3: Equivalent Single Layer theory. Displacement variables through the thickness.

Classical plate theory (CPT) In this theory the Kirchhoff's hypothesis are applied. It is assumed that straight lines perpendicular to the mid-surface remain straight and normal to it after deformation and that the thickness of the plate does not change. Thus, Eq. 2.1 becomes:

$$\begin{aligned} u_x(x,y,z) &= u_{x_0}(x,y) - z\frac{\partial u_{z_0}}{\partial x} \\ u_y(x,y,z) &= u_{y_0}(x,y) - z\frac{\partial u_{z_0}}{\partial y} \\ u_z(x,y,z) &= u_{z_0}(x,y) \end{aligned} \tag{2.2}$$

As a consequence of these assumptions the transverse shear and normal effects are neglected. This theory can provide accurate results only for thin plates and with low levels of anisotropy.

First-order shear deformation theory (FSDT) The Kirchhoff hypothesis are relaxed. In particular, straight lines perpendicular to the mid-surface do not remain as such during deformation. The resulting axiomatic model becomes:

$$\begin{aligned} u_x(x,y,z) &= u_{x0}(x,y) + zu_{x1}(x,y) \\ u_y(x,y,z) &= u_{y0}(x,y) + zu_{y1}(x,y) \\ u_z(x,y,z) &= u_{z0}(x,y) \end{aligned} \tag{2.3}$$

where u_{x1} and u_{y1} have the meaning of rotation of a transverse normal about the y and x axis respectively. These hypothesis allows a constant transverse shear to exist. Nonetheless a constant shear is not physically possible for equilibrium consideration and a correction factor is often used.

High-order shear deformation theories (HSDT) Increasing the order of the polynomial, more accurate and complex theories can be developed. The higher order coefficients do not present a classical interpretation (e.g. rotations). These theories do not need a shear correction factor because they allow the shear stresses to go to zero on the top and bottom of the plate. An example of higher order theory reported below:

$$\begin{aligned} u_x(x,y,z) &= u_{x0}(x,y) + zu_{x1}(x,y) + z^2 u_{x2}(x,y) \\ u_y(x,y,z) &= u_{y0}(x,y) + zu_{y1}(x,y) + z^2 u_{y2}(x,y) \\ u_z(x,y,z) &= u_{z0}(x,y) + zu_{z1}(x,y) \end{aligned} \tag{2.4}$$

But many other options are available, as the commonly used third-order laminated plate theory of Reddy [35].

2.1.2 Layerwise theories

The ESL theories can accurately predict the global behavior of the plate, especially if thin. But they can not capture the three-dimensional state of stress with adequate accuracy. This issue is overcome modeling each ply separately with an ESL theory (see Fig. 2.4). The most general expression is:

$$\begin{aligned} u_x^k(x,y,z) &= \sum_{i=0}^{n_x} \left(z - \frac{z_{\text{top}_k} + z_{\text{bot}_k}}{2} \right)^i \phi_{x_i}^k(x,y) \\ u_y^k(x,y,z) &= \sum_{i=0}^{n_y} \left(z - \frac{z_{\text{top}_k} + z_{\text{bot}_k}}{2} \right)^i \phi_{y_i}^k(x,y) \quad z_{\text{bot}_k} \leq z \leq z_{\text{top}_k} \\ u_z^k(x,y,z) &= \sum_{i=0}^{n_z} \left(z - \frac{z_{\text{top}_k} + z_{\text{bot}_k}}{2} \right)^i \phi_{z_i}^k(x,y) \end{aligned} \tag{2.5}$$

where k denotes the ply number. The term $(z_{top_k} + z_{bot_k})/2$ has been added because the ESL theories use as reference frame the middle plane of the corresponding layer instead of the entire plate.

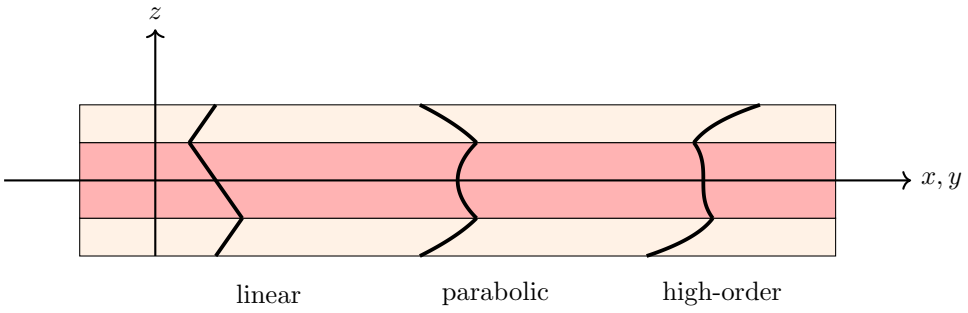

Figure 2.4: Layer-Wise displacement variables.

In case a first order shear deformation theory is used for the inplane displacement and a constant

value for the out-of-plane displacement at each layer Eq. 2.5 becomes:

$$\begin{aligned} u_x^k(x,y,z) &= u_{x0}^k(x,y) + \left(z - \frac{z_{top_k} + z_{bot_k}}{2}\right) u_{x1}^k(x,y) \\ u_y^k(x,y,z) &= u_{y0}^k(x,y) + \left(z - \frac{z_{top_k} + z_{bot_k}}{2}\right) u_{y1}^k(x,y) \quad z_{bot_k} \leq z \leq z_{top_k} \\ u_z^k(x,y,z) &= u_{z0}^k(x,y) \end{aligned} \tag{2.6}$$

In the practical modeling a Taylor expansion is not ideal to describe the thickness variation of a LW theory. It makes the imposition of the inter-laminar continuity a cumbersome process. An axiomatic expansion based on Legendre polynomial is far more convenient, because it allows for an effective application of the interlaminar compatibility of the displacements (i.e., the displacements must be continuous functions in the thickness direction). The expansion (Fig. 2.5) using the Legendre polynomial becomes:

$$\begin{aligned} u_x^k(x,y,z) &= \sum_{i=0}^{n_x} F_{i+1}^k(z)\, \psi_{x_i}^k(x,y) \\ u_y^k(x,y,z) &= \sum_{i=0}^{n_y} F_{i+1}^k(z)\, \psi_{y_i}^k(x,y) \\ u_z^k(x,y,z) &= \sum_{i=0}^{n_z} F_{i+1}^k(z)\, \psi_{z_i}^k(x,y) \end{aligned} \tag{2.7}$$

where $\psi_{x_i}^k$, $\psi_{y_i}^k$, $\psi_{z_i}^k$ are the unknowns and F_{i+1}^k are the known coefficients that depend on the thickness through the Legendre polynomials. Their explicit expression is as follow:

$$\begin{aligned} F_1^k &= \frac{P_0^k + P_1^k}{2} \\ F_i^k &= P_i^k - P_{i-2}^k \quad i = 2, n_x \\ F_{n_x+1}^k &= \frac{P_0^k - P_1^k}{2} \end{aligned} \tag{2.8}$$

where P_i is the Legendre polynomial of order i. The Legendre polynomials are defined between -1 and 1, so a transformation of the thickness coordinate is needed before evaluating them:

$$\zeta_k = \frac{2}{z_{\mathrm{top}_k} - z_{\mathrm{bot}_k}} z - \frac{z_{\mathrm{top}_k} + z_{\mathrm{bot}_k}}{z_{\mathrm{top}_k} - z_{\mathrm{bot}_k}} \tag{2.9}$$

The advantage resides on the fact that the first and last unknown terms in equation 2.7 represent the displacement of the top and bottom surface of the layer respectively when equation 2.8 is adopted. Thus,

the compatibility condition between layer k and $k+1$ simply becomes:

$$\begin{aligned} \psi^k_{x_0} &= \psi^{k+1}_{x_{n_x}} \\ \psi^k_{y_0} &= \psi^{k+1}_{y_{n_y}} \\ \psi^k_{z_0} &= \psi^{k+1}_{z_{n_z}} \end{aligned} \tag{2.10}$$

Although the stress state is considerably improved with respect to the ESL theories, the continuity of the transverse stresses is still not guaranteed. For this reason mixed theory can be used where also the transverse stress variables are modeled with an axiomatic theory [36–39]. This kind of theories are called mixed layer-wise theories and they guarantee continuity of the transverse stress, but in this dissertation only displacement based axiomatic theory are considered.

2.1.3 Partially-layerwise theory

It is possible to combine all the theories listed. For example the inplane displacements can be modeled with a LW theory and the out-of-plane displacement with an ESL one:

$$\begin{aligned} u^k_x(x,y,z) &= u^k_{x0}(x,y) + \left(z - \frac{z_{\text{top}_k} + z_{\text{bot}_k}}{2}\right) u^k_{x1}(x,y) \quad z_{\text{bot}_k} \leq z \leq z_{\text{top}_k} \\ u^k_y(x,y,z) &= u^k_{y0}(x,y) + \left(z - \frac{z_{\text{top}_k} + z_{\text{bot}_k}}{2}\right) u^k_{y1}(x,y) \quad z_{\text{bot}_k} \leq z \leq z_{\text{top}_k} \\ u_z(x,y,z) &= u_{z0} \end{aligned} \tag{2.11}$$

Other options are available.

2.1.4 Zig-Zag theories

Zig-zag theories are ESL theories but are treated separately in this dissertation for their capability to be as accurate as the more complex LW ones. One of the shortcoming of the classical ESL theories is their incapability to take into account the discontinuity of the first displacements' derivatives in the thickness direction [26]. Zig-Zag theories have been developed to overcome this issue [30–33]. From an historical perspective [40], this type of theories can be subdivided into 3 major categories: Lekhnitskii Multilayered Theory (LMT) [41], Ambartsumian Multilayered Theory (AMT) [42–46], and Reissner Multilayered Theory (RMT) [39, 47, 48].

The Zig-Zag models were applied to displacement-based formulations [49] but also postulated for mixed variational statements. This is the case of Murakami [34] who adopted Reissner's Mixed Variational Theorem (RMVT) [39, 47]. This framework was the base of later work [50, 51] which indicated the effective-

ness of considering the discontinuity of the first displacement derivative in the axiomatic modeling. Mixed Zig-Zag theories were also proposed on the basis of Hu-Washizu [38] and Hellinger-Reissner principles [52]. The high numerical performance of these models has also been confirmed for the case of curvilinear fibers [53] with particular reference to the calculation of the stress fields.

Recently, different Zig-Zag approaches emerged: the continuity of the transverse stresses is a priori enforced without increasing the number of degrees of freedom [54, 55]. This is achieved by using a strain enhancement able to obtain the interlaminar stress continuity while maintaining the value of strain energy. A different approach is followed in Ref. [56], where the multilayered Zig-Zag theory is built by using C_z^0 warping functions.

Zig-Zag models have also been used for geometrically nonlinear structural analysis due to the relatively low computational cost with respect to layerwise models [57]. Ref. [48] used Murakami's Zig-Zag Function (MZZF) to enhance the in-plane displacements of an RMVT framework. The nonlinearity was based on von-Kármán strains. The moderately large displacement model has also been adopted in Ref. [58], where cubic expansion for the displacement field was enriched with a Zig-Zag function for the analysis of composite plates in the postbuckled region. Results showed that the Zig-Zag modeling was superior to the FSDT especially when the laminate had drastically different transverse stiffness properties from ply to ply and for low length-to-thickness aspect ratios. A linear Zig-Zag model [59] was used to formulate a first order sublaminate theory with a Total Lagrangian Formulation (TLF). A Zig-Zag FSDT was proposed in Ref. [60], where the von-Kármán strain model was used to represent the geometric nonlinearity. A mixed approach allowed the formulation to take into account the continuity of the stresses and boundary conditions. Moreover, shear correction factor was not required.

More recently, Flores [61] introduced a Zig-Zag term to a FSDT for the large displacement analysis of shells. Finally, a higher-order shear deformation Zig-Zag theory [62] was proposed for the aerothermoelastic analysis of composite panels subjected to supersonic airflow under the assumption of moderately large displacement field (von-Kármán sense).

In this dissertation the Murakammi's Zig-Zag Function (MZZF) have been used to augment the axiomatic displacement field. Its expression is the following:

$$\text{MZZF:} \quad (-1)^k \xi_k = (-1)^k \left(\frac{2}{z_{\text{top}_k} - z_{\text{bot}_k}} z - \frac{z_{\text{top}_k} + z_{\text{bot}_k}}{z_{\text{top}_k} - z_{\text{bot}_k}} \right) \tag{2.12}$$

where ζ_k is a thickness non-dimensional coordinate and its value is between -1 and 1. This function is added

to the ESL displacement variables (see Fig. 2.5). For example:

$$\begin{aligned} u_x(x,y,z) &= u_{x0}(x,y) + zu_{x1}(x,y) + z^2u_{x2}(x,y) + (-1)^k\xi_k u_{x_\zeta}(x,y) \\ u_y(x,y,z) &= u_{y0}(x,y) + zu_{y1}(x,y) + z^2u_{y2}(x,y) + (-1)^k\xi_k u_{y_\zeta}(x,y) \\ u_z(x,y,z) &= u_{z0}(x,y) + zu_{z1}(x,y) + (-1)^k\xi_k u_{z_\zeta}(x,y) \end{aligned} \tag{2.13}$$

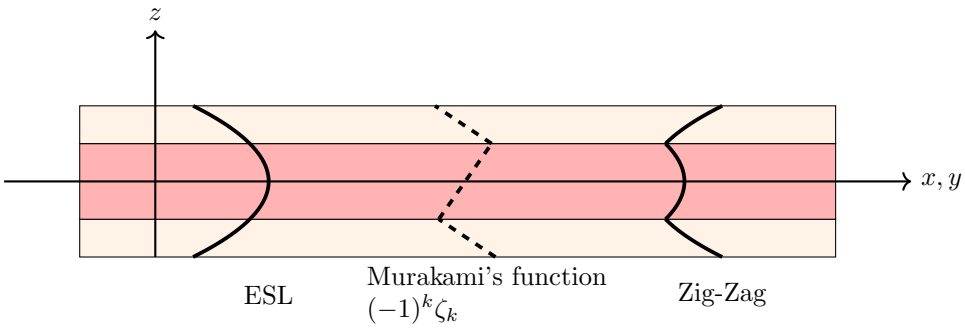

Figure 2.5: Equivalent Single Layer theory enhancement of the displacement variables with Murakami's Zig-Zag function.

2.2 Global-local methods

The objective of the global-local methods is to maximize the solution accuracy given a certain amount of computational resources. In absence of analytical solutions, the only way this can be done is through numerical methods that are able to locally increase their resolution. This locality is usually enough because either only specific areas of the structure have a complex stress field or the designer is only interested in getting data from a specific part of it. During the years several different algorithms have been developed for this purpose and researchers proposed different definitions of the term *global-local analysis*. Here some examples:

> Global/local stress analysis methodology is defined as a procedure to determine local, detailed stress states for specific structural regions using information obtained from an independent global stress analysis [63].

> Global-local analysis refers to a solution procedure where the entire structure is modeled in two steps. In the first step, a global model is analyzed and in the next step the area of interest, called the local model, is analyzed using relevant data from the global solution [64].

> Global-local analysis refers to a special case of the more general multiple model analysis; the

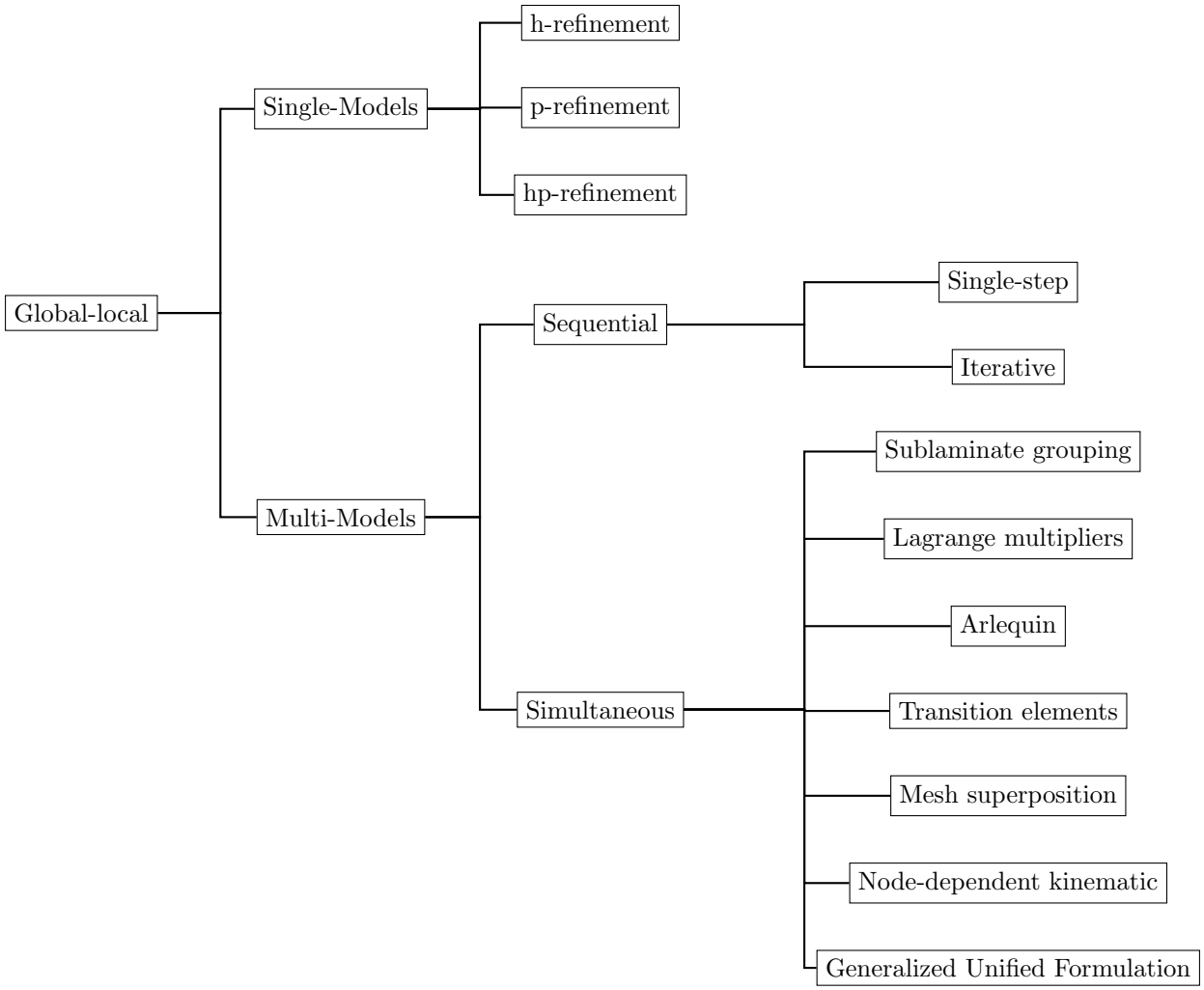

Figure 2.6: Global-local analysis algorithms for Finite Element methods

former term is typically used when there exist a typical subregion of interest that occupies a small portion of the computational domain [35].

In computational structural mechanics, the term global-local analysis refers to a variety of hierarchical modeling strategies used to study structural response phenomena covering a wide range of length scales [65].

In this dissertation the term global-local analysis refers to a generic numerical method that allows to obtain different level of accuracy in different part of the structural domain. The global-local method utilized in FEM can be classified in single-model and multi-model methods. Fig. 2.6 shows a list of method used for global-local analysis.

2.2.1 Single-model methods

The first class of method relies on one mathematical model and the localization is done either refining the mesh in the area of interest (h-refinement) [66] or increasing the degree of the basis functions (p-refinement) [67]. Also a combination of the two have been used (hp-refinement) [68]. These methods do not change the kinematic theory and for this reason are called single-models.

2.2.2 Multi-model methods

Multi-model methods for global-local analysis can be subdivided in sequential and simultaneous. There is a wide variety of simultaneous models e.g. transition elements, sublaminate grouping and others. Here a description of the methods is provided.

Sequential These methods rely on the use of a simple model to obtain an approximate solution on the entire domain (global region), immediately followed by a new simulation with a more refined model considering only the zone of interest (local region). The results of the first simulation are used as boundary condition for the latter [63, 69]. These methods have the shortcoming that there is no feedback from the local region to the global one and consequently equilibrium is not guaranteed. To solve this issue iterative methods were introduce, where a loop between the solution is performed [70–73].

Sublaminate grouping In the sublaminate grouping method the local zone is composed by selected plies of the laminates. These plies are well resolved using three-dimensional solid elements or higher order plate theories. This method was introduced by Wang [74] and it relays on the Saint-Venant's principle. The idea is that the interlaminar stresses between two layer are not affected if the force distribution of other layers acting on the layer of interest is substituted with a statically equivalent force. The idea is to use an ESL theory to model the layers not of interest. Later Jones [75] applied this technique by adopting three-dimensional elements, whereas Pagano [76] employed two-dimensional elements. Sun [77] proposed this technique to study delamination of thick laminates.

Transition elements Another way is to have different element types for different areas of the structure and join them together with special transition elements [78–81]. The disadvantage is that there should be a transition element for every element combination.

Lagrange multipliers Another solution is to augment the weak form of the elasticity problem to enforce the compatibility of the displacements between the global and local zone where different discretization or/and

mathematical models are used. This operation is done through Lagrange multipliers. The advantage is that transitional elements are not necessary. Aminpour [82] applied this technique for the study of plates with hole and a composite laminate fuselage panel. Carrera [83] used Lagrange multipliers for beam elements together with the unified formulation for variable kinematic.

Mesh superposition Fish [84] introduced the s-Finite element method. It consists of an additional mesh superimposed to the existing one. The new mesh can be finer or having higher polynomial order elements allowing to more accurately capture higher gradient. This method can be seen as a generalization of the h-, p- and hp- methods. It has been applied to the study of multilayered plates [85]. The continuity of the displacement field between the two meshes is ensured through the use of homogeneous boundary conditions of the superimposed mesh.

Arlequine In this method the laminate is subdivided in overlapping domains that can be modeled independently with different finite element and kinematic theories. The weak statement is formed by weighting the potential energies associated with each domain an additional gluing term through Lagrange multiplier. Ben Dhia [86] introduced the method and used it for global-local analysis of plates [87]; Biscani [88] implemented it in the context of a unified formulation where both ESL and LW theories were used simultaneously for the analysis of square thick plates.

Node-dependent kinematics The node-dependent kinematics has been used in the framework of the Carrera Unified formulation [89, 90]. This method focuses the attention on the finite element nodes and not on the element itself. Each node can be modeled with a different axiomatic theory. The elements that have nodes with different theory are practically transition elements, but the compatibility is automatically ensured thanks to the shape function property and no special modeling is necessary [91–93].

2.3 Unified formulations

In the traditional FEM a two-dimensional plate element is built upon a single axiomatic theory (see section 2.1). As a consequence codes have limited element libraries (only few axiomatic theories are available). If an additional element is needed, heavy and time consuming modification of the code may be required with the risk of introducing bugs. The Unified Formulations (UFs) enable to create polymorphic elements capable to change the underlying axiomatic model by user request. This is achieved by means of a compact notation that makes use of indicial notation. Practically, a code that uses an Unified Formulation has an infinite number of elements in its library, each one associated with an axiomatic model. This feature

makes the UF an ideal tool for multi-model analysis with the objective to reduce the number of degree of freedom of the problem.

In this dissertation the Generalized Unified Formulation (GUF) is used. It is a direct extension of Carrera Unified Formulation (CUF) [89, 90, 94]. In the latter all displacement components are described using the same expansion in the thickness direction of order $\mathcal{N}$. The displacement field for a layer k is as follow:

$$\text{CUF}: \begin{cases} u_x^k(x,y,z) & = F_{\alpha_u}^k(z^k) u_{x_{\alpha_u}}^k(x,y) \\ u_y^k(x,y,z) & = F_{\alpha_u}^k(z^k) u_{y_{\alpha_u}}^k(x,y) \quad \alpha_u = t,l,b \quad l = 2,\ldots,\mathcal{N} \\ u_z^k(x,y,z) & = F_{\alpha_u}^k(z^k) u_{z_{\alpha_u}}^k(x,y) \end{cases} \tag{2.14}$$

where $u_{x_{\alpha_u}}^k$,$u_{y_{\alpha_u}}^k$,$u_{z_{\alpha_u}}^k$ are the unknown function depending only on the in-plane coordinates. These are the functions discretized using the two-dimensional Finite Element approximation. Instead $F_{\alpha_u}^k$ are the thickness functions. They contain the thickness coordinate (z) dependence in the displacement field decomposition. The symbol t and b are used for the first and last term of the expansion (instead of 1 and $\mathcal{N}+1$), because if Legendre polynomials are used the first and last unknown coefficient of the expansion are the displacements at the top and bottom of the layer respectively. If an ESL theory, the layer identification k can be dropped from Eq.2.14.

On the contrary, the Generalized Unified Formulation permits an independent modeling of each displacement component, allowing a greater number of axiomatic theories. The bigger design space has the potential to reduce the total number of dofs necessary to obtain a more accurate solution at less computational cost. The displacement field for a layer k becomes:

$$\text{GUF}: \begin{cases} u_x^k & = {}^x F_{\alpha_{u_x}}^k(z^k) u_{x\alpha_{u_x}}^k(x,y) \quad \alpha_{u_x} = t,l,b \quad l = 2,\ldots,\mathcal{N}_x \\ u_y^k & = {}^y F_{\alpha_{u_y}}^k(z^k) u_{y\alpha_{u_y}}^k(x,y) \quad \alpha_{u_y} = t,m,b \quad m = 2,\ldots,\mathcal{N}_y \\ u_z^k & = {}^z F_{\alpha_{u_z}}^k(z^k) u_{z\alpha_{u_z}}^k(x,y) \quad \alpha_{u_z} = t,n,b \quad n = 2,\ldots,\mathcal{N}_z \end{cases} \tag{2.15}$$

where $\mathcal{N}_x$, $\mathcal{N}_y$, $\mathcal{N}_z$ are the order of expansion in each directions. To note that different thickness functions can be used for different directions. Also in this case the unknown functions depend on the in-plane coordinates and discretized using two dimensional shape functions.

To explain how the equivalent GUF notation is adopted in the practice, an example is now introduced. Let's take the x displacement and assume we have a parabolic expansion in the thickness direction,

as reported in the following equations:

$$u_x = u_{x0} + z u_{x1} + z^2 u_{x2} + z^3 u_{x3} \tag{2.16}$$

The thickness function are introduced. In this particular case:

$$^{x}F_t = 1 \quad ^{x}F_2 = z \quad ^{x}F_3 = z^2 \quad ^{x}F_b = z^3 \tag{2.17}$$

and Eq. 2.16 can be rewritten as:

$$u_x = {}^{x}F_t(z)u_{x_0} + {}^{x}F_2(z)u_{x_1} + {}^{x}F_3(z)u_{x_2} + {}^{x}F_b(z)u_{x_3} \tag{2.18}$$

then the expansion coefficient are renamed using the GUF convention:

$$\begin{aligned} u_{x_t} &= u_{x0}; \quad u_{x_3} = u_{x2} \\ u_{x_2} &= u_{x1}; \quad u_{x_b} = u_{x3} \end{aligned} \tag{2.19}$$

and Eq. 2.16 is rewritten as

$$u_x = {}^{x}F_t(z)u_{x_t} + {}^{x}F_2(z)u_{x_2} + {}^{x}F_3(z)u_{x_3} + {}^{x}F_b(z)u_{x_b} \tag{2.20}$$

or using Einstein's notation:

$$u_x^k = {}^{x}F^k_{\alpha_{u_x}} u_{x\alpha_{u_x}} \quad \alpha_{u_x} = t, l, b \quad l = 2, \ldots, \mathcal{N}_x \tag{2.21}$$

Finally, the FEM approximation is applied to the two-dimensional unknown functions. The value at each point (x,y) can be obtained as an interpolation of the nodal value of the element it belongs to:

$$u_{x_t}(x, y) \quad = \quad {}^{x}N_i(x, y)\, {}^{x}U_{t_i} \tag{2.22}$$

where i and ${}^{x}N_i$ are the local node number of the element and the associated shape function. The final GUF approximation of the displacement component becomes:

$$u_x = {}^{x}F_t(z)\, {}^{x}N_i\, {}^{x}U_{t_i} + {}^{x}F_2(z)\, {}^{x}N_i\, {}^{x}U_{2_i} + {}^{x}F_3(z)\, {}^{x}N_i\, {}^{x}U_{3_i} + {}^{x}F_b(z)\, {}^{x}N_i\, {}^{x}U_{b_i} \tag{2.23}$$

or using Einstein's notation again:

$$u_x = {}^{x}F_{\alpha_{u_x}}(z)\,{}^{x}N_i\,{}^{x}U_{\alpha_{u_x i}} \tag{2.24}$$

2.3.1 Thickness functions

The expression of the thickness function depends on the axiomatic theory used. If layer-wise:

$$\begin{aligned} {}^{x}F_t^k &= \frac{P_0^k + P_1^k}{2} \\ {}^{x}F_l^k &= P_l^k - P_{l-2}^k \quad l = 2, \ldots, \mathcal{N}_{u_x}^k \\ {}^{x}F_b^k &= \frac{P_0^k - P_1^k}{2} \end{aligned} \tag{2.25}$$

For an ESL theory a Taylor expansion is used and the thickness functions are:

$$\begin{aligned} {}^{x}F_t^k &= 1 \\ {}^{x}F_l^k &= z^{l-1} \quad l = 2, \ldots, \mathcal{N}_{u_x}^k \\ {}^{x}F_b^k &= z^{\mathcal{N}_{u_x}} \end{aligned} \tag{2.26}$$

The Zig-Zag theory are build from the ESL with the addition of the Murakami's zig-zag function. So the notation becomes:

$$\begin{aligned} {}^{x}F_t^k &= 1 \\ {}^{x}F_l^k &= z^{l-1} \quad l = 2, \ldots, \mathcal{N}_{u_x}^k + 1 \\ {}^{x}F_b^k &= (-1)^k \zeta_k \end{aligned} \tag{2.27}$$

where $(-1)^k \zeta_k$ is MZZF defined in Eq. 2.12.

2.3.2 Model classification

An acronym is used to identify the kinematic theory used for a specific element:

$$\mathrm{D}_{u_x}\mathrm{D}_{u_y}\mathrm{D}_{u_z}\mathrm{PVD}_{\mathcal{N}_{u_x}\mathcal{N}_{u_y}\mathcal{N}_{u_z}}$$

where D_{u_j} and $\mathcal{N}_{u_j}$ are the kinematic theory (E: ESL, L: LW and Z for Zig-Zag) and the order of the polynomial used for the j direction. PVD stands for Principle of Virtual Displacements and it indicates that the displacements are the only unknown, as opposed to mixed formulations like RMVT. The stress field is

reconstructed through Hooke's law or using ad-hoc post-processing procedure.

For example the theory $_{\text{LZE}}\text{PVD}_{324}$ is :

$$\begin{cases} u_x^k &= \dfrac{P_0^k + P_1^k}{2} u_{xt}^k + (P_2^k - P_0^k) u_{x2}^k + (P_3^k - P_1^k) u_{x3}^k + \dfrac{P_0^k - P_1^k}{2} u_{xb}^k \\ u_y^k &= u_{y0} + z u_{y1} + z^2 u_{y2} + (-1)^k \zeta_k u_{y3} \\ u_z &= u_{z0} + z u_{z1} + z^2 u_{z2} + z^3 u_{z3} + z^4 u_{z4} \end{cases} \tag{2.28}$$

2.3.3 Finite element implementation

The application of the Finite Element method to GUF follows the same steps used for a classical axiomatic theory. First the weak form of the governing equation is derived. This can be obtained through the principle of the virtual displacements [35, 95], that states that the internal and external virtual work are equal

$$\delta W_{in} = \delta W_{ext} \tag{2.29}$$

where the symbol δ indicate a virtual variation. The expression for the internal work for linear analysis and a multilayered plate is:

$$\delta W_{in} = \int_V \delta \epsilon_{ij} \sigma_{ij} \mathrm{d}V = \sum_{k=1}^{NL} \int_{V^k} \delta \epsilon_{ij}^k \sigma_{ij}^k \mathrm{d}V^k = \sum_{k=1}^{NL} \delta W_{in}^k \tag{2.30}$$

where ϵ_{ij} and σ_{ij} are the component of the strain and stress tensor. V is the volume occupied by the body and NL is the total number of layers. The virtual internal work can be written in vector form using Voigt's notation:

$$\delta W_{in} = \int_V \delta \boldsymbol{\epsilon}^T \boldsymbol{\sigma} \mathrm{d}V = \sum_{k=1}^{NL} \int_{V^k} \left(\delta \boldsymbol{\epsilon}^k\right)^T \boldsymbol{\sigma}^k \mathrm{d}V^k \tag{2.31}$$

where $\boldsymbol{\epsilon}$ and $\boldsymbol{\sigma}$ are the strain and stress vector

$$\boldsymbol{\epsilon} = [\epsilon_{xx}\ \epsilon_{yy}\ \gamma_{xy}\ \gamma_{xz} \gamma_{yz}\ \epsilon_{zz}]^T \tag{2.32}$$

$$\boldsymbol{\sigma} = [\sigma_x\ \sigma_y\ \sigma_{xy}\ \sigma_{xz}\ \sigma_{yz}\ \sigma_{zz}]^T \tag{2.33}$$

The external work due to the traction forces $\mathbf{F}$ is

$$\delta W_{ext} = \int_A \delta \mathbf{u}^T \mathbf{F} \mathrm{d}A \tag{2.34}$$

where A is the surface where the forces are applied. The equilibrium equation is expressed as a function of the displacements and consequently as a function of the in-plane unknown of the unified formulation $(u^k_{x\alpha_{u_x}}, u^k_{y\alpha_{u_y}}, u^k_{z\alpha_{u_z}})$ through the strain-displacement relationships

$$\boldsymbol{\epsilon}^k = \begin{bmatrix} \epsilon^k_{xx} \\ \epsilon^k_{yy} \\ \gamma^k_{xy} \\ \gamma^k_{xz} \\ \gamma^k_{yz} \\ \epsilon^k_{zz} \end{bmatrix} = \begin{bmatrix} u^k_{x,x} \\ u^k_{y,y} \\ u^k_{x,y} + u^k_{y,z} \\ u^k_{x,z} + u^k_{z,x} \\ u^k_{y,z} + u^k_{z,y} \\ u^k_{z,z} \end{bmatrix} = \begin{bmatrix} {}^xF^k_{\alpha_{u_x}} u^k_{x\alpha_{u_x},x} \\ {}^yF^k_{\alpha_{u_y}} u^k_{y\alpha_{u_y},y} \\ {}^xF^k_{\alpha_{u_x}} u^k_{x\alpha_{u_x},y} + {}^yF^k_{\alpha_{u_y}} u^k_{y\alpha_{u_y},x} \\ {}^xF^k_{\alpha_{u_{x,z}}} u^k_{x\alpha_{u_x}} + {}^zF^k_{\alpha_{u_z}} u^k_{z\alpha_{u_z},x} \\ {}^yF^k_{\alpha_{u_{y,z}}} u^k_{y\alpha_{u_y}} + {}^zF^k_{\alpha_{u_z}} u^k_{z\alpha_{u_z},y} \\ {}^zF^k_{\alpha_{u_{z,z}}} u^k_{z\alpha_{u_z}} \end{bmatrix} \tag{2.35}$$

and Hooke's law

$$\boldsymbol{\sigma}^k = \mathbf{C}^k \boldsymbol{\epsilon}^k \tag{2.36}$$

Finally the FEM approximation is introduced. The plate is divided in elements and the displacement values at each point can be derived as interpolation of the nodal values.

$$\begin{aligned} u^k_{x\alpha_{u_x}} &= {}^xN_i \, {}^xU^k_{\alpha_{u_x} i} \\ u^k_{y\alpha_{u_y}} &= {}^yN_i \, {}^yU^k_{\alpha_{u_y} i} \\ u^k_{z\alpha_{u_z}} &= {}^zN_i \, {}^zU^k_{\alpha_{u_z} i} \end{aligned} \tag{2.37}$$

Substituting the expression of the stress (Eq. 2.36), strains (Eq. 2.35) and the displacements discretization (Eq. 2.37) in (Eq. 2.31) the discretized expression of the internal virtual work can be found. The contribution for a single ply is:

$$\begin{aligned} \delta W^k_{int} = {} & \delta \, {}^xU^k_{\alpha_{u_x} I} \, K^{k\alpha_{u_x}\beta_{u_x} IJ}_{u_x u_x} \, {}^xU^k_{\beta_{u_x} J} + \delta U^k_{x\alpha_{u_x} I} \, K^{k\alpha_{u_x}\beta_{u_y} IJ}_{u_x u_y} \, {}^yU^k_{\beta_{u_y} J} + \\ & + \delta \, {}^xU^k_{\alpha_{u_x} I} \, K^{k\alpha_{u_x}\beta_{u_z} IJ}_{u_x u_z} \, {}^zU^k_{\beta_{u_Z} J} + \delta U^k_{y\alpha_{u_y} I} \, K^{k\alpha_{u_y}\beta_{u_x} IJ}_{u_y u_x} \, {}^xU^k_{\beta_{u_x} J} + \\ & + \delta \, {}^yU^k_{\alpha_{u_y} I} \, K^{k\alpha_{u_y}\beta_{u_y} IJ}_{u_y u_y} \, {}^yU^k_{\beta_{u_y} J} + \delta \, {}^yU^k_{\alpha_{u_y} I} \, K^{k\alpha_{u_y}\beta_{u_z} IJ}_{u_y u_z} \, {}^zU^k_{\beta_{u_Z} J} + \\ & + \delta \, {}^zU^k_{\alpha_{u_z} I} \, K^{k\alpha_{u_z}\beta_{u_x} IJ}_{u_z u_x} \, {}^xU^k_{\beta_{u_x} J} + \delta \, {}^zU^k_{\alpha_{u_z} I} \, K^{k\alpha_{u_z}\beta_{u_y} IJ}_{u_z u_y} \, {}^yU^k_{\beta_{u_y} J} + \\ & + \delta \, {}^zU^k_{\alpha_{u_z} I} \, K^{k\alpha_{u_z}\beta_{u_z} IJ}_{u_z u_z} \, {}^zU^k_{\beta_{u_Z} J} \end{aligned} \tag{2.38}$$

Terms like $K^{k\alpha_{u_x}\beta_{u_x} IJ}_{u_x u_x}$ are scalars and they are called the *kernels* of the Generalized Unified Formulation. Although they are functions of the axiomatic theory, material properties and geometry of the structure their expression is *formally* invariant and they are the building blocks of the formulation. Full

expression can be found in Appendix A. Only six of them are independent because of the symmetry property of the elastic stiffness matrix. From this scalar invariant it is possible to build the stiffness matrix of the multilayered plate (see Fig. 2.7).

Eq. 2.38 can be written more conveniently in matrix form:

$$\begin{aligned}
\delta W_{int}^k &= \left(\delta \mathbf{U}_x^k\right)^T \mathbf{K}_{u_x u_x}^k \mathbf{U}_x^k + \left(\delta \mathbf{U}_x^k\right)^T \mathbf{K}_{u_x u_y}^k \mathbf{U}_y^k + \left(\delta \mathbf{U}_x^k\right)^T \mathbf{K}_{u_x u_z}^k \mathbf{U}_z^k + \\
&+ \left(\delta \mathbf{U}_y^k\right)^T \mathbf{K}_{u_y u_x}^k \mathbf{U}_x^k + \left(\delta \mathbf{U}_y^k\right)^T \mathbf{K}_{u_y u_y}^k \mathbf{U}_y^k + \left(\delta \mathbf{U}_y^k\right)^T \mathbf{K}_{u_y u_z}^k \mathbf{U}_z^k + \\
&+ \left(\delta \mathbf{U}_z^k\right)^T \mathbf{K}_{u_z u_x}^k \mathbf{U}_x^k + \left(\delta \mathbf{U}_z^k\right)^T \mathbf{K}_{u_z u_y}^k \mathbf{U}_y^k + \left(\delta \mathbf{U}_z^k\right)^T \mathbf{K}_{u_z u_z}^k \mathbf{U}_z^k
\end{aligned} \tag{2.39}$$

and after assembling:

$$\delta W_{int}^k = \begin{bmatrix} \delta \mathbf{U}_x^k \\ \delta \mathbf{U}_y^k \\ \delta \mathbf{U}_z^k \end{bmatrix}^T \begin{bmatrix} \mathbf{K}_{u_x u_x}^k & \mathbf{K}_{u_x u_y}^k & \mathbf{K}_{u_x u_z}^k \\ \mathbf{K}_{u_y u_x}^k & \mathbf{K}_{u_y u_y}^k & \mathbf{K}_{u_y u_z}^k \\ \mathbf{K}_{u_z u_x}^k & \mathbf{K}_{u_z u_y}^k & \mathbf{K}_{u_z u_z}^k \end{bmatrix} \begin{bmatrix} \mathbf{U}_x^k \\ \mathbf{U}_y^k \\ \mathbf{U}_z^k \end{bmatrix} = \left(\delta \mathbf{U}^k\right)^T \mathbf{K}^k \mathbf{U}^k \tag{2.40}$$

$\mathbf{K}^k$ is the layer stiffness matrix.

Similar procedure is done for the virtual work of the external forces and the linear system of equation for a single lamina is as follows:

$$\begin{bmatrix} \mathbf{K}_{u_x u_x}^k & \mathbf{K}_{u_x u_y}^k & \mathbf{K}_{u_x u_z}^k \\ \mathbf{K}_{u_y u_x}^k & \mathbf{K}_{u_y u_y}^k & \mathbf{K}_{u_y u_z}^k \\ \mathbf{K}_{u_z u_x}^k & \mathbf{K}_{u_z u_y}^k & \mathbf{K}_{u_z u_z}^k \end{bmatrix} \begin{bmatrix} \mathbf{U}_x^k \\ \mathbf{U}_y^k \\ \mathbf{U}_z^k \end{bmatrix} = \begin{bmatrix} \mathbf{F}_x^k \\ \mathbf{F}_y^k \\ \mathbf{F}_z^k \end{bmatrix} \tag{2.41}$$

The multilayered finite element stiffness is obtained through a thickness assembly procedure of Eq. 2.41. Particular attention has to be taken during this process since it depends on the combination of the selected theories. Fig. 2.8 shows the actual implementation for the term $\mathbf{K}_{u_x u_y}$. In case of ESL theories the layers are merged in one and consequently the layer stiffness terms are summed. For LW the layers are kept separate and there is no superposition of the matrices with the consequence of a greater number of dofs necessary. The interlayer displacement compatibility is imposed by applying Eq. 2.10. This results in the superimposition of the bottom right corner of the upper layer matrix with the top left corner of the bottom layer one (second case of Fig. 2.8). A combination of the two previous operations is obtained in case and ESL and LW theories are used simultaneously.

A scalar kernel, instead of a 3×3 matrix kernel (CUF), derives from the hypothesis of indepen-

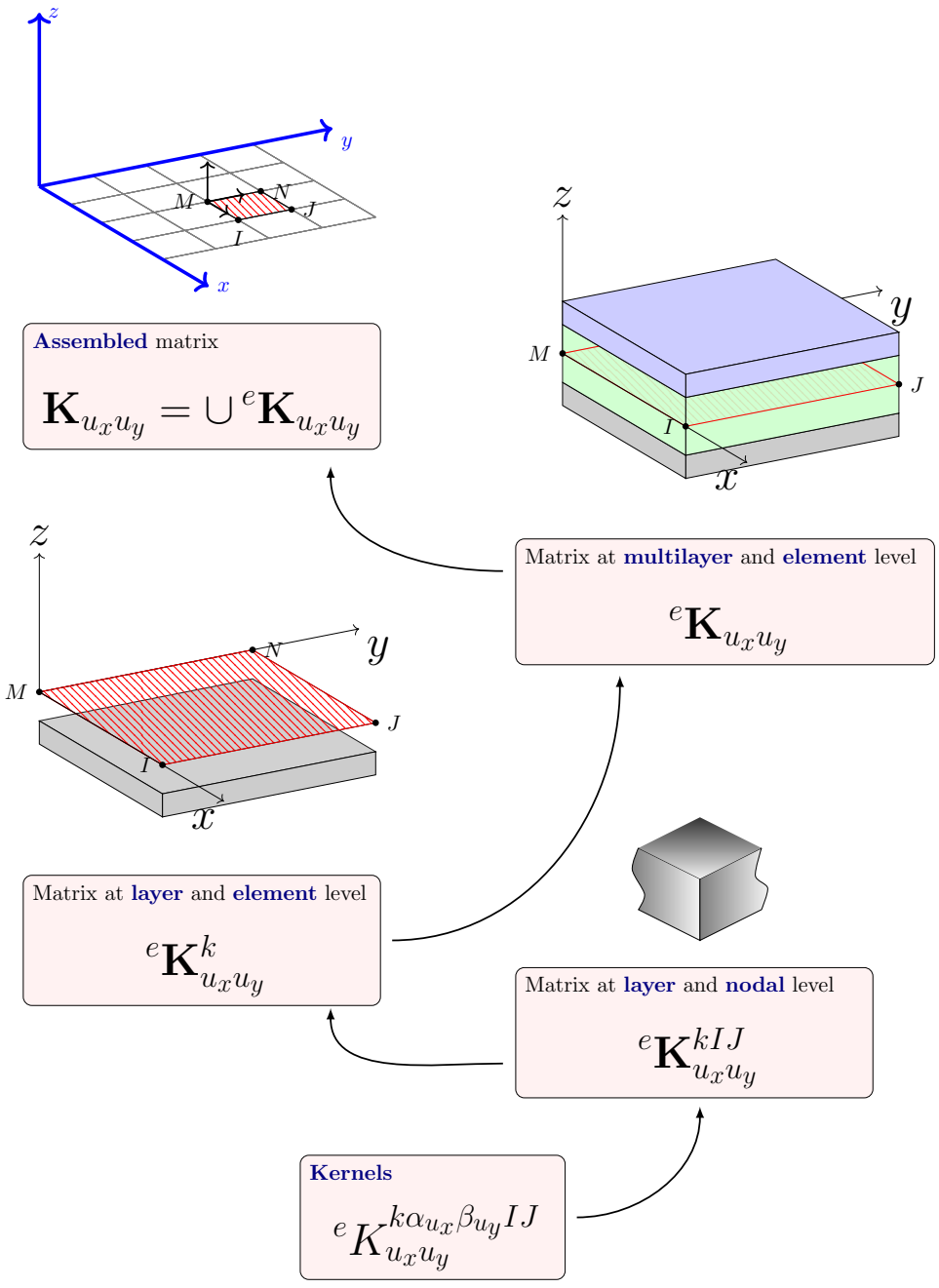

Figure 2.7: Elastic stiffness matrix construction. From invariant kernels to assembled structure. Example shown for one kernel.

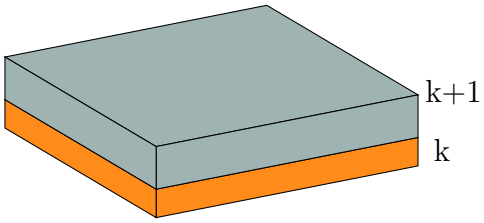

$$\mathbf{K}_{u_x u_y} = \mathbf{K}^{k}_{u_x u_y} + \mathbf{K}^{k+1}_{u_x u_y} \qquad U_x \qquad U_y$$

$$\begin{bmatrix}
K^{ktt}_{u_xu_y} + K^{(k+1)tt}_{u_xu_y} & K^{kt2}_{u_xu_y} + K^{(k+1)t2}_{u_xu_y} & K^{kt3}_{u_xu_y} + K^{(k+1)t3}_{u_xu_y} & K^{ktb}_{u_xu_y} + K^{(k+1)tb}_{u_xu_y} \\
K^{k2t}_{u_xu_y} + K^{(k+1)2t}_{u_xu_y} & K^{k22}_{u_xu_y} + K^{(k+1)22}_{u_xu_y} & K^{k23}_{u_xu_y} + K^{(k+1)23}_{u_xu_y} & K^{k2b}_{u_xu_y} + K^{(k+1)2b}_{u_xu_y} \\
K^{kbt}_{u_xu_y} + K^{(k+1)bt}_{u_xu_y} & K^{kb2}_{u_xu_y} + K^{(k+1)b2}_{u_xu_y} & K^{kb3}_{u_xu_y} + K^{(k+1)b3}_{u_xu_y} & K^{kbb}_{u_xu_y} + K^{(k+1)bb}_{u_xu_y}
\end{bmatrix}$$

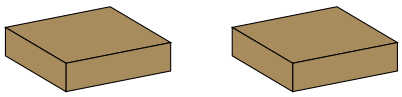

EELPVD$_{233}$

$$\begin{bmatrix}
K^{(k+1)tt}_{u_xu_y} & K^{(k+1)t2}_{u_xu_y} & K^{(k+1)t3}_{u_xu_y} & K^{(k+1)tb}_{u_xu_y} & 0 & 0 & 0 \\
K^{(k+1)2t}_{u_xu_y} & K^{(k+1)22}_{u_xu_y} & K^{(k+1)23}_{u_xu_y} & K^{(k+1)2b}_{u_xu_y} & 0 & 0 & 0 \\
K^{(k+1)bt}_{u_xu_y} & K^{(k+1)b2}_{u_xu_y} & K^{(k+1)b3}_{u_xu_y} & K^{(k+1)bb}_{u_xu_y} + K^{ktt}_{u_xu_y} & K^{kt2}_{u_xu_y} & K^{kt3}_{u_xu_y} & K^{ktb}_{u_xu_y} \\
0 & 0 & 0 & K^{k2t}_{u_xu_y} & K^{k22}_{u_xu_y} & K^{k23}_{u_xu_y} & K^{k2b}_{u_xu_y} \\
0 & 0 & 0 & K^{kbt}_{u_xu_y} & K^{kb2}_{u_xu_y} & K^{kb3}_{u_xu_y} & K^{kbb}_{u_xu_y}
\end{bmatrix}$$

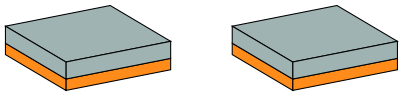

LLLPVD$_{233}$

$$\begin{bmatrix}
K^{(k+1)tt}_{u_xu_y} & K^{(k+1)t2}_{u_xu_y} & K^{(k+1)t3}_{u_xu_y} & K^{(k+1)tb}_{u_xu_y} + K^{ktt}_{u_xu_y} & K^{kt2}_{u_xu_y} & K^{kt3}_{u_xu_y} & K^{ktb}_{u_xu_y} \\
K^{(k+1)2t}_{u_xu_y} & K^{(k+1)22}_{u_xu_y} & K^{(k+1)23}_{u_xu_y} & K^{(k+1)2b}_{u_xu_y} + K^{k2t}_{u_xu_y} & K^{k22}_{u_xu_y} & K^{k23}_{u_xu_y} & K^{k2b}_{u_xu_y} \\
K^{(k+1)bt}_{u_xu_y} & K^{(k+1)b2}_{u_xu_y} & K^{(k+1)b3}_{u_xu_y} & K^{(k+1)bb}_{u_xu_y} + K^{kbt}_{u_xu_y} & K^{kb2}_{u_xu_y} & K^{kb3}_{u_xu_y} & K^{kbb}_{u_xu_y}
\end{bmatrix}$$

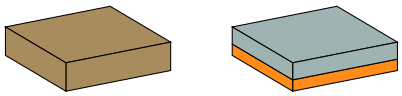

ELLPVD$_{233}$

$$\begin{bmatrix}
K^{(k+1)tt}_{u_xu_y} & K^{(k+1)t2}_{u_xu_y} & K^{(k+1)t3}_{u_xu_y} & K^{(k+1)tb}_{u_xu_y} \\
K^{(k+1)2t}_{u_xu_y} & K^{(k+1)22}_{u_xu_y} & K^{(k+1)23}_{u_xu_y} & K^{(k+1)2b}_{u_xu_y} \\
K^{(k+1)bt}_{u_xu_y} + K^{ktt}_{u_xu_y} & K^{(k+1)b2}_{u_xu_y} + K^{kt2}_{u_xu_y} & K^{(k+1)b3}_{u_xu_y} + K^{kt3}_{u_xu_y} & K^{(k+1)bb}_{u_xu_y} + K^{ktb}_{u_xu_y} \\
K^{k2t}_{u_xu_y} & K^{k22}_{u_xu_y} & K^{k23}_{u_xu_y} & K^{k2b}_{u_xu_y} \\
K^{kbt}_{u_xu_y} & K^{kb2}_{u_xu_y} & K^{kb3}_{u_xu_y} & K^{kbb}_{u_xu_y}
\end{bmatrix}$$

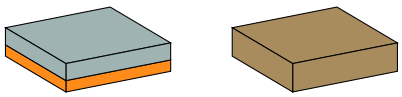

LELPVD$_{233}$

Figure 2.8: Example of thickness assembly for the term $\mathbf{K}_{u_x u_y}$ of the stiffness matrix. Different combinations of axiomatic model (ESL and LW) for in-plane displacements (u_x, u_y) are shown. On the left the assembled matrix and on the right the corresponding axiomatic model used for each component.

dently model the components of the displacement vector. This provides the flexibility to assemble stiffness contribution of "mixed" terms that are modeled with different theories. This fact implies that assembled kernels ($\mathbf{K}_{u_x u_y}$, $\mathbf{K}_{u_y u_z}$) can be rectangular and of different sizes. Fig. 2.9 shows a simple example of matrix structure in case there are two nodes and different theories.

2.3.4 In-plane assembly

Elements based on the GUF are polymorphic because an infinite number of kinematics can be associated to them. These characteristic make the elements useful for a global-local analysis (see Fig. 2.10).

In the current formulation each finite element can have a different kinematic model assigned in the local element reference system. This produces incompatibility between elements. A node can be described by different kinematic theory depending which element is considered belonging to. This issue is solved through a weak imposition of the interelement compatibility using a penalty method.

2.4 Acknowledgments

Chapter 2 is in part a reprint of:

- "*Large displacement models for composites based on Murakami's Zig-Zag Function, Green-Lagrange Strain Tensor, and Generalized Unified Formulation*", *Thin-Walled Structures*, 2020 and co-authored by Luciano Demasi. The author of this dissertation is the primary investigator and author of this paper.

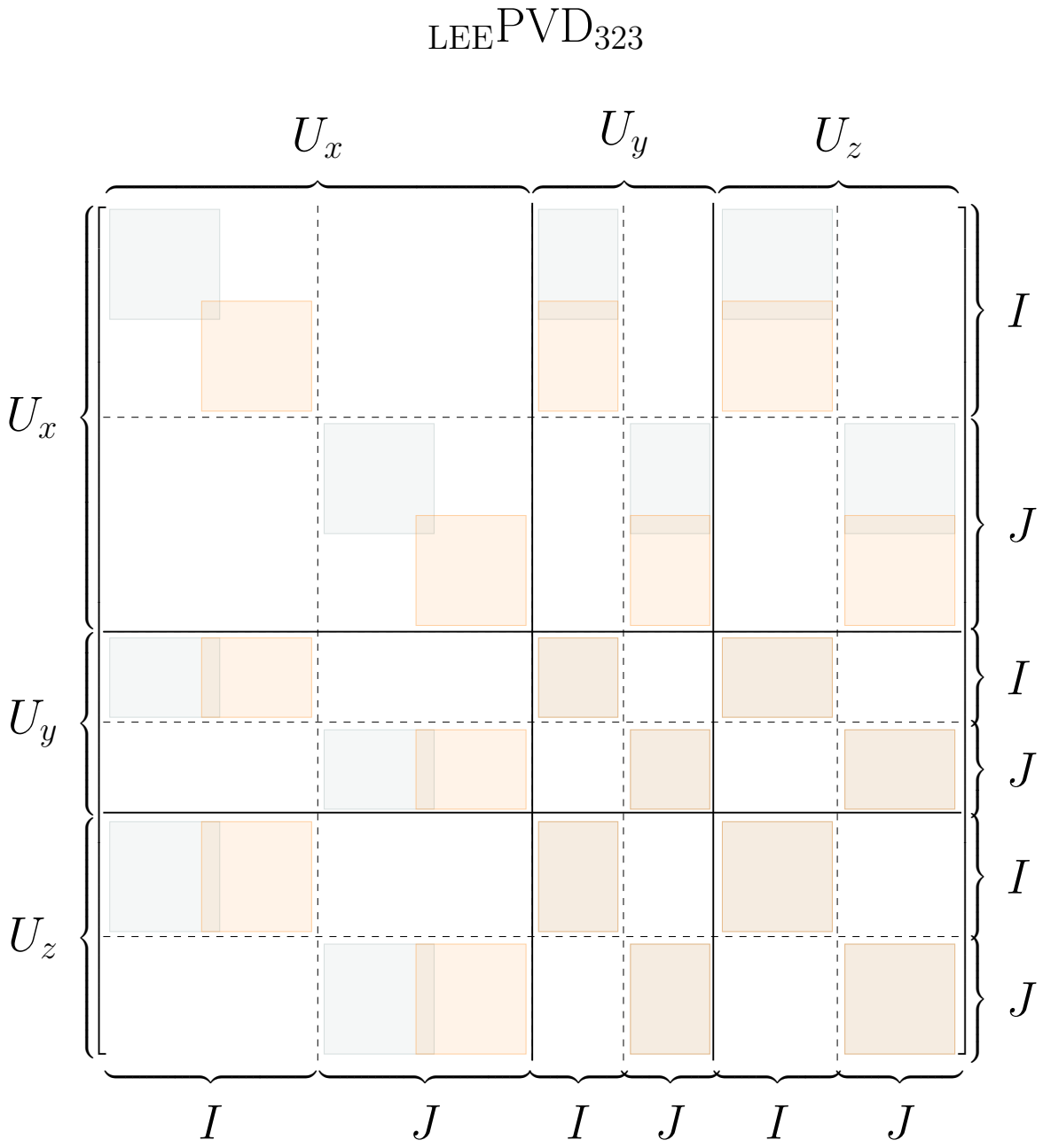

Figure 2.9: Assembled stiffness matrix of a two layer plate using the axiomatic theory $_{\text{LEE}}\text{PVD}_{323}$. Only two nodes I,J are shown. Blue and orange squares represent the stiffness of the top and bottom layer respectively

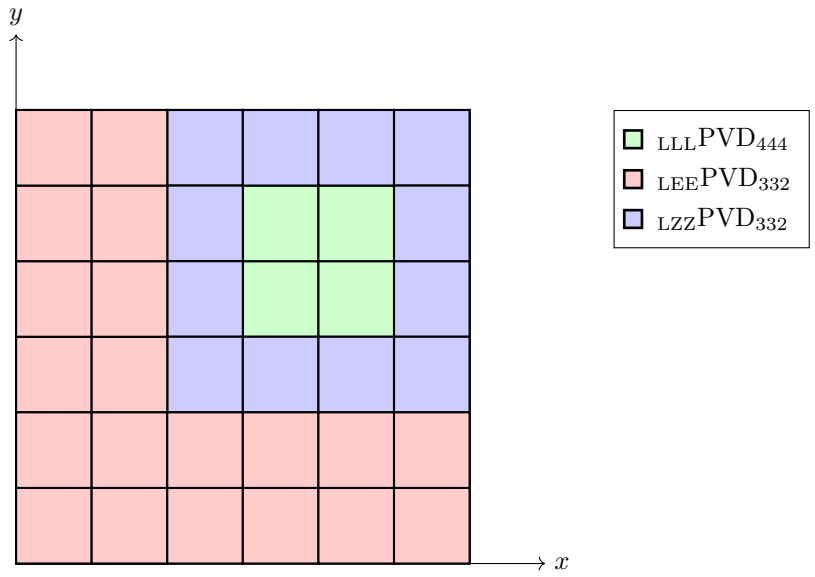

Figure 2.10: Application of GUF for global-local analysis. Different color corresponds to different kinematic theories.

Chapter 3

Geometrically Nonlinear Static Analysis of Anisotropic Laminates

3.1 Governing equations

In this chapter it is described the procedure to solve a geometrically nonlinear problem for a anisotropic laminate with variable thickness using a variable axiomatic plate model with the Finite Element Method. The first step is to find a suitable form of the governing equations that allows an easy application of the numerical algorithm. This form is called weak form. It can be derived from the differential expression of the equilibrium equation using the Weighted Residual Method and an integration by parts. The resulting equation is still difficult to solve because of the nonlinearity. Then a linearization is performed and the solution is obtained incrementally.

3.1.1 Strong form of the boundary value problem

The equations that it is intended to solve are the ones of static elasticity of a general body subjected to both Dirichlet and Neumann boundary conditions. The elastic body during the deformation is supposed to occupy a region V of the three-dimensional space with boundary Γ (see Fig. 3.1). A left subscript 0 is used to indicate the initial configuration. The body is subjected to both conservative volume forces ($\mathbf{b}$), surface forces ($\mathbf{h}$) acting on part of the boundary (Γ_h) and it is constrained on the remaining part of the boundary (Γ_g) where a displacement field is given ($\mathbf{g}$). Defined a fixed Cartesian reference frame, it is possible to identify each point on the solid by its position at the initial undeformed configuration ($\mathbf{X}$) and at the deformed (current) one ($\mathbf{x}$), after a displacement field $\mathbf{u}$ is applied.

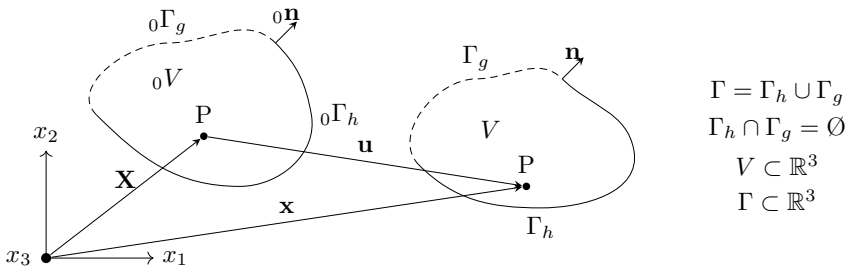

Figure 3.1: Solid domain at initial undeformed configuration and after deformation occurs.

$$\mathbf{x} = \mathbf{X} + \mathbf{u} \tag{3.1}$$

The most natural way to define the equilibrium is to express it in the deformed configuration using the Cauchy stress tensor σ_{ij}. The associated system of differential equations (strong form) is shown in Box 3.2.

Strong form at current configuration

Given $b_i : V \to \mathbb{R}$, $\hat{g}_i : \Gamma_{g_i} \to \mathbb{R}$, $\hat{h}_i : \Gamma_{h_i} \to \mathbb{R}$, find $u_i : V \to \mathbb{R}$, such that

$$\begin{cases} \sigma_{ji,j}(\mathbf{x}) + b_i(\mathbf{x}) = 0 & \text{in } V \\ u_i(\mathbf{x}) = \hat{g}_i(\mathbf{x}) & \text{on } \Gamma_{g_i} \\ n_j(\mathbf{x})\sigma_{ji}(\mathbf{x}) = \hat{h}_i(\mathbf{x}) & \text{on } \Gamma_{h_i} \end{cases} \tag{3.2}$$

This form turns out to be difficult to deal with using the current variable axiomatic theory due to the continuous update of the current reference systems during the incremental algorithm. As a matter of fact *it is not possible to apply a rotation matrix* to a quantity which components along a certain direction are described by polynomials of different order. Other methods can be used like a least-square solution, but it will degrade the performance. This issue can be avoided if the equilibrium is expressed in the initial undeformed configuration ($_0V$) using the Second Piola-Kirchhoff stress tensor $\mathbf{S}$ ($SPKST$) and the Green-Lagrange strain tensor $\mathbf{E}$ ($GLST$) [96]. The strong form in the undeformed configuration is shown in Box 3.3 (see Appendix B for derivation). Here $\mathbf{G}$ is the deformation gradient and $\mathcal{J}$ its determinant.

3.1.2 Weak form of the boundary value problem

The strong form of the boundary value problem (Eq. 3.3) is not easily solved. There are other forms that can be used to solve it: such as the weighted residual forms or the weak forms (virtual work) and the variational forms (energy principles). Since we allow the forces to be non-conservative, it is not possible to

Strong form at undeformed configuration

Given $b_i : {}_0V \to \mathbb{R}$, $\hat{g}_i : \Gamma_{g_i} \to \mathbb{R}$, ${}_0\hat{h}_i : {}_0\Gamma_{h_i} \to \mathbb{R}$, find $u_i : {}_0V \to \mathbb{R}$, such that

$$\begin{cases} \left(G_{ip}(\mathbf{X})S_{pj}(\mathbf{X})\right)_{,j} + Jb_i(\mathbf{X}) &= \mathcal{J}\rho(\mathbf{X})\ddot{u}_i(\mathbf{X}) & \text{in} \quad {}_0V \\ u_i(\mathbf{X}) &= \hat{g}_i(\mathbf{X}) & \text{on} \quad {}_0\Gamma_{g_i} \\ G_{ik}(\mathbf{X})S_{kj}(\mathbf{X})\,{}_0n_j(\mathbf{X}) &= {}_0\hat{h}_i(\mathbf{X}) & \text{on} \quad {}_0\Gamma_{h_i} \end{cases} \tag{3.3}$$

obtain a potential energy for the system and consequently it is not possible to use an energy principle like the principle of minimum potential energy. In the Finite Element Method the weak form is often used. In order to rewrite the system of equations (Eq. 3.3) in the corresponding weak form it is necessary to introduce the trial functions (u_i) and the weighting functions (δu_i) defined as follows:

$$u_i \in S_i \qquad S_i = \{u_i \mid u_i \in H^1, u_i = \hat{g}_i \text{ on } {}_0\Gamma_{g_i}\} \tag{3.4}$$

$$\delta u_i \in W_i \qquad W_i = \{\delta u_i \mid \delta u_i \in H^1, \delta u_i = 0 \text{ on } {}_0\Gamma_{g_i}\} \tag{3.5}$$

where H^1 is the space of functions with square-integrable derivatives.

The first step is to multiply the equilibrium equation 3.3 by the weighting functions and integrate over the domain

$$-\int_{{}_0V} \delta u_i \left(G_{ip}S_{pj}\right)_{,j} \,\mathrm{d}\,{}_0V = \int_{{}_0V} \delta u_i \mathcal{J} b_i \,\mathrm{d}\,{}_0V \tag{3.6}$$

This form corresponds to the weighted residual form. To obtain the weak form an integration by part is used:

$$\int_{{}_0V} \delta u_i \left(G_{ip}S_{pj}\right)_{,j} \,\mathrm{d}\,{}_0V = -\int_{{}_0V} \delta u_{i,j} G_{ip}S_{pj} \,\mathrm{d}\,{}_0V + \int_{{}_0V} \left(\delta u_i G_{ip}S_{pj}\right)_{,j} \,\mathrm{d}\,{}_0V \tag{3.7}$$

Using Gauss theorem on the last term of the right-hand side of the equation 3.7:

$$\int_{{}_0V} \delta u_i \left(G_{ip}S_{pj}\right)_{,j} \,\mathrm{d}\,{}_0V = -\int_{{}_0V} \delta u_{i,j} G_{ip}S_{pj} \,\mathrm{d}\,{}_0V \int_{{}_0\Gamma} \delta u_i G_{ip}S_{pj}\,{}_0n_j \,\mathrm{d}\,{}_0\Gamma \tag{3.8}$$

Since $\delta u_i = 0$ on Γ_{g_i} by definition of weighting function (see Eq. 3.4) it is possible to write the following:

$$\int_{{}_0V} \delta u_i \left(G_{ip}S_{pj}\right)_{,j} \,\mathrm{d}\,{}_0V = -\int_V \delta u_{i,j} G_{ip}S_{pj}\,\mathrm{d}\,{}_0V + \sum_i \int_{{}_0\Gamma_{h_i}} \delta u_i G_{ip}S_{pj}\,{}_0n_j\,\mathrm{d}\,{}_0\Gamma \tag{3.9}$$

Using the Neumann boundary condition (see Eq. 3.3) in Eq. 3.9:

$$\int_{{}_0V} \delta u_i \left(G_{ip}S_{pj}\right)_{,j} \,\mathrm{d}\,{}_0V = -\int_{{}_0V} \delta u_{i,j} G_{ip}S_{pj}\,\mathrm{d}\,{}_0V + \sum_i \int_{{}_0\Gamma_{h_i}} \delta u_i\,{}_0\hat{h}_i\,\mathrm{d}\,{}_0\Gamma \tag{3.10}$$

Substituting Eq. 3.10 in Eq. 3.6

$$\int_{{}_0V} \delta u_{i,j} G_{ip}S_{pj}\,\mathrm{d}\,{}_0V = \int_{{}_0V} \delta u_i \mathcal{J} b_i\,\mathrm{d}\,{}_0V + \sum_i \int_{{}_0\Gamma_{h_i}} \delta u_i\,{}_0\hat{h}_i\,\mathrm{d}\,{}_0\Gamma \tag{3.11}$$

Using the following relations $\delta u_{i,j} = \delta G_{ij}$:

$$\int_{{}_0V} \delta G_{ij} G_{ip}S_{pj}\mathrm{d}\,{}_0V = \int_{{}_0V} \delta u_i \mathcal{J} b_i\,\mathrm{d}\,{}_0V + \sum_i \int_{{}_0\Gamma_{h_i}} \delta u_i\,{}_0\hat{h}_i\,\mathrm{d}\,{}_0\Gamma \tag{3.12}$$

The left-hand side of Eq. 3.12 can be rewritten as a function of the Green-Lagrange strain and Second-Piola Kirchhoff stress tensor. Introducing the variation of the Green-Lagrange strain:

$$\delta E_{pj} = \frac{1}{2}\left(\delta G_{ip}G_{ij} + G_{ip}\delta G_{ij}\right) \tag{3.13}$$

it is possible to show that using the symmetry of the stress tensor, the product of the strain variation with the stress is:

$$\begin{aligned}
\delta E_{pj}S_{pj} &= \frac{1}{2}\left(\delta G_{ip}G_{ij} + G_{ip}\delta G_{ij}\right)S_{pj} = \frac{1}{2}\delta G_{ip}G_{ij}S_{pj} + \frac{1}{2}\delta G_{ij}G_{ip}S_{pj} && (3.14)\\
&= \frac{1}{2}\delta G_{ij}G_{ip}S_{jp} + \frac{1}{2}\delta G_{ij}G_{ip}S_{pj} = \frac{1}{2}\delta G_{ij}G_{ip}S_{pj} + \frac{1}{2}\delta G_{ij}G_{ip}S_{pj} && (3.15)\\
&= \delta G_{ij}G_{ip}S_{pj} && (3.16)
\end{aligned}$$

Substituting Eq. 3.14 in Eq. 3.12 the weak form is obtained. The statement is as follows:

Weak form undeformed configuration

Given $b_i : {}_0V \to \mathbb{R}$, $\hat{g}_i : {}_0\Gamma_{g_i} \to \mathbb{R}$, ${}_0\hat{h}_i : {}_0\Gamma_{h_i} \to \mathbb{R}$, find $u_i \in S_i$, such that for all $\delta u_i \in W_i$

$$\int_{{}_0V} \delta E_{ij}S_{ij}\,\mathrm{d}\,{}_0V = \int_{{}_0V} \delta u_i \mathcal{J} b_i\,\mathrm{d}\,{}_0V + \sum_i \int_{{}_0\Gamma_{h_i}} \delta u_i\,{}_0\hat{h}_i\,\mathrm{d}\,{}_0\Gamma \tag{3.17}$$

This form is equivalent to the work of virtual displacements. The left hand side represents the virtual internal work and the right-hand side the work of the external forces.

3.1.3 Essential boundary condition

The weak form (Eq. 3.17) does not include the essential boundary conditions. There are different methods to enforce them, e.g. direct substitution method, penalty method, Lagrange multiplier, Nitche's method. In this work the penalty method has been chosen for its simplicity and for not increasing the number of unknown variables. In this method the energy of the system is modified due to the constraint. The energy contribution of the constraint is:

$$U_{\mathrm{G}} = \frac{1}{2}\int_{{}_0\Gamma^g} (\mathbf{u}-\mathbf{g})^T \boldsymbol{\psi} (\mathbf{u}-\mathbf{g}) \,\mathrm{d}\,{}_0\Gamma^g \tag{3.18}$$

where $\boldsymbol{\psi}$ is a diagonal matrix with the penalty factors.

$$\boldsymbol{\psi} = \begin{bmatrix} \psi_x & 0 & 0 \\ 0 & \psi_y & 0 \\ 0 & 0 & \psi_z \end{bmatrix} \tag{3.19}$$

The variation of the potential energy is taken:

$$\begin{aligned} \delta U_{\mathrm{G}} &= \delta\left[\frac{1}{2}\int_{{}_0\Gamma^g} (\mathbf{u}-\mathbf{g})^T \boldsymbol{\psi} (\mathbf{u}-\mathbf{g}) \,\mathrm{d}\,{}_0\Gamma^g\right] = \\ &= \frac{1}{2}\int_{{}_0\Gamma^g} \delta(\mathbf{u}-\mathbf{g})^T \boldsymbol{\psi} (\mathbf{u}-\mathbf{g}) \,\mathrm{d}\,{}_0\Gamma^g + \frac{1}{2}\int_{{}_0\Gamma^g} (\mathbf{u}-\mathbf{g})^T \boldsymbol{\psi} \delta(\mathbf{u}-\mathbf{g}) \,\mathrm{d}\,{}_0\Gamma^g = \\ &= \frac{1}{2}\int_{{}_0\Gamma^g} \delta\mathbf{u}^T \boldsymbol{\psi} (\mathbf{u}-\mathbf{g}) \,\mathrm{d}\,{}_0\Gamma^g + \frac{1}{2}\int_{{}_0\Gamma^g} (\mathbf{u}-\mathbf{g})^T \boldsymbol{\psi} \delta\mathbf{u} \,\mathrm{d}\,{}_0\Gamma^g = \\ &= \int_{{}_0\Gamma^g} \delta\mathbf{u}^T \boldsymbol{\psi} (\mathbf{u}-\mathbf{g}) \mathrm{d}\,{}_0\Gamma^g = \int_{{}_0\Gamma^g} \delta\mathbf{u}^T \boldsymbol{\psi} \mathbf{u} \,\mathrm{d}\,{}_0\Gamma^g - \int_{{}_0\Gamma^g} \delta\mathbf{u}^T \boldsymbol{\psi} \mathbf{g} \,\mathrm{d}\,{}_0\Gamma^g \end{aligned} \tag{3.20}$$

This variation is then added to the weak form (Box 3.21).

3.1.4 Interelement compatibility

The weak form derived (Eq. 3.21) is applicable to a standard FEM in which a single axiomatic theory is chosen for all elements and all displacement direction. An additional issue arises if this condition is removed and different elements are allowed to have different theories and order of expansions. Foreseeing this issue, the weak form is augmented with additional terms to take into account the inter-element displacement compatibility. In doing so we imagine that the continuum solid to be splits into pieces. Each

Weak form undeformed configuration

Given $b_i : {}_0V \to \mathbb{R}$, $\hat{g}_i : {}_0\Gamma_{g_i} \to \mathbb{R}$, ${}_0\hat{h}_i : {}_0\Gamma_{h_i} \to \mathbb{R}$, find $u_i \in S_i$, such that for all $\delta u_i \in W_i$

$$\int_{{}_0V} \delta E_{ij} S_{ij} \, \mathrm{d}\, {}_0V + \int_{{}_0\Gamma_{g_i}} \delta u_i \psi_{ii} u_i \, \mathrm{d}\, {}_0\Gamma_{g_i} = \sum_i \int_{{}_0\Gamma_{h_i}} \delta u_i \, {}_0\hat{h}_i \, \mathrm{d}\, {}_0\Gamma + \sum_i \int_{{}_0\Gamma_{g_i}} \delta u_i \psi_{ii} g_i \, \mathrm{d}\, {}_0\Gamma_{g_i} + \int_{{}_0V} \delta u_i \mathcal{J} b_i \mathrm{d}\, {}_0V \tag{3.21}$$

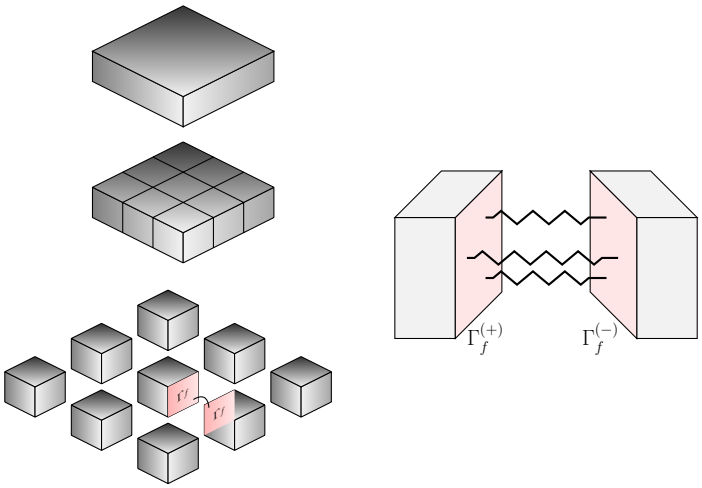

Figure 3.2: Solid is subdivided into elements. Elements are connected through a distribution of springs attached to the new generated faces.

piece corresponding to a future finite element. The division generates new internal surfaces (Γ_f). Then the surfaces are kept together using again a penalty method, that can be imagined as a distribution of springs connecting the new generated surfaces (see Fig. 3.2).

The energy associated to the springs connecting each pair of faces is:

$$U_{\mathrm{COMP}} = \sum_{f=1}^{n_f} U_{\mathrm{COMP}}^{(f)} \tag{3.22}$$

$$U_{\mathrm{COMP}}^{(f)} = \frac{1}{2} \int_{{}_0\Gamma_f} (\mathbf{u}_{\Gamma_{f(+)}} - \mathbf{u}_{\Gamma_{f(-)}})^T \boldsymbol{\gamma} (\mathbf{u}_{\Gamma_{f(+)}} - \mathbf{u}_{\Gamma_{f(-)}}) \, \mathrm{d}\, {}_0\Gamma_f \tag{3.23}$$

where

$$\boldsymbol{\gamma} = \begin{bmatrix} \gamma_x & 0 & 0 \\ 0 & \gamma_y & 0 \\ 0 & 0 & \gamma_z \end{bmatrix} \tag{3.24}$$

Note that the surface $\Gamma_{f^{(+)}}$ and $\Gamma_{f^{(-)}}$ are supposed to be equal. The variation of the energy is:

$$\begin{aligned}
\delta U^{(f)}_{\text{COMP}} &= \delta\left[\frac{1}{2}\int_{{}_0\Gamma_f} (\mathbf{u}_{\Gamma_{f^{(+)}}} - \mathbf{u}_{\Gamma_{f^{(-)}}})^T \boldsymbol{\gamma} (\mathbf{u}_{\Gamma_{f^{(+)}}} - \mathbf{u}_{\Gamma_{f^{(-)}}}) \,\mathrm{d}\,{}_0\Gamma_f\right] = \\
&= \frac{1}{2}\int_{{}_0\Gamma_f} \delta\mathbf{u}^T_{\Gamma_{f^{(+)}}} \boldsymbol{\gamma} (\mathbf{u}_{\Gamma_{f^{(+)}}} - \mathbf{u}_{\Gamma_{f^{(-)}}}) \,\mathrm{d}\,{}_0\Gamma_f - \frac{1}{2}\int_{{}_0\Gamma_f} \delta\mathbf{u}^T_{\Gamma_{f^{(-)}}} \boldsymbol{\gamma} (\mathbf{u}_{\Gamma_{f^{(+)}}} - \mathbf{u}_{\Gamma_{f^{(-)}}}) \,\mathrm{d}\,{}_0\Gamma_f + \\
&+ \frac{1}{2}\int_{{}_0\Gamma_f} (\mathbf{u}_{\Gamma_{f^{(+)}}} - \mathbf{u}_{\Gamma_{f^{(-)}}})^T \boldsymbol{\gamma} \delta\mathbf{u}_{\Gamma_{f^{(+)}}} \,\mathrm{d}\,{}_0\Gamma_f - \frac{1}{2}\int_{{}_0\Gamma_f} (\mathbf{u}_{\Gamma_{f^{(+)}}} - \mathbf{u}_{\Gamma_{f^{(-)}}})^T \boldsymbol{\gamma} \delta\mathbf{u}_{\Gamma_{f^{(-)}}} \,\mathrm{d}\,{}_0\Gamma_f = \\
&= \int_{{}_0\Gamma_f} \delta\mathbf{u}^T_{\Gamma_{f^{(+)}}} \boldsymbol{\gamma} \mathbf{u}_{\Gamma_{f^{(+)}}} \,\mathrm{d}\,{}_0\Gamma_f - \int_{{}_0\Gamma_f} \delta\mathbf{u}^T_{\Gamma_{f^{(+)}}} \boldsymbol{\gamma} \mathbf{u}_{\Gamma_{f^{(-)}}} \,\mathrm{d}\,{}_0\Gamma_f + \\
&+ \int_{{}_0\Gamma_f} \delta\mathbf{u}^T_{\Gamma_{f^{(-)}}} \boldsymbol{\gamma} \mathbf{u}_{\Gamma_{f^{(-)}}} \,\mathrm{d}\,{}_0\Gamma_f - \int_{{}_0\Gamma_f} \delta\mathbf{u}^T_{\Gamma_{f^{(-)}}} \boldsymbol{\gamma} \mathbf{u}_{\Gamma_{f^{(+)}}} \,\mathrm{d}\,{}_0\Gamma_f
\end{aligned} \tag{3.25}$$

Adding this contribution to the weak form, the final expression for the variable kinematic plate is obtained:

Weak form for the variable kinematic plate theory in the undeformed configuration

Given $b_i : {}_0V \to \mathbb{R}$, $\hat{g}_i : {}_0\Gamma_{g_i} \to \mathbb{R}$, ${}_0\hat{h}_i : {}_0\Gamma_{h_i} \to \mathbb{R}$, find $u_i \in S_i$, such that for all $\delta u_i \in W_i$

$$\begin{aligned}
&\underbrace{\int_{{}_0V} \delta E_{ij} S_{ij} \,\mathrm{d}\,{}_0V}_{\text{Internal work}} + \underbrace{\int_{{}_0\Gamma_{g_i}} \delta u_i \psi_{ii} u_i \,\mathrm{d}\,{}_0\Gamma_{g_i}}_{\substack{\text{homogeneous part of} \\ \text{essential b.c.}}} - \underbrace{\int_{{}_0\Gamma_{g_i}} \delta u_i \psi_{ii} g_i \,\mathrm{d}\,{}_0\Gamma_{g_i}}_{\substack{\text{Non-homogeneous part of} \\ \text{essential b.c.}}} = \\
&\underbrace{\underbrace{\int_{{}_0V} \delta u_i \mathcal{J} b_i \mathrm{d}\,{}_0V}_{\text{Volume forces}} + \underbrace{\sum_i \int_{{}_0\Gamma_{h_i}} \delta u_i \,{}_0\hat{h}_i \,\mathrm{d}\,{}_0\Gamma}_{\text{Surface forces}}}_{\text{External work}} - \\
&\underbrace{- \sum_i \sum_{f=1}^{n_f} \int_{{}_0\Gamma_f} \left(\delta u_{i\,\Gamma_{f^{(+)}}} - \delta u_{i\,\Gamma_{f^{(-)}}}\right) \gamma_{ii} \left(u_{i\,\Gamma_{f^{(+)}}} - u_{i\,\Gamma_{f^{(-)}}}\right) \,\mathrm{d}\,{}_0\Gamma_f}_{\text{Interelement compatibility}}
\end{aligned} \tag{3.26}$$

The weak form derived has the same expression of the equation that it would have been obtained if the principle of the virtual displacements (PVD) had been used. It states that the internal work due to the virtual displacements (virtual work) is equal to the external virtual work with the addition of energy

constraints to impose the boundary condition.

$$\delta W_{\mathrm{INT}} + \delta U_{\mathrm{G}} + \delta U_{\mathrm{COMP}} = \delta W_{\mathrm{EXT}} \tag{3.27}$$

where

$$\delta W_{\mathrm{INT}} = \int_{{}_0V} \delta E_{ij} S_{ij} \, \mathrm{d}\,{}_0V \tag{3.28}$$

$$\delta W_{\mathrm{EXT}} = \int_{{}_0V} \delta u_i \mathcal{J} b_i \, \mathrm{d}\,{}_0V + \sum_i \int_{{}_0\Gamma_{h_i}} \delta u_i \, {}_0\hat{h}_i \, \mathrm{d}\,{}_0\Gamma \tag{3.29}$$

$$\delta U_{\mathrm{G}} = \int_{{}_0\Gamma_{g_i}} \delta u_i \psi_{ii} u_i \mathrm{d}\,{}_0\Gamma_{g_i} - \int_{\Gamma_{g_i}} \delta u_i \psi_{ii} g_i \, \mathrm{d}\,{}_0\Gamma_{g_i} \tag{3.30}$$

$$\begin{aligned} \delta U^{(f)}_{\mathrm{COMP}} \;=\; & \sum_i \sum_{f=1}^{n_f} \int_{{}_0\Gamma_f} \delta u_{i\,\Gamma_{f(+)}} \gamma_{ii} u_{i\,\Gamma_{f(+)}} \, \mathrm{d}\,{}_0\Gamma_f + \sum_i \sum_{f=1}^{n_f} \int_{{}_0\Gamma_f} \delta u_{i\,\Gamma_{f(-)}} \gamma_{ii} u_{i\,\Gamma_{f(-)}} \, \mathrm{d}\,{}_0\Gamma_f - \\ - \; & \sum_i \sum_{f=1}^{n_f} \int_{{}_0\Gamma_f} \delta u_{i\,\Gamma_{f(+)}} \gamma_{ii} u_{i\,\Gamma_{f(-)}} \, \mathrm{d}\,{}_0\Gamma_f - \sum_i \sum_{f=1}^{n_f} \int_{{}_0\Gamma_f} \delta u_{i\,\Gamma_{f(-)}} \gamma_{ii} u_{i\,\Gamma_{f(+)}} \, \mathrm{d}\,{}_0\Gamma_f \end{aligned} \tag{3.31}$$

3.1.5 Linearization for load stepping algorithm

During the linearization process the left sub- and super- scripts on a field variable refer to the configuration in which that variable has *measured* and *occurred* respectively. Thus, for example, ${}^{t}_{0}\delta W_{\mathrm{tot}}$ indicates that the total virtual work δW_{tot} is calculated at the pseudo-time t and is referred to the initial configuration. This is a static analysis. Thus, from a formal point of view, time t is not adopted. However, the solution strategy requires the conceptual subdivisions in steps, which are easily identified by the "time" t. For that reason, even when the quantities contain reference to the variable t, the reader needs to assume that a nonlinear static solution of the structural problem is sought.

The nonlinear equation provided by the weak form (see Eq. 3.26) has to be linearized using a *load step algorithm* in order to be solved with the Finite Element Method. In the present capability Newton-Raphson technique has been implemented. Assuming that the solution corresponding to a load level identified by the pseudo-time t is known, the algorithm needs to be able to identify the response to a load level corresponding to an incremented pseudo-time $t + \Delta t$, where Δt is the pseudo-time increment. Following this logic, the weak form (see Eq. 3.27) is written at pseudo-time $t + \Delta t$ as follows:

$${}^{t+\Delta t}_{0}\delta W_{\mathrm{TOT}} = {}^{t+\Delta t}_{0}\delta W_{\mathrm{INT}} - {}^{t+\Delta t}_{0}\delta W_{\mathrm{EXT}} + {}^{t+\Delta t}_{0}\delta U_G + {}^{t+\Delta t}_{0}\delta U_{COMP} = 0 \tag{3.32}$$

In the practice [97] an incremental decomposition of the variables is adopted as shown below for the generic quantity $\square$:

$$\overbrace{{}^{t+\Delta t}_{0}\square}^{\text{unknown}} = \overbrace{{}^{t}_{0}\square}^{\text{known}} + \overbrace{{}_{0}\Delta\square}^{\text{unknown}} \tag{3.33}$$

Using the approach described in Eq. 3.33 for the cases of displacement u_i, strain E_{ij}, and stress S_{ij} components, the following relations can be written:

$$\begin{aligned} {}^{t+\Delta t}_{0}u_i &= {}^{t}_{0}u_i + {}_{0}\Delta u_i \\ {}^{t+\Delta t}_{0}E_{ij} &= {}^{t}_{0}E_{ij} + {}_{0}\Delta E_{ij} \\ {}^{t+\Delta t}_{0}S_{ij} &= {}^{t}_{0}S_{ij} + {}_{0}\Delta S_{ij} \end{aligned} \tag{3.34}$$

The $GLST$ is a nonlinear function of the displacements as described in the following expression:

$$E_{ij} = \frac{1}{2}\left(G_{ki}G_{kj} - \delta_{ij}\right) = \frac{1}{2}\left(u_{i,j} + u_{j,i} + u_{k,i}u_{k,j}\right) \tag{3.35}$$

where $\mathbf{G}$ is the deformation gradient and is explicitly defined below:

$${}^{t}_{0}G_{ij} = \delta_{ij} + {}^{t}_{0}u_{i,j} \tag{3.36}$$

The symbol δ_{ij} is Kronecker's delta and the subscript "," is used to indicate differentiation.

The expression for the increment ${}_{0}\Delta E_{ij}$ of the $GLST$ (see Eqs. 3.34 and 3.35) can be derived by subtracting the strains at time t from the ones at $t + \Delta t$:

$${}_{0}\Delta E_{ij} = \frac{1}{2}\left({}_{0}\Delta u_{i,j} + {}_{0}\Delta u_{j,i} + {}^{t}_{0}u_{k,i}\,{}_{0}\Delta u_{k,j} + {}_{0}\Delta u_{k,i}\,{}^{t}_{0}u_{k,j}\right) + \frac{1}{2}\,{}_{0}\Delta u_{k,i}\,{}_{0}\Delta u_{k,j} \tag{3.37}$$

The increment ${}_{0}\Delta E_{ij}$ is conveniently decomposed as follows:

$${}_{0}\Delta E_{ij} = {}_{0}\Delta e_{ij} + {}_{0}\Delta \eta_{ij} \tag{3.38}$$

where term ${}_{0}\Delta e_{ij}$ is a *linear function of the displacement increments*, whereas ${}_{0}\Delta \eta_{ij}$ is a *nonlinear function of the displacement increments*. Their explicit expressions are reported below:

$${}_{0}\Delta e_{ij} = \frac{1}{2}\left({}_{0}\Delta u_{i,j} + {}_{0}\Delta u_{j,i} + {}^{t}_{0}u_{k,i}\;{}_{0}\Delta u_{k,j} + {}_{0}\Delta u_{k,i}\;{}^{t}_{0}u_{k,j}\right) \tag{3.39}$$

$${}_{0}\Delta \eta_{ij} = \frac{1}{2}\,{}_{0}\Delta u_{k,i}\;{}_{0}\Delta u_{k,j} \tag{3.40}$$

To apply PVD the variations $\delta\,{}_0\Delta e_{ij}$ and $\delta\,{}_0\Delta\eta_{ij}$ need to be calculated from Eqs. 3.39 and 3.40, as reported in the following relations:

$$\delta\,{}_0\Delta e_{ij} = \frac{1}{2}\left(\delta\,{}_0\Delta u_{i,j} + \delta\,{}_0\Delta u_{j,i} + {}^{t}_{0}u_{k,i}\;\delta\,{}_0\Delta u_{k,j} + \delta\,{}_0\Delta u_{k,i}\;{}^{t}_{0}u_{k,j}\right) \tag{3.41}$$

$$\delta\,{}_0\Delta\eta_{ij} = \frac{1}{2}\left(\delta\,{}_0\Delta u_{k,i}\;{}_0\Delta u_{k,j} + \;{}_0\Delta u_{k,i}\;\delta\,{}_0\Delta u_{k,j}\right) \tag{3.42}$$

To obtain an equation that is a function of the displacements only, the $SPKST$ increments are related to the $GLST$ increments through the *Classical Form of Hooke's Law* (CFHL):

$${}_0\Delta S_{ij} = \;{}_0C_{ijrs}\;{}_0\Delta E_{rs} \tag{3.43}$$

where C_{ijrs} are Hooke's coefficients and are the ones usually adopted for linear analysis, provided that the material can be assumed to behave in a linear manner even in the presence of large displacements [95]. Substituting Eqs. 3.34, 3.41, 3.42, and 3.43 into the expression for the internal virtual work (see Eq. 3.27) the following result is obtained:

$$\begin{aligned} {}^{t+\Delta t}_{0}\delta W_{\text{INT}} \;=\; & \int_{{}_0V} \delta\,{}_0\Delta e_{ij}\;{}^{t}_{0}S_{ij}\,\mathrm{d}\,{}_0V + \int_{{}_0V} \delta\,{}_0\Delta\eta_{ij}\;{}^{t}_{0}S_{ij}\,\mathrm{d}\,{}_0V + \\ & + \int_{{}_0V} \delta\,{}_0\Delta e_{ij}\;{}_0C_{ijrs}\;{}_0\Delta E_{rs}\,\mathrm{d}\,{}_0V + \int_{{}_0V} \delta\,{}_0\Delta\eta_{ij}\;{}_0C_{ijrs}\;{}_0\Delta E_{rs}\,\mathrm{d}\,{}_0V \end{aligned} \tag{3.44}$$

In the practical solution process, the terms representing higher order infinitesimal quantities are neglected. The order of dependence with respect to the displacement increments can be directly deduced from Eq. 3.44:

$$\begin{aligned} {}^{t+\Delta t}_{0}\delta W_{\text{INT}} = & \boxed{\int_{{}_0V} \delta\,{}_0\Delta e_{ij}\;{}^{t}_{0}S_{ij}\,\mathrm{d}\,{}_0V} && (\sim\;{}_0\Delta u^0) \\ & + \boxed{\int_{{}_0V} \delta\,{}_0\Delta e_{ij}\;{}_0C_{ijrs}\;{}_0\Delta e_{rs}\,\mathrm{d}\,{}_0V} + \boxed{\int_{{}_0V} \delta\,{}_0\Delta\eta_{ij}\;{}^{t}_{0}S_{ij}\,\mathrm{d}\,{}_0V} && (\sim\;{}_0\Delta u^1) \\ & + \int_{{}_0V} \delta\,{}_0\Delta e_{ij}\;{}_0C_{ijrs}\;{}_0\Delta\eta_{rs}\,\mathrm{d}\,{}_0V && (\sim\;{}_0\Delta u^2) \\ & + \int_{{}_0V} \delta\,{}_0\Delta\eta_{ij}\;{}_0C_{ijrs}\;{}_0\Delta\eta_{rs}\,\mathrm{d}\,{}_0V && (\sim\;{}_0\Delta u^3) \end{aligned} \tag{3.45}$$

The constant and linear terms appearing in Eq. 3.45 are boxed for convenience of the reader. Discarding the higher order terms and substituting Eq. 3.45 into the PVD statement (Eqs. 3.27 and 3.32), the following

approximation for the PVD is obtained:

$$ {}^{t+\Delta t}_{0}\delta W^{\text{ct }1}_{\text{INT}} + {}^{t+\Delta t}_{0}\delta W^{\text{ct }2}_{\text{INT}} + {}^{t+\Delta t}_{0}\delta U_G + {}^{t+\Delta t}_{0}\delta U_{COMP} = - {}^{t+\Delta t}_{0}\delta W^{\text{ct }3}_{\text{INT}} + {}^{t+\Delta t}_{0}\delta W_{\text{EXT}} \tag{3.46} $$

where the definitions reported below have been used:

$$ \begin{aligned}
{}^{t+\Delta t}_{0}\delta W^{\text{ct }1}_{\text{INT}} &= \int_{{}_0V} \delta\, {}_0\Delta e_{ij}\, {}_0C_{ijrs}\, {}_0\Delta e_{rs} \mathrm{d}\, {}_0V \\
{}^{t+\Delta t}_{0}\delta W^{\text{ct }2}_{\text{INT}} &= \int_{{}_0V} \delta\, {}_0\Delta \eta_{ij}\, {}^{t}_{0}S_{ij} \mathrm{d}\, {}_0V \\
{}^{t+\Delta t}_{0}\delta W^{\text{ct }3}_{\text{INT}} &= \int_{{}_0V} \delta\, {}_0\Delta e_{ij}\, {}^{t}_{0}S_{ij} \mathrm{d}\, {}_0V \\
{}^{t+\Delta t}_{0}\delta W_{\text{EXT}} &= \int_{{}_0\Gamma_h} \delta\, {}_0\Delta u_i\ {}^{t+\Delta t}_{0}\hat{h}_i\ \mathrm{d}\, {}_0\Gamma_h + \int_{{}_0V} \delta u_i \mathcal{J} b_i \mathrm{d}\, {}_0V + \sum_p \delta\, {}_0\Delta u_{p_i}\ {}^{t+\Delta t}_{0}f_{p\,i} \\
{}^{t+\Delta t}_{0}\delta U_{\text{G}} &= \int_{{}_0\Gamma_{g_i}} \delta\, {}_0\Delta u_i \psi_{ii}\, {}_0\Delta u_i \mathrm{d}\, {}_0\Gamma_{g_i} + \int_{{}_0\Gamma_{g_i}} \delta\, {}_0\Delta u_i \psi_{ii}\, {}^{t}_{0}u_i \mathrm{d}\, {}_0\Gamma_{g_i} - \int_{{}_0\Gamma_{g_i}} \delta\, {}_0\Delta u_i \psi_{ii} g_i \mathrm{d}\, {}_0\Gamma_{g_i} \\
{}^{t+\Delta t}_{0}\delta U_{\text{COMP}} &= \sum_i \sum_{f=1}^{n_f} \int_{\Gamma_f} \delta\, {}_0\Delta u_{i\,\Gamma_{f^{(+)}}}\, \gamma_{ii}\, {}_0\Delta u_{i\,\Gamma_{f^{(+)}}} \mathrm{d}\Gamma_f + \sum_i \sum_{f=1}^{n_f} \int_{\Gamma_f} \delta\, {}_0\Delta u_{i\,\Gamma_{f^{(+)}}}\, \gamma_{ii}\, {}^{t}_{0}u_{i\,\Gamma_{f^{(+)}}} \mathrm{d}\Gamma_f + \\
&+ \sum_i \sum_{f=1}^{n_f} \int_{\Gamma_f} \delta\, {}_0\Delta u_{i\,\Gamma_{f^{(-)}}}\, \gamma_{ii}\, {}_0\Delta u_{i\,\Gamma_{f^{(-)}}} \mathrm{d}\Gamma_f + \sum_i \sum_{f=1}^{n_f} \int_{\Gamma_f} \delta\, {}_0\Delta u_{i\,\Gamma_{f^{(-)}}}\, \gamma_{ii}\, {}^{t}_{0}u_{i\,\Gamma_{f^{(-)}}} \mathrm{d}\Gamma_f - \\
&- \sum_i \sum_{f=1}^{n_f} \int_{\Gamma_f} \delta\, {}_0\Delta u_{i\,\Gamma_{f^{(+)}}}\, \gamma_{ii}\, {}_0\Delta u_{i\,\Gamma_{f^{(-)}}} \mathrm{d}\Gamma_f - \sum_i \sum_{f=1}^{n_f} \int_{\Gamma_f} \delta\, {}_0\Delta u_{i\,\Gamma_{f^{(+)}}}\, \gamma_{ii}\, {}^{t}_{0}u_{i\,\Gamma_{f^{(-)}}} \mathrm{d}\Gamma_f - \\
&- \sum_i \sum_{f=1}^{n_f} \int_{\Gamma_f} \delta\, {}_0\Delta u_{i\,\Gamma_{f^{(-)}}}\, \gamma_{ii}\, {}_0\Delta u_{i\,\Gamma_{f^{(+)}}} \mathrm{d}\Gamma_f - \sum_i \sum_{f=1}^{n_f} \int_{\Gamma_f} \delta\, {}_0\Delta u_{i\,\Gamma_{f^{(-)}}}\, \gamma_{ii}\, {}^{t}_{0}u_{i\,\Gamma_{f^{(+)}}} \mathrm{d}\Gamma_f
\end{aligned} \tag{3.47} $$

Eq. 3.46 is the *linear* relation that has to be solved at each pseudo-time step t to obtain the solution at $t + \Delta t$. The solution is numerically obtained by using the finite element discretization in the framework of GUF.

3.2 Variable axiomatic thickness expansion

The general idea is to represent the governing equations with the displacement arrays written in indicial form, allowing the user to master a virtually infinite number of theories. Each displacement component had its own independent indicial representation allowing a different structural theory for each finite element coordinate direction.

To show how the GUF is extended to the large displacement model, let X, Y, Z be a coordinate system located at finite element level (at this stage we assume that the reference undeformed geometry is considered). The $X - Y$ plane is coincident with the plate's mid-plane and Z is the thickness coordinate.

The incremental displacement ${}_0\Delta u_i$ (see Eq. 3.34) within GUF framework and at layer level is the following:

$$
\begin{aligned}
{}_0\Delta u^k_X(X,Y,Z^k) &= {}^X_0F^k_{\alpha_{u_X}}(Z^k)\,{}_0\Delta u^k_{X\alpha_{u_X}}(X,Y) \quad \alpha_{u_X}=t,l,b \quad l=2,\ldots,\mathcal{N}_{u_X}\\
{}_0\Delta u^k_Y(X,Y,Z^k) &= {}^Y_0F^k_{\alpha_{u_Y}}(Z^k)\,{}_0\Delta u^k_{Y\alpha_{u_Y}}(X,Y) \quad \alpha_{u_Y}=t,m,b \quad m=2,\ldots,\mathcal{N}_{u_Y}\\
{}_0\Delta u^k_Z(X,Y,Z^k) &= {}^Z_0F^k_{\alpha_{u_Z}}(Z^k)\,{}_0\Delta u^k_{Z\alpha_{u_Z}}(X,Y) \quad \alpha_{u_Z}=t,n,b \quad n=2,\ldots,\mathcal{N}_{u_Z}
\end{aligned}
\tag{3.48}
$$

where t, b, and l, m, n are indices adopted for the axiomatic expansion in the thickness direction. Including more terms is equivalent of having accurate higher-order theories, but the number of degrees of freedom and related computational cost are increased. More in detail, $\mathcal{N}_{u_X}$, $\mathcal{N}_{u_Y}$, and $\mathcal{N}_{u_Z}$ are the orders of the layerwise theories used for the different displacement components. For instance, $\mathcal{N}_{u_Y}=3$ means that the displacement in the Y direction and layer k is expressed with a cubic expansion obtained by combining Legendre polynomials (terms of the type ${}^Y_0F^k_{\alpha_{u_Y}}(Z)$).

The in-plane expressions of the displacements (terms ${}_0\Delta u^k_{X\alpha_{u_X}}(X,Y)$, ${}_0\Delta u^k_{Y\alpha_{u_Y}}(X,Y)$, and ${}_0\Delta u^k_{Z\alpha_{u_Z}}(X,Y)$ in Eq. 3.48) are unknown functions at this stage. Within the typical finite element discretization, these unknowns are further expressed in terms of shape functions and nodal (unknown) incremental displacements as follows:

$$
\begin{aligned}
{}_0\Delta u^k_{X\alpha_{u_X}} &= {}^X_0N_I(X,Y)\ {}_0\Delta U^k_{X\alpha_{u_X}I} \quad I=1,2,\ldots M_n\\
{}_0\Delta u^k_{Y\alpha_{u_Y}} &= {}^Y_0N_I(X,Y)\ {}_0\Delta U^k_{Y\alpha_{u_Y}I} \quad I=1,2,\ldots M_n\\
{}_0\Delta u^k_{Z\alpha_{u_Z}} &= {}^Z_0N_I(X,Y)\ {}_0\Delta U^k_{Z\alpha_{u_Z}I} \quad I=1,2,\ldots M_n
\end{aligned}
\tag{3.49}
$$

where ${}^X_0N_I$, ${}^Y_0N_I$, and ${}^Z_0N_I$ are shape functions used for the displacements in the X, Y, and Z directions, respectively. Subscript I indicates the identity of the node (local numbering) and the summation convention is applied. M_n is the number of element nodes. As it is realized by inspection of Eq. 3.49, the formulation is formally independent of the type of finite element (i.e., quadrilater with 9 nodes or triangular with 15 nodes).

3.3 Finite element discretization and solution of the system

The linearized system of governing equations (see Eq. 3.46) is rewritten by using FEM and GUF notation (Eqs. 3.48 and 3.49). The resulting set of equations for a generic finite element is the following:

$$
\left({}^t_0\mathbf{K}_{\mathrm{L}} + {}^t_0\mathbf{K}_{\mathrm{NL+}} + {}^t_0\mathbf{K}_{\mathrm{SP}}\right)\,{}_0\Delta\mathbf{U} = \left({}^t_0\mathbf{K}_{\mathrm{T}} + {}^t_0\mathbf{K}_{\mathrm{SP}}\right)\,{}_0\Delta\mathbf{U} = {}^{t+\Delta t}_0\mathbf{F}_{\mathrm{EXT}} - {}^t_0\mathbf{F}_{\mathrm{INT}} - {}^t_0\mathbf{F}_{\mathrm{SP}}
\tag{3.50}
$$

where ${}^{t}_{0}\mathbf{K}_{\mathrm{L}}$, ${}^{t}_{0}\mathbf{K}_{\mathrm{NL}}$ are the linear and nonlinear parts of the *tangent stiffness matrix* ${}^{t}_{0}\mathbf{K}_{\mathrm{T}}$, respectively. The quantity ${}^{t+\Delta t}_{0}\mathbf{F}_{\mathrm{EXT}}$ is the external force vector and ${}^{t}_{0}\mathbf{F}_{\mathrm{INT}}$ represents the internal forces. ${}_{0}\Delta\mathbf{U}$ contains the unknown nodal displacements. In the GUF architecture different axiomatic theories and number of degrees of freedoms per finite element are allowed, so it is not generally possible to assemble the element stiffness and force arrays using the typical standard procedure (which usually involves transformations from local to global coordinate systems and then additions of portions of the stiffness matrices of the single elements to get the stiffness matrix at structural level). In the present approach as have been shown in the previous sections of this chapter the displacement compatibility of elements sharing the same node is imposed weakly by using the penalty method, which, from a physical perspective, could be interpreted as a set of distributed springs along the thickness. This compatibility imposition generates an additional stiffness matrix ${}^{t}_{0}\mathbf{K}_{\mathrm{SP}}$ and force vector ${}^{t}_{0}\mathbf{F}_{\mathrm{SP}}$. Box 3.51 show the connection between the weak form and the FEM arrays.

Linearized weak form for load stepping algorithm

$$
\begin{aligned}
&\underbrace{\int_{{}_0V} \delta\,{}_0\Delta e_{ij}\;{}_0C_{ijrs}\;{}_0\Delta e_{rs}\,\mathrm{d}\,{}_0V}_{\substack{\text{Stiffness matrix (linear)}\\ \delta\,{}_0\Delta\mathbf{U}\;{}^{t}_{0}\mathbf{K}_{\mathrm{L}}\;{}_0\Delta\mathbf{U}}} + \underbrace{\int_{{}_0V} \delta\,{}_0\Delta\eta_{ij}\;{}^{t}_{0}S_{ij}\,\mathrm{d}\,{}_0V}_{\substack{\text{Stiffness matrix (nonlinear)}\\ \delta\,{}_0\Delta\mathbf{U}\;{}^{t}_{0}\mathbf{K}_{\mathrm{NL}}\;{}_0\Delta\mathbf{U}}} + \underbrace{\int_{{}_0\Gamma_{g_i}} \delta\,{}_0\Delta u_i\psi_{ii}\;{}_0\Delta u_i\,\mathrm{d}\,{}_0\Gamma_{g_i}}_{\substack{\text{Spring stiffness (b.c.)}\\ \delta\,{}_0\Delta\mathbf{U}\;{}^{t}_{0}\mathbf{K}_{\mathrm{SP}}\;{}_0\Delta\mathbf{U}}} + \\
&\underbrace{\sum_i\sum_{f=1}^{n_f}\int_{\Gamma_f}\left(\delta\,{}_0\Delta u_{i\,\Gamma_{f(+)}} - \delta\,{}_0\Delta u_{i\,\Gamma_{f(-)}}\right)\gamma_{ii}\left({}_0\Delta u_{i\,\Gamma_{f(+)}} - {}_0\Delta u_{i\,\Gamma_{f(-)}}\right)\mathrm{d}\,{}_0\Gamma_f}_{\substack{\text{Spring stiffness (inter-element)}\\ \delta\,{}_0\Delta\mathbf{U}\;{}^{t}_{0}\mathbf{K}_{\mathrm{SP}}\;{}_0\Delta\mathbf{U}}} = \\
&= \underbrace{\int_{{}_0\Gamma_h}\delta\,{}_0\Delta u_i\;{}^{t+\Delta t}_{0}\hat{h}_i\,\mathrm{d}\,{}_0\Gamma_h + \int_{{}_0V}\delta u_i\mathcal{J}b_i\,\mathrm{d}\,{}_0V + \sum_p \delta\,{}_0\Delta u_{p_i}\;{}^{t+\Delta t}_{0}f_{p\,i}}_{\substack{\text{External forces}\\ \delta\,{}_0\Delta\mathbf{U}\;{}^{t+\Delta t}_{0}\mathbf{F}_{\mathrm{EXT}}}} - \underbrace{\int_{{}_0V}\delta\,{}_0\Delta e_{ij}\;{}^{t}_{0}S_{ij}\mathrm{d}\,{}_0V}_{\substack{\text{Internal forces}\\ \delta\,{}_0\Delta\mathbf{U}\;{}^{t}_{0}\mathbf{F}_{\mathrm{INT}}}} - \\
&\underbrace{\int_{{}_0\Gamma_{g_i}}\delta\,{}_0\Delta u_i\psi_{ii}\,{}^{t}_{0}u_i\mathrm{d}\,{}_0\Gamma_{g_i}}_{\substack{\text{Spring forces (b.c.)}\\ \delta\,{}_0\Delta\mathbf{U}\;{}^{t}_{0}\mathbf{F}_{\mathrm{SP}}}} + \underbrace{\int_{{}_0\Gamma_{g_i}}\delta\,{}_0\Delta u_i\psi_{ii}g_i\mathrm{d}\,{}_0\Gamma_{g_i}}_{\substack{\text{Spring forces (b.c. nonhomog.)}\\ \delta\,{}_0\Delta\mathbf{U}\;{}^{t}_{0}\mathbf{F}_{\mathrm{SP}}}} - \\
&\underbrace{\sum_i\sum_{f=1}^{n_f}\int_{\Gamma_f}\left(\delta\,{}_0\Delta u_{i\,\Gamma_{f(+)}} - \delta\,{}_0\Delta u_{i\,\Gamma_{f(-)}}\right)\gamma_{ii}\left({}^{t}_{0}u_{i\,\Gamma_{f(+)}} - {}^{t}_{0}u_{i\,\Gamma_{f(-)}}\right)\mathrm{d}\,{}_0\Gamma_f}_{\substack{\text{Spring forces (inter-element)}\\ \delta\,{}_0\Delta\mathbf{U}\;{}^{t}_{0}\mathbf{F}_{\mathrm{SP}}}}
\end{aligned}
\tag{3.51}
$$

The explicit expression of the finite element equation (see Eq. 3.50) is reported below:

$$\begin{bmatrix} {}^{t}_{0}\mathbf{K}_{\mathrm{T}\,u_X u_X} + {}^{t}_{0}\mathbf{K}_{\mathrm{SP}\,u_X u_X} & {}^{t}_{0}\mathbf{K}_{\mathrm{T}\,u_X u_Y} + {}^{t}_{0}\mathbf{K}_{\mathrm{SP}\,u_X u_Y} & {}^{t}_{0}\mathbf{K}_{\mathrm{T}\,u_X u_Z} + {}^{t}_{0}\mathbf{K}_{\mathrm{SP}\,u_X u_Z} \\ {}^{t}_{0}\mathbf{K}_{\mathrm{T}\,u_Y u_X} + {}^{t}_{0}\mathbf{K}_{\mathrm{SP}\,u_Y u_X} & {}^{t}_{0}\mathbf{K}_{\mathrm{T}\,u_Y u_Y} + {}^{t}_{0}\mathbf{K}_{\mathrm{SP}\,u_Y u_Y} & {}^{t}_{0}\mathbf{K}_{\mathrm{T}\,u_Y u_Z} + {}^{t}_{0}\mathbf{K}_{\mathrm{SP}\,u_Y u_Z} \\ {}^{t}_{0}\mathbf{K}_{\mathrm{T}\,u_Z u_X} + {}^{t}_{0}\mathbf{K}_{\mathrm{SP}\,u_Z u_X} & {}^{t}_{0}\mathbf{K}_{\mathrm{T}\,u_Z u_Y} + {}^{t}_{0}\mathbf{K}_{\mathrm{SP}\,u_Z u_X} & {}^{t}_{0}\mathbf{K}_{\mathrm{T}\,u_Z u_Z} + {}^{t}_{0}\mathbf{K}_{\mathrm{SP}\,u_Z u_X} \end{bmatrix} \begin{bmatrix} {}_{0}\Delta\mathbf{U}_X \\ {}_{0}\Delta\mathbf{U}_Y \\ {}_{0}\Delta\mathbf{U}_Z \end{bmatrix} = \begin{bmatrix} {}^{t+\Delta t}_{0}\mathbf{F}_{\mathrm{EXT}\,X} - {}^{t}_{0}\mathbf{F}_{\mathrm{INT}\,X} - {}^{t}_{0}\mathbf{F}_{\mathrm{SP}\,X} \\ {}^{t+\Delta t}_{0}\mathbf{F}_{\mathrm{EXT}\,Y} - {}^{t}_{0}\mathbf{F}_{\mathrm{INT}\,Y} - {}^{t}_{0}\mathbf{F}_{\mathrm{SP}\,Y} \\ {}^{t+\Delta t}_{0}\mathbf{F}_{\mathrm{EXT}\,Z} - {}^{t}_{0}\mathbf{F}_{\mathrm{INT}\,Z} - {}^{t}_{0}\mathbf{F}_{\mathrm{SP}\,Z} \end{bmatrix} \tag{3.52}$$

where, for example, it is

$${}_{0}\Delta\mathbf{U}_X = \left[{}_{0}\Delta\mathbf{U}^T_{X\,1} \cdots {}_{0}\Delta\mathbf{U}^T_{X\,I} \cdots {}_{0}\Delta\mathbf{U}^T_{X\,M_n} \right]^T \tag{3.53}$$

${}_{0}\Delta\mathbf{U}^T_{X\,I}$ is the vector containing the nodal displacements relative to node I of the element.

The system is solved iteratevely through Newton-Raphson iterations until a user-selected convergence criterium is satisfied. In the following paragraphs, the GUF kernels of each term of the discretized linearized system of equations will be derived for the first time.

3.3.1 Kernels of linear stiffness matrix

The linear stiffness matrix ${}^{t}_{0}\mathbf{K}_{\mathrm{L}}$ is built from the first term on the LHS of Eq. 3.46:

$${}^{t+\Delta t}_{0}\delta W^{\mathrm{ct}\,1}_{\mathrm{INT}} = \int_{{}_{0}V} \delta\, {}_{0}\Delta e_{ij}\, {}_{0}C_{ijrs}\, {}_{0}\Delta e_{rs} \mathrm{d}\, {}_{0}V \tag{3.54}$$

The array representation of the linear part ${}_{0}\Delta e_{ij}$ of the *GLST* (see Eq. 3.39) can be expressed in matrix form using Voigt notation:

$${}_{0}\Delta\mathbf{e} = {}^{t}_{0}\mathbf{L}\, {}_{0}\Delta\mathbf{u} \tag{3.55}$$

where the following definitions have been used:

$${}_{0}\Delta\mathbf{e} = [\, {}_{0}\Delta e_{XX} \quad {}_{0}\Delta e_{YY} \quad 2\,{}_{0}\Delta e_{XY} \quad 2\,{}_{0}\Delta e_{XZ} \quad 2\,{}_{0}\Delta e_{YZ} \quad {}_{0}\Delta e_{ZZ}]^T \tag{3.56}$$

$${}_{0}\Delta\mathbf{u} = [\, {}_{0}\Delta u_X \quad {}_{0}\Delta u_Y \quad {}_{0}\Delta u_Z]^T \tag{3.57}$$

$$
{}^{t}_{0}\mathbf{L} = \begin{bmatrix}
{}^{t}_{0}G_{XX}\,{}_{0}\partial_X & {}^{t}_{0}G_{YX}\,{}_{0}\partial_X & {}^{t}_{0}G_{ZX}\,{}_{0}\partial_X \\
{}^{t}_{0}G_{XY}\,{}_{0}\partial_Y & {}^{t}_{0}G_{YY}\,{}_{0}\partial_Y & {}^{t}_{0}G_{ZY}\,{}_{0}\partial_Y \\
{}^{t}_{0}G_{XX}\,{}_{0}\partial_Y + G_{XY}\,{}_{0}\partial_X & {}^{t}_{0}G_{YX}\,{}_{0}\partial_Y + G_{YY}\,{}_{0}\partial_X & {}^{t}_{0}G_{ZX}\,{}_{0}\partial_Y + {}^{t}_{0}G_{ZY}\,{}_{0}\partial_X \\
{}^{t}_{0}G_{XZ}\,{}_{0}\partial_X + G_{XX}\,{}_{0}\partial_Z & {}^{t}_{0}G_{YZ}\,{}_{0}\partial_X + G_{YX}\,{}_{0}\partial_Z & {}^{t}_{0}G_{ZZ}\,{}_{0}\partial_X + {}^{t}_{0}G_{ZX}\,{}_{0}\partial_Z \\
{}^{t}_{0}G_{XY}\,{}_{0}\partial_Z + G_{XZ}\,{}_{0}\partial_Y & {}^{t}_{0}G_{YY}\,{}_{0}\partial_Z + G_{YZ}\,{}_{0}\partial_Y & {}^{t}_{0}G_{ZY}\,{}_{0}\partial_Z + {}^{t}_{0}G_{ZZ}\,{}_{0}\partial_Y \\
{}^{t}_{0}G_{XZ}\,{}_{0}\partial_Z & {}^{t}_{0}G_{YZ}\,{}_{0}\partial_Z & {}^{t}_{0}G_{ZZ}\,{}_{0}\partial_Z
\end{bmatrix} \tag{3.58}
$$

The expression for the deformation gradient within the GUF formalism can be found in Appendix C. The displacement increments can be expressed as a function of the nodal displacements of the element. Thus, the strains can be expressed as a function of the unknowns (at finite element level) as follows:

$$
{}_{0}\Delta\mathbf{e} = {}^{t}_{0}\mathbf{B}_{\mathrm{L}}\,{}_{0}\Delta\mathbf{U} \tag{3.59}
$$

where

$$
{}_{0}\Delta\mathbf{U} = \left[\ {}_{0}\Delta\mathbf{U}_1^T \quad \ldots \quad {}_{0}\Delta\mathbf{U}_J^T \quad \ldots \quad {}_{0}\Delta\mathbf{U}_{M_n}^T\ \right]^T \tag{3.60}
$$

$$
{}^{t}_{0}\mathbf{B}_{\mathrm{L}} = \left[\ {}^{t}_{0}\mathbf{B}_L^1 \quad \ldots \quad {}^{t}_{0}\mathbf{B}_L^J \quad \ldots \quad {}^{t}_{0}\mathbf{B}_L^{M_n}\ \right] \tag{3.61}
$$

The index $J = 1, \ldots, M_n$ is the identity of the local element node.

Introducing the GUF notation (see Eqs. 3.48 and 3.49) we can rewrite ${}_{0}\Delta\mathbf{e}$ (see Eq. 3.55) for an element as follows:

$$
{}_{0}\Delta\mathbf{e} = {}^{t}_{0}\mathbf{B}_{\mathrm{L}}^{J}\,{}_{0}\Delta\mathbf{U}_J = \begin{bmatrix}
{}^{t}_{0}B_{L\,11}^{\beta_{u_X} J} & {}^{t}_{0}B_{L\,12}^{\beta_{u_Y} J} & {}^{t}_{0}B_{L\,13}^{\beta_{u_Z} J} \\
{}^{t}_{0}B_{L\,21}^{\beta_{u_X} J} & {}^{t}_{0}B_{L\,22}^{\beta_{u_Y} J} & {}^{t}_{0}B_{L\,23}^{\beta_{u_Z} J} \\
{}^{t}_{0}B_{L\,31}^{\beta_{u_X} J} & {}^{t}_{0}B_{L\,32}^{\beta_{u_Y} J} & {}^{t}_{0}B_{L\,33}^{\beta_{u_Z} J} \\
{}^{t}_{0}B_{L\,41}^{\beta_{u_X} J} & {}^{t}_{0}B_{L\,42}^{\beta_{u_Y} J} & {}^{t}_{0}B_{L\,43}^{\beta_{u_Z} J} \\
{}^{t}_{0}B_{L\,51}^{\beta_{u_X} J} & {}^{t}_{0}B_{L\,52}^{\beta_{u_Y} J} & {}^{t}_{0}B_{L\,53}^{\beta_{u_Z} J} \\
{}^{t}_{0}B_{L\,61}^{\beta_{u_X} J} & {}^{t}_{0}B_{L\,62}^{\beta_{u_Y} J} & {}^{t}_{0}B_{L\,63}^{\beta_{u_Z} J}
\end{bmatrix}
\begin{bmatrix}
{}_{0}\Delta U_{X\beta_{u_X} J} \\
{}_{0}\Delta U_{Y\beta_{u_Y} J} \\
{}_{0}\Delta U_{Z\beta_{u_Z} J}
\end{bmatrix} \tag{3.62}
$$

The components of the GUF *linear strain-displacement matrix* ${}^{t}_{0}\mathbf{B}_L^J$ are defined in D. ${}^{t}_{0}\mathbf{B}_L^J$ is conveniently

written in a more compact form, as reported below:

$$ {}^{t}_{0}\mathbf{B}^{J}_{\mathrm{L}} = \left[\begin{array}{ccc} {}^{t}_{0}\mathbf{B}^{\beta_{u_X}\,J}_{\mathrm{L}\,1} & {}^{t}_{0}\mathbf{B}^{\beta_{u_Y}\,J}_{\mathrm{L}\,2} & {}^{t}_{0}\mathbf{B}^{\beta_{u_Z}\,J}_{\mathrm{L}\,3} \end{array} \right] \tag{3.63} $$

where the following definitions are used:

$$ {}^{t}_{0}\mathbf{B}^{\beta_{u_X}\,J}_{\mathrm{L}\,q} = [\, {}^{t}_{0}B^{\beta_{u_X}\,J}_{L\,1q} \;\; {}^{t}_{0}B^{\beta_{u_X}\,J}_{L\,2q} \;\; {}^{t}_{0}B^{\beta_{u_X}\,J}_{L\,3q} \;\; {}^{t}_{0}B^{\beta_{u_X}\,J}_{L\,4q} \;\; {}^{t}_{0}B^{\beta_{u_X}\,J}_{L\,5q} \;\; {}^{t}_{0}B^{\beta_{u_X}\,J}_{L\,6q} \,]^{T} \quad q = 1, 2, 3 \tag{3.64} $$

The linear part ${}_{0}\mathbf{\Delta e}$ of the incremental strains (see Eq. 3.62) are explicitly written by the means of Eq. 3.63 and explicitly indicating the nodal contributions:

$$ {}_{0}\mathbf{\Delta e} = {}^{t}_{0}\mathbf{B}^{J}_{L}\;{}_{0}\mathbf{\Delta U}_{J} = \left[{}^{t}_{0}\mathbf{B}^{\beta_{u_X}\,J}_{L\,1} \;\; {}^{t}_{0}\mathbf{B}^{\beta_{u_Y}\,J}_{L\,2} \;\; {}^{t}_{0}\mathbf{B}^{\beta_{u_Z}\,J}_{L\,3} \right] \left[\begin{array}{c} {}_{0}\Delta U_{X\beta_{u_X}\,J} \\ {}_{0}\Delta U_{Y\beta_{u_Y}\,J} \\ {}_{0}\Delta U_{Z\beta_{u_Z}\,J} \end{array} \right] \tag{3.65} $$

Next, the linear stiffness matrix contribution is obtained. To reach that goal, Eq. 3.54 can be rewritten through Eq. 3.59 in the following form:

$$ {}^{t+\Delta t}_{0}\delta W^{\mathrm{ct}\;1}_{\mathrm{INT}} = \delta\,{}_{0}\mathbf{\Delta U}^{T}_{I} \left(\int_{{}_{0}V} {}^{t}_{0}\mathbf{B}^{I\;T}_{L}\;\tilde{\mathbf{C}}\;{}^{t}_{0}\mathbf{B}^{J}_{L}\,\mathrm{d}\,{}_{0}V \right) {}_{0}\mathbf{\Delta U}_{J} = \delta\,{}_{0}\mathbf{\Delta U}^{T}_{I}\;{}^{t}_{0}\mathbf{K}^{IJ}_{L}\;{}_{0}\mathbf{\Delta U}_{J} \tag{3.66} $$

where the *linear stiffness matrix* has been defined as

$$ {}^{t}_{0}\mathbf{K}^{IJ}_{L} = \int_{{}_{0}V} {}^{t}_{0}\mathbf{B}^{I\;T}_{L}\;\tilde{\mathbf{C}}\;{}^{t}_{0}\mathbf{B}^{J}_{L}\,\mathrm{d}\,{}_{0}V \tag{3.67} $$

Examples of *kernels of the linear stiffness matrix* are reported below:

$$ {}^{t}_{0}K^{\alpha_{u_X}\beta_{u_X}\,IJ}_{\mathrm{L}\,u_X u_X} = \int_{{}_{0}V} {}^{t}_{0}\mathbf{B}^{\alpha_{u_X}\,I\;T}_{\mathrm{L}\,1}\;\tilde{\mathbf{C}}\;{}^{t}_{0}\mathbf{B}^{\beta_{u_X}\,J}_{L\,1}\,\mathrm{d}\,{}_{0}V \tag{3.68} $$

$$ {}^{t}_{0}K^{\alpha_{u_X}\beta_{u_Z}\,IJ}_{\mathrm{L}\,u_Y u_Z} = \int_{{}_{0}V} {}^{t}_{0}\mathbf{B}^{\alpha_{u_Y}\,I\;T}_{L\,2}\;\tilde{\mathbf{C}}\;{}^{t}_{0}\mathbf{B}^{\beta_{u_Z}\,J}_{L\,3}\,\mathrm{d}\,{}_{0}V \tag{3.69} $$

The explicit details and examples of fully expanded kernels are discussed in E.

3.3.2 Kernels of the nonlinear stiffness matrix

The nonlinear stiffness matrix ${}^{t}_{0}\mathbf{K}_{\mathrm{NL}}$ is obtained from ${}^{t+\Delta t}_{0}\delta W^{\mathrm{ct}\,2}_{\mathrm{INT}}$ (see its definition in Eq. 3.47):

$$ {}^{t+\Delta t}_{0}\delta W^{\mathrm{ct}\,2}_{\mathrm{INT}} = \int_{{}_0V} \delta\, {}_0\Delta\eta_{ij}\, {}^{t}_{0}S_{ij}\, \mathrm{d}\, {}_0V \tag{3.70} $$

Using Eq. 3.40 for the definition of ${}_0\Delta\eta_{ij}$, it is possible to obtain the following relation:

$$ {}^{t+\Delta t}_{0}\delta W^{\mathrm{ct}\,2}_{\mathrm{INT}} = \int_{{}_0V} \delta\, {}_0\Delta u_{k,i}\, {}^{t}_{0}S_{ij}\, {}_0\Delta u_{k,j}\, \mathrm{d}\, {}_0V \tag{3.71} $$

Introducing the GUF relations (see Eqs. 3.48 and 3.49), it can be shown that Eq. 3.71 leads to the stiffness matrix at nodal level. The matrix relating nodes I and J is:

$$ {}^{t}_{0}\mathbf{K}^{IJ}_{\mathrm{NL}} = \int_{{}_0V} {}_0\mathbf{B}^{I\,T}_{NL}\ {}^{t}_{0}\boldsymbol{\tau}\ {}_0\mathbf{B}^{J}_{NL}\, \mathrm{d}\, {}_0V \tag{3.72} $$

where

$$ {}_0\mathbf{B}^{J}_{\mathrm{NL}} = \begin{bmatrix} {}^{X}_{0}F_{\beta_{u_X}} & {}^{X}_{0}N_{J,X} & 0 & 0 \\ {}^{X}_{0}F_{\beta_{u_X}} & {}^{X}_{0}N_{J,Y} & 0 & 0 \\ {}^{X}_{0}F_{\beta_{u_{X,Z}}} & {}^{X}_{0}N_{J} & 0 & 0 \\ 0 & {}^{Y}_{0}F_{\beta_{u_Y}} & {}^{Y}_{0}N_{J,X} & 0 \\ 0 & {}^{Y}_{0}F_{\beta_{u_Y}} & {}^{Y}_{0}N_{J,Y} & 0 \\ 0 & {}^{Y}_{0}F_{\beta_{u_{Y,Z}}} & {}^{Y}_{0}N_{J} & 0 \\ 0 & 0 & {}^{Z}_{0}F_{\beta_{u_Z}} & {}^{Z}_{0}N_{J,X} \\ 0 & 0 & {}^{Z}_{0}F_{\beta_{u_Z}} & {}^{Z}_{0}N_{J,Y} \\ 0 & 0 & {}^{Z}_{0}F_{\beta_{u_{Z,Z}}} & {}^{Z}_{0}N_{J} \end{bmatrix} \tag{3.73} $$

and

$$ {}^{t}_{0}\boldsymbol{\tau} = \begin{bmatrix} {}^{t}_{0}\mathbf{S} & \mathbf{0} & \mathbf{0} \\ \mathbf{0} & {}^{t}_{0}\mathbf{S} & \mathbf{0} \\ \mathbf{0} & \mathbf{0} & {}^{t}_{0}\mathbf{S} \end{bmatrix} \tag{3.74} $$

The kernels of the nonlinear stiffness matrix can be expressed in compact form introducing the following notation for the nonlinear strain-displacement matrix:

$$ {}_0\mathbf{B}^J_{\mathrm{NL}} = \begin{bmatrix} {}_0\mathbf{T}_X^{\beta_{u_X}\,J} & \mathbf{0} & \mathbf{0} \\ \mathbf{0} & {}_0\mathbf{T}_Y^{\beta_{u_Y}\,J} & \mathbf{0} \\ \mathbf{0} & \mathbf{0} & {}_0\mathbf{T}_Z^{\beta_{u_Z}\,J} \end{bmatrix} \tag{3.75} $$

where

$$ \begin{aligned} {}_0\mathbf{T}_X^{\beta_{u_X}\,J} &= [\ {}^X_0F_{\beta_{u_X}}\ {}^X_0N_{J,X} \qquad {}^X_0F_{\beta_{u_X}}\ {}^X_0N_{J,Y} \qquad {}^X_0F_{\beta_{u_{X,Z}}}\ {}^X_0N_J\ ]^T \\ {}_0\mathbf{T}_Y^{\beta_{u_Y}\,J} &= [\ {}^Y_0F_{\beta_{u_Y}}\ {}^Y_0N_{J,X} \qquad {}^Y_0F_{\beta_{u_Y}}\ {}^Y_0N_{J,Y} \qquad {}^Y_0F_{\beta_{u_{Y,Z}}}\ {}^Y_0N_J\ ]^T \\ {}_0\mathbf{T}_Z^{\beta_{u_Z}\,J} &= [\ {}^Z_0F_{\beta_{u_Z}}\ {}^Z_0N_{J,X} \qquad {}^Z_0F_{\beta_{u_Z}}\ {}^Z_0N_{J,Y} \qquad {}^Z_0F_{\beta_{u_{Z,Z}}}\ {}^Z_0N_J\ ]^T \end{aligned} \tag{3.76} $$

Using Eqs. 3.72-3.76, it is deduced that the the nonzero kernels generating the nonlinear stiffness matrix are the following:

$$ {}^t_0K^{\alpha_{u_X}\beta_{u_X}\,IJ}_{\mathrm{NL}\,u_X u_X} = \int_{{}_0V} {}_0\mathbf{T}_X^{\alpha_{u_X}\,I\,T}\ {}^t_0\mathbf{S}\ {}_0\mathbf{T}_X^{\beta_{u_X}\,J}\ \mathrm{d}\,{}_0V \tag{3.77} $$

$$ {}^t_0K^{\alpha_{u_Y}\beta_{u_Y}\,IJ}_{\mathrm{NL}\,u_Y u_Y} = \int_{{}_0V} {}_0\mathbf{T}_Y^{\alpha_{u_Y}\,I\,T}\ {}^t_0\mathbf{S}\ {}_0\mathbf{T}_Y^{\beta_{u_Y}\,J}\ \mathrm{d}\,{}_0V \tag{3.78} $$

$$ {}^t_0K^{\alpha_{u_Z}\beta_{u_Z}\,IJ}_{\mathrm{NL}\,u_Z u_Z} = \int_{{}_0V} {}_0\mathbf{T}_Z^{\alpha_{u_Z}\,I\,T}\ {}^t_0\mathbf{S}\ {}_0\mathbf{T}_Z^{\beta_{u_Z}\,J}\ \mathrm{d}\,{}_0V \tag{3.79} $$

3.3.3 Internal forces

The unbalanced load is the difference between the vector of external forces and the array containing the internal forces. In this section how to determine the internal forces is discussed.

The internal force vector generates from ${}^{t+\Delta t}_0\delta W^{\mathrm{ct}\ 3}_{\mathrm{INT}}$ (see Eq. 3.47):

$$ {}^{t+\Delta t}_0\delta W^{\mathrm{ct}\ 3}_{\mathrm{INT}} = \int_{{}_0V} \delta\,{}_0\Delta e_{ij}\ {}^t_0S_{ij}\ \mathrm{d}\,{}_0V \tag{3.80} $$

here the $SPKST$ is known and the variation of the linear part of the $GLST$ can be expressed in matrix form (see Eq. 3.65) to obtain at finite element level an expression involving the internal forces:

$$ \int_{{}_0V} \delta\,{}_0\Delta\mathbf{e}\ {}^t_0\mathbf{S}\ \mathrm{d}\,{}_0V = \delta\,{}_0\Delta\mathbf{U}^T\ {}^t_0\mathbf{F}_{\mathrm{INT}} \tag{3.81} $$

where the internal force array ${}^{t}_{0}\mathbf{F}_{\mathrm{INT}}$ is partitioned to separate the contributions of each finite element node as follows:

$$ {}^{t}_{0}\mathbf{F}_{\mathrm{INT}} = [{}^{t}_{0}\mathbf{F}^{T}_{\mathrm{INT}\,1} \cdots {}^{t}_{0}\mathbf{F}^{T}_{\mathrm{INT}\,I} \cdots {}^{t}_{0}\mathbf{F}^{T}_{\mathrm{INT}\,M_n}]^{T} \tag{3.82} $$

The force array at nodal level has the expression reported below:

$$ {}^{t}_{0}\mathbf{F}_{\mathrm{INT}\,I} = \int_{{}_0V} {}^{t}_{0}\mathbf{B}^{I\,T}_{L}\ {}^{t}_{0}\mathbf{S}\ \mathrm{d}\,{}_0V \tag{3.83} $$

where ${}^{t}_{0}\mathbf{B}^{I}_{L}$ can be deduced from equations 3.63 and 3.64.

3.3.4 External forces

The external force vector due to the surface traction and point loads is derived from the external virtual work ${}^{t+\Delta t}_{0}\delta W_{\mathrm{EXT}}$ appearing in Eq. 3.47:

$$ {}^{t+\Delta t}_{0}\delta W_{\mathrm{EXT}} = {}^{t+\Delta t}_{0}\delta W^{\mathrm{ct}\,1}_{\mathrm{EXT}} + {}^{t+\Delta t}_{0}\delta W^{\mathrm{ct}\,2}_{\mathrm{EXT}} + {}^{t+\Delta t}_{0}\delta W^{\mathrm{ct}\,3}_{\mathrm{EXT}} \tag{3.84} $$

where

$$ \begin{aligned} {}^{t+\Delta t}_{0}\delta W^{\mathrm{ct}\,1}_{\mathrm{EXT}} &= \int_{{}_0\Gamma_h} \delta\,{}_0\Delta u_i\ {}^{t+\Delta t}_{0}\hat{h}_i\,\mathrm{d}\,{}_0A \\ {}^{t+\Delta t}_{0}\delta W^{\mathrm{ct}\,2}_{\mathrm{EXT}} &= \sum_{p} \delta\,{}_0\Delta u_i\,{}^{t+\Delta t}_{0}f_{p\,i} \\ {}^{t+\Delta t}_{0}\delta W^{\mathrm{ct}\,3}_{\mathrm{EXT}} &= \int_{{}_0V} \delta u_i \mathcal{J} b_i \mathrm{d}\,{}_0V \end{aligned} \tag{3.85} $$

Distributed surface loads and concentrated forces are taken into account by ${}^{t+\Delta t}_{0}\delta W^{\mathrm{ct}\,1}_{\mathrm{EXT}}$ and ${}^{t+\Delta t}_{0}\delta W^{\mathrm{ct}\,2}_{\mathrm{EXT}}$, respectively. The body forces are not considered in this dissertation. Moreover the load stiffness correction matrix has been neglected.

Concentrated Loads

The case of structure subjected to concentrated loads is now analyzed. In this formulation the types of theories and orders of expansion are in general different if different finite elements are considered. This requires a special attention in the formulation of the concentrated loads, since the finite element quantities need to be referred to a local element coordinate system. The methodology adopted here to write the finite element equations is a TLF. This means that the integrals and geometry transformations are evaluated at the initial geometry. So far we indicated with X, Y, Z the coordinates of a generic point *at element level* in the undeformed continuum. We need now to introduce (see Figure 3.3) the coordinates $\mathcal{X}$, $\mathcal{Y}$, and $\mathcal{Z}$ which

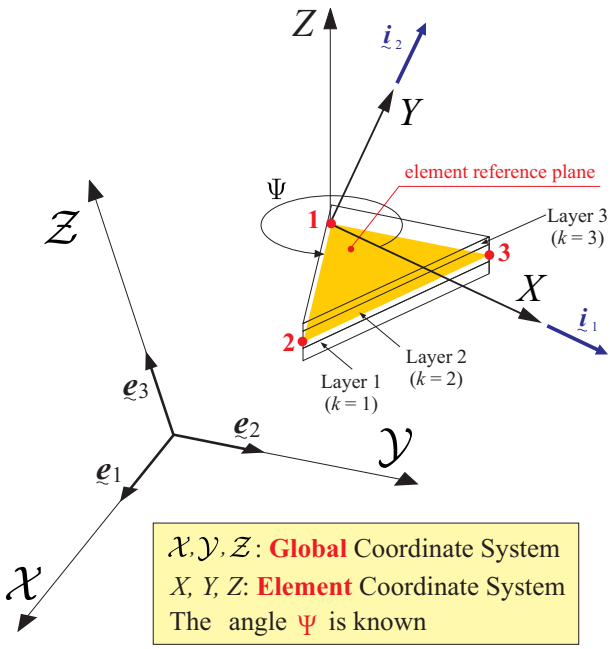

Figure 3.3: Global and local coordinate systems (undeformed geometry) [98].

identify the initial position of that point but referred to a global coordinate frame (i.e., the frame is the same for the entire structure made of a collection of finite elements).

Let now ${}^{0}_{0}a^{k}_{ij}$ be the generic coefficient of the transformation matrix that relates the *global* to *local* coordinate systems (centered on node 1 in the local numbering of the element, see Fig. 3.3) at layer level in the *undeformed configuration*. For example, it is

$$ {}^{0}_{0}a^{k}_{12} = {}^{0}_{0}\underset{\sim}{i}^{k}_{1} \bullet \underset{\sim}{e}_2 = {}^{0}_{0}\underset{\sim}{i}_{1} \bullet \underset{\sim}{e}_2 = {}^{0}_{0}a_{12} \tag{3.86} $$

where ${}^{0}_{0}\underset{\sim}{i}_{1}$ is the unit vector in the local X direction and $\underset{\sim}{e}_2$ is the unit vector in the global $\mathcal{Y}$ direction.

Consider now a force applied to a position defined by local coordinates X, Y, and Z^k (it is now necessary to identify the layer in which the force is applied to properly calculate the equivalent forces) on a triangular finite element. The algorithm usually employed to solve the nonlinear equations adopts the concept of load step to gradually apply the external loads to the structure. Thus, to take into account this fact, concentrated forces are written as products between a load factor ${}^{t+\Delta t}\lambda$ and nominal load which has components ${}_{0}f^{k}_{p\mathcal{X}}$, ${}_{0}f^{k}_{p\mathcal{Y}}$, and ${}_{0}f^{k}_{p\mathcal{Z}}$ in the *global* coordinate system (undeformed state). For simplicity it is shown the case in which the loads are not "follower" forces. That is, the directions and magnitudes do not change while the structure deforms. The first operation is to express the force by using the local coordinate

system on the element. This is easily achieved by setting

$$\begin{aligned}
{}^{t+\Delta t}_{0}f^{k}_{X} &= {}^{t+\Delta t}\lambda\left({}^{0}_{0}a^{k}_{11}\,{}_{0}f^{k}_{\mathcal{X}} + {}^{0}_{0}a^{k}_{12}\,{}_{0}f^{k}_{\mathcal{Y}} + {}^{0}_{0}a^{k}_{13}\,{}_{0}f^{k}_{\mathcal{Z}}\right)\\
{}^{t+\Delta t}_{0}f^{k}_{Y} &= {}^{t+\Delta t}\lambda\left({}^{0}_{0}a^{k}_{21}\,{}_{0}f^{k}_{\mathcal{X}} + {}^{0}_{0}a^{k}_{22}\,{}_{0}f^{k}_{\mathcal{Y}} + {}^{0}_{0}a^{k}_{23}\,{}_{0}f^{k}_{\mathcal{Z}}\right)\\
{}^{t+\Delta t}_{0}f^{k}_{Z} &= {}^{t+\Delta t}\lambda\left({}^{0}_{0}a^{k}_{31}\,{}_{0}f^{k}_{\mathcal{X}} + {}^{0}_{0}a^{k}_{32}\,{}_{0}f^{k}_{\mathcal{Y}} + {}^{0}_{0}a^{k}_{33}\,{}_{0}f^{k}_{\mathcal{Z}}\right)
\end{aligned} \tag{3.87}$$

Since the coordinate transformations of Eq. 3.87 are done in the undeformed configuration, the related matrices are computed only once at the beginning of the simulation (this would not be true in a corotational [99–101] approach). Now the nodal forces (not yet expressed consistently to the actual degrees of freedom at this stage) can be found by using an energetic approach based on the concept of the virtual work of the applied generic force, as reported below:

$$\begin{aligned}
{}^{t+\Delta t}_{0}\delta W^{\mathrm{ct}\ 2}_{\mathrm{EXT}} = {}&{}^{t+\Delta t}_{0}f^{k}_{X}\left(X,Y,Z^{k}\right)\ \delta\,{}_{0}\Delta u^{k}_{X}\left(X,Y,Z^{k}\right) +\\
&{}^{t+\Delta t}_{0}f^{k}_{Y}\left(X,Y,Z^{k}\right)\ \delta\,{}_{0}\Delta u^{k}_{Y}\left(X,Y,Z^{k}\right) +\\
&{}^{t+\Delta t}_{0}f^{k}_{Z}\left(X,Y,Z^{k}\right)\ \delta\,{}_{0}\Delta u^{k}_{Z}\left(X,Y,Z^{k}\right)
\end{aligned} \tag{3.88}$$

The finite element discretization and GUF expansion imply the writing reported below:

$$\begin{aligned}
{}_{0}\Delta u^{k}_{X}\left(X,Y,Z^{k}\right) &= {}^{X}_{0}F^{k}_{\alpha_{u_X}}\left(Z^{k}\right)\ {}_{0}\Delta u^{k}_{X\alpha_{u_X}}\left(X,Y\right)\\
&= {}^{X}_{0}N_{I}\left(X,Y\right)\ {}^{X}_{0}F^{k}_{\alpha_{u_X}}\left(Z^{k}\right)\ {}_{0}\Delta U^{k}_{X\alpha_{u_X}\,I}
\end{aligned} \tag{3.89}$$

thus,

$$\delta\,{}_{0}\Delta u^{k}_{X}\left(X,Y,Z^{k}\right) = {}^{X}_{0}N_{I}\left(X,Y\right)\ {}^{X}_{0}F^{k}_{\alpha_{u_X}}\left(Z^{k}\right)\ \delta\,{}_{0}\Delta U^{k}_{X\alpha_{u_X}\,I} \tag{3.90}$$

similar expressions can be obtained for the other virtual displacements:

$$\delta\,{}_{0}\Delta u^{k}_{Y}\left(X,Y,Z^{k}\right) = {}^{Y}_{0}N_{I}\left(X,Y\right)\ {}^{Y}_{0}F^{k}_{\alpha_{u_Y}}\left(Z^{k}\right)\ \delta\,{}_{0}\Delta U^{k}_{Y\alpha_{u_Y}\,I} \tag{3.91}$$

$$\delta\,{}_{0}\Delta u^{k}_{Z}\left(X,Y,Z^{k}\right) = {}^{Z}_{0}N_{I}\left(X,Y\right)\ {}^{Z}_{0}F^{k}_{\alpha_{u_Z}}\left(Z^{k}\right)\ \delta\,{}_{0}\Delta U^{k}_{Z\alpha_{u_Z}\,I} \tag{3.92}$$

Substituting Eqs. 3.90, 3.91, and 3.92 into the expression of the external concentrated force virtual work

(see Eq. (3.88)) the obtained result is the following:

$$
\begin{aligned}
{}^{t+\Delta t}_{0}\delta W^{\text{ct 2}}_{\text{EXT}} = {}& {}^{t+\Delta t}_{0}f^{k}_{X} \;\; {}^{X}_{0}N_{I} \;\; {}^{X}_{0}F^{k}_{\alpha_{u_X}} \;\; \delta\,{}_{0}\Delta U^{k}_{X\alpha_{u_X}\,I} \\
& + {}^{t+\Delta t}_{0}f^{k}_{Y} \;\; {}^{Y}_{0}N_{I} \;\; {}^{Y}_{0}F^{k}_{\alpha_{u_Y}} \;\; \delta\,{}_{0}\Delta U^{k}_{Y\alpha_{u_Y}\,I} \\
& + {}^{t+\Delta t}_{0}f^{k}_{Z} \;\; {}^{Z}_{0}N_{I} \;\; {}^{Z}_{0}F^{k}_{\alpha_{u_Z}} \;\; \delta\,{}_{0}\Delta U^{k}_{Z\alpha_{u_Z}\,I}
\end{aligned}
\tag{3.93}
$$

An alternative expression for the virtual work produced by the external load can be written in terms of *finite element equivalent forces* as reported below:

$$
\begin{aligned}
{}^{t+\Delta t}_{0}\delta W^{\text{ct 2}}_{\text{EXT}} = {}& {}^{t+\Delta t}_{0}f^{k}_{x\alpha_{u_X}\,I} \;\; \delta\,{}_{0}\Delta U^{k}_{X\alpha_{u_X}\,I} + {}^{t+\Delta t}_{0}f^{k}_{Y\alpha_{u_Y}\,I} \;\; \delta\,{}_{0}\Delta U^{k}_{Y\alpha_{u_Y}\,I} \\
& + {}^{t+\Delta t}_{0}f^{k}_{Z\alpha_{u_Z}\,I} \;\; \delta\,{}_{0}\Delta U^{k}_{Z\alpha_{u_Z}\,I}
\end{aligned}
\tag{3.94}
$$

Direct comparison of Eqs. 3.93 and 3.94 leads to the nodal forces written in a form consistent with the actual degrees of freedom:

$$
\begin{aligned}
{}^{t+\Delta t}_{0}f^{k}_{X\alpha_{u_X}\,I} &= {}^{t+\Delta t}_{0}f^{k}_{X} \;\; {}^{X}_{0}N_{I} \;\; {}^{X}_{0}F^{k}_{\alpha_{u_X}} \\
{}^{t+\Delta t}_{0}f^{k}_{Y\alpha_{u_Y}\,I} &= {}^{t+\Delta t}_{0}f^{k}_{Y} \;\; {}^{Y}_{0}N_{I} \;\; {}^{Y}_{0}F^{k}_{\alpha_{u_Y}} \\
{}^{t+\Delta t}_{0}f^{k}_{Z\alpha_{u_Z}\,I} &= {}^{t+\Delta t}_{0}f^{k}_{Z} \;\; {}^{Z}_{0}N_{I} \;\; {}^{Z}_{0}F^{k}_{\alpha_{u_Z}}
\end{aligned}
\tag{3.95}
$$

The local forces expressed as a function of the global components (see Eq. 3.87) can be substituted into Eq. 3.95. The result is the represented by the finite element consistent nodal forces:

$$
\begin{aligned}
{}^{t+\Delta t}_{0}f^{k}_{X\alpha_{u_X}\,I} &= {}^{t+\Delta t}\lambda \left({}^{0}_{0}a^{k}_{11}\,{}_{0}f^{k}_{\mathcal{X}} + {}^{0}_{0}a^{k}_{12}\,{}_{0}f^{k}_{\mathcal{Y}} + {}^{0}_{0}a^{k}_{13}\,{}_{0}f^{k}_{\mathcal{Z}} \right) \; {}^{X}_{0}N_{I} \; {}^{x}_{0}F^{k}_{\alpha_{u_X}} \\
{}^{t+\Delta t}_{0}f^{k}_{Y\alpha_{u_Y}\,I} &= {}^{t+\Delta t}\lambda \left({}^{0}_{0}a^{k}_{21}\,{}_{0}f^{k}_{\mathcal{X}} + {}^{0}_{0}a^{k}_{22}\,{}_{0}f^{k}_{\mathcal{Y}} + {}^{0}_{0}a^{k}_{23}\,{}_{0}f^{k}_{\mathcal{Z}} \right) \; {}^{Y}_{0}N_{I} \; {}^{y}_{0}F^{k}_{\alpha_{u_Y}} \\
{}^{t+\Delta t}_{0}f^{k}_{Z\alpha_{u_Z}\,I} &= {}^{t+\Delta t}\lambda \left({}^{0}_{0}a^{k}_{31}\,{}_{0}f^{k}_{\mathcal{X}} + {}^{0}_{0}a^{k}_{32}\,{}_{0}f^{k}_{\mathcal{Y}} + {}^{0}_{0}a^{k}_{33}\,{}_{0}f^{k}_{\mathcal{Z}} \right) \; {}^{Z}_{0}N_{I} \; {}^{z}_{0}F^{k}_{\alpha_{u_Z}}
\end{aligned}
\tag{3.96}
$$

Expansion of the indices of Eq. 3.96 and assembling in the thickness direction lead to the nodal forces equivalent to the external loadings.

Distributed load

Now we consider the case we have an arbitrary load distribution ${}^{t+\Delta t}_{0}\hat{h}(X,Y)$ applied on the surface (Z^k) of the layer of an element. This load distribution can have a component normal to the surface (pressure) and a tangential component (shear).

The surface forces are written as products between a load factor ${}^{t+\Delta t}\lambda$ and nominal load which has components $\hat{h}_{\mathcal{X}}, \hat{h}_{\mathcal{Y}}$, and $\hat{h}_{\mathcal{Z}}$ in the global coordinate system.

The force is expressed in the local coordinate system of the element at time step $t+\Delta t$ as follow:

$$\begin{aligned}
{}^{t+\Delta t}_{0}\hat{h}_X &= {}^{t+\Delta t}\lambda \left({}^{0}_{0}a^k_{11}\hat{h}_{\mathcal{X}} + {}^{0}_{0}a^k_{12}\hat{h}_{\mathcal{Y}} + {}^{0}_{0}a^k_{13}\hat{h}_{\mathcal{Z}} \right) \\
{}^{t+\Delta t}_{0}\hat{h}_Y &= {}^{t+\Delta t}\lambda \left({}^{0}_{0}a^k_{21}\hat{h}_{\mathcal{X}} + {}^{0}_{0}a^k_{22}\hat{h}_{\mathcal{Y}} + {}^{0}_{0}a^k_{23}\hat{h}_{\mathcal{Z}} \right) \\
{}^{t+\Delta t}_{0}\hat{h}_Z &= {}^{t+\Delta t}\lambda \left({}^{0}_{0}a^k_{31}\hat{h}_{\mathcal{X}} + {}^{0}_{0}a^k_{32}\hat{h}_{\mathcal{Y}} + {}^{0}_{0}a^k_{33}\hat{h}_{\mathcal{Z}} \right)
\end{aligned} \tag{3.97}$$

The external work contribution (see Eq. 3.85) is:

$$\begin{aligned}
{}^{t+\Delta t}_{0}\delta W^{ct\,1}_{\mathrm{EXT}} &= \int_{{}_0\Gamma_h} \delta\, {}_0\Delta\mathbf{u}^T\, {}^{t+\Delta t}_{0}\hat{h}\, \mathrm{d}\, {}_0\Gamma_h = \\
&= \int_{{}_0\Gamma_h} \delta\, {}_0\Delta u_X\, {}^{t+\Delta t}_{0}\hat{h}_X\, \mathrm{d}\, {}_0\Gamma_h + \int_{{}_0\Gamma_h} \delta\, {}_0\Delta u_Y\, {}^{t+\Delta t}_{0}\hat{h}_Y\, \mathrm{d}\, {}_0\Gamma_h + \int_{{}_0\Gamma_h} \delta\, {}_0\Delta u_Z\, {}^{t+\Delta t}_{0}\hat{h}_Z\, \mathrm{d}\, {}_0\Gamma_h
\end{aligned} \tag{3.98}$$

where ${}^{t+\Delta t}_{0}\hat{h} = [{}^{t+\Delta t}_{0}\hat{h}_X \;\; {}^{t+\Delta t}_{0}\hat{h}_Y \;\; {}^{t+\Delta t}_{0}\hat{h}_Z]^T$

Using GUF to express the variation of the displacement increments:

$$\begin{aligned}
{}^{t+\Delta t}_{0}\delta W^{ct\,1}_{\mathrm{EXT}} &= \delta\, {}_0\Delta U^k_{X\alpha_{u_X}\,I} \int_{{}_0\Gamma_h} {}^{X}_{0}N_I(X,Y)\, {}^{X}_{0}F^k_{\alpha_{u_X}}(Z^k)\, {}^{t+\Delta t}_{0}\hat{h}_X\, \mathrm{d}\, {}_0\Gamma_h + \\
&+ \delta\, {}_0\Delta U^k_{Y\alpha_{u_Y}\,I} \int_{{}_0\Gamma_h} {}^{Y}_{0}N_I(X,Y)\, {}^{Y}_{0}F^k_{\alpha_{u_Y}}(Z^k)\, {}^{t+\Delta t}_{0}\hat{h}_Y\, \mathrm{d}\, {}_0\Gamma_h + \\
&+ \delta\, {}_0\Delta U^k_{Z\alpha_{u_Z}\,I} \int_{{}_0\Gamma_h} {}^{Z}_{0}N_I(X,Y)\, {}^{Z}_{0}F^k_{\alpha_{u_Z}}(Z^k)\, {}^{t+\Delta t}_{0}\hat{h}_Z\, \mathrm{d}\, {}_0\Gamma_h
\end{aligned} \tag{3.99}$$

The equivalent nodal forces can be found comparing the above expression (eq. 3.99) with the following:

$$\begin{aligned}
{}^{t+\Delta t}_{0}\delta W^{ct\,1}_{\mathrm{EXT}} &= \delta\, {}_0\Delta U^k_{X\alpha_{u_X}\,I}\, {}^{t+\Delta t}_{0}f^k_{X\alpha_{u_X}\,I} + \delta\, {}_0\Delta U^k_{Y\alpha_{u_Y}\,I}\, {}^{t+\Delta t}_{0}f^k_{Y\alpha_{u_Y}\,I} + \\
&+ \delta\, {}_0\Delta U^k_{Z\alpha_{u_Z}\,I}\, {}^{t+\Delta t}_{0}f^k_{Z\alpha_{u_Z}\,I}
\end{aligned} \tag{3.100}$$

The equivalent nodal forces then can be recognized:

$$\begin{aligned}
{}^{t+\Delta t}_{0}f^k_{X\alpha_{u_X}\,I} &= \int_{{}_0\Gamma_h} {}^{X}_{0}N_I(X,Y)\, {}^{X}_{0}F^k_{\alpha_{u_X}}\left(Z^k\right)\, {}^{t+\Delta t}_{0}\hat{h}_X(X,Y)\, \mathrm{d}\, {}_0\Gamma_h \\
{}^{t+\Delta t}_{0}f^k_{Y\alpha_{u_Y}\,I} &= \int_{{}_0\Gamma_h} {}^{Y}_{0}N_I(X,Y)\, {}^{Y}_{0}F^k_{\alpha_{u_Y}}\left(Z^k\right)\, {}^{t+\Delta t}_{0}\hat{h}_Y(X,Y)\, \mathrm{d}\, {}_0\Gamma_h \\
{}^{t+\Delta t}_{0}f^k_{Z\alpha_{u_Z}\,I} &= \int_{{}_0\Gamma_h} {}^{Z}_{0}N_I(X,Y)\, {}^{Z}_{0}F^k_{\alpha_{u_Z}}\left(Z^k\right)\, {}^{t+\Delta t}_{0}\hat{h}_Z(X,Y)\, \mathrm{d}\, {}_0\Gamma_h
\end{aligned} \tag{3.101}$$

3.3.5 Boundary conditions

The essential boundary conditions are imposed weakly by using the penalty method [27, 102]. This can be physically interpreted as placing a distribution of translational springs along the thickness. When a boundary condition is imposed (for example the structure is externally "fixed"), one end of the spring connects to the ground and a zero displacement is prescribed. When the springs are used to impose Dirichlet boundary condition, also a point spring can be used in cases the rotational dofs are set free (e.g. hinges).

The springs modify the linear system to solve as shown in Eq. (3.50), introducing an additional contribution to the tangent stiffness matrix and residual (${}^{t}_{0}\mathbf{K}_{\mathrm{SP}}$ and ${}^{t}_{0}\mathbf{F}_{\mathrm{SP}}$, respectively). To highlight the main concepts, we start the discussion by showing how the kernels of the spring stiffness matrix are derived.

Let's recall the contribution to the linearized weak form of the boundary condition (see Eq.3.47):

$$ {}^{t+\Delta t}_{0}\delta U_{\mathrm{G}} = \int_{{}_0\Gamma_{g_i}} \delta\, {}_0\Delta u_i \psi_{ii}\, {}_0\Delta u_i \mathrm{d}\, {}_0\Gamma_{g_i} + \int_{{}_0\Gamma_{g_i}} \delta\, {}_0\Delta u_i \psi_{ii}\, {}^{t}_{0}u_i \mathrm{d}\, {}_0\Gamma_{g_i} - \int_{{}_0\Gamma_{g_i}} \delta\, {}_0\Delta u_i \psi_{ii} g_i \mathrm{d}\, {}_0\Gamma_{g_i} \tag{3.102} $$

In the current implementation the essential boundary conditions are applied directly at the element nodes (not the element sides). Then Eq. 3.102 is rewritten:

$$ \begin{aligned} {}^{t+\Delta t}_{0}\delta U_{\mathrm{G}} &= \sum_I \sum_k \int_{Z_{bot_k}}^{Z_{top_k}} \delta\, {}_0\Delta u_i^k(\mathcal{X}_I, \mathcal{Y}_I, Z)\, \psi_{ii}\, {}_0\Delta u_i^k(\mathcal{X}_I, \mathcal{Y}_I, Z)\mathrm{d}Z + \\ &+ \sum_I \sum_k \int_{Z_{bot_k}}^{Z_{top_k}} \delta\, {}_0\Delta u_i^k(\mathcal{X}_I, \mathcal{Y}_I, Z)\, \psi_{ii}\, {}^{t}_{0}u_i^k(\mathcal{X}_I, \mathcal{Y}_I, Z)\mathrm{d}Z - \\ &- \sum_I \sum_k \int_{Z_{bot_k}}^{Z_{top_k}} \delta\, {}_0\Delta u_i^k(\mathcal{X}_I, \mathcal{Y}_I, Z)\, \psi_{ii}\, g_i^k(\mathcal{X}_I, \mathcal{Y}_I, Z)\mathrm{d}Z \end{aligned} \tag{3.103} $$

where I are the ID of the nodes to be constrained.

The first term on the right-hand side is the contribution to the tangent stiffness matrix, the second and third terms are the contribution to the internal force vector.

Stiffness

The first term on the right-hand side of Eq. 3.103 generates an additional stiffness matrix to be added to the tangent stiffness.

$$ {}^{t+\Delta t}_{0}\delta U_{\mathrm{G}}^{\mathrm{stiff}} = \sum_I \sum_k \int_{Z_{bot_k}}^{Z_{top_k}} \delta\, {}_0\Delta u_i^k(\mathcal{X}_I, \mathcal{Y}_I, Z)\, \psi_{ii}\, {}_0\Delta u_i^k(\mathcal{X}_I, \mathcal{Y}_I, Z)\mathrm{d}Z \tag{3.104} $$

For simplicity let's consider only a single node I connected to the ground and a single layer. Then Eq. 3.104 can be expanded as

$$\begin{aligned}\int_{Z_{bot_k}}^{Z_{top_k}} \delta\,{}_0\Delta u_{i_I}^k\,\psi_{ii}\,{}_0\Delta u_{i_I}^k \mathrm{d}Z &= \int_{Z_{bot_k}}^{Z_{top_k}} \delta\,{}_0\Delta u_{\mathcal{X}_I}^k\,\psi_{\mathcal{X}\mathcal{X}}\,{}_0\Delta u_{\mathcal{X}_I}^k \mathrm{d}Z + \int_{Z_{bot_k}}^{Z_{top_k}} \delta\,{}_0\Delta u_{\mathcal{Y}_I}^k\,\psi_{\mathcal{Y}\mathcal{Y}}\,{}_0\Delta u_{\mathcal{Y}_I}^k \mathrm{d}Z + \\ &+ \int_{Z_{bot_k}}^{Z_{top_k}} \delta\,{}_0\Delta u_{\mathcal{Z}_I}^k\,\psi_{\mathcal{Z}\mathcal{Z}}\,{}_0\Delta u_{\mathcal{Z}_I} \mathrm{d}Z\end{aligned} \tag{3.105}$$

where ${}_0\Delta u_{i_I}^k = {}_0\Delta u_i^k(\mathcal{X}_I, \mathcal{Y}_I, Z)$ has been used. The resulting contribution to the stiffness matrix has to be expressed in the local reference system of the element that has the node I. Thus, a transformation is necessary to express the global displacements $(\mathcal{X}, \mathcal{Y}, \mathcal{Z})$ in the element reference systems (X, Y, Z):

$$\begin{aligned}{}_0\Delta u_{\mathcal{X}_I}^k &= {}_0^0a_{11}^k\,{}_0\Delta u_{X_I}^k + {}_0^0a_{21}^k\,{}_0\Delta u_{Y_I}^k + {}_0^0a_{31}^k\,{}_0\Delta u_{Z_I}^k \\ {}_0\Delta u_{\mathcal{Y}_I}^k &= {}_0^0a_{12}^k\,{}_0\Delta u_{X_I}^k + {}_0^0a_{22}^k\,{}_0\Delta u_{Y_I}^k + {}_0^0a_{32}^k\,{}_0\Delta u_{Z_I}^k \\ {}_0\Delta u_{\mathcal{Z}_I}^k &= {}_0^0a_{13}^k\,{}_0\Delta u_{X_I}^k + {}_0^0a_{23}^k\,{}_0\Delta u_{Y_I}^k + {}_0^0a_{33}^k\,{}_0\Delta u_{Z_I}^k\end{aligned} \tag{3.106}$$

The finite element discretization and GUF expansion applied at the local displacements results in the following expressions:

$$\begin{aligned}{}_0\Delta u_{X_I}^k &= {}_0^X F_{\alpha_{u_X}}^k\,{}_0\Delta U_{X\alpha_{u_X}\,I}^k \\ {}_0\Delta u_{Y_I}^k &= {}_0^Y F_{\alpha_{u_Y}}^k\,{}_0\Delta U_{Y\alpha_{u_Y}\,I}^k \\ {}_0\Delta u_{Z_I}^k &= {}_0^Z F_{\alpha_{u_Z}}^k\,{}_0\Delta U_{Z\alpha_{u_Z}\,I}^k\end{aligned} \tag{3.107}$$

and the virtual displacements

$$\begin{aligned}\delta\,{}_0\Delta u_{Z_I}^k &= {}_0^X F_{\alpha_{u_X}}^k\,\delta\,{}_0\Delta U_{X\alpha_{u_X}\,I}^k \\ \delta\,{}_0\Delta u_{Y_I}^k &= {}_0^Y F_{\alpha_{u_Y}}^k\,\delta\,{}_0\Delta U_{Y\alpha_{u_Y}\,I}^k \\ \delta\,{}_0\Delta u_{Z_I}^k &= {}_0^Z F_{\alpha_{u_Z}}^k\,\delta\,{}_0\Delta U_{Z\alpha_{u_Z}\,I}^k\end{aligned} \tag{3.108}$$

Substituting Eq. 3.106-3.108 in Eq. 3.103 it is possible to recognize the kernels of the boundary condition contribution to the tangent stiffness matrix:

$$\begin{aligned}{}_0^{t+\Delta t}\delta U_{\mathrm{G}\,I}^{k\,\mathrm{stiff}} &= \delta\,{}_0\Delta U_{X\alpha_{u_X}\,I}^k\,K_{\mathrm{sp}\,u_x u_x}^{k\alpha_{ux}\beta_{ux}II}\,{}_0\Delta U_{X\alpha_{u_X}\,I}^k + \delta\,{}_0\Delta U_{X\alpha_{u_X}\,I}^k\,K_{\mathrm{sp}\,u_x u_y}^{k\alpha_{ux}\beta_{uy}II}\,{}_0\Delta U_{Y\alpha_{u_Y}\,I}^k + \\ &+ \delta\,{}_0\Delta U_{X\alpha_{u_X}\,I}^k\,K_{\mathrm{sp}\,u_x u_z}^{k\alpha_{ux}\beta_{uz}II}\,{}_0\Delta U_{Z\alpha_{u_Z}\,I}^k + \text{other terms}\end{aligned} \tag{3.109}$$

where for example:

$$ {}^{t}_{0}K^{k\,\alpha_{u_X}\beta_{u_X}\,II}_{\mathrm{SP}\,u_X u_X}=\Big[\big({}^{0}_{0}a^{k}_{11}\big)^2\ \psi_{\mathcal{X}\mathcal{X}}+\big({}^{0}_{0}a^{k}_{12}\big)^2\ \psi_{\mathcal{Y}\mathcal{Y}}+\big({}^{0}_{0}a^{k}_{13}\big)^2\ \psi_{\mathcal{Z}\mathcal{Z}}\Big]\int_{Z_{bot_k}}^{Z_{top_k}} {}^{X}_{0}F^{k}_{\alpha_{u_X}}\ {}^{X}_{0}F^{k}_{\beta_{u_X}}\,\mathrm{d}Z \tag{3.110} $$

These terms are components of the spring stiffness matrix ${}^{t}_{0}\mathbf{K}_{\mathrm{SP}}$. From a computational point of view it is also relevant to point out that the springs' kernels, generating the related matrix, are constant during the solution of the nonlinear set of equations, with relevant advantages in terms of CPU time. This means

$$ {}^{t}_{0}\mathbf{K}_{\mathrm{SP}} = {}^{0}_{0}\mathbf{K}_{\mathrm{SP}} \tag{3.111} $$

Internal forces

The last two terms on the left-hand side of Eq. 3.103 generates an additional force contribution to be added to the internal force vector.

$$ {}^{t+\Delta t}_{0}\delta U^{\mathrm{hom.}}_{\mathrm{G}} = \sum_I \sum_k \int_{Z_{bot_k}}^{Z_{top_k}} \delta\,{}_0\Delta u^k_i(\mathcal{X}_I,\mathcal{Y}_I,Z)\,\psi_{ii}\ {}^{t}_{0}u^k_i(\mathcal{X}_I,\mathcal{Y}_I,Z)\mathrm{d}Z \tag{3.112} $$

$$ {}^{t+\Delta t}_{0}\delta U^{\mathrm{nonhom.}}_{\mathrm{G}} = \sum_I \sum_k \int_{Z_{bot_k}}^{Z_{top_k}} \delta\ {}_0\Delta u^k_i(\mathcal{X}_I,\mathcal{Y}_I,Z)\,\psi_{ii}\,g^k_i(\mathcal{X}_I,\mathcal{Y}_I,Z)\mathrm{d}Z \tag{3.113} $$

Also in this case a generic node I and layer is considered. The procedure follows the same steps performed for the stiffness matrix. The virtual displacements are manipulated as before. The term ${}^{t}_{0}u^k_i(\mathcal{X}_I,\mathcal{Y}_I,Z)$ represent the displacement at the beginning of the current load step. Its value can be obtained as a sum of all the incremental displacements of the previous converged iterations. And since in the total Lagrangian formulation the reference configuration is the initial one, the value of the thickness functions and rotation matrix do not change. These allows to treat the cumulative displacements as the incremental displacements. Then, it is possible to express it in terms of local variables:

$$ \begin{aligned} {}^{t}_{0}u^k_{\mathcal{X}_I} &= {}^{0}_{0}a^k_{11}\,{}^{t}_{0}u^k_{X_I} + {}^{0}_{0}a^k_{21}\,{}^{t}_{0}u^k_{Y_I} + {}^{0}_{0}a^k_{31}\,{}^{t}_{0}u^k_{Z_I} \\ {}^{t}_{0}u^k_{\mathcal{Y}_I} &= {}^{0}_{0}a^k_{12}\,{}^{t}_{0}u^k_{X_I} + {}^{0}_{0}a^k_{22}\,{}^{t}_{0}u^k_{Y_I} + {}^{0}_{0}a^k_{32}\,{}^{t}_{0}u^k_{Z_I} \\ {}^{t}_{0}u^k_{\mathcal{Z}_I} &= {}^{0}_{0}a^k_{13}\,{}^{t}_{0}u^k_{X_I} + {}^{0}_{0}a^k_{23}\,{}^{t}_{0}u^k_{Y_I} + {}^{0}_{0}a^k_{33}\,{}^{t}_{0}u^k_{Z_I} \end{aligned} \tag{3.114} $$

and apply the finitie element discretization and GUF expansion as in Eq. 3.107:

$$
\begin{aligned}
{}^{t}_{0}u^{k}_{X_I} &= {}^{X}_{0}F^{k}_{\alpha_{u_X}} \, {}^{t}_{0}U^{k}_{X\alpha_{u_X} I} \\
{}^{t}_{0}u^{k}_{Y_I} &= {}^{Y}_{0}F^{k}_{\alpha_{u_Y}} \, {}^{t}_{0}U^{k}_{Y\alpha_{u_Y} I} \\
{}^{t}_{0}u^{k}_{Z_I} &= {}^{Z}_{0}F^{k}_{\alpha_{u_Z}} \, {}^{t}_{0}U^{k}_{Z\alpha_{u_Z} I}
\end{aligned}
\tag{3.115}
$$

The final results shows, as expected, that the contribution to the internal force due to the spring is computed as the product of the spring stiffness by the cumulative displacements:

$$
\begin{aligned}
{}^{t+\Delta t}_{0}\delta U^{k\,\mathrm{hom}}_{\mathrm{G}_I} &= \delta \, {}_{0}\Delta U^{k}_{X\alpha_{u_X} I} \, K^{k\alpha_{ux}\beta_{ux} II}_{\mathrm{SP}\, u_x u_x} \, {}^{t}_{0}U^{k}_{X\alpha_{u_X} I} + \delta \, {}_{0}\Delta U^{k}_{X\alpha_{u_X} I} \, K^{k\alpha_{ux}\beta_{uy} II}_{\mathrm{SP}\, u_x u_y} \, {}^{t}_{0}U^{k}_{Y\alpha_{u_Y} I} + \\
&+ \delta \, {}_{0}\Delta U^{k}_{X\alpha_{u_X} I} \, K^{k\alpha_{ux}\beta_{uz} II}_{\mathrm{SP}\, u_x u_z} \, {}^{t}_{0}U^{k}_{Z\alpha_{u_Z} I} + \dots
\end{aligned}
\tag{3.116}
$$

After assembly:

$$
{}^{t}_{0}\mathbf{F}_{\mathrm{SP}} = {}^{t}_{0}\mathbf{K}_{\mathrm{SP}} \, {}^{t}_{0}\mathbf{U} \tag{3.117}
$$

Since the stiffness matrix of the springs is constant, the spring force vector at a generic load step is:

$$
{}^{t}_{0}\mathbf{F}^{\mathrm{sp}} = {}^{0}_{0}\mathbf{K}_{\mathrm{sp}} \, {}^{t}_{0}\mathbf{U} \tag{3.118}
$$

The non-homogeneous contribution is not shown, because in this dissertation only homogeneous boundary condition have been used, although the derivation is straightforward.

3.3.6 Inter-element compatibility

The compatibility of the displacements [86–88, 103] between adjacent nodes of different elements is imposed weakly by using the penalty method as done for the essential boundary conditions. The springs modify the linear system to solve as shown in Eq. (3.50), introducing an additional contribution to the spring stiffness matrix and spring force vector already computed for the boundary condition ($^{t}_{0}\mathbf{K}_{\mathrm{SP}}$ and $^{t}_{0}\mathbf{F}_{\mathrm{SP}}$, respectively). The construction of the stiffness matrix follows the same steps used for the essential boundary condition. For this reason an alternative procedure is shown based on the derivative of the potential energy.

To highlight the main concepts, we start the discussion by showing how the kernels of the spring stiffness matrix are derived when there is a point spring connecting node J of element c and node L of element d. The identity of the connected layer is k.

First, the total potential energy $\mathcal{V}^k$ is written considering the displacements (at generic locations of

elements c and d respectively) expressed in global coordinates:

$$ {}^{t+\Delta t}_{0}\mathcal{V}^{k} = \frac{1}{2}\left({}^{t+\Delta t}_{0}\mathbf{u}^{k\,c} - {}^{t+\Delta t}_{0}\mathbf{u}^{k\,d}\right)^{T}\boldsymbol{\gamma}^{k}\left({}^{t+\Delta t}_{0}\mathbf{u}^{k\,c} - {}^{t+\Delta t}_{0}\mathbf{u}^{k\,d}\right) \tag{3.119} $$

where $\boldsymbol{\gamma}^{k}$ is a diagonal matrix containing the value of the spring stiffness (penalty constants) in each direction (global frame).

Second, an incremental decomposition, as shown in Eq. 3.34, is done for the node displacements:

$$ \begin{aligned} {}^{t+\Delta t}_{0}\mathbf{u}^{k\,c} &= {}^{t}_{0}\mathbf{u}^{k\,c} + {}_{0}\Delta\mathbf{u}^{k\,c} \\ {}^{t+\Delta t}_{0}\mathbf{u}^{k\,d} &= {}^{t}_{0}\mathbf{u}^{k\,d} + {}_{0}\Delta\mathbf{u}^{k\,d} \end{aligned} \tag{3.120} $$

Third, the incremental displacement of layer k is written from global coordinate system to local element frame (both systems referred to the undeformed geometry) through a rotation matrix. For the node J of element c we have:

$$ \begin{aligned} {}_{0}\Delta u^{k\,c}_{\mathcal{X}J} &= {}^{0}_{0}a^{k\,c}_{11}\ {}_{0}\Delta u^{k\,c}_{XJ} + {}^{0}_{0}a^{k\,c}_{21}\ {}_{0}\Delta u^{k\,c}_{YJ} + {}^{0}_{0}a^{k\,c}_{31}\ {}_{0}\Delta u^{k\,c}_{ZJ} \\ {}_{0}\Delta u^{k\,c}_{\mathcal{Y}J} &= {}^{0}_{0}a^{k\,c}_{12}\ {}_{0}\Delta u^{k\,c}_{XJ} + {}^{0}_{0}a^{k\,c}_{22}\ {}_{0}\Delta u^{k\,c}_{YJ} + {}^{0}_{0}a^{k\,c}_{32}\ {}_{0}\Delta u^{k\,c}_{ZJ} \\ {}_{0}\Delta u^{k\,c}_{\mathcal{Z}J} &= {}^{0}_{0}a^{k\,c}_{13}\ {}_{0}\Delta u^{k\,c}_{XJ} + {}^{0}_{0}a^{k\,c}_{23}\ {}_{0}\Delta u^{k\,c}_{YJ} + {}^{0}_{0}a^{k\,c}_{33}\ {}_{0}\Delta u^{k\,c}_{ZJ} \end{aligned} \tag{3.121} $$

Notice that the incremental displacements are referred to the undeformed configuration. Thus, the transformation matrix does not change with time.

Fourth, the incremental displacement is written using the GUF formalism (see Eqs. 3.48 and 3.49). For node J of element c we have the following relations:

$$ \begin{aligned} {}_{0}\Delta u^{k\,c}_{XJ} &= {}^{X}_{0}F^{k\,c}_{\alpha_{u_X}}\ {}_{0}\Delta U^{k\,c}_{X\alpha_{u_X}J} \\ {}_{0}\Delta u^{k\,c}_{YJ} &= {}^{Y}_{0}F^{k\,c}_{\alpha_{u_Y}}\ {}_{0}\Delta U^{k\,c}_{Y\alpha_{u_Y}J} \\ {}_{0}\Delta u^{k\,c}_{ZJ} &= {}^{Z}_{0}F^{k\,c}_{\alpha_{u_Z}}\ {}_{0}\Delta U^{k\,c}_{Z\alpha_{u_Z}J} \end{aligned} \tag{3.122} $$

substituting Eq. 3.122 into Eq. 3.121, the incremental displacements in the global coordinate system are

obtained:

$$
\begin{aligned}
{}_0\Delta u^{k\,c}_{\mathcal{X}J} &= {}^{0}_{0}a^{k\,c}_{11}\,{}^{X}_{0}F^{k\,c}_{\alpha_{u_X}}\,{}_0\Delta U^{k\,c}_{X\alpha_{u_X}J} + {}^{0}_{0}a^{k\,c}_{21}\,{}^{Y}_{0}F^{k\,c}_{\alpha_{u_Y}}\,{}_0\Delta U^{k\,c}_{Y\alpha_{u_Y}J} \\
&\quad + {}^{0}_{0}a^{k\,c}_{31}\,{}^{Z}_{0}F^{k\,c}_{\alpha_{u_Z}}\,{}_0\Delta U^{k\,c}_{Z\alpha_{u_Z}J} \\
{}_0\Delta u^{k\,c}_{\mathcal{Y}J} &= {}^{0}_{0}a^{k\,c}_{12}\,{}^{X}_{0}F^{k\,c}_{\alpha_{u_X}}\,{}_0\Delta U^{k\,c}_{X\alpha_{u_X}J} + {}^{0}_{0}a^{k\,c}_{22}\,{}^{Y}_{0}F^{k\,c}_{\alpha_{u_Y}}\,{}_0\Delta U^{k\,c}_{Y\alpha_{u_Y}J} \\
&\quad + {}^{0}_{0}a^{k\,c}_{32}\,{}^{Z}_{0}F^{k\,c}_{\alpha_{u_Z}}\,{}_0\Delta U^{k\,c}_{Z\alpha_{u_Z}J} \\
{}_0\Delta u^{k\,c}_{\mathcal{Z}J} &= {}^{0}_{0}a^{k\,c}_{13}\,{}^{X}_{0}F^{k\,c}_{\alpha_{u_X}}\,{}_0\Delta U^{k\,c}_{X\alpha_{u_X}J} + {}^{0}_{0}a^{k\,c}_{23}\,{}^{Y}_{0}F^{k\,c}_{\alpha_{u_Y}}\,{}_0\Delta U^{k\,c}_{Y\alpha_{u_Y}J} \\
&\quad + {}^{0}_{0}a^{k\,c}_{33}\,{}^{Z}_{0}F^{k\,c}_{\alpha_{u_Z}}\,{}_0\Delta U^{k\,c}_{Z\alpha_{u_Z}J}
\end{aligned}
\tag{3.123}
$$

Similar operations and relations can be performed for element d and on the generic node L. The details are omitted for brevity.

Fifth, it is observed that the total potential energy ${}^{t+\Delta t}_{0}\mathcal{V}^{k}$ reported in Eq. 3.119 ca be conceptually written in terms of 3 distinct contributions. In particular, the first one depends only on the unknown incremental displacements and is indicated with ${}^{t+\Delta t}_{0}\mathcal{V}_{\Delta t-\Delta t}$. The second contribution is a "mixed" term and is indicated with the symbol ${}^{t+\Delta t}_{0}\mathcal{V}_{\Delta t-t}$. The last energy contribution depends only on the cumulative displacement at pseudo-time t and is indicated with ${}^{t+\Delta t}_{0}\mathcal{V}_{t-t}$. In mathematical terms, the conceptual subdivision earlier mentioned is expressed as

$$
{}^{t+\Delta t}_{0}\mathcal{V}^{k} = {}^{t+\Delta t}_{0}\mathcal{V}^{k}_{\Delta t-\Delta t} + {}^{t+\Delta t}_{0}\mathcal{V}^{k}_{\Delta t-t} + {}^{t+\Delta t}_{0}\mathcal{V}^{k}_{t-t} \tag{3.124}
$$

Sixth, the second derivatives of the potential energy (see Eq. 3.124 and the mathematical derivations presented in Appendix F) with respect to the incremental nodal displacement unknowns evaluated at time t of the three energy contribution are performed. Since the rotation matrix relating global and local coordinates is evaluated at the reference undeformed geometry, it is also known and not dependent on the displacements. Thus, only ${}^{t+\Delta t}\mathcal{V}_{\Delta t-\Delta t}$ gives nonzero values of the kernels of the spring contribution to the tangent stiffness matrix. Also in this case the springs' kernels, generating the related matrix, are constant during the solution of the nonlinear set of equations.

Since the stiffness matrix of the springs is constant (consequence of the TLF), the spring force vector at a generic load step is (see Eq. F.13):

$$
{}^{t+\Delta t}_{0}\mathbf{F}_{\mathrm{SP}} = {}^{0}_{0}\mathbf{K}_{\mathrm{SP}}\,{}^{t+\Delta t}_{0}\mathbf{U} \tag{3.125}
$$

3.4 Acknowledgments

Chapter 3 is in part a edited reprint of :

- "*Large displacement models for composites based on Murakami's Zig-Zag Function, Green-Lagrange Strain Tensor, and Generalized Unified Formulation*", *Thin-Walled Structures*, 2020 and co-authored by Luciano Demasi. The author of this dissertation is the primary investigator and author of this paper.

Chapter 4

Dynamics

4.1 Governing equations

The geometrically nonlinear formulation developed in the previous chapter is applied to dynamical systems. As for the static case, the starting point are the governing equations in strong form.

4.1.1 Strong form of the boundary value problem

The problem statement for dynamical system is an extension of the nonlinear static one (Eq. 3.2) with the addition of the inertial forces and the initial conditions. It can be expressed in the current (see Box. 4.1) or undeformed configuration (see Box. 4.2). where ρ is the density, $\bar{\dot{u}}_i$ is the initial velocity field, $\bar{S}_{ij}$ the initial state of stress and t is the time variable.

Strong form current configuration

Given $b_i : V \to \mathbb{R}$, $\rho : V \to \mathbb{R}$, $\hat{g}_i : \Gamma_{g_i} \to \mathbb{R}$, $\hat{h}_i : \Gamma_{h_i} \to \mathbb{R}$, $\bar{\dot{u}} : V \to \mathbb{R}$, $\bar{\sigma}_{ij} : V \to \mathbb{R}$, find $u_i : V \to \mathbb{R}$, such that

$$\begin{cases} \sigma_{ji,j}(\mathbf{x},t) + b_i(\mathbf{X},t) &= \rho(\mathbf{x})\ddot{u}_i(\mathbf{x},t) \quad \text{in} \quad V \\ u_i(\mathbf{x},t) &= \hat{g}_i(\mathbf{x},t) \quad \text{on} \quad \Gamma_{g_i} \\ n_j(\mathbf{x},t)\sigma_{ji}(\mathbf{x},t) &= \hat{h}_i(\mathbf{x},t) \quad \text{on} \quad \Gamma_{h_i} \\ \dot{u}_i(\mathbf{x},0) &= \bar{\dot{u}}_i \quad \text{in} \quad V \\ \sigma_{ij}(\mathbf{x},0) &= \bar{\sigma}_{ij} \quad \text{in} \quad V \end{cases} \tag{4.1}$$

Strong form undeformed configuration

Given $b_i : {}_0V \to \mathbb{R}$, $\rho : {}_0V \to \mathbb{R}$, $\hat{g}_i : {}_0\Gamma_{g_i} \to \mathbb{R}$, ${}_0\hat{h}_i : {}_0\Gamma_{h_i} \to \mathbb{R}$, $\bar{\dot{u}} : V \to \mathbb{R}$, $\bar{\sigma}_{ij} : V \to \mathbb{R}$, find $u_i : {}_0V \to \mathbb{R}$, such that

$$\begin{cases} (G_{ip}(\mathbf{X},t)S_{pj}(\mathbf{X},t))_{,j} + \mathcal{J}b_i(\mathbf{X},t) = \mathcal{J}\rho(\mathbf{X})\ddot{u}_i(\mathbf{X},t) & \text{in} \quad {}_0V \\ u_i(\mathbf{X},t) = \hat{g}_i(\mathbf{X},t) & \text{on} \quad {}_0\Gamma_{g_i} \\ G_{ik}S_{kj}(\mathbf{X},t)\,{}_0n_j(\mathbf{X},t) = {}_0\hat{h}_i(\mathbf{X},t) & \text{on} \quad {}_0\Gamma_{h_i} \\ \dot{u}_i(\mathbf{X},0) = \bar{\dot{u}}_i & \text{in} \quad {}_0V \\ S_{ij}(\mathbf{X},0) = \bar{S}_{ij} & \text{in} \quad {}_0V \end{cases} \tag{4.2}$$

4.1.2 Weak form of the boundary value problem

The derivation of the weak form follows the same steps already shown for the static case (see paragraph 3.1.2). The definition of the space of the weighting function remains as defined in Eq. 3.4 for the static analysis. Instead the space of the trial functions (u_i) is now time dependent. The differential equation is multiplied by the weighting functions and integrated over the domain in the undeformed configuration at time $t = 0$:

$$\int_{{}_0V} \delta u_i \left((G_{ip}S_{pj})_{,j} + \mathcal{J}b_i - \mathcal{J}\rho\ddot{u}_i \right) \mathrm{d}\,{}_0V = 0 \tag{4.3}$$

Follows an integration by part, application of the divergence theorem and the natural boundary condition with the following results:

$$\int_{{}_0V} \delta u_{i,j} G_{ip}S_{pj} \,\mathrm{d}\,{}_0V = \int_{{}_0V} \delta u_i \mathcal{J}b_i \,\mathrm{d}\,{}_0V - \int_{{}_0V} \delta u_i \mathcal{J}\rho\ddot{u}_i \,\mathrm{d}\,{}_0V + \sum_i \int_{{}_0\Gamma_{h_i}} \delta u_i \,{}_0\hat{h}_i \,\mathrm{d}\,{}_0\Gamma \tag{4.4}$$

Introducing the relations between the variation of strain and the variation of the displacement, the weak form for the dynamical system is obtained:

$$\int_{{}_0V} \delta E_{ij} S_{ij} \,\mathrm{d}\,{}_0V = \int_{{}_0V} \delta u_i \mathcal{J}b_i \,\mathrm{d}\,{}_0V - \int_{{}_0V} \delta u_i \mathcal{J}\rho\ddot{u}_i \,\mathrm{d}\,{}_0V + \sum_i \int_{{}_0\Gamma_{h_i}} \delta u_i \,{}_0\hat{h}_i \,\mathrm{d}\,{}_0\Gamma \tag{4.5}$$

The complete statement of the weak form is shown in Box 4.6. Eq. 4.6 can be interpreted using the principle of virtual displacements:

$$\delta W_{\mathrm{INT}} + \delta W_{\mathrm{KIN}} = \delta W_{\mathrm{EXT}} \tag{4.7}$$

the additional term is the virtual work of the inertial forces:

$$\delta W_{\mathrm{KIN}} = \int_{{}_0V} \delta u_i \mathcal{J}\rho\ddot{u}_i \,\mathrm{d}\,{}_0V \tag{4.8}$$

Weak form undeformed configuration

Given $b_i : {}_0V \to \mathbb{R}$, $\rho : {}_0V \to \mathbb{R}$, $\hat{g}_i : {}_0\Gamma_{g_i} \to \mathbb{R}$, ${}_0\hat{h}_i : {}_0\Gamma_{h_i} \to \mathbb{R}$, find $u_i \in S_i$, such that for all $\delta u_i \in W_i$

$$\underbrace{\int_{{}_0V} \delta E_{ij} S_{ij} \mathrm{d}\,{}_0V}_{\text{Internal work}} + \underbrace{\int_{{}_0V} \delta u_i \mathcal{J} \rho \ddot{u}_i \mathrm{d}\,{}_0V}_{\text{Inertial work}} = \underbrace{\int_{{}_0V} \delta u_i \mathcal{J} f_i \mathrm{d}\,{}_0V + \sum_i \int_{{}_0\Gamma_{h_i}} \delta u_i \, {}_0\hat{h}_i \mathrm{d}\,{}_0\Gamma}_{\text{External work}} \tag{4.6}$$

4.1.3 Imposition of time-dependent boundary conditions and interelement compatibility

In the dynamic case the boundary conditions and the displacement compatibility between elements are imposed weakly. The weak form is augmented with the variation of the potential energy as shown in section 3.1.3 and 3.1.4. The resulting weak form for a geometrically nonlinear dynamical system in a inertial reference frame is shown in Box 4.9.

Weak form for the variable kinematic plate theory in the undeformed configuration

Given $b_i : {}_0V \to \mathbb{R}$, $\rho : {}_0V \to \mathbb{R}$, $\hat{g}_i : {}_0\Gamma_{g_i} \to \mathbb{R}$, ${}_0\hat{h}_i : {}_0\Gamma_{h_i} \to \mathbb{R}$, find $u_i \in S_i$, such that for all $\delta u_i \in W_i$

$$\begin{aligned}
&\underbrace{\int_{{}_0V} \delta E_{ij} S_{ij} \mathrm{d}\,{}_0V}_{\text{Internal work}} + \underbrace{\int_{{}_0\Gamma_{g_i}} \delta u_i \psi_{ii} u_i \mathrm{d}\,{}_0\Gamma_{g_i}}_{\substack{\text{homogeneous part of} \\ \text{essential b.c.}}} - \underbrace{\int_{{}_0\Gamma_{g_i}} \delta u_i \psi_{ii} g_i \mathrm{d}\,{}_0\Gamma_{g_i}}_{\substack{\text{Non-homogeneous part of} \\ \text{essential b.c.}}} = \\
&\underbrace{\underbrace{\int_{{}_0V} \delta u_i \mathcal{J} b_i \mathrm{d}\,{}_0V}_{\text{Volume forces}} + \underbrace{\sum_i \int_{{}_0\Gamma_{h_i}} \delta u_i \, {}_0\hat{h}_i \mathrm{d}\,{}_0\Gamma}_{\text{Surface forces}}}_{\text{External work}} - \underbrace{\int_{{}_0V} \delta u_i \mathcal{J} \rho \ddot{u}_i \mathrm{d}\,{}_0V}_{\text{Inertial work}} - \\
&\underbrace{- \sum_i \sum_{f=1}^{n_f} \int_{{}_0\Gamma_f} \left(\delta u_{i\,{}_0\Gamma_{f^{(+)}}} - \delta u_{i\,{}_0\Gamma_{f^{(-)}}} \right) \gamma_{ii} \left(u_{i\,{}_0\Gamma_{f^{(+)}}} - u_{i\,{}_0\Gamma_{f^{(-)}}} \right) \mathrm{d}\,{}_0\Gamma_f}_{\text{Interelement compatibility}}
\end{aligned} \tag{4.9}$$

4.2 Finite element discretization

The spacial discretization is obtained by means of the finite element approximation and axiomatic plate models expressed in GUF notation. But, unlike the static case, the weak form is not yet fully discretized because it is still a continuous function of time. The finite element matrices and vector are unchanged with

respect to the static case. The only new term is the mass matrix ($\mathbf{M}$) obtained by the discretization of the inertial contribution (see paragraph 4.2.1).

For time integration purpose it is convenient to recast the finite element equation in residual form:

$$\mathbf{R} = \mathbf{M}\ddot{\mathbf{U}} + \mathbf{F}_{\mathrm{INT}}(\mathbf{U}) + \mathbf{K}_{\mathrm{SP}}\mathbf{U} - \mathbf{F}_{\mathrm{EXT}} + \mathbf{F}_{\mathrm{SP}} = \mathbf{0} \tag{4.10}$$

This residual equation should be satisfied at every time instant. The internal force vector is a nonlinear function of the displacement field. Its linearization will be performed for convenience during the time discretization phase.

4.2.1 Kernels of the mass matrix

The mass matrix is computed through discretization of Eq. 4.8, reported here for convenience

$$^{t+\Delta t}_{0}\delta W_{\mathrm{KIN}} = \int_{_0V} \delta u_i \mathcal{J}\rho \, ^{t+\Delta t}_{0}\ddot{u}_i \, \mathrm{d}\,{}_0V \tag{4.11}$$

Its kernels are obtained after expressing the virtual displacements (δu_i) and accelerations ($\ddot{u}_i$) as a function of the GUF unknown. For example the X components for a layer k are:

$$_0\delta u^k_X(X,Y,Z^k) = {}^X_0F^k_{\alpha_{u_X}}(Z^k)\, {}^X_0N_I(X,Y)\ {}_0\delta U^k_{X\alpha_{u_X}I} \quad \alpha_{u_X}=t,l,b \quad l=2,\dots,N_{u_X} \quad I=1,2,\dots M_n \tag{4.12}$$

$$_0\ddot{u}^k_X(X,Y,Z^k,t) = {}^X_0F^k_{\alpha_{u_X}}(Z^k)\, {}^X_0N_I(X,Y)\ {}_0\ddot{U}^k_{X\alpha_{u_X}I}(t) \quad \alpha_{u_X}=t,l,b \quad l=2,\dots,N_{u_X} \quad I=1,2,\dots M_n \tag{4.13}$$

And then substituting Eq. 4.12 and Eq. 4.13 in Eq. 4.11 the virtual work as a function of the nodal variables is found:

$$\begin{aligned}
^{t+\Delta t}_{0}\delta W_{\mathrm{KIN}} \quad = \quad & {}_0\delta U^k_{X\alpha_{u_X}I}\left[\int_{_0V} \mathcal{J}\rho\, {}^X_0N_I\ {}^X_0F^k_{\alpha_{u_X}}\ {}^X_0F^k_{\alpha_{u_X}}\ {}^X_0N_J\ \mathrm{d}\,{}_0V\right] {}_0\ddot{U}^k_{X\beta_{u_X}J} + \\
& {}_0\delta U^k_{Y\alpha_{u_Y}I}\left[\int_{_0V} \mathcal{J}\rho\, {}^Y_0N_I\ {}^Y_0F^k_{\alpha_{u_Y}}\ {}^Y_0F^k_{\alpha_{u_Y}}\ {}^Y_0N_J\ \mathrm{d}\,{}_0V\right] {}_0\ddot{U}^k_{Y\beta_{u_Y}J} + \\
& {}_0\delta U^k_{Z\alpha_{u_Z}I}\left[\int_{_0V} \mathcal{J}\rho\, {}^Z_0N_I\ {}^Z_0F^k_{\alpha_{u_Z}}\ {}^Z_0F^k_{\alpha_{u_Z}}\ {}^Z_0N_J\ \mathrm{d}\,{}_0V\right] {}_0\ddot{U}^k_{Z\beta_{u_Z}J}
\end{aligned} \tag{4.14}$$

The mass matrix is identified:

$$
\begin{aligned}
{}^{t+\Delta t}_{0}\delta W_{\text{KIN}} &= \delta\mathbf{U}^T\mathbf{M}\ddot{\mathbf{U}} = \\
&= {}_0\delta U^k_{X\alpha_{u_X}I}\left[{}^0_0M^{\alpha_{u_X}\beta_{u_X}IJ}_{u_Xu_X}\right]{}_0\ddot{U}^k_{X\beta_{u_X}J} + \\
&\quad {}_0\delta U^k_{Y\alpha_{u_Y}I}\left[{}^0_0M^{\alpha_{u_Y}\beta_{u_Y}IJ}_{u_Yu_Y}\right]{}_0\ddot{U}^k_{Y\beta_{u_Y}J} + \\
&\quad {}_0\delta U^k_{Z\alpha_{u_Z}I}\left[{}^0_0M^{\alpha_{u_Z}\beta_{u_Z}IJ}_{u_Zu_Z}\right]{}_0\ddot{U}^k_{Z\beta_{u_Z}J}
\end{aligned}
\tag{4.15}
$$

where

$$
\begin{aligned}
{}^0_0M^{\alpha_{u_X}\beta_{u_X}IJ}_{u_Xu_X} &= \int_{{}_0V}\mathcal{J}\rho\,{}^X_0N_I\;{}^X_0F^k_{\alpha_{u_X}}\;{}^X_0F^k_{\alpha_{u_X}}\;{}^X_0N_J\,\mathrm{d}\,{}_0V \\
{}^0_0M^{\alpha_{u_Y}\beta_{u_Y}IJ}_{u_Yu_Y} &= \int_{{}_0V}\mathcal{J}\rho\,{}^Y_0N_I\;{}^Y_0F^k_{\alpha_{u_Y}}\;{}^Y_0F^k_{\alpha_{u_Y}}\;{}^Y_0N_J\,\mathrm{d}\,{}_0V \\
{}^0_0M^{\alpha_{u_Z}\beta_{u_Z}IJ}_{u_Zu_Z} &= \int_{{}_0V}\mathcal{J}\rho\,{}^Z_0N_I\;{}^Z_0F^k_{\alpha_{u_Z}}\;{}^Z_0F^k_{\alpha_{u_Z}}\;{}^Z_0N_J\,\mathrm{d}\,{}_0V
\end{aligned}
\tag{4.16}
$$

are its kernels. The mass matrix is block diagonal and only three kernels exist for this matrix.

4.3 Non-inertial reference frame

The equations derived so far are valid for an inertial reference frame. For the study of rotors or flapping wing is often convenient to derive the equations in a reference frame that moves synchronously with the elastic body (corotational) [104, 105]. The weak form can be expressed in this moving reference frame with the addition of the apparent forces.

With the presence of multiple frames it is necessary to introduce new quantities and notations. The transformation matrix between two coordinate system is indicated as $\mathbf{T}_{\alpha\beta}$. This matrix transform the component of a vector from the reference system β to α

$$
{}_\alpha\mathbf{v} = \mathbf{T}_{\alpha\beta}\,{}_\beta\mathbf{v} \tag{4.17}
$$

where the subscript indicates the reference system in which the vector components are projected. The letter I and G are used for identify the inertial and the global/body reference system respectively. Then $\mathbf{T}_{IG}$ project the components of an array from the global/body coordinate system to the inertial one.

The vector $\boldsymbol{\omega}$ is the angular velocity of the moving frame with respect to the inertial one. And $\boldsymbol{\Omega}$ is the matrix associated with the cross product operation $\boldsymbol{\omega}\times$. The time derivative of the transformation matrix is

$$
\dot{\mathbf{T}}_{\alpha\beta} = {}_\alpha\boldsymbol{\Omega}\mathbf{T}_{\alpha\beta} \tag{4.18}
$$

In the following paragraph arrays that are expressed in the inertial coordinate systems (I) have a tilde on top of them, e.g. $\widetilde{(\bullet)}$.

4.3.1 Position, velocity and acceleration of a point

The position of a point in an inertial reference frame can be expressed as:

$$\tilde{\mathbf{r}} = \tilde{\mathbf{r}}_o + \tilde{\mathbf{x}} = \tilde{\mathbf{r}}_o + \mathbf{T}_{IG}\mathbf{x} \tag{4.19}$$

where $\tilde{\mathbf{r}}_o$ is the origin of the moving frame and $\tilde{\mathbf{x}}$ is the position of the point measured from this origin (see Fig. 4.1). The velocity obtained from the time derivative of Eq. 4.19 is:

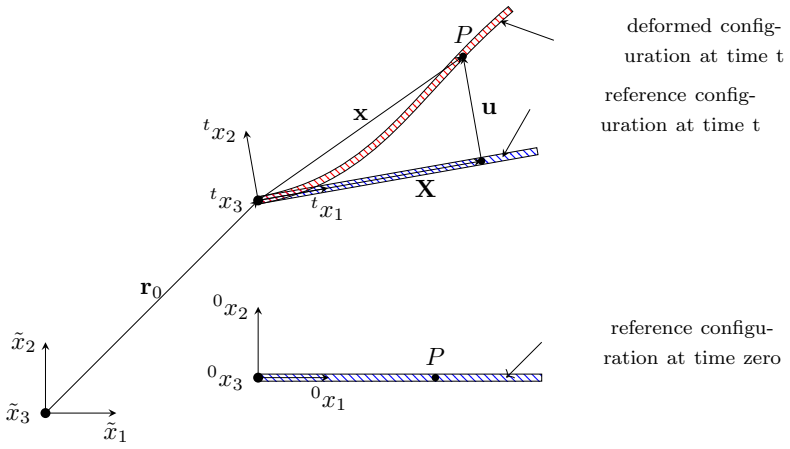

Figure 4.1: Reference systems and position of a point P during deformation.

$$\dot{\tilde{\mathbf{r}}} = \dot{\tilde{\mathbf{r}}}_o + \dot{\mathbf{T}}_{IG}\mathbf{x} + \mathbf{T}_{IG}\dot{\mathbf{x}} = \dot{\tilde{\mathbf{r}}}_o + \widetilde{\boldsymbol{\Omega}}\mathbf{T}_{IG}\mathbf{x} + \mathbf{T}_{IG}\dot{\mathbf{x}} \tag{4.20}$$

And in the same way the acceleration is:

$$\begin{aligned}
\ddot{\tilde{\mathbf{r}}} &= \ddot{\tilde{\mathbf{r}}}_o + \dot{\widetilde{\boldsymbol{\Omega}}}\mathbf{T}_{IG}\mathbf{x} + \widetilde{\boldsymbol{\Omega}}\dot{\mathbf{T}}_{IG}\mathbf{x} + \widetilde{\boldsymbol{\Omega}}\mathbf{T}_{IG}\dot{\mathbf{x}} + \dot{\mathbf{T}}_{IG}\dot{\mathbf{x}} + \mathbf{T}_{IG}\ddot{\mathbf{x}} \\
&= \ddot{\tilde{\mathbf{r}}}_o + \dot{\widetilde{\boldsymbol{\Omega}}}\mathbf{T}_{IG}\mathbf{x} + \widetilde{\boldsymbol{\Omega}}\widetilde{\boldsymbol{\Omega}}\mathbf{T}_{IG}\mathbf{x} + \widetilde{\boldsymbol{\Omega}}\mathbf{T}_{IG}\dot{\mathbf{x}} + \widetilde{\boldsymbol{\Omega}}\mathbf{T}_{IG}\dot{\mathbf{x}} + \mathbf{T}_{IG}\ddot{\mathbf{x}} \\
&= \ddot{\tilde{\mathbf{r}}}_o + \dot{\widetilde{\boldsymbol{\Omega}}}\mathbf{T}_{IG}\mathbf{x} + \widetilde{\boldsymbol{\Omega}}\widetilde{\boldsymbol{\Omega}}\mathbf{T}_{IG}\mathbf{x} + 2\widetilde{\boldsymbol{\Omega}}\mathbf{T}_{IG}\dot{\mathbf{x}} + \mathbf{T}_{IG}\ddot{\mathbf{x}}
\end{aligned} \tag{4.21}$$

Using the relation 3.1 in Eq. 4.21:

$$\ddot{\tilde{\mathbf{r}}} = \ddot{\tilde{\mathbf{r}}}_o + \dot{\widetilde{\boldsymbol{\Omega}}}\mathbf{T}_{IG}\mathbf{X} + \dot{\widetilde{\boldsymbol{\Omega}}}\mathbf{T}_{IG}\mathbf{u} + \widetilde{\boldsymbol{\Omega}}\widetilde{\boldsymbol{\Omega}}\mathbf{T}_{IG}\mathbf{X} + \widetilde{\boldsymbol{\Omega}}\widetilde{\boldsymbol{\Omega}}\mathbf{T}_{IG}\mathbf{u} + 2\widetilde{\boldsymbol{\Omega}}\mathbf{T}_{IG}\dot{\mathbf{u}} + \mathbf{T}_{IG}\ddot{\mathbf{u}} \tag{4.22}$$

The governing equations are referred to the body reference frame (G), for this reason the components of the acceleration are projected in such reference:

$$\ddot{\mathbf{r}} \quad = \quad \mathbf{T}_{IG}^T \ddot{\tilde{\mathbf{r}}} = \ddot{\mathbf{r}}_o + \dot{\mathbf{\Omega}}\mathbf{X} + \dot{\mathbf{\Omega}}\mathbf{u} + \mathbf{\Omega}\mathbf{\Omega}\mathbf{X} + \mathbf{\Omega}\mathbf{\Omega}\mathbf{u} + 2\mathbf{\Omega}\dot{\mathbf{u}} + \ddot{\mathbf{u}} \tag{4.23}$$

where :

$$\mathbf{\Omega} = \mathbf{T}_{IG}^T \widetilde{\mathbf{\Omega}} \mathbf{T}_{IG} \tag{4.24}$$

4.3.2 Weak form modifications

To express the weak form (Eq. 4.9) in a relative reference frame it suffices to include an appropriate expression for the acceleration in the inertia contribution. The virtual work of the inertial forces in the inertial reference frame is:

$$\delta W_{\text{KIN}} = \int_{{}_0V} \mathcal{J}\rho\delta\tilde{\mathbf{x}}^T \ddot{\tilde{\mathbf{x}}} \, \mathrm{d}\,{}_0V \tag{4.25}$$

and the virtual displacements of the position vector (Eq. 4.19) is

$$\delta\tilde{\mathbf{r}} = \mathbf{T}_{IG}\delta\mathbf{u} \tag{4.26}$$

where $\delta\tilde{\mathbf{r}}_o = 0$ has been used. This is due to the fact that the rigid motion of the body is predetermined as well the position of the origin of the attached reference system ($\tilde{\mathbf{r}}_o$). Substituting the expression of the variation of the position (Eq. 4.26) and the acceleration (Eq. 4.23) in the variation of the inertial virtual work (Eq. 4.25):

$$\begin{aligned} \delta W_{\text{KIN}} \quad &= \quad \int_{{}_0V} \mathcal{J}\rho\delta\mathbf{u}^T \left(\ddot{\mathbf{r}}_o + \dot{\mathbf{\Omega}}\mathbf{X} + \mathbf{\Omega}\mathbf{\Omega}\mathbf{X} \right) \mathrm{d}\,{}_0V + \int_{{}_0V} \mathcal{J}\rho\delta\mathbf{u}^T \left(\dot{\mathbf{\Omega}} + \mathbf{\Omega}\mathbf{\Omega} \right) \mathbf{u} \, \mathrm{d}\,{}_0V + \\ &+ \quad \int_{{}_0V} \mathcal{J}\rho\delta\mathbf{u}^T \left(2\mathbf{\Omega} \right) \dot{\mathbf{u}} \, \mathrm{d}\,{}_0V + \int_{{}_0V} \mathcal{J}\rho\delta\mathbf{u}^T \ddot{\mathbf{u}} \, \mathrm{d}\,{}_0V \end{aligned} \tag{4.27}$$

or in indicial notation

$$\begin{aligned} \delta W_{\text{KIN}} \quad &= \quad \int_{{}_0V} \mathcal{J}\rho\delta u_i \left[\ddot{r}_{o_i} + \dot{\Omega}_{ij} X_j + \Omega_{ip}\Omega_{pj} X_j \right] \mathrm{d}\,{}_0V + \int_{{}_0V} \mathcal{J}\rho\delta u_i \left(\dot{\Omega}_{ij} + \Omega_{ip}\Omega_{pj} \right) u_j \, \mathrm{d}\,{}_0V + \\ &+ \quad \int_{{}_0V} \mathcal{J}\rho\delta u_i 2\Omega_{ij}\dot{u}_j \, \mathrm{d}\,{}_0V + \int_{{}_0V} \mathcal{J}\rho\delta u_i \ddot{u}_i \, \mathrm{d}\,{}_0V \end{aligned} \tag{4.28}$$

After substitution of Eq. 4.28 in Eq. 4.9, the weak form of the elastic body deforming in a non-inertial reference frame is obtained (see Box 4.29).

Weak form of undeformed configuration in body coordinate system

Given $b_i : {}_0V \to \mathbb{R}$, $\rho : {}_0V \to \mathbb{R}$, $\hat{g}_i : {}_0\Gamma_{g_i} \to \mathbb{R}$, ${}_0\hat{h}_i : {}_0\Gamma_{h_i} \to \mathbb{R}$, find $u_i \in S_i$, such that for all $\delta u_i \in W_i$

$$\underbrace{\int_{{}_0V} \delta E_{pj} S_{pj} \, \mathrm{d}\,{}_0V}_{\substack{\text{Virtual work of}\\ \text{internal forces}}} + \underbrace{\int_{{}_0V} \mathcal{J}\rho\delta u_i \ddot{u}_i \, \mathrm{d}\,{}_0V}_{\substack{\text{Virtual work of inertia}\\ \text{in body coord. syst.}}} + \underbrace{\int_{{}_0V} \mathcal{J}\rho\delta u_i \left(\Omega_{ip}\Omega_{pj}u_j + \Omega_{ip}\Omega_{pj}X_j\right) \, \mathrm{d}\,{}_0V}_{\substack{\text{Virtual work of}\\ \text{centrifugal forces}}} +$$

$$\underbrace{\int_{{}_0V} \mathcal{J}\rho\delta u_i \ddot{x}_{o_i} \, \mathrm{d}\,{}_0V}_{\substack{\text{Virtual work of}\\ \text{rigid body translation}}} + + \underbrace{\int_{{}_0V} \mathcal{J}\rho\delta u_i \left(\dot{\Omega}_{ij}u_j + \dot{\Omega}_{ij}X_j\right) \, \mathrm{d}\,{}_0V}_{\substack{\text{Virtual work of}\\ \text{Euler forces}}} + \underbrace{\int_{{}_0V} \mathcal{J}\rho\delta u_i 2\Omega_{ij}\dot{u}_j \, \mathrm{d}\,{}_0V}_{\substack{\text{Virtual work of}\\ \text{Coriolis forces}}} +$$

$$\underbrace{\int_{{}_0\Gamma_{g_i}} \delta u_i \psi_{ii} u_i \, \mathrm{d}\,{}_0\Gamma_{g_i}}_{\substack{\text{homogeneous part of}\\ \text{essential b.c.}}} - - \underbrace{\int_{{}_0\Gamma_{g_i}} \delta u_i \psi_{ii} g_i \mathrm{d}\,{}_0\Gamma_{g_i}}_{\substack{\text{Non-homogeneous part of}\\ \text{essential b.c.}}} +$$

$$\underbrace{+ \sum_i \sum_{f=1}^{n_f} \int_{{}_0\Gamma_f} \left(\delta u_{i\,{}_{\Gamma_{f^{(+)}}}} - \delta u_{i\,{}_{\Gamma_{f^{(-)}}}}\right) \gamma_{ii} \left(u_{i\,{}_{\Gamma_{f^{(+)}}}} - u_{i\,{}_{\Gamma_{f^{(-)}}}}\right) \, \mathrm{d}\,{}_0\Gamma_f}_{\text{Interelement compatibility constraint}} =$$

$$= \underbrace{\int_{{}_0V} \delta u_i \mathcal{J} b_i \, \mathrm{d}V}_{\substack{\text{Virtual work of}\\ \text{body forces}}} + \underbrace{\sum_i \int_{{}_0\Gamma_{h_i}} \delta u_i \, {}_0\hat{h}_i \, \mathrm{d}\,{}_0\Gamma}_{\substack{\text{Virtual work of}\\ \text{surface forces}}} \tag{4.29}$$

4.3.3 Finite element discretization

The virtual work of inertial forces (Eq. 4.28) written in a moving frame provides several FEM arrays when discretized, in addition to the mass matrix. Here the expression for each array are derived. The virtual work is decomposed as follows:

$$\delta W_{\mathrm{KIN}} = \delta W_{\mathrm{M}} + \delta W_{\mathrm{TR}} + \delta W_{\mathrm{CF}} + \delta W_{\mathrm{EU}} + \delta W_{\mathrm{CR}} \tag{4.30}$$

where

$$\begin{aligned}
\delta W_{\mathrm{TR}} &= \int_{{}_0V} \mathcal{J}\rho\delta u_i \ddot{r}_{o_i} \,\mathrm{d}\,{}_0V \\
\delta W_{\mathrm{CF}} &= \int_{{}_0V} \mathcal{J}\rho\delta u_i \Omega_{ip}\Omega_{pj} X_j \,\mathrm{d}\,{}_0V + \int_{{}_0V} \mathcal{J}\rho\delta u_i \Omega_{ip}\Omega_{pj} u_j \,\mathrm{d}\,{}_0V \\
\delta W_{\mathrm{EU}} &= \int_{{}_0V} \mathcal{J}\rho\delta u_i \dot{\Omega}_{ij} u_j \,\mathrm{d}\,{}_0V + \int_{{}_0V} \mathcal{J}\rho\delta u_i \dot{\Omega}_{ij} X_j \,\mathrm{d}\,{}_0V \\
\delta W_{\mathrm{CR}} &= \int_{{}_0V} \mathcal{J}\rho\delta u_i 2\Omega_{ij} \dot{u}_j \,\mathrm{d}\,{}_0V \\
\delta W_{\mathrm{M}} &= \int_{{}_0V} \mathcal{J}\rho\delta u_i \ddot{u}_i \,\mathrm{d}\,{}_0V
\end{aligned}$$

The nodal unknown are expressed in the undeformed element coordinate systems (E) that move rigidly with the global/body systems. Then another constant transformation $\mathbf{T}_{GE}$ is implicity used since the expression are formally invariant. The virtual work is then decomposed at element level

$$\delta W_{\mathrm{KIN}} = \sum_e \delta W^e_{\mathrm{KIN}} \tag{4.31}$$

Translation forces

The first contribution is due to the rigid translation of the body identified by the motion of the body reference frame origin ($\mathbf{r}_o$). The corresponding virtual work term (see Eq. 4.30) at element level is:

$${}^{t+\Delta t}_{0}\delta W^{\mathrm{e}}_{\mathrm{TR}} = \int_{{}_0V^e} \mathcal{J}\rho\delta u_i \ddot{r}_{o_j} \,\mathrm{d}\,{}_0V \tag{4.32}$$

Once the virtual displacements are spatially discretize Eq. 4.32 is rewritten as:

$$\begin{aligned}
{}^{t+\Delta t}_{0}\delta W^{e}_{\mathrm{TR}} &= {}_0\delta U^k_{X\alpha_{u_X} I} \left[\int_{{}_0V^e} \mathcal{J}\rho\, {}^{X}_{0}N_I \; {}^{X}_{0}F^k_{\alpha_{u_X}} \; \ddot{r}_{o_j} \,\mathrm{d}\,{}_0V \right] + \\
&\quad {}_0\delta U^k_{Y\alpha_{u_Y} I} \left[\int_{{}_0V^e} \mathcal{J}\rho\, {}^{Y}_{0}N_I \; {}^{Y}_{0}F^k_{\alpha_{u_Y}} \; \ddot{r}_{o_j} \,\mathrm{d}\,{}_0V \right] + \\
&\quad {}_0\delta U^k_{Z\alpha_{u_Z} I} \left[\int_{{}_0V^e} \mathcal{J}\rho\, {}^{Z}_{0}N_I \; {}^{Z}_{0}F^k_{\alpha_{u_Z}} \; \ddot{r}_{o_j} \,\mathrm{d}\,{}_0V \right]
\end{aligned} \tag{4.33}$$

In this form it is possible to recognize the equivalent nodal forces generated by the apparent force due to rigid translation of the body $\mathbf{F}_{TR}$:

$$\begin{aligned} {}^{t+\Delta t}_{0}\delta W^{e}_{\mathrm{TR}} &= {}_{0}\delta U^{k}_{X\alpha_{u_X}I}\,{}^{t+\Delta t}_{0}F^{\alpha_{u_X}I}_{\mathrm{TR}\,u_X} + {}_{0}\delta U^{k}_{Y\alpha_{u_Y}I}\,{}^{t+\Delta t}_{0}F^{\alpha_{u_Y}I}_{\mathrm{TR}\,u_Y} + {}_{0}\delta U^{k}_{Z\alpha_{u_Z}I}\,{}^{t+\Delta t}_{0}F^{\alpha_{u_Z}I}_{\mathrm{TR}\,u_Z} = \\ &= \delta\mathbf{U}^{T}\mathbf{F}_{\mathrm{TR}} \end{aligned} \tag{4.34}$$

Its kernels are:

$$\begin{aligned} {}^{t+\Delta t}_{0}F^{\alpha_{u_X}I}_{T\,u_X} &= \int_{{}_0V^e} \mathcal{J}\rho\,{}^{X}_{0}N_I\;{}^{X}_{0}F^{k}_{\alpha_{u_X}}\;\ddot{r}_{0_j}\,\mathrm{d}\,{}_0V \\ {}^{t+\Delta t}_{0}F^{\alpha_{u_Y}I}_{T\,u_Y} &= \int_{{}_0V^e} \mathcal{J}\rho\,{}^{Y}_{0}N_I\;{}^{Y}_{0}F^{k}_{\alpha_{u_Y}}\;\ddot{r}_{0_j}\,\mathrm{d}\,{}_0V \\ {}^{t+\Delta t}_{0}F^{\alpha_{u_Z}I}_{T\,u_Z} &= \int_{{}_0V^e} \mathcal{J}\rho\,{}^{Z}_{0}N_I\;{}^{Z}_{0}F^{k}_{\alpha_{u_Z}}\;\ddot{r}_{0_j}\,\mathrm{d}\,{}_0V \end{aligned} \tag{4.35}$$

Centrifugal forces

The centrifugal acceleration in a finite element formulation generates both an additional stiffness matrix and an apparent force vector. Its contribution to the virtual work is:

$${}^{t+\Delta t}_{0}\delta W^{e\,\mathrm{stiff.}}_{\mathrm{CF}} = \int_{{}_0V^e} \mathcal{J}\rho\delta u_i\,(\Omega_{ip}\Omega_{pj})\,u_j\,\mathrm{d}\,{}_0V \tag{4.36}$$

$${}^{t+\Delta t}_{0}\delta W^{e\,\mathrm{force}}_{\mathrm{CF}} = \int_{{}_0V^e} \mathcal{J}\rho\delta u_i\,(\Omega_{ip}\Omega_{pj}X_j)\;\mathrm{d}\,{}_0V \tag{4.37}$$

Performing the spatial discretization of both terms:

$$\begin{aligned} {}^{t+\Delta t}_{0}\delta W^{e\,\mathrm{stiff.}}_{\mathrm{CF}} = {}& {}_{0}\delta U^{k}_{X\alpha_{u_X}I}\left[\int_{{}_0V^e} \mathcal{J}\rho\,{}^{X}_{0}N_I\;{}^{X}_{0}F^{k}_{\alpha_{u_X}}\;\Omega_{1p}\Omega_{p1}\,{}^{X}_{0}F^{k}_{\alpha_{u_X}}\;{}^{X}_{0}N_J\,\mathrm{d}\,{}_0V\right]{}_{0}\ddot{U}^{k}_{X\beta_{u_X}J} + \\ & {}_{0}\delta U^{k}_{X\alpha_{u_X}I}\left[\int_{{}_0V^e} \mathcal{J}\rho\,{}^{X}_{0}N_I\;{}^{X}_{0}F^{k}_{\alpha_{u_X}}\;\Omega_{1p}\Omega_{p2}\,{}^{Y}_{0}F^{k}_{\alpha_{u_Y}}\;{}^{Y}_{0}N_J\,\mathrm{d}\,{}_0V\right]{}_{0}\dot{U}^{k}_{Y\beta_{u_Y}J} + \\ & {}_{0}\delta U^{k}_{X\alpha_{u_X}I}\left[\int_{{}_0V^e} \mathcal{J}\rho\,{}^{X}_{0}N_I\;{}^{X}_{0}F^{k}_{\alpha_{u_X}}\;\Omega_{1p}\Omega_{p3}\,{}^{Z}_{0}F^{k}_{\alpha_{u_Z}}\;{}^{Z}_{0}N_J\,\mathrm{d}\,{}_0V\right]{}_{0}\dot{U}^{k}_{Z\beta_{u_Z}J} + \ldots \end{aligned} \tag{4.38}$$

$$\begin{aligned} {}^{t+\Delta t}_{0}\delta W^{e\,\mathrm{force}}_{\mathrm{CF}} = {}& {}_{0}\delta U^{k}_{X\alpha_{u_X}I}\left[\int_{{}_0V^e} \mathcal{J}\rho\,{}^{X}_{0}N_I\;{}^{X}_{0}F^{k}_{\alpha_{u_X}}\;\Omega_{1p}\Omega_{pq}X_j\mathrm{d}\,{}_0V\right] + \\ & {}_{0}\delta U^{k}_{Y\alpha_{u_Y}I}\left[\int_{{}_0V^e} \mathcal{J}\rho\,{}^{Y}_{0}N_I\;{}^{Y}_{0}F^{k}_{\alpha_{u_Y}}\;\Omega_{2p}\Omega_{pq}X_j\mathrm{d}\,{}_0V\right] + \\ & {}_{0}\delta U^{k}_{Z\alpha_{u_Z}I}\left[\int_{{}_0V^e} \mathcal{J}\rho\,{}^{Z}_{0}N_I\;{}^{Z}_{0}F^{k}_{\alpha_{u_Z}}\;\Omega_{3p}\Omega_{pq}X_j\mathrm{d}\,{}_0V\right] \end{aligned} \tag{4.39}$$

The stiffness and force kernels of the apparent centrifugal force due to the rotation of the body can be identified:

$$
\begin{aligned}
{}^{t+\Delta t}_{0}\delta W^{e}_{\mathrm{CF}} &= \delta\mathbf{U}^{T}\mathbf{F}_{\mathrm{CF}} + \delta\mathbf{U}^{T}\mathbf{K}_{\mathrm{CF}}\ddot{\mathbf{U}} = \\
&= {}_{0}\delta U^{k}_{X\alpha_{u_X}I}\,{}^{t+\Delta t}_{0}F^{\alpha_{u_X}I}_{\mathrm{CF}\,u_X} + {}_{0}\delta U^{k}_{Y\alpha_{u_Y}I}\,{}^{t+\Delta t}_{0}F^{\alpha_{u_Y}I}_{\mathrm{CF}\,u_Y} + {}_{0}\delta U^{k}_{Z\alpha_{u_Z}I}\,{}^{t+\Delta t}_{0}F^{\alpha_{u_Z}I}_{\mathrm{CF}\,u_Z} + \\
&+ {}_{0}\delta U^{k}_{X\alpha_{u_X}I}\left[{}^{0}_{0}K^{\alpha_{u_X}\beta_{u_X}IJ}_{\mathrm{CF}\,u_X u_X}\right]{}_{0}\dot{U}^{k}_{X\beta_{u_X}J} + {}_{0}\delta U^{k}_{X\alpha_{u_X}I}\left[{}^{0}_{0}K^{\alpha_{u_X}\beta_{u_Y}IJ}_{\mathrm{CF}\,u_X u_Y}\right]{}_{0}\dot{U}^{k}_{Y\beta_{u_Y}J} + \\
&+ {}_{0}\delta U^{k}_{X\alpha_{u_X}I}\left[{}^{0}_{0}K^{\alpha_{u_X}\beta_{u_Z}IJ}_{\mathrm{CF}\,u_X u_Z}\right]{}_{0}\dot{U}^{k}_{Z\beta_{u_Z}J} + {}_{0}\delta U^{k}_{Y\alpha_{u_Y}I}\left[{}^{0}_{0}K^{\alpha_{u_Y}\beta_{u_X}IJ}_{\mathrm{CF}\,u_Y u_X}\right]{}_{0}\dot{U}^{k}_{X\beta_{u_X}J} + \\
&+ {}_{0}\delta U^{k}_{Y\alpha_{u_Y}I}\left[{}^{0}_{0}K^{\alpha_{u_Y}\beta_{u_Y}IJ}_{\mathrm{CF}\,u_Y u_Y}\right]{}_{0}\dot{U}^{k}_{Y\beta_{u_Y}J} + {}_{0}\delta U^{k}_{Y\alpha_{u_Y}I}\left[{}^{0}_{0}K^{\alpha_{u_Y}\beta_{u_Z}IJ}_{\mathrm{CF}\,u_Y u_Z}\right]{}_{0}\dot{U}^{k}_{Z\beta_{u_Z}J} + \\
&+ {}_{0}\delta U^{k}_{Z\alpha_{u_Z}I}\left[{}^{0}_{0}K^{\alpha_{u_Z}\beta_{u_X}IJ}_{\mathrm{CF}\,u_Z u_X}\right]{}_{0}\dot{U}^{k}_{X\beta_{u_X}J} + {}_{0}\delta U^{k}_{Z\alpha_{u_Z}I}\left[{}^{0}_{0}K^{\alpha_{u_Z}\beta_{u_Y}IJ}_{\mathrm{CF}\,u_Z u_Y}\right]{}_{0}\dot{U}^{k}_{Y\beta_{u_Y}J} + \\
&+ {}_{0}\delta U^{k}_{Z\alpha_{u_Z}I}\left[{}^{0}_{0}K^{\alpha_{u_Z}\beta_{u_Z}IJ}_{\mathrm{CF}\,u_Z u_Z}\right]{}_{0}\dot{U}^{k}_{Z\beta_{u_Z}J}
\end{aligned}
\tag{4.40}
$$

For example:

$$
{}^{t+\Delta t}_{0}F^{\alpha_{u_X}I}_{\mathrm{CF}\,u_X} = \int_{{}_{0}V^{e}} \mathcal{J}\rho\,{}^{X}_{0}N_I\;{}^{X}_{0}F^{k}_{\alpha_{u_X}}\;\Omega_{1p}\Omega_{pj}X_j\,\mathrm{d}\,{}_{0}V \tag{4.41}
$$

$$
{}^{0}_{0}K^{\alpha_{u_X}\beta_{u_X}IJ}_{\mathrm{CF}\,u_X u_X} = \int_{{}_{0}V^{e}} \mathcal{J}\rho\,{}^{X}_{0}N_I\;{}^{X}_{0}F^{k}_{\alpha_{u_X}}\;\Omega_{1p}\Omega_{p1}\,{}^{X}_{0}F^{k}_{\alpha_{u_X}}\;{}^{X}_{0}N_J\,\mathrm{d}\,{}_{0}V \tag{4.42}
$$

Euler forces

As the centrifugal force also the Euler force provides an additional stiffness matrix and an apparent force vector. Its contribution to the virtual work is:

$$
{}^{t+\Delta t}_{0}\delta W^{e\,\mathrm{stiff}}_{\mathrm{EU}} = \int_{{}_{0}V^{e}} \mathcal{J}\rho\delta u_i\dot{\Omega}_{ij}u_j\,\mathrm{d}\,{}_{0}V \tag{4.43}
$$

$$
{}^{t+\Delta t}_{0}\delta W^{e\,\mathrm{force}}_{\mathrm{EU}} = \int_{{}_{0}V^{e}} \mathcal{J}\rho\delta u_i\dot{\Omega}_{ij}X_j\,\mathrm{d}\,{}_{0}V \tag{4.44}
$$

Performing the spatial discretization of both terms:

$$
\begin{aligned}
{}^{t+\Delta t}_{0}\delta W^{e\,\mathrm{stiff.}}_{\mathrm{EU}} &= \delta\mathbf{U}^{T}\mathbf{K}_{\mathrm{EU}}\mathbf{U} = \\
&= {}_{0}\delta U^{k}_{X\alpha_{u_X}I}\left[\int_{{}_{0}V^{e}} \mathcal{J}\rho\,{}^{X}_{0}N_I\;{}^{X}_{0}F^{k}_{\alpha_{u_X}}\;\dot{\Omega}_{11}\,{}^{X}_{0}F^{k}_{\alpha_{u_X}}\;{}^{X}_{0}N_J\,\mathrm{d}\,{}_{0}V\right]{}_{0}U^{k}_{X\beta_{u_X}J} + \\
&\quad {}_{0}\delta U^{k}_{X\alpha_{u_X}I}\left[\int_{{}_{0}V^{e}} \mathcal{J}\rho\,{}^{X}_{0}N_I\;{}^{X}_{0}F^{k}_{\alpha_{u_X}}\;\dot{\Omega}_{12}\,{}^{Y}_{0}F^{k}_{\alpha_{u_Y}}\;{}^{Y}_{0}N_J\,\mathrm{d}\,{}_{0}V\right]{}_{0}U^{k}_{Y\beta_{u_Y}J} + \\
&\quad {}_{0}\delta U^{k}_{X\alpha_{u_X}I}\left[\int_{{}_{0}V^{e}} \mathcal{J}\rho\,{}^{X}_{0}N_I\;{}^{X}_{0}F^{k}_{\alpha_{u_X}}\;\dot{\Omega}_{13}\,{}^{Z}_{0}F^{k}_{\alpha_{u_Z}}\;{}^{Z}_{0}N_J\,\mathrm{d}\,{}_{0}V\right]{}_{0}U^{k}_{Z\beta_{u_Z}J} + \ldots
\end{aligned}
\tag{4.45}
$$

$$
\begin{aligned}
{}^{t+\Delta t}_{0}\delta W^{e\,\text{force}}_{\text{EU}} &= \delta\mathbf{U}^T\mathbf{F}_{\text{EU}} = \\
&= {}_0\delta U^k_{X\alpha_{u_X}I}\left[\int_{{}_0V^e}\mathcal{J}\rho\,{}^X_0N_I\;{}^X_0F^k_{\alpha_{u_X}}\;\dot\Omega_{1j}X_j\,\mathrm{d}\,{}_0V\right]+ \\
&\quad {}_0\delta U^k_{Y\alpha_{u_Y}I}\left[\int_{{}_0V^e}\mathcal{J}\rho\,{}^Y_0N_I\;{}^Y_0F^k_{\alpha_{u_Y}}\;\dot\Omega_{2j}X_j\,\mathrm{d}\,{}_0V\right]+ \\
&\quad {}_0\delta U^k_{Z\alpha_{u_Z}I}\left[\int_{{}_0V^e}\mathcal{J}\rho\,{}^Z_0N_I\;{}^Z_0F^k_{\alpha_{u_Z}}\;\dot\Omega_{3j}X_j\,\mathrm{d}\,{}_0V\right]
\end{aligned}
\tag{4.46}
$$

The relative kernels can be identified, e.g.:

$$
{}^{t+\Delta t}_{0}F^{\alpha_{u_X}I}_{\text{EU}\,u_X} = \int_{{}_0V^e}\mathcal{J}\rho\,{}^X_0N_I\;{}^X_0F^k_{\alpha_{u_X}}\;\dot\Omega_{1j}X_j\,\mathrm{d}\,{}_0V \tag{4.47}
$$

$$
{}^0_0K^{\alpha_{u_X}\beta_{u_X}IJ}_{\text{EU}\,u_Xu_X} = \int_{{}_0V^e}\mathcal{J}\rho\,{}^X_0N_I\;{}^X_0F^k_{\alpha_{u_X}}\;\dot\Omega_{11}X_j\,\mathrm{d}\,{}_0V \tag{4.48}
$$

Coriolis forces

The Coriolis acceleration provides an additional damping matrix added, if present, to the structural ones. The virtual work contribution is:

$$
{}^{t+\Delta t}_{0}\delta W^e_{\text{CR}} = \int_{{}_0V^e}\mathcal{J}\rho\delta u_i 2\,{}_I\Omega_{ij}\dot u_j\,\mathrm{d}\,{}_0V \tag{4.49}
$$

GUF as well the spatial discretization are applied to both the virtual displacement and the velocity. e.g.

$$
{}_0\delta u^k_X(X,Y,Z^k) = {}^X_0F^k_{\alpha_{u_X}}(Z^k)\,{}^X_0N_I(X,Y)\;{}_0\delta U^k_{X\alpha_{u_X}I}(X,Y)\quad \alpha_{u_X}=t,l,b\quad l=2,\ldots,N^k_{u_X}\quad I=1,2,\ldots M_n \tag{4.50}
$$

$$
{}_0\dot u^k_X(X,Y,Z^k) = {}^X_0F^k_{\alpha_{u_X}}(Z^k)\,{}^X_0N_I(X,Y)\;{}_0\dot U^k_{X\alpha_{u_X}I}(X,Y)\quad \alpha_{u_X}=t,l,b\quad l=2,\ldots,N^k_{u_X}\quad I=1,2,\ldots M_n \tag{4.51}
$$

The explicit expression for the semi-discretized form of Eq. 4.49 is

$$
\begin{aligned}
{}^{t+\Delta t}_{0}\delta W^e_{\text{CR}} &= {}_0\delta U^k_{X\alpha_{u_X}I}\left[2\int_{{}_0V^e}\mathcal{J}\rho\,{}^X_0N_I\;{}^X_0F^k_{\alpha_{u_X}}\;\Omega_{11}\,{}^X_0F^k_{\alpha_{u_X}}\;{}^X_0N_J\,\mathrm{d}\,{}_0V\right]{}_0\dot U^k_{X\beta_{u_X}J}+ \\
&\quad {}_0\delta U^k_{X\alpha_{u_X}I}\left[2\int_{{}_0V^e}\mathcal{J}\rho\,{}^X_0N_I\;{}^X_0F^k_{\alpha_{u_X}}\;\Omega_{12}\,{}^Y_0F^k_{\alpha_{u_Y}}\;{}^Y_0N_J\,\mathrm{d}\,{}_0V\right]{}_0\dot U^k_{Y\beta_{u_Y}J}+ \\
&\quad {}_0\delta U^k_{X\alpha_{u_X}I}\left[2\int_{{}_0V^e}\mathcal{J}\rho\,{}^X_0N_I\;{}^X_0F^k_{\alpha_{u_X}}\;\Omega_{13}\,{}^Z_0F^k_{\alpha_{u_Z}}\;{}^Z_0N_J\,\mathrm{d}\,{}_0V\right]{}_0\dot U^k_{Z\beta_{u_Z}J}+\ldots
\end{aligned}
\tag{4.52}
$$

It is possible to recognize the damping matrix:

$$
\begin{aligned}
{}^{t+\Delta t}_{0}\delta W^{e}_{\mathrm{CR}} &= \delta\mathbf{U}^{T}\mathbf{D}_{\mathrm{CR}}\dot{\mathbf{U}} = \\
&= {}_{0}\delta U^{k}_{X\alpha_{u_X}I}\left[{}^{0}_{0}D^{\alpha_{u_X}\beta_{u_X}IJ}_{u_X u_X}\right]{}_{0}\dot{U}^{k}_{X\beta_{u_X}J} + {}_{0}\delta U^{k}_{X\alpha_{u_X}I}\left[{}^{0}_{0}D^{\alpha_{u_X}\beta_{u_Y}IJ}_{u_X u_Y}\right]{}_{0}\dot{U}^{k}_{Y\beta_{u_Y}J} + \\
&+ {}_{0}\delta U^{k}_{X\alpha_{u_X}I}\left[{}^{0}_{0}D^{\alpha_{u_X}\beta_{u_Z}IJ}_{u_X u_Z}\right]{}_{0}\dot{U}^{k}_{Z\beta_{u_Z}J} + {}_{0}\delta U^{k}_{Y\alpha_{u_Y}I}\left[{}^{0}_{0}D^{\alpha_{u_Y}\beta_{u_X}IJ}_{u_Y u_X}\right]{}_{0}\dot{U}^{k}_{X\beta_{u_X}J} + \\
&+ {}_{0}\delta U^{k}_{Y\alpha_{u_Y}I}\left[{}^{0}_{0}D^{\alpha_{u_Y}\beta_{u_Y}IJ}_{u_Y u_Y}\right]{}_{0}\dot{U}^{k}_{Y\beta_{u_Y}J} + {}_{0}\delta U^{k}_{Y\alpha_{u_Y}I}\left[{}^{0}_{0}D^{\alpha_{u_Y}\beta_{u_Z}IJ}_{u_Y u_Z}\right]{}_{0}\dot{U}^{k}_{Z\beta_{u_Z}J} + \\
&+ {}_{0}\delta U^{k}_{Z\alpha_{u_Z}I}\left[{}^{0}_{0}D^{\alpha_{u_Z}\beta_{u_X}IJ}_{u_Z u_X}\right]{}_{0}\dot{U}^{k}_{X\beta_{u_X}J} + {}_{0}\delta U^{k}_{Z\alpha_{u_Z}I}\left[{}^{0}_{0}D^{\alpha_{u_Z}\beta_{u_Y}IJ}_{u_Z u_Y}\right]{}_{0}\dot{U}^{k}_{Y\beta_{u_Y}J} + \\
&+ {}_{0}\delta U^{k}_{Z\alpha_{u_Z}I}\left[{}^{0}_{0}D^{\alpha_{u_Z}\beta_{u_Z}IJ}_{u_Z u_Z}\right]{}_{0}\dot{U}^{k}_{Z\beta_{u_Z}J}
\end{aligned}
\tag{4.53}
$$

where for example the kernel of the matrix relating the α_{ux} term of the polynomial/Legendre function for the x displacement of the node I and the α_{uy} for the y velocity function of node J is

$$
{}^{0}_{0}D^{\alpha_{u_X}\beta_{u_Y}IJ}_{\mathrm{CR}u_X u_Y} = 2\int_{{}_{0}V^{e}} \mathcal{J}\rho\, {}^{X}_{0}N_I\ {}^{X}_{0}F^{k}_{\alpha_{u_X}}\ \Omega_{12}\, {}^{Y}_{0}F^{k}_{\alpha_{u_Y}}\ {}^{Y}_{0}N_J\ \mathrm{d}\,{}_{0}V \tag{4.54}
$$

Residual equation

The choice of a moving frame attached to the body alter the expression of the semidiscrete residual equation (see Eq. 4.10). It modifies the effective stiffness, damping matrices and the external force vector. At a generic instant the residual is:

$$
\mathbf{R} = \mathbf{M}\ddot{\mathbf{U}} + \mathbf{D}_{GYR}(\boldsymbol{\Omega})\dot{\mathbf{U}} + \mathbf{K}_{\mathrm{DYN}}(\boldsymbol{\Omega},\dot{\boldsymbol{\Omega}})\mathbf{U} + \mathbf{F}_{\mathrm{INT}}(\mathbf{U}) - \mathbf{F}_{\mathrm{EXT}} + \mathbf{F}_{\mathrm{TR}}(\ddot{\mathbf{r}}_o) + \mathbf{F}_{\mathrm{EU}}(\dot{\boldsymbol{\Omega}}) + \mathbf{F}_{\mathrm{CF}}(\boldsymbol{\Omega}) = \mathbf{0} \tag{4.55}
$$

where $\mathbf{D}_{\mathrm{GYR}}$ is the *gyroscopic damping matrix* (Eq. 4.53) and $\mathbf{K}_{\mathrm{DYN}}$ is the *dynamic stiffness matrix*:

$$
\begin{aligned}
\mathbf{D}_{\mathrm{GYR}} &= \mathbf{D}_{\mathrm{CR}} \\
\mathbf{K}_{\mathrm{DYN}} &= \mathbf{K}_{\mathrm{CR}} + \mathbf{K}_{\mathrm{EU}}
\end{aligned}
\tag{4.56}
$$

4.4 Time integration algorithm

Up to this point the weak form has been discretized in space through the use of a finite element method. The resulting semidiscrete equation has been derived for both inertial (see Eq. 4.10) and body (see Eq. 4.55) reference systems. These equations now have to be discretized in time and solved with a time integration algorithm. In structural dynamic the most common is the Newmark β-method [106]. Its characteristics like stability, accuracy and numerical dissipation are controlled by two free parameters. In many application it is useful to have some numerical dissipation to remove the high-frequency content from

the solution. This is possible with the Newmark method, but at the cost of loosing the quadratic convergence rate. Several other methods were developed to mantain second order accuracy and dissipate high-frequency modes like the HHT-α method [107] and Bossak-Newmark method [108]. The integration algorithm adopted in this dissertation is the generalized α-method [109]. This method encompass many family of methods, including the few just cited. This section will provide an overview of the procedure to derived the discretized equation of motion and its practical implementation in a software used to generate the results that will be shown in the next chapters.

4.4.1 Generalized α-method

For the analysis of the method is convenient to use the semidiscretized finite element equation derived from the weak form in residual form:

$$\mathbf{R} = \mathbf{M}\ddot{\mathbf{U}} + \mathbf{D}\dot{\mathbf{U}} + \mathbf{F}_{\text{INT}}(\mathbf{U}) - \mathbf{F}_{\text{EXT}} = \mathbf{0} \tag{4.57}$$

This residual should be satisfied always, but in a numerical method only the satisfaction at discrete times are requested. In general the solution a time step t is known and we are looking for the value of the displacement field at time $t + \Delta t$ that satisfy the residual equation:

$$^{t+\Delta t}\mathbf{R} = \mathbf{M}\,{}^{t+\Delta t}\ddot{\mathbf{U}} + {}^{t+\Delta t}\mathbf{F}_{\text{EXT}} - {}^{t+\Delta t}\mathbf{F}_{\text{INT}}({}^{t+\Delta t}\mathbf{U}) = \mathbf{0} \tag{4.58}$$

In the generalized α-method intermediate values inside the time step are considered and a modified version of the residual has to be satisfied:

$$^{t+\Delta t}\mathbf{R} = \mathbf{M}\,{}^{\alpha_m}\ddot{\mathbf{U}} + \mathbf{D}\,{}^{\alpha_f}\dot{\mathbf{U}} + {}^{\alpha_f}\mathbf{F}_{\text{INT}} - {}^{\alpha_f}\mathbf{F}_{\text{EXT}} = \mathbf{0} \tag{4.59}$$

where α_f and α_m are parameter used to interpolate the displacement solution:

$$\begin{aligned}
{}^{\alpha_f}\mathbf{U} &= (1-\alpha_f)\,{}^{t}\mathbf{U} + \alpha_f\,{}^{t+\Delta t}\mathbf{U} &&= {}^{t}\mathbf{U} + \alpha_f\Delta\mathbf{U} \\
{}^{\alpha_f}\dot{\mathbf{U}} &= (1-\alpha_f)\,{}^{t}\dot{\mathbf{U}} + \alpha_f\,{}^{t+\Delta t}\dot{\mathbf{U}} &&= {}^{t}\dot{\mathbf{U}} + \alpha_f\Delta\dot{\mathbf{U}} \\
{}^{\alpha_m}\ddot{\mathbf{U}} &= (1-\alpha_m)\,{}^{t}\ddot{\mathbf{U}} + \alpha_m\,{}^{t+\Delta t}\ddot{\mathbf{U}} &&= {}^{t}\ddot{\mathbf{U}} + \alpha_m\Delta\ddot{\mathbf{U}} \\
{}^{\alpha_f}\mathbf{F}_{\text{EXT}} &= (1-\alpha_f)\,{}^{t}\mathbf{F}_{\text{EXT}} + \alpha_f\,{}^{t+\Delta t}\mathbf{F}_{\text{EXT}} &&= {}^{t}\mathbf{F}_{\text{EXT}} + \alpha_f\Delta\mathbf{F}_{\text{EXT}}
\end{aligned} \tag{4.60}$$

The Newmark approximation [106] is also used:

$$\begin{cases} {}^{t+\Delta t}\mathbf{U} = {}^{t}\mathbf{U} + \Delta t\, {}^{t}\dot{\mathbf{U}} + \Delta t^2 \left[\left(\frac{1}{2} - \beta \right) {}^{t}\ddot{\mathbf{U}} + \beta\, {}^{t+\Delta t}\ddot{\mathbf{U}} \right] \\ {}^{t+\Delta t}\dot{\mathbf{U}} = {}^{t}\dot{\mathbf{U}} + \Delta t \left[(1-\gamma)\, {}^{t}\ddot{\mathbf{U}} + \gamma\, {}^{t+\Delta t}\ddot{\mathbf{U}} \right] \end{cases} \tag{4.61}$$

where β and γ are parameters that regulate how much the acceleration at the end of the time steps affect the displacement and velocity values. Rearranging it is possible to express the velocity and acceleration at the end of the time step $(t + \Delta t)$ as a function of their initial values (t) and the displacement increments:

$$\begin{cases} {}^{t+\Delta t}\dot{\mathbf{U}} = \frac{\gamma}{\beta \Delta t} \Delta \mathbf{U} + \left(1 - \frac{\gamma}{\beta} \right) {}^{t}\dot{\mathbf{U}} + \Delta t \left(1 - \frac{\gamma}{2\beta} \right) {}^{t}\ddot{\mathbf{U}} \\ {}^{t+\Delta t}\ddot{\mathbf{U}} = \frac{1}{\beta \Delta t^2}\, \Delta \mathbf{U} - \frac{1}{\beta \Delta t}\, {}^{t}\dot{\mathbf{U}} + \left(1 - \frac{1}{2\beta} \right) {}^{t}\ddot{\mathbf{U}} \end{cases} \tag{4.62}$$

with $\Delta \mathbf{U} = {}^{t+\Delta t}\mathbf{U} - {}^{t}\mathbf{U}$. Substituting the Newmark approximation in Eq. 4.60 the velocities and accelerations at the intermediate times are known as a function of the incremental displacements:

$$\begin{aligned} {}^{\alpha_f}\mathbf{U} &= {}^{t}\mathbf{U} + \alpha_f \Delta \mathbf{U} \\ {}^{\alpha_f}\dot{\mathbf{U}} &= \left(1 - \alpha_f \frac{\gamma}{\beta} \right) {}^{t}\dot{\mathbf{U}} + \alpha_f \Delta t \left(1 - \frac{\gamma}{2\beta} \right) {}^{t}\ddot{\mathbf{U}} + \frac{\alpha_f \gamma}{\beta \Delta t} \Delta \mathbf{U} \\ {}^{\alpha_m}\ddot{\mathbf{U}} &= \left(1 - \frac{\alpha_m}{2\beta} \right) {}^{t}\ddot{\mathbf{U}} - \frac{\alpha_m}{\beta \Delta t}\, {}^{t}\dot{\mathbf{U}} + \frac{\alpha_m}{\beta \Delta t^2} \Delta \mathbf{U} \end{aligned}$$

And then substituting Eq. 4.63 in Eq. 4.59 the residual expression for the generalized α-method can be found:

$$\begin{aligned} {}^{t+\Delta t}\mathbf{R} = {} & \frac{\alpha_m}{\beta \Delta t^2} \mathbf{M} \Delta \mathbf{U} + \frac{\alpha_f \gamma}{\beta \Delta t} \mathbf{D} \Delta \mathbf{U} + \alpha_f\, {}^{t+\Delta t}\mathbf{F}_{\mathrm{INT}}(\mathbf{U}) + (1-\alpha_f)\, {}^{t}\mathbf{F}_{\mathrm{INT}} - (1-\alpha_f)\, {}^{t}\mathbf{F}_{\mathrm{EXT}} + \\ & - \alpha_f\, {}^{t+\Delta t}\mathbf{F}_{\mathrm{EXT}} + \left[\left(1 - \frac{\alpha_m}{2\beta} \right) \mathbf{M} + \alpha_f \Delta t \left(1 - \frac{\gamma}{2\beta} \right) \mathbf{D} \right] {}^{t}\ddot{\mathbf{U}} + \left[-\frac{\alpha_m}{\beta \Delta t} \mathbf{M} + \left(1 - \alpha_f \frac{\gamma}{\beta} \right) \mathbf{D} \right] {}^{t}\dot{\mathbf{U}} = \mathbf{0} \end{aligned} \tag{4.63}$$

Since the equation is nonlinear an iterative algorithm should be used to solve a series of linearized systems. If we use Newton-Raphson to drive the residual to zero:

$$\mathbf{0} = {}^{t+\Delta t}\mathbf{R}^{i} + \left(\frac{\partial\, {}^{t+\Delta t}\mathbf{R}^{i}}{\partial\, {}^{t+\Delta t}\mathbf{U}} \right) \Delta \mathbf{U}^{i+1} \tag{4.64}$$

where i is the iteration counter and $\Delta\mathbf{U}^{i+1} = {}^{t+\Delta t}\mathbf{U}^{i+1} - {}^{t+\Delta t}\mathbf{U}^{i}$. The resulting linearized equation:

$$\left[\frac{\alpha_m}{\beta\Delta t^2}\mathbf{M} + \frac{\alpha_f\gamma}{\beta\Delta t}\mathbf{D} + \alpha_f\mathbf{K}^i_{\mathrm{TAN}}\right]\Delta\mathbf{U}^{i+1} = \left(-\frac{\alpha_m}{\beta\Delta t^2}\mathbf{M} - \frac{\alpha_f\gamma}{\beta\Delta t}\mathbf{D}\right)\Delta\mathbf{U}^{i} + \alpha_f\left({}^{t+\Delta t}\mathbf{F}^i_{\mathrm{EXT}} - {}^{t+\Delta t}\mathbf{F}^i_{\mathrm{INT}}\right) -$$
$$-(1-\alpha_f)\left({}^{t}\mathbf{F}_{\mathrm{EXT}} - {}^{t}\mathbf{F}_{\mathrm{INT}}\right) - \left[\left(1-\frac{\alpha_m}{2\beta}\right)\mathbf{M} + \alpha_f\Delta t\left(1-\frac{\gamma}{2\beta}\right)\mathbf{D}\right]{}^{t}\ddot{\mathbf{U}} - \left[-\frac{\alpha_m}{\beta\Delta t}\mathbf{M} + \left(1-\alpha_f\frac{\gamma}{\beta}\right)\mathbf{D}\right]{}^{t}\dot{\mathbf{U}} \tag{4.65}$$

This equation can be used for both an inertial and a moving reference system and the actual arrays expressions depend on which is chosen. The complete expressions are shown in table 4.1. The material stiffness matrices $\mathbf{K}_{\mathrm{L}}$ and $\mathbf{K}_{\mathrm{NL}}$, the spring stiffness matrix $\mathbf{K}_{\mathrm{SP}}$, the internal $\mathbf{F}_{\mathrm{INT}}$ and external force vector $\mathbf{F}_{\mathrm{EXT}}$ have been derived in chapter 3 because unchanged with respect the static case.

Table 4.1: Finite element arrays for time integration algorithm used in Eq. 4.65. The terms in the last two columns are the arrays as computed in the previous sections.

Array	Symbols (Eq.4.65)	Inertial coord. sys.	Body coord. sys.
tangent stiffness matrix	$\mathbf{K}_{TAN}$	$\mathbf{K}_{\mathrm{L}} + \mathbf{K}_{\mathrm{NL}} + \mathbf{K}_{\mathrm{SP}}$	$\mathbf{K}_{\mathrm{L}} + \mathbf{K}_{\mathrm{NL}} + \mathbf{K}_{\mathrm{SP}} + \mathbf{K}_{\mathrm{DYN}}$
damping matrix	$\mathbf{D}$	$\mathbf{0}$	$\mathbf{D}_{GYR}$
mass matrix	$\mathbf{M}$	$\mathbf{M}$	$\mathbf{M}$
external force vector	$\mathbf{F}_{\mathrm{EXT}}$	$\mathbf{F}_{\mathrm{EXT}}$	$\mathbf{F}_{\mathrm{EXT}}$ - $\mathbf{F}_{\mathrm{TR}}$ - $\mathbf{F}_{\mathrm{EU}}$ - $\mathbf{F}_{\mathrm{CF}}$
internal force vector	$\mathbf{F}_{\mathrm{INT}}$	$\mathbf{F}_{\mathrm{INT}} + \mathbf{F}_{\mathrm{SP}}$	$\mathbf{F}_{\mathrm{INT}} + \mathbf{F}_{\mathrm{SP}}$

4.4.2 Predictor

The convergence, number of iteration, of the Newton-Raphson method can be accelerated with a good initial guess of the final solution. These guessed values are based only on the current converged state (t) of the systems and they are called *predictors*. In the current dissertation the following expression are used:

$$\begin{cases} {}^{t+\Delta t}\mathbf{U}^p = {}^{t}\mathbf{U} + \Delta t\,{}^{t}\dot{\mathbf{U}} + (1-2\beta)\dfrac{\Delta t^2}{2}\,{}^{t}\ddot{\mathbf{U}} & (4.66) \\ {}^{t+\Delta t}\dot{\mathbf{U}}^p = {}^{t}\dot{\mathbf{U}} + (1-\gamma)\Delta t\,{}^{t}\ddot{\mathbf{U}} & (4.67) \\ {}^{t+\Delta t}\ddot{\mathbf{U}}^p = 0 & (4.68) \end{cases}$$

Then Newmark approximation (see Eq. 4.61) can be rewritten as:

$$\begin{cases} {}^{t+\Delta t}\ddot{\mathbf{U}} = \dfrac{1}{\beta\Delta t^2}\left({}^{t+\Delta t}\mathbf{U} - {}^{t+\Delta t}\mathbf{U}^p\right) & (4.69) \\ {}^{t+\Delta t}\dot{\mathbf{U}} = {}^{t+\Delta t}\dot{\mathbf{U}}^p + \dfrac{\gamma}{\beta\Delta t}\left({}^{t+\Delta t}\mathbf{U} - {}^{t+\Delta t}\mathbf{U}^p\right) & (4.70) \end{cases}$$

From this new expression the linearized residual (Eq. 4.65) can be recasted as follows:

$$\left[\frac{\alpha_m}{\beta\Delta t^2}\mathbf{M}+\frac{\alpha_f\gamma}{\beta\Delta t}\mathbf{D}+\alpha_f\mathbf{K}^i_{\text{TAN}}\right]\left({}^{t+\Delta t}\mathbf{U}^{i+1}-{}^{t+\Delta t}\mathbf{U}^{i}\right)=\left(-\frac{\alpha_m}{\beta\Delta t^2}\mathbf{M}-\frac{\alpha_f\gamma}{\beta\Delta t}\mathbf{D}\right)\left({}^{t+\Delta t}\mathbf{U}^{i}-{}^{t+\Delta t}\mathbf{U}^{p}\right)$$
$$-\alpha_f\mathbf{D}\,{}^{t+\Delta t}\dot{\mathbf{U}}^{p}-(1-\alpha_f)\mathbf{D}\,{}^{t}\dot{\mathbf{U}}-(1-\alpha_m)\mathbf{M}\,{}^{t}\ddot{\mathbf{U}}+\alpha_f\left({}^{t+\Delta t}\mathbf{F}^i_{\text{EXT}}-{}^{t+\Delta t}\mathbf{F}^i_{\text{INT}}\right)$$
$$+(1-\alpha_f)\left({}^{t}\mathbf{F}_{\text{EXT}}-{}^{t}\mathbf{F}_{\text{INT}}\right) \tag{4.71}$$

From a purely implementation point of view it is convenient to compute and store the terms of the residual that are not updated during the Newton-Raphson iterations at the beginning of the time step. These terms are collected in the following arrays:

$$\begin{aligned}{}^{t+\Delta t}\mathbf{R}^{p} &= \left(\frac{\alpha_m}{\beta\Delta t^2}\mathbf{M}+\frac{\alpha_f\gamma}{\beta\Delta t}\mathbf{D}\right){}^{t+\Delta t}\mathbf{U}^{p}-\alpha_f\mathbf{D}\,{}^{t+\Delta t}\dot{\mathbf{U}}^{p}-(1-\alpha_f)\mathbf{D}\,{}^{t}\dot{\mathbf{U}}-(1-\alpha_m)\mathbf{M}\,{}^{t}\ddot{\mathbf{U}}\\ &+ (1-\alpha_f)\left({}^{t}\mathbf{F}_{\text{EXT}}-{}^{t}\mathbf{F}_{\text{INT}}\right)\end{aligned} \tag{4.72}$$

$$\mathbf{K}_{KIN}=\frac{\alpha_m}{\beta\Delta t^2}\mathbf{M}+\frac{\alpha_f\gamma}{\beta\Delta t}\mathbf{D} \tag{4.73}$$

And the equation to be solve at each iteration is:

$$\left[\mathbf{K}_{\text{KIN}}+\alpha_f\mathbf{K}^i_{\text{TAN}}\right]\Delta\mathbf{U}^{i+1}=-\mathbf{K}_{\text{KIN}}\,{}^{t+\Delta t}\mathbf{U}^{i}+\alpha_f\left({}^{t+\Delta t}\mathbf{F}^i_{\text{EXT}}-{}^{t+\Delta t}\mathbf{F}^i_{\text{INT}}\right)+{}^{t+\Delta t}\mathbf{R}^{p} \tag{4.74}$$

The iteration is stopped when the displacement increment and/or the residual norm are below certain tolerance value set by the user.

Chapter 5

Variable Angle Tow fiber model and stress recovery procedure

5.1 Variable Angle Tow

In a finite element method the modeling of the fiber's path comes down to the correct evaluation of the material coefficients and their in-plane derivatives at the Gauss points. This information is then used for the numerical integration over the domain to compute the elastic stiffness of the structure and for the correct evaluation of the transverse stresses through a recovery procedure.

5.1.1 Path definition

In the proposed formulation it is possible to define a different fiber's path for each layer. In accordance with the plate model the fiber path is defined on a plane parallel to the element X-Y plane. Moreover the fiber pattern associated with each layer is generated by translation of a single fiber called *fundamental curve* (see Fig. 5.1). The problem of describing the pattern is then shifted to the description of this fundamental curve. Its definition requires the introduction of multiple coordinate systems:

- global coordinate system ($\mathcal{X}$,$\mathcal{Y}$,$\mathcal{Z}$)
- local element coordinate system (X,Y,Z)
- local layer coordinate system ($\widehat{X}^k$,$\widehat{Y}^k$,$\widehat{Z}^k$)
- material coordinate systems (X_M^k, Y_M^k, Z_M^k)
- fundamental curve coordinate system (ξ^k,η^k)

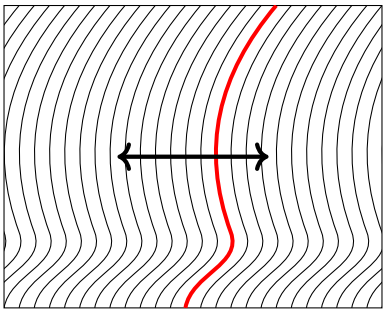

Figure 5.1: Allowed curvilinear pattern. It is generated by translation of a single fiber, *fundamental curve*, (in red).

The pattern for each layer is build in their layer coordinate systems ($\widehat{X}^k$,$\widehat{Y}^k$). It is generated from the translation of the fundamental curve along the $\widehat{X}^k$ axis. However the actual paths needs to be known through the point-wise definition of the angle ϑ^k between the element X-axis and the fibers' tangent (see Fig. 5.2). The stiffness matrix is build in the element reference system and consequently also the material coefficients have to be expressed in such reference.

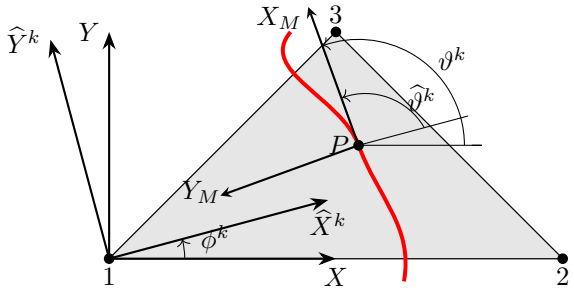

Figure 5.2: Layer coordinate systems and angles.

The spatial variation of the angle ϑ^k is provided by the user as input. Successively the equation of the fundamental fiber is approximated as a combination of Legendre polynomials whose coefficients can be determined through a collocation method.

$$\vartheta^k\left(\mu^k\right) = a_0^k P_0^k\left(\mu^k\right) + a_1^k P_1^k\left(\mu^k\right) + ... = a_t^k P_t^k\left(\mu^k\right) \qquad t = 0, 1, ..., T \tag{5.1}$$

Legendre polynomials are function of the parameter μ^k restricted in the interval [-1,1]. The mapping between this variable and the physical ones is obtained through the introduction of a new coordinate system (ξ^k,η^k) as shown in Fig. 5.3.

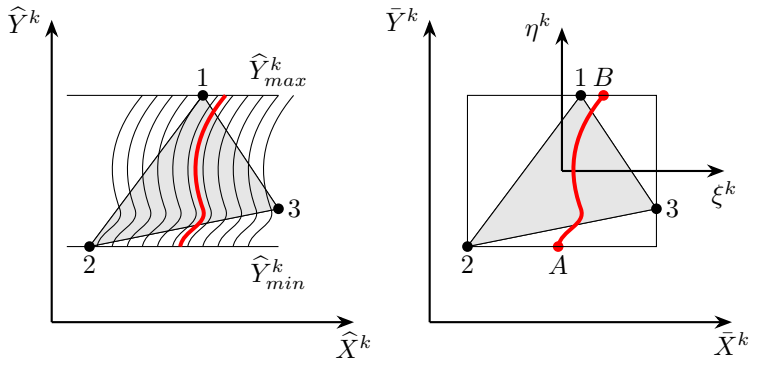

Figure 5.3: Fundamental curve coordinate system. (ξ^k,η^k)

The coordinate relations between the layer coordinate system and the auxiliary one are:

$$\begin{aligned}\widehat{X}^{\,k} &= \frac{\widehat{X}^{\,k}_{\max} + \widehat{X}^{\,k}_{\min}}{2} + \frac{\widehat{X}^{\,k}_{\max} - \widehat{X}^{\,k}_{\min}}{2}\xi^{\,k} \\ \widehat{Y}^{\,k} &= \frac{\widehat{Y}^{\,k}_{\max} + \widehat{Y}^{\,k}_{\min}}{2} + \frac{\widehat{Y}^{\,k}_{\max} - \widehat{Y}^{\,k}_{\min}}{2}\eta^{\,k}\end{aligned} \tag{5.2}$$

or equivalently

$$\begin{aligned}\xi^{\,k} &= -\frac{\widehat{X}^{\,k}_{\max} + \widehat{X}^{\,k}_{\min}}{\widehat{X}^{\,k}_{\max} - \widehat{X}^{\,k}_{\min}} + \frac{2}{\widehat{X}^{\,k}_{\max} - \widehat{X}^{\,k}_{\min}}\widehat{X}^{\,k} \\ \eta^{\,k} &= -\frac{\widehat{Y}^{\,k}_{\max} + \widehat{Y}^{\,k}_{\min}}{\widehat{Y}^{\,k}_{\max} - \widehat{Y}^{\,k}_{\min}} + \frac{2}{\widehat{Y}^{\,k}_{\max} - \widehat{Y}^{\,k}_{\min}}\widehat{Y}^{\,k}\end{aligned} \tag{5.3}$$

where $\widehat{X}^{\,k}_{\min}$, $\widehat{X}^{\,k}_{\max}$, $\widehat{Y}^{\,k}_{\min}$, $\widehat{Y}^{\,k}_{\max}$ are the minimum and maximum coordinate values of the element in consideration. The coordinate η^k, as $\mu^{\,k}$, is defined in the interval [-1,1]. It is assumed:

$$\mu^k = \begin{cases} +\eta^{\,k} & \text{if } \mu^k_A = -1 \\ -\eta^{\,k} & \text{if } \mu^k_A = +1 \end{cases} \tag{5.4}$$

then

$$\mu^{\,k} = \pm\eta^{\,k} \tag{5.5}$$

Thus, the transformation in Eq. 5.2 becomes:

$$\widehat{Y}^{\,k} = \frac{\widehat{Y}^{\,k}_{\max} + \widehat{Y}^{\,k}_{\min}}{2} \pm \frac{\widehat{Y}^{\,k}_{\max} - \widehat{Y}^{\,k}_{\min}}{2}\mu^{\,k} = \frac{\widehat{Y}^{\,k}_{\max} + \widehat{Y}^{\,k}_{\min}}{2} + \frac{\mu^{\,k}}{F} \tag{5.6}$$

where

$$F = \mp\frac{2}{\widehat{Y}^{\,k}_{\max} - \widehat{Y}^{\,k}_{\min}} \tag{5.7}$$

Expression 5.6 allows to perform the derivatives of the material properties using the path approxi-

mation in Eq. 5.1:

$$\frac{\partial(\square)}{\partial \widehat{Y}^{\,k}} = F \frac{\partial(\square)}{\partial \mu^{\,k}} \tag{5.8}$$

$\partial(\square)/\partial \widehat{X}^{\,k} = 0$ by construction (see Fig. 5.3).

5.1.2 Material coefficients

If the strain are small the constitutive relations developed for linear analysis can be used also for large displacement and large rotation analysis. The material is suppose to be orthotropic in the material reference frame and the stress-strain relation in terms of $SPKST$ and $GLST$ is

$$\begin{bmatrix} S_{XX} \\ S_{YY} \\ S_{XY} \\ S_{XZ} \\ S_{YZ} \\ S_{ZZ} \end{bmatrix}^k = \begin{bmatrix} \overline{C}_{11} & \overline{C}_{12} & \overline{C}_{16} & 0 & 0 & \overline{C}_{13} \\ \overline{C}_{12} & \overline{C}_{22} & \overline{C}_{26} & 0 & 0 & \overline{C}_{23} \\ \overline{C}_{16} & \overline{C}_{26} & \overline{C}_{66} & 0 & 0 & \overline{C}_{36} \\ 0 & 0 & 0 & \overline{C}_{55} & \overline{C}_{45} & 0 \\ 0 & 0 & 0 & \overline{C}_{45} & \overline{C}_{44} & 0 \\ \overline{C}_{13} & \overline{C}_{23} & \overline{C}_{36} & 0 & 0 & \overline{C}_{33} \end{bmatrix}^k \begin{bmatrix} E_{XX} \\ E_{YY} \\ 2E_{XY} \\ 2E_{XZ} \\ 2E_{YZ} \\ E_{ZZ} \end{bmatrix}^k \tag{5.9}$$

$\overline{C}^k_{ij}$ are the material coefficient (C^k_{ij}) rotated in the element reference frame:

$$\begin{aligned}
&C^k_{11} = \frac{1-\upsilon^k_{23}\upsilon^k_{32}}{\Delta^k} E^k_{11} \qquad C^k_{12} = \frac{\upsilon^k_{21}+\upsilon^k_{23}\upsilon_{31}}{\Delta^k} E^k_{11} \qquad C^k_{22} = \frac{1-\upsilon^k_{13}\upsilon^k_{31}}{\Delta^k} E^k_{22} \\
&C^k_{13} = \frac{\upsilon^k_{21}\upsilon^k_{32}+\upsilon_{31}}{\Delta^k} E^k_{11} \quad C^k_{23} = \frac{\upsilon^k_{32}+\upsilon^k_{12}\upsilon_{31}}{\Delta^k} E^k_{22} \qquad C^k_{33} = \frac{1-\upsilon^k_{12}\upsilon^k_{21}}{\Delta^k} E^k_{33} \\
&C^k_{44} = G^k_{23} \qquad C^k_{55} = G^k_{13} \qquad C^k_{66} = G^k_{12} \\
&\Delta^k = 1-\upsilon^k_{23}\upsilon^k_{32}-\upsilon^k_{12}\upsilon_{21}-\upsilon^k_{13}\upsilon^k_{31}-2\upsilon^k_{21}\upsilon^k_{32}\upsilon^k_{13} \\
&\upsilon^k_{32} = \frac{E^k_{33}}{E^k_{22}}\upsilon^k_{23} \qquad \upsilon^k_{21} = \frac{E^k_{22}}{E^k_{11}}\upsilon^k_{12} \qquad \upsilon^k_{31} = \frac{E^k_{33}}{E^k_{11}}\upsilon^k_{13}
\end{aligned} \tag{5.10}$$

where E^k_{11}, E^k_{22}, E^k_{33}, G^k_{12}, G^k_{13}, G^k_{23}, ν^k_{12}, ν^k_{13}, ν^k_{23} are the the elastic moduli and Poisson's ratios.

The rotation of the fourth-order stiffness tensor can be shown to be:

$$
\begin{aligned}
\overline{C}^k_{11} &= c^4_\vartheta C^k_{11} + 2c^2_\vartheta s^2_\vartheta C^k_{12} + s^4_\vartheta C^k_{22} + 4c^2_\vartheta s^2_\vartheta C^k_{66} \\
\overline{C}^k_{12} &= c^4_\vartheta C^k_{12} + s^4_\vartheta C^k_{12} + c^2_\vartheta s^2_\vartheta C^k_{11} + c^2_\vartheta s^2_\vartheta C^k_{22} - 4c^2_\vartheta s^2_\vartheta C^k_{66} \\
\overline{C}^k_{16} &= c^3_\vartheta s_\vartheta C^k_{11} - c^3_\vartheta s_\vartheta C^k_{12} + c_\vartheta s^3_\vartheta C^k_{12} - c_\vartheta s^3_\vartheta C^k_{22} + 2c_\vartheta s^3_\vartheta C^k_{66} - 2c^3_\vartheta s_\vartheta C^k_{66} \\
\overline{C}^k_{13} &= c^2_\vartheta C^k_{13} + s^2_\vartheta C^k_{23} \\
\overline{C}^k_{22} &= c^4_\vartheta C^k_{22} + 2c^2_\vartheta s^2_\vartheta C^k_{12} + s^4_\vartheta C^k_{11} + 4c^2_\vartheta s^2_\vartheta C^k_{66} \\
\overline{C}^k_{26} &= c_\vartheta s^3_\vartheta C^k_{11} + c^3_\vartheta s_\vartheta C^k_{12} - c_\vartheta s^3_\vartheta C^k_{12} - c^3_\vartheta s_\vartheta C^k_{22} + 2c^3_\vartheta s_\vartheta C^k_{66} - 2c_\vartheta s^3_\vartheta C^k_{66} \\
\overline{C}^k_{23} &= c^2_\vartheta C^k_{23} + s^2_\vartheta C^k_{13} \\
\overline{C}^k_{66} &= c^4_\vartheta C^k_{66} - 2c^2_\vartheta s^2_\vartheta C^k_{66} + s^4_\vartheta C^k_{66} + c^2_\vartheta s^2_\vartheta C^k_{11} - 2c^2_\vartheta s^2_\vartheta C^k_{12} + c^2_\vartheta s^2_\vartheta C^k_{22} \\
\overline{C}^k_{36} &= c_\vartheta s_\vartheta C^k_{13} - c_\vartheta s_\vartheta C^k_{23} \\
\overline{C}^k_{55} &= c^2_\vartheta C^k_{55} + s^2_\vartheta C^k_{44} \\
\overline{C}^k_{44} &= c^2_\vartheta C^k_{44} + s^2_\vartheta C^k_{55} \\
\overline{C}^k_{45} &= -c_\vartheta s_\vartheta C^k_{44} + c_\vartheta s_\vartheta C^k_{55} \\
\overline{C}^k_{33} &= C^k_{33}
\end{aligned}
\tag{5.11}
$$

where $c_\vartheta = \cos\vartheta^k$, $s_\vartheta = \sin\vartheta^k$.

5.2 Stress derivatives

During the proposed stress recovery procedure, as shown in the next section, it is necessary to perform the derivatives of the $SPKST$.

$$
\begin{aligned}
\mathbf{S}^k_{,X} &= \overline{\mathbf{C}}^k_{,X}\mathbf{E}^k + \overline{\mathbf{C}}^k\mathbf{E}^k_{,X} \\
\mathbf{S}^k_{,Y} &= \overline{\mathbf{C}}^k_{,Y}\mathbf{E}^k + \overline{\mathbf{C}}^k\mathbf{E}^k_{,Y}
\end{aligned}
\tag{5.12}
$$

For example the Y derivative of the inplane stress S_{YY} is compute as follow:

$$
\begin{aligned}
S^k_{YY,Y} &= \bar{C}^k_{12}E^k_{XX,Y} + \bar{C}^k_{22}E^k_{YY,Y} + \bar{C}^k_{26}2E^k_{XY,Y} + \bar{C}^k_{23}E^k_{ZZ,Y} + \\
&\quad \bar{C}^k_{12,Y}E^k_{XX} + \bar{C}^k_{22,Y}E^k_{YY} + \bar{C}^k_{26,Y}2E^k_{XY} + \bar{C}^k_{23,Y}E^k_{ZZ}
\end{aligned}
\tag{5.13}
$$

where $\bar{C}_{ij}^k$ are the material coefficient already rotated in the local element reference systems. To demonstrate the procedure the derivative of $\bar{C}_{12}^k$ with respect to Y is chosen. Using Eq. 5.11

$$\begin{aligned}\frac{\partial \bar{C}_{12}^k}{\partial Y} &= \left(4(\cos\vartheta^k)^3\frac{\partial\cos\vartheta^k}{\partial Y}+4(\sin\vartheta^k)^3\frac{\partial\sin\vartheta^k}{\partial Y}\right)C_{12}^k+\\ &+ \left(2(\cos\vartheta^k)^2\sin\vartheta^k\frac{\partial\sin\vartheta^k}{\partial Y}+2(\sin\vartheta^k)^2\cos\vartheta^k\frac{\partial\cos\vartheta^k}{\partial Y}\right)\left(C_{11}^k+C_{22}^k-4C_{66}^k\right)\end{aligned} \tag{5.14}$$

The derivatives of the trigonometric functions with respect the in-plane coordinate are computed:

$$\begin{aligned}\frac{\partial\cos\vartheta^k}{\partial X} &= \widehat{\nabla}(\cos\vartheta^k)\cdot\mathbf{i}_1 = \frac{\partial\cos\vartheta^k}{\partial\widehat{X}^k}\widehat{\mathbf{i}}_1^k\cdot\mathbf{i}_1 + \frac{\partial\cos\vartheta^k}{\partial\widehat{Y}^k}\widehat{\mathbf{i}}_2^k\cdot\mathbf{i}_1\\ \frac{\partial\cos\vartheta^k}{\partial Y} &= \widehat{\nabla}(\cos\vartheta^k)\cdot\mathbf{i}_2 = \frac{\partial\cos\vartheta^k}{\partial\widehat{X}^k}\widehat{\mathbf{i}}_1^k\cdot\mathbf{i}_2 + \frac{\partial\cos\vartheta^k}{\partial\widehat{Y}^k}\widehat{\mathbf{i}}_2^k\cdot\mathbf{i}_2\\ \frac{\partial\sin\vartheta^k}{\partial X} &= \widehat{\nabla}(\sin\vartheta^k)\cdot\mathbf{i}_1 = \frac{\partial\sin\vartheta^k}{\partial\widehat{X}^k}\widehat{\mathbf{i}}_1^k\cdot\mathbf{i}_1 + \frac{\partial\sin\vartheta^k}{\partial\widehat{Y}^k}\widehat{\mathbf{i}}_2^k\cdot\mathbf{i}_1\\ \frac{\partial\sin\vartheta^k}{\partial Y} &= \widehat{\nabla}(\sin\vartheta^k)\cdot\mathbf{i}_2 = \frac{\partial\sin\vartheta^k}{\partial\widehat{X}^k}\widehat{\mathbf{i}}_1^k\cdot\mathbf{i}_2 + \frac{\partial\sin\vartheta^k}{\partial\widehat{Y}^k}\widehat{\mathbf{i}}_2^k\cdot\mathbf{i}_2\end{aligned} \tag{5.15}$$

where $(\widehat{\mathbf{i}}_1^k,\widehat{\mathbf{i}}_2^k)$ are the unit versor of the layer coordinate systems and $(\mathbf{i}_1,\mathbf{i}_2)$ are the ones of the element coordinate system (see Fig. 5.2).

$$\begin{aligned}\widehat{\mathbf{i}}_1^k\cdot\mathbf{i}_1 &= \cos\phi^k\\ \widehat{\mathbf{i}}_1^k\cdot\mathbf{i}_2 &= \sin\phi^k\\ \widehat{\mathbf{i}}_2^k\cdot\mathbf{i}_1 &= -\sin\phi^k\\ \widehat{\mathbf{i}}_2^k\cdot\mathbf{i}_2 &= \cos\phi^k\end{aligned} \tag{5.16}$$

Using the following angular relationships

$$\vartheta^k = \widehat{\vartheta}^k + \phi^k \tag{5.17}$$

and the trigonometric identities Eq. 5.15 can be rewritten as:

$$\begin{aligned}
\frac{\partial \cos\vartheta^k}{\partial X} &= \left(\cos\phi^k \frac{\partial \cos\widehat{\vartheta}^k}{\partial \widehat{X}^k} - \sin\phi^k \frac{\partial \sin\widehat{\vartheta}^k}{\partial \widehat{X}^k}\right)\cos\phi^k - \frac{\partial \cos\vartheta^k}{\partial \widehat{Y}^k}\sin\phi^k \\
\frac{\partial \cos\vartheta^k}{\partial Y} &= \left(\cos\phi^k \frac{\partial \cos\widehat{\vartheta}^k}{\partial \widehat{X}^k} - \sin\phi^k \frac{\partial \sin\widehat{\vartheta}^k}{\partial \widehat{X}^k}\right)\sin\phi^k + \frac{\partial \cos\vartheta^k}{\partial \widehat{Y}^k}\cos\phi^k \\
\frac{\partial \sin\vartheta^k}{\partial X} &= \left(\sin\phi^k \frac{\partial \sin\widehat{\vartheta}^k}{\partial \widehat{X}^k} + \cos\phi^k \frac{\partial \cos\widehat{\vartheta}^k}{\partial \widehat{X}^k}\right)\cos\phi^k - \frac{\partial \sin\widehat{\vartheta}^k}{\partial \widehat{Y}^k}\sin\phi^k \\
\frac{\partial \sin\vartheta^k}{\partial Y} &= \left(\sin\phi^k \frac{\partial \sin\widehat{\vartheta}^k}{\partial \widehat{X}^k} + \cos\phi^k \frac{\partial \cos\widehat{\vartheta}^k}{\partial \widehat{X}^k}\right)\sin\phi^k + \frac{\partial \sin\vartheta^k}{\partial \widehat{Y}^k}\cos\phi^k
\end{aligned} \tag{5.18}$$

where the fact that $\partial\phi^k/\partial\hat{X}^k = 0$ has been used. The fiber is rigidly translated along the $\hat{X}^k$ then $\widehat{\vartheta}$ is constant along that directions and Eq. 5.18 is simplified:

$$\begin{aligned}
\frac{\partial \cos\vartheta^k}{\partial X} &= -\frac{\partial \cos\vartheta^k}{\partial \widehat{Y}^k}\sin\phi^k \\
\frac{\partial \cos\vartheta^k}{\partial Y} &= \frac{\partial \cos\vartheta^k}{\partial \widehat{Y}^k}\cos\phi^k \\
\frac{\partial \sin\vartheta^k}{\partial X} &= -\frac{\partial \sin\vartheta^k}{\partial \widehat{Y}^k}\sin\phi^k \\
\frac{\partial \sin\vartheta^k}{\partial Y} &= \frac{\partial \sin\vartheta^k}{\partial \widehat{Y}^k}\cos\phi^k
\end{aligned} \tag{5.19}$$

The angle ϑ is known as a function of the parameter μ^k and it will be simpler to compute the derivative with respect to that parameter. This can be done using Eq. 5.8 in Eq. 5.19:

$$\begin{aligned}
\frac{\partial \cos\vartheta^k}{\partial X} &= -F\frac{\partial \cos\vartheta^k}{\partial \mu^k}\sin\phi^k &&= F\sin\vartheta^k\frac{\partial\vartheta^k}{\partial\mu^k}\sin\phi^k \\
\frac{\partial \cos\vartheta^k}{\partial Y} &= F\frac{\partial \cos\vartheta^k}{\partial \mu^k}\cos\phi^k &&= -F\sin\vartheta\frac{\partial\vartheta^k}{\partial\mu^k}\cos\phi^k \\
\frac{\partial \sin\vartheta^k}{\partial X} &= -F\frac{\partial \sin\vartheta^k}{\partial \mu^k}\sin\phi^k &&= -F\cos\vartheta\frac{\partial\vartheta^k}{\partial\mu^k}\sin\phi^k \\
\frac{\partial \sin\vartheta^k}{\partial Y} &= F\frac{\partial \sin\vartheta^k}{\partial \mu^k}\cos\phi^k &&= F\cos\vartheta^k\frac{\partial\vartheta^k}{\partial\mu^k}\cos\phi^k
\end{aligned} \tag{5.20}$$

The angle derivative is calculated through Eq. 5.1:

$$\frac{\partial\vartheta^k}{\partial\mu^k} = a_t^k \frac{\mathrm{d}P_t^k}{\mathrm{d}\mu^k} \tag{5.21}$$

and the final expression of the trigonometric function derivatives as a function of the known Legendre

polynomial coefficient are obtained:

$$\begin{array}{rcl} \dfrac{\partial \cos\vartheta^k}{\partial X} &=& F\sin\left(a_t^k P_t^k\right) a_t^k \dfrac{\mathrm{d}P_t^k}{\mathrm{d}\mu^k}\sin\phi^k \\ \dfrac{\partial \cos\vartheta^k}{\partial Y} &=& -F\sin\left(a_t^k P_t^k\right) a_t^k \dfrac{\mathrm{d}P_t^k}{\mathrm{d}\mu^k}\cos\phi^k \\ \dfrac{\partial \sin\vartheta^k}{\partial X} &=& -F\cos\left(a_t^k P_t^k\right) a_t^k \dfrac{\mathrm{d}P_t^k}{\mathrm{d}\mu^k}\sin\phi^k \\ \dfrac{\partial \sin\vartheta^k}{\partial Y} &=& F\cos\left(a_t^k P_t^k\right) a_t^k \dfrac{\mathrm{d}P_t^k}{\mathrm{d}\mu^k}\cos\phi^k \end{array} \tag{5.22}$$

Eq. 5.22 allows to compute the derivative of the material coefficient (Eq. 5.14) from the knowledge of μ^k and consequently of $\widehat{Y}^k$ using Eq. 5.6.

In conclusion, it is now possible to compute the derivatives of the $SPKST$ (Eq. 5.12) once the $GLST$ is computed through kinematic relationship from the displacement solution and the user input fiber equation given by Eq. 5.1.

5.3 The proposed stress recovery procedure

PVD-based theories have only displacements as primary unknowns. This means that the stress field caused by the nonlinear deformation of the structure has to be computed successively during a post-processing phase. The stresses can be computed by using CFHL (Eq. (3.43)). This method provides excellent in-plane SPKST stress components, but the transverse stresses are not accurately calculated and the interlaminar continuity violated. The *Cauchy Stress Tensor* (CST), directly obtained from SPKST, are also inaccurate.

The same problem have been encountered also in linear analysis. It has been shown that the integration of equilibrium equations

$$\left\{\begin{array}{rcl} \dfrac{\partial \sigma_{zx}^k}{\partial z} &=& -\dfrac{\partial \sigma_{xx}^k}{\partial x} - \dfrac{\partial \sigma_{yx}^k}{\partial y} \\ \dfrac{\partial \sigma_{zy}^k}{\partial z} &=& -\dfrac{\partial \sigma_{xy}^k}{\partial x} - \dfrac{\partial \sigma_{yy}^k}{\partial y} \\ \dfrac{\partial \sigma_{zz}^k}{\partial z} &=& -\dfrac{\partial \sigma_{xz}^k}{\partial x} - \dfrac{\partial \sigma_{yz}^k}{\partial y} \end{array}\right. \tag{5.23}$$

along the thickness improves the results. Suppose the value of the stress is needed at a point ($\bar{x}$,$\bar{y}$) of the plate. The inplane stresses are computed using the Hooke's formula and the transverse stresses as follows:

$$
\begin{aligned}
\sigma^k_{zx}(\bar{x},\bar{y},z) &= \sigma^k_{zx}(\bar{x},\bar{y},z_0) - \int_{z_0}^{z} \left(\frac{\partial \sigma^k_{xx}}{\partial x} - \frac{\partial \sigma^k_{yx}}{\partial y} \right) \mathrm{d}z \\
\sigma^k_{zy}(\bar{x},\bar{y},z) &= \sigma^k_{zy}(\bar{x},\bar{y},z_0) - \int_{z_0}^{z} \left(\frac{\partial \sigma^k_{xy}}{\partial x} - \frac{\partial \sigma^k_{yy}}{\partial y} \right) \mathrm{d}z \\
\sigma^k_{zz}(\bar{x},\bar{y},z) &= \sigma^k_{zz}(\bar{x},\bar{y},z_0) - \int_{z_0}^{z} \left(\frac{\partial \sigma^k_{xz}}{\partial x} - \frac{\partial \sigma^k_{yz}}{\partial y} \right) \mathrm{d}z
\end{aligned}
\tag{5.24}
$$

where z_0 is a point where the stresses are known. At the start of the integration usually this point is at the top ($k = n_l$) or bottom ($k = 1$) of the plate. If the stress at the bottom of the plate is known the stress integration starts from $k = 1$ up to the layer where the stress is wanted. The intermediate layers will use the stress at the top (bottom) of the lower (current) layer as starting point, where the stress have been already computed. The first two equations are independent and they can be solved separately. The transverse shear stresses obtained should then be substituted in the third equation to obtain the correct expression of the normal transverse stress. Although, previous numerical results have shown that using the transverse shear stresses obtained from Hooke's law does not affect the accuracy of the normal transverse stress [28]. This fact will be used later also in the nonlinear case.

This problem for nonlinear analysis has been studied by few authors [18–21] and tackled with different strategies, often for higher-order theories and von-Kármán strain model. Here a dedicated procedure is proposed. It is based on the integration of the equilibrium equations written in terms of SPKST [98]. The procedure is tailored to take into account the variability of stiffness coefficients as prescribed by VAT laminates.

Starting point is represented by the equilibrium equations [96, 110] written in the undeformed configuration

$$
\frac{\partial \left(G^k_{im} S^k_{mj} \right)}{\partial X_j} = 0 \quad i,j = 1,2,3 \tag{5.25}
$$

If the coordinates X_1, X_2, X_3 are replaced with X, Y, Z and i, j, and m take the values of X, Y, and Z, respectively Eq. (5.25) becomes

$$
\begin{cases}
\dfrac{\partial \left(G^k_{Xm} S^k_{mX} \right)}{\partial X} + \dfrac{\partial \left(G^k_{Xm} S^k_{mY} \right)}{\partial Y} + \dfrac{\partial \left(G^k_{Xm} S^k_{mZ} \right)}{\partial Z} = 0 \\
\dfrac{\partial \left(G^k_{Ym} S^k_{mX} \right)}{\partial X} + \dfrac{\partial \left(G^k_{Ym} S^k_{mY} \right)}{\partial Y} + \dfrac{\partial \left(G^k_{Ym} S^k_{mZ} \right)}{\partial Z} = 0 \qquad m = X,Y,Z \\
\dfrac{\partial \left(G^k_{Zm} S^k_{mX} \right)}{\partial X} + \dfrac{\partial \left(G^k_{Zm} S^k_{mY} \right)}{\partial Y} + \dfrac{\partial \left(G^k_{Zm} S^k_{mZ} \right)}{\partial Z} = 0
\end{cases}
\tag{5.26}
$$

As opposed to the linear case all three equations are coupled and they have to be solved simultaneously. In this dissertation the following assumption is made: *only the derivatives of the transverse stress with respect to Z are considered unknowns*. The remaining terms are accurately computed with the $CFHL$. This hypothesis allows to use an integration method similar to the one used for linear analysis. All terms with the derivative of the stresses with respect to Z are kept on the left-hand side and all others are moved on the right-hand side.

$$\begin{cases} \dfrac{\partial \left(G^k_{Xm} S^k_{mZ}\right)}{\partial Z} = -\dfrac{\partial \left(G^k_{Xm} S^k_{mX}\right)}{\partial X} - \dfrac{\partial \left(G^k_{Xm} S^k_{mY}\right)}{\partial Y} \\ \dfrac{\partial \left(G^k_{Ym} S^k_{mZ}\right)}{\partial Z} = -\dfrac{\partial \left(G^k_{Ym} S^k_{mX}\right)}{\partial X} - \dfrac{\partial \left(G^k_{Ym} S^k_{mY}\right)}{\partial Y} \qquad m = X, Y, Z \\ \dfrac{\partial \left(G^k_{Zm} S^k_{mZ}\right)}{\partial Z} = -\dfrac{\partial \left(G^k_{Zm} S^k_{mX}\right)}{\partial X} - \dfrac{\partial \left(G^k_{Zm} S^k_{mY}\right)}{\partial Y} \end{cases} \tag{5.27}$$

As an example the first equilibrium relation of Eq. (5.26) is rewritten as

$$\begin{aligned} G^k_{XX} S^k_{XZ,Z} + G^k_{XY} S^k_{YZ,Z} + G^k_{XZ} S^k_{ZZ,Z} = & - S^k_{XX}\, G^k_{XX,X} - S^k_{YY}\, G^k_{XY,Y} - S^k_{XY}\, G^k_{XY,X} \\ & - S^k_{XY}\, G^k_{XX,Y} - G^k_{XX}\, S^k_{XX,X} - G^k_{XY}\, S^k_{YX,X} \\ & - G^k_{XX}\, S^k_{XY,Y} - G^k_{XY}\, S^k_{YY,Y} - S^k_{XZ}\, G^k_{XZ,X} \\ & - S^k_{XZ}\, G^k_{XX,Z} - S^k_{YZ}\, G^k_{XZ,Y} - S^k_{YZ}\, G^k_{XY,Z} \\ & - S^k_{ZZ}\, G^k_{XZ,Z} - G^k_{XZ}\, S^k_{ZX,X} - G^k_{XZ}\, S^k_{ZY,Y} \end{aligned} \tag{5.28}$$

To simplify the notation, the deformation gradient is expressed as a function of the position vector $\mathbf{R}$:

$$\mathbf{G}^k = \begin{bmatrix} \mathbf{R}^k_{,X} & \mathbf{R}^k_{,Y} & \mathbf{R}^k_{,Z} \end{bmatrix} \tag{5.29}$$

where

$$\mathbf{R}^k = \begin{bmatrix} X + u^k_X \\ Y + u^k_Y \\ Z + u^k_Z \end{bmatrix} \tag{5.30}$$

Using the rule of differentiation of product the equilibrium equations take the form reported below:

$$\begin{aligned}\frac{\partial(\mathbf{G}^k\widehat{\mathbf{S}}^k)}{\partial Z} &= -S^k_{XX}\mathbf{R}^k_{,XX} - S^k_{XX,X}\mathbf{R}^k_{,X} - S^k_{YY}\mathbf{R}^k_{,YY} - S^k_{YY,Y}\mathbf{R}^k_{,Y} - S^k_{XY,Y}\mathbf{R}^k_{,X} - S^k_{XY,X}\mathbf{R}^k_{,Y} \\ &\quad -2S^k_{XY}\mathbf{R}^k_{,XY} - S^k_{XZ,X}\mathbf{R}^k_{,Z} - S^k_{XZ}\mathbf{R}^k_{,XZ} - S^k_{YZ,Y}\mathbf{R}^k_{,Z} - S^k_{YZ}\mathbf{R}^k_{,YZ}\end{aligned} \tag{5.31}$$

where

$$\widehat{\mathbf{S}}^k = \left[S^k_{XZ}\ S^k_{YZ}\ S^k_{ZZ}\right]^T \tag{5.32}$$

Eq. (5.31) is the nonlinear counterpart of Eq. 5.23. It is integrated along the thickness of the element starting from either the top or bottom surface. The values of the transverse stresses at a coordinate Z is obtained as follow:

$$\widehat{\mathbf{S}}^k = \left(\mathbf{G}^k\right)^{-1}\left[\left(\mathbf{G}^k\widehat{\mathbf{S}}^k\right)_{Z_0} + \int_{Z_0}^{Z}\frac{\partial\left(\mathbf{G}^k\widehat{\mathbf{S}}^{k\,H}\right)}{\partial Z}\mathrm{d}Z\right] \tag{5.33}$$

In this case Z_0 is the coordinate of the layer where the stress is known. Usually this happens at the top or bottom of the laminate. In case it is of interest the stress field in an internal layer the same procedure used for the linear case (Eq. 5.24) should be followed. The stresses in the right-hand side of Eq. (5.31) are known and computed by using CFHL ($\hat{\mathbf{S}}^H$). The main steps of the method are shown in Fig. 5.4.

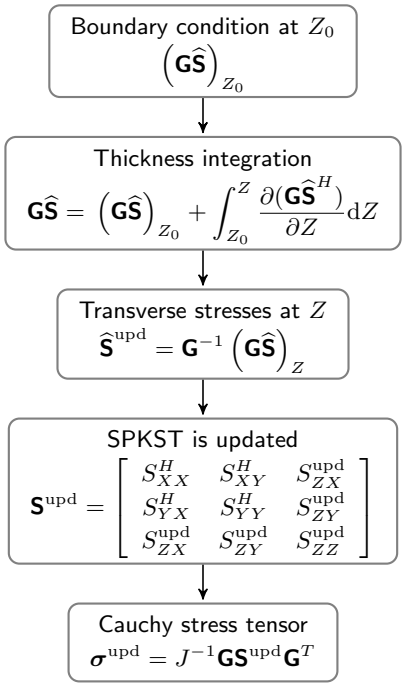

Figure 5.4: Stress integration algorithm. $\mathbf{G}$ is known everywhere and computed from the solution vector. $\mathbf{S}^H$ is the SPKST computed by CFHL.

As it can be seen from Eq. 5.31, it is necessary to compute the in-plane derivatives of SPKST and

particular attention should be paid if the material coefficients are not constant in the element coordinate systems as for VAT composites [28]. This issue has been dealt with in section 5.2 (see Eq. 5.12).

In this work the acronym Q3D will be used to indicate that the transverse stresses have been computed with this procedure.

5.3.1 Dynamic extension

In dynamical problems the stress recovery algorithm is formally unchanged. Eq. 5.33 still holds. The main difference is the introduction of the inertial forces in the governing equation (Eq. 5.25):

$$\frac{\partial \left(G^k_{im} S^k_{mj}\right)}{\partial X_j} = \rho^k \ddot{u}^k_i \quad i,j = 1,2,3 \tag{5.34}$$

The additional term is known since both the density distribution and the acceleration field are available. The density is given as input and the acceleration field is computed during the solution process from the displacement field. The inertial contribution modifies only the right-hand side of Eq. 5.31:

$$\begin{aligned} \frac{\partial(\mathbf{G}^k\widehat{\mathbf{S}}^k)}{\partial Z} \quad = \quad & -S^k_{XX}\mathbf{R}^k_{,XX} - S^k_{XX,X}\mathbf{R}^k_{,X} - S^k_{YY}\mathbf{R}^k_{,YY} - S^k_{YY,Y}\mathbf{R}^k_{,Y} - S^k_{XY,Y}\mathbf{R}^k_{,X} - S^k_{XY,X}\mathbf{R}^k_{,Y} \\ & -2S^k_{XY}\mathbf{R}^k_{,XY} - S^k_{XZ,X}\mathbf{R}^k_{,Z} - S^k_{XZ}\mathbf{R}^k_{,XZ} - S^k_{YZ,Y}\mathbf{R}^k_{,Z} - S^k_{YZ}\mathbf{R}^k_{,YZ} + \rho^k\ddot{\mathbf{u}}^k \end{aligned} \tag{5.35}$$

5.4 Acknowledgments

Chapter 5 is in part a edited reprint of :

- *"Computational Architecture Based on Murakami's Zig-Zag function for the Geometrically Nonlinear Analysis of Variable Angle Tow Laminates"*, AIAA Scitech Forum, Orlando, Florida, January 2020 and co-authored by Luciano Demasi. The author of this dissertation is the primary investigator and author of this paper.

Chapter 6

Numerical examples

In this chapter the multi-theory and multi-fidelity model for nonlinear static and dynamic analysis of composite laminates is tested on a series of benchmark problems from literature or direct comparison with commercial codes.

In static analysis the stress and displacement fields are considered at specific in-plane global coordinates $(\mathcal{X}, \mathcal{Y})$ of the plate. At such points, the variation of their components along the thickness $(\mathcal{Z})$ direction is visualized. This allows us to check if the models adopted provide a solution that satisfies the physical constraints, e.g. continuity of transverse stress at lamina interface.

In dynamic analysis, from the point of view of an aerolastic design it is of great interested to evaluate the displacement correctly, because they change the boundary condition of the aerodynamic solver and consequently the effective loads applied to the structure. The stress are checked monitoring a material particle locate at specific points $(\mathcal{X}, \mathcal{Y}, \mathcal{Z})$ during time.

In this dissertation only the quartic triangular element is used. It proved to perform well in linear analysis and to be locking free.

6.1 Static analysis

The following test are performed:

- *Clamped, antisymmetric cross-ply laminated square plate under uniform load*: a preliminary validation of the nonlinear algorithm. The capability to capture the stress-stiffening along with the LW models are checked. LW will be used as reference solution for other less refined theories (ESL, ZZ).
- *Cantilever composite plate subjected to a tip load*: this is a problem where very large displacements and rotation comes into play. Here the performance of different axiomatic models in presence of

geometrically nonlinear are compared as well as the stress recovery procedure.

- *Thick three-layered simply supported plate with bottom surface pressure*: In case of sandwich plates the core and skins have different material properties making predominant the Zig-Zag form of the displacement field.

- *Thick three-layered VAT simply supported plate with bottom surface pressure*: same problem as before but with inclusion of VAT composites. Both the curvilinear fiber path definition and the stress integration algorithm for anisotropic materials are tested.

6.1.1 Clamped, antisymmetric cross-ply laminated square plate under uniform load

This test involves the large displacement bending of a clamped square plate with a antisymmetric cross-ply laminate (0/90/0/90/0/90) subjected to uniform load of 1800 psi. The material properties are the following:

$$\begin{aligned} &E_2 = 10^6 \text{ psi} \qquad \tfrac{E_1}{E_2} = 40 \qquad \tfrac{E_3}{E_2} = 1 \qquad G_{12} = G_{13} = \tfrac{6}{10} \cdot E_2 \\ &G_{23} = \tfrac{1}{2} \cdot E_2 \qquad \nu_{12} = \nu_{13} = \nu_{23} = \tfrac{1}{4} \end{aligned} \tag{6.1}$$

The plate has an edge length of 12 in and a thickness of 0.3 in. In Fig. 6.1 the deflection (expressed in inches) of the six-layered laminate together with at two-layer (0/90) case are compared against result obtained by Reddy [57] who used a first order shear deformation theory (FSDT). Also the in-plane Cauchy stresses at the middle of the plate (see Fig. 6.2) are compared with NASTRAN (results obtained with CHEXA solid elements). The stresses are calculated in the undeformed global coordinate system indicated with $\mathcal{X}, \mathcal{Y}, \mathcal{Z}$. The correlation is excellent.

6.1.2 Cantilevered composite plate subjected to a tip load

This test case has been adapted from Ref. [111], the geometry, constraints and material properties are shown in Fig. 6.3 (see also Refs. [112, 113]). Two laminations schemes [111] are analyzed:

- Stacking Sequence # 1 (SS 1): -45/45/-45/45

- Stacking Sequence # 2 (SS 2): 30/-60/-60/30

The plate is subject to very large displacements of about eighty times the thickness. Using various layerwise theories indicated as $_{\text{LLL}}\text{PVD}_{222}$, $_{\text{LLL}}\text{PVD}_{333}$, and $_{\text{LLL}}\text{PVD}_{444}$ for the parabolic, cubic, and fourth-order cases, respectively, it was verified that the convergence of the SPKST was, as expected, slower than the

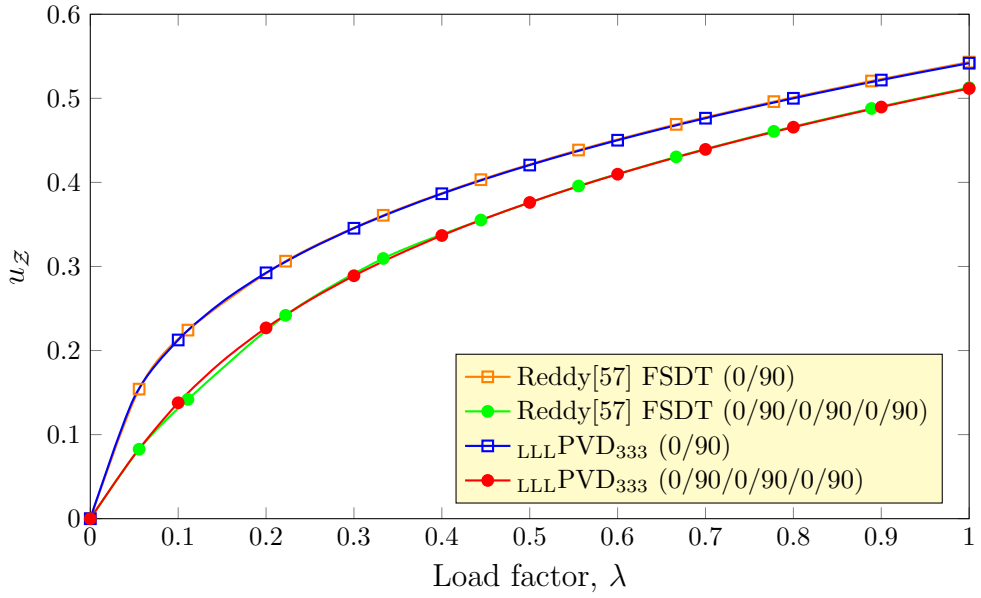

Figure 6.1: Load-deflection curve for clamped anisymmetric cross-ply laminated square plates under uniform load [57]. The displacements are expressed in inches.

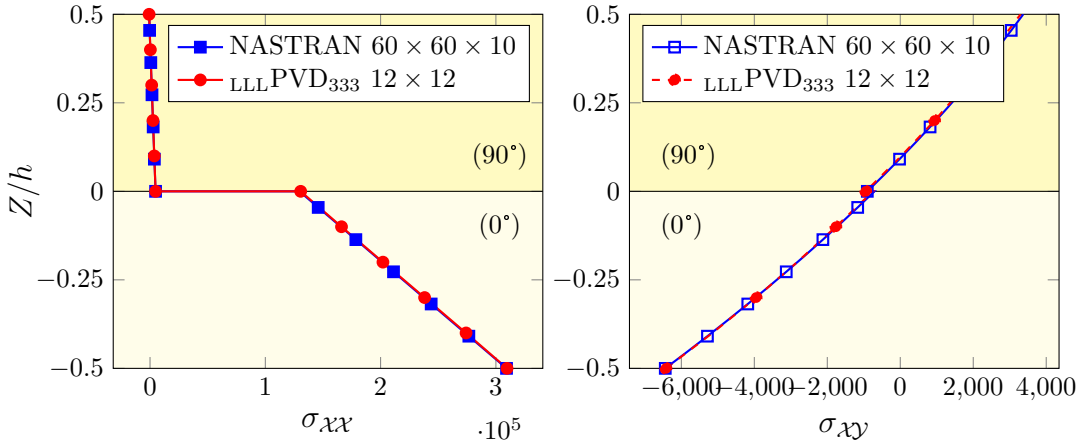

Figure 6.2: Cauchy stress (expressed in psi) σ_{xx} and σ_{xy} evaluated in the middle of the plate.

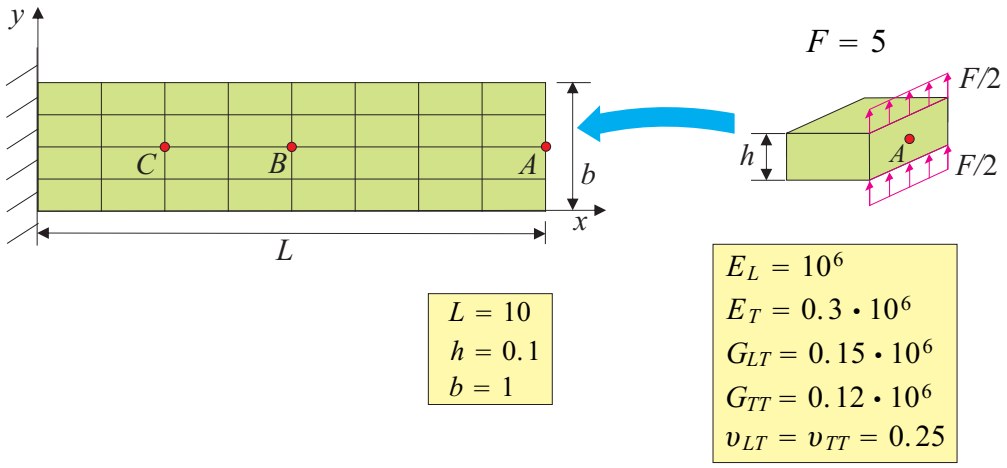

Figure 6.3: Cantilever plate strip subjected to end shear loading [111]. Figure from [98].

displacements. Figs. 6.4 and 6.5 present the convergence[1] for the SPKST component S_{yz}. With an appropriate in-plane approximation, all layerwise theories considered provide a good accuracy. The symbols "Q3D" is used in this work to indicate that the proposed post-processing SPKST stress recovery procedure is applied. Based on these data a mesh 16×4 will be used for all following results shown for this benchmark problem. And the fourth-order theory $_{\text{LLL}}\text{PVD}_{444}$ it will be used as a reference for the other axiomatic models.

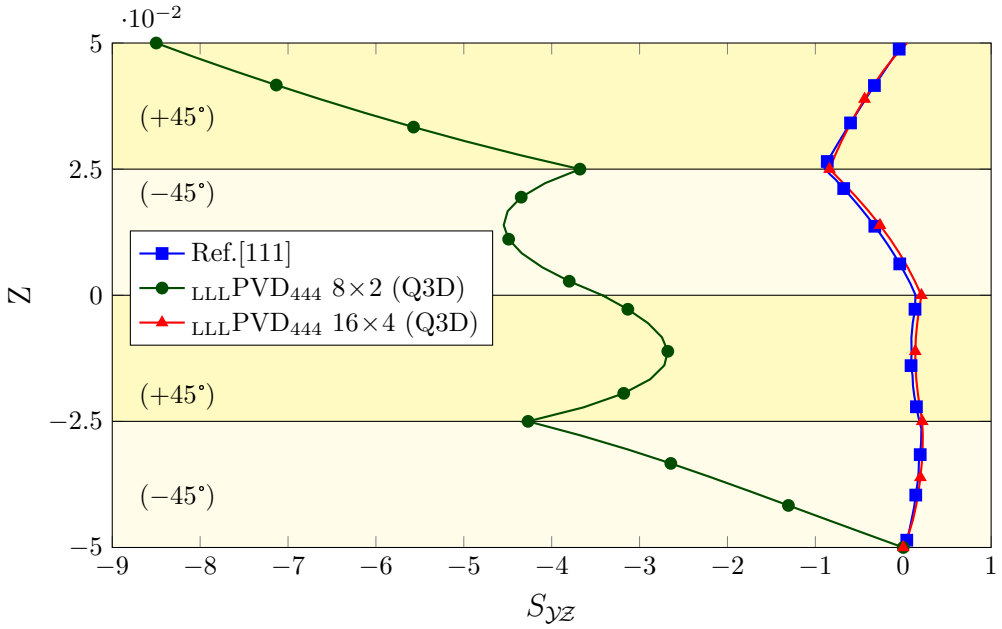

Figure 6.4: SPKST component S_{yz} at point B: convergence test with respect to the mesh

[1]Kulikov's results for the stresses have been extracted from Ref. [111] by using the software *WebPlotDigitizer* and this is the reason why the curves are not always perfectly smooth.

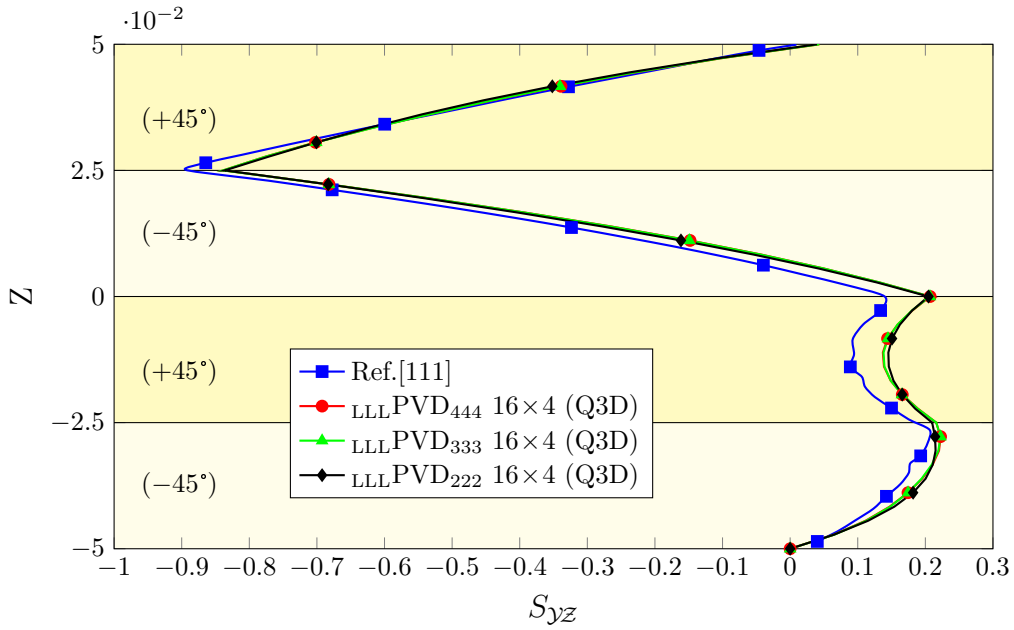

Figure 6.5: SPKST component S_{yz} at point B: convergence test with respect to the order of expansion along the thickness.

Displacements The displacements of the plate tip (point A) provided by the ESL and ZZ theories are compared in Figs. 6.6 and 6.7, indicating the excellence performance in capturing displacements at global level also by low order theories. As we will show later, the case of thick plate needs an accurate formulation to correctly represents three-dimensional effects and the Zig-Zag models built by using MZZF achieve that.

Stress field: layerwise models The state of stress along the plate thickness can be obtained using both the CFHL and the stress integration algorithm. On this regard, Fig. 6.8 compare the SPKST component S_{zz} at point C indicating the superior performance of the proposed recovery procedure with respect to CFHL. In this case, the layerwise approach provides a satisfactory performance even by applying the constitutive equations (see Fig. 6.8). However, it is anticipated that for ESL theories the recovery procedure is necessary to correctly reproduce these stresses. The excellent correlation with publish data is also confirmed for the (30/-60/-60/30) stacking sequence, as documented in Figs. 6.9 and 6.10.

SPKST results are summarized in Fig. 6.11. These results are relative to points B and C (whose locations are depicted in Fig. 6.3). Since results presenting transverse components of SPKST are not very abundant in the literature, Tables 6.1 and 6.2 report numerical values of these stresses and could be used to compare other theories. The present results are also validated using ABAQUS element C3D20R. In particular, the SPKST (the transverse components of SPKST are evaluated using the proposed stress recovery procedure) is transformed into the Cauchy Stress Tensor referred to the undeformed geometry. The excellent correlation and the relevant stress values are reported in Figs. 6.12 and 6.13.

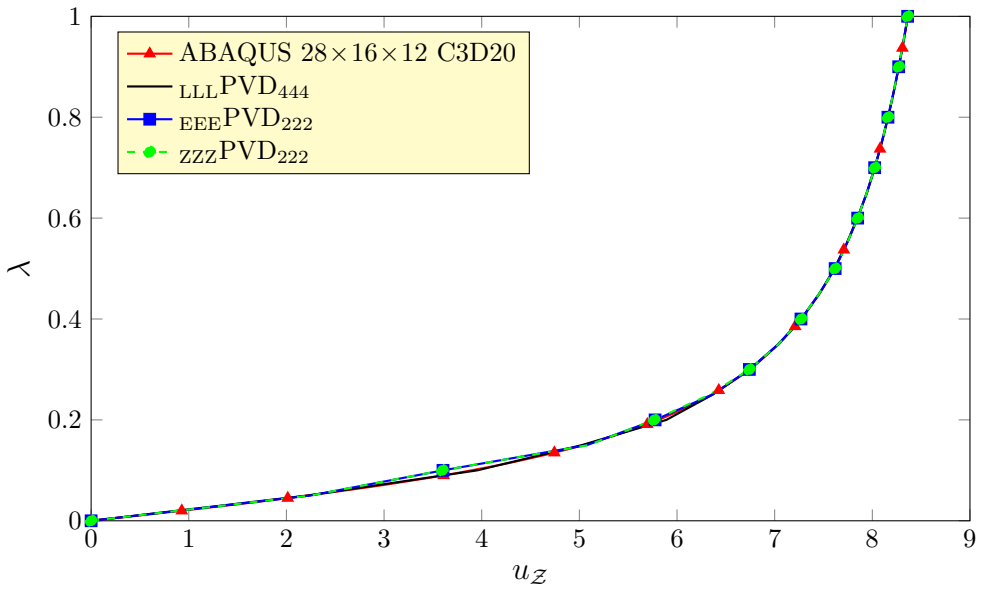

Figure 6.6: Case of SS1. Transverse displacement point A.

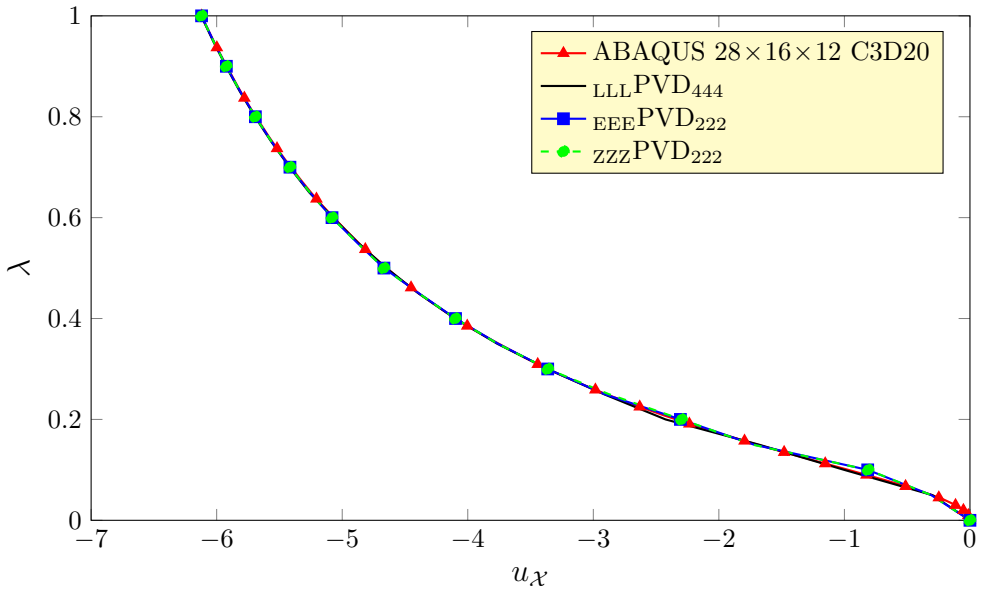

Figure 6.7: Case of SS1. Axial displacement point A.

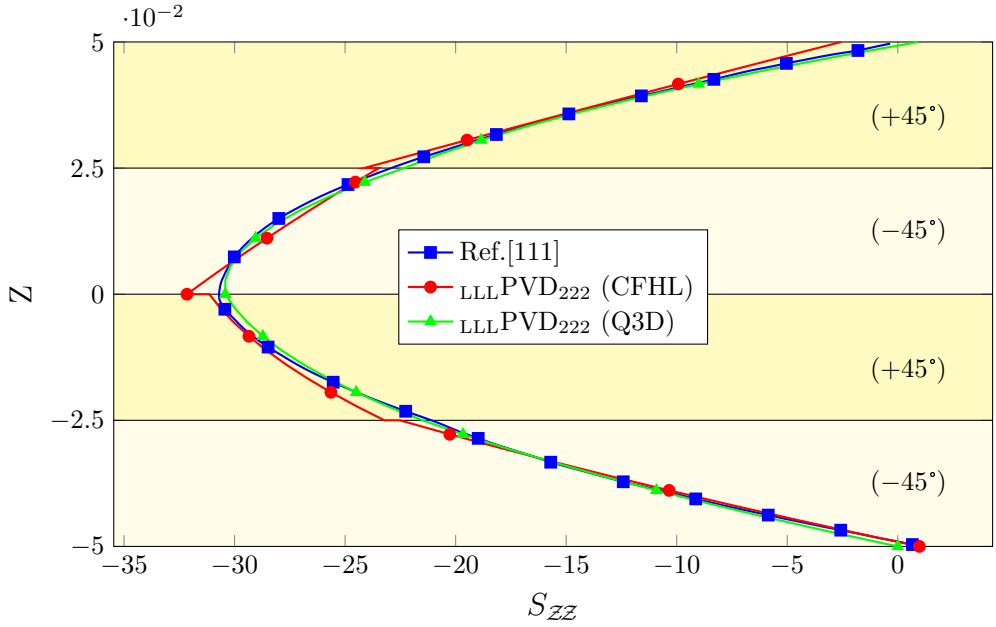

Figure 6.8: SPKST component S_{zz} at point C: evaluation using the present stress recovery procedure and CFHL.

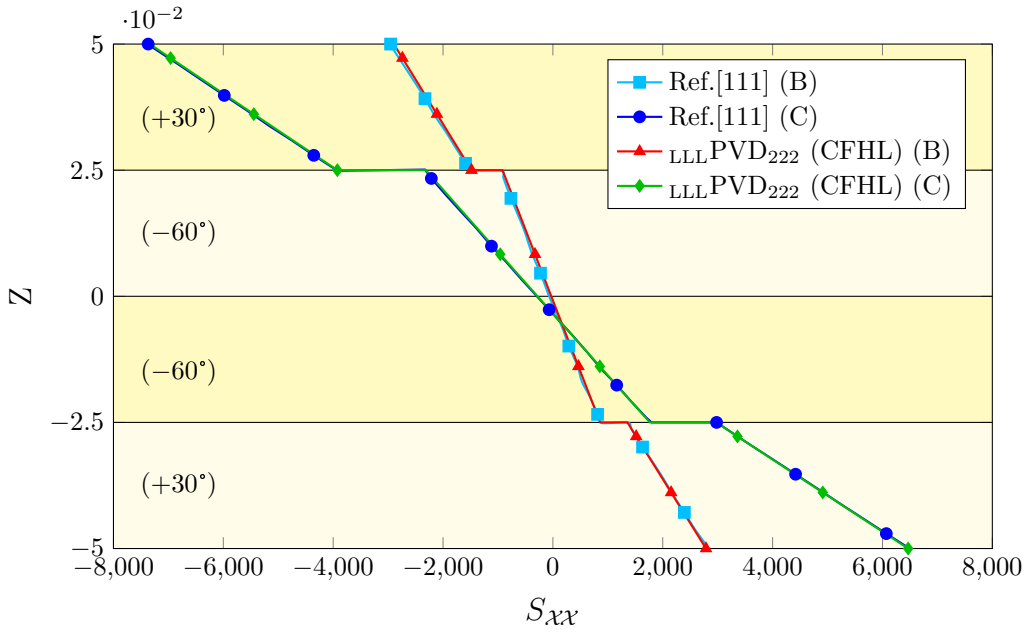

Figure 6.9: SPKST component S_{xx} at points B and C using CFHL.

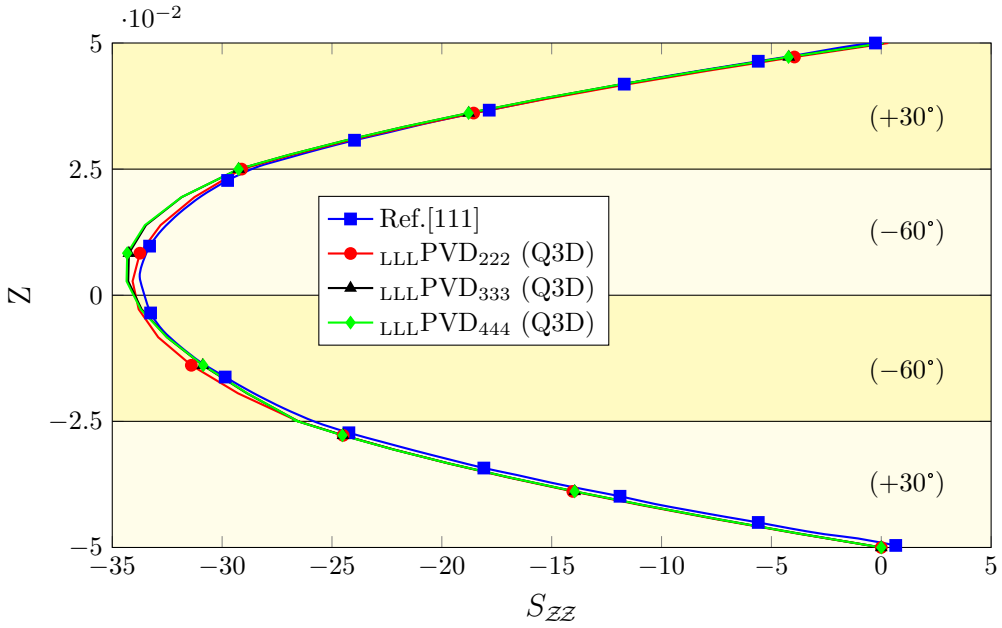

Figure 6.10: SPKST component S_{zz} at point C using the proposed stress recovery procedure.

Table 6.1: Kulikov's test case [111]: present evaluations of SPKST components S_{xx} and S_{xz} calculated at points B and C with LLLPVD$_{444}$ theory. Lamination scheme (-45/45/-45/45).

Location		Point B		Point C	
(Layer)	Z	S_{xx}	S_{xz}	S_{xx}	S_{xz}
1^{bot}	$-h/2$	+1961.43	+0.00	+4805.72	+0.00
1^{top}	$-h/4$	+929.13	+7.69	+2104.43	+24.60
2^{bot}	$-h/4$	+1089.47	+7.69	+2531.63	+24.60
2^{top}	-0	+57.10	+10.33	−144.25	+34.26
3^{bot}	$+0$	−98.01	+10.33	−569.17	+34.26
3^{top}	$+h/4$	−1122.42	+7.57	−3223.81	+24.40
4^{bot}	$+h/4$	−970.79	+7.57	−2794.50	+24.40
4^{top}	$+h/2$	−1996.80	−0.15	−5429.63	−0.01

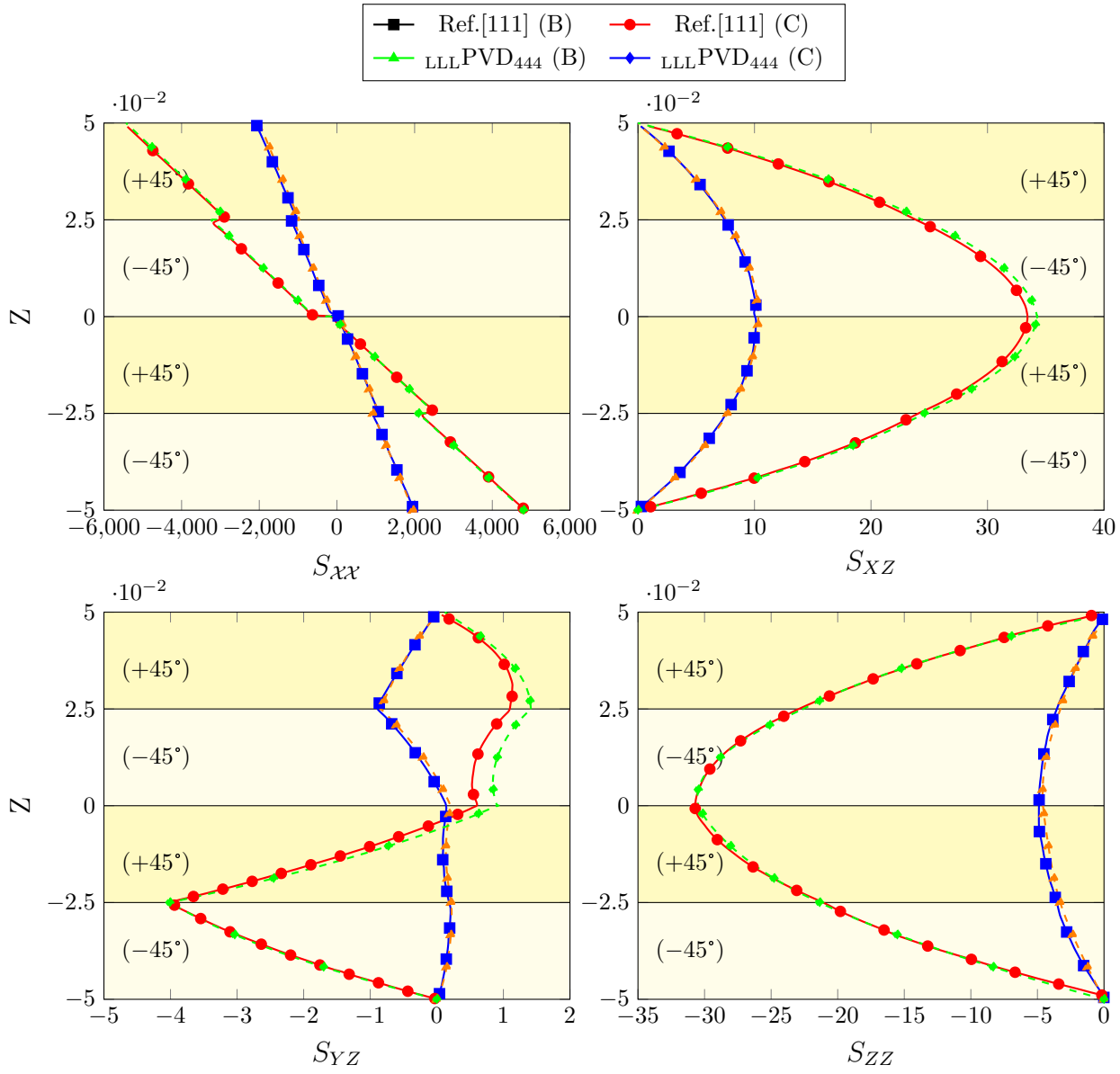

Figure 6.11: Distribution of the SPKST stresses. Lamination scheme (-45/45/-45/45).

Table 6.2: Kulikov's test case [111]: present evaluations of SPKST components S_{yz} and S_{zz} calculated at points B and C with $_{\text{LLL}}\text{PVD}_{444}$ theory. Lamination scheme (-45/45/-45/45).

Location		Point B		Point C	
(Layer)	Z	S_{yz}	S_{zz}	S_{yz}	S_{zz}
1^{bot}	$-h/2$	$+0.00$	-0.00	-0.00	-0.00
1^{top}	$-h/4$	$+0.22$	-3.29	-4.01	-21.35
2^{bot}	$-h/4$	$+0.22$	-3.29	-4.01	-21.35
2^{top}	-0	$+0.21$	-4.58	$+0.90$	-30.48
3^{bot}	$+0$	$+0.21$	-4.58	$+0.90$	-30.48
3^{top}	$+h/4$	-0.84	-3.27	$+1.41$	-22.59
4^{bot}	$+h/4$	-0.84	-3.27	$+1.41$	-22.59
4^{top}	$+h/2$	$+0.04$	$+0.43$	$+0.12$	$+0.75$

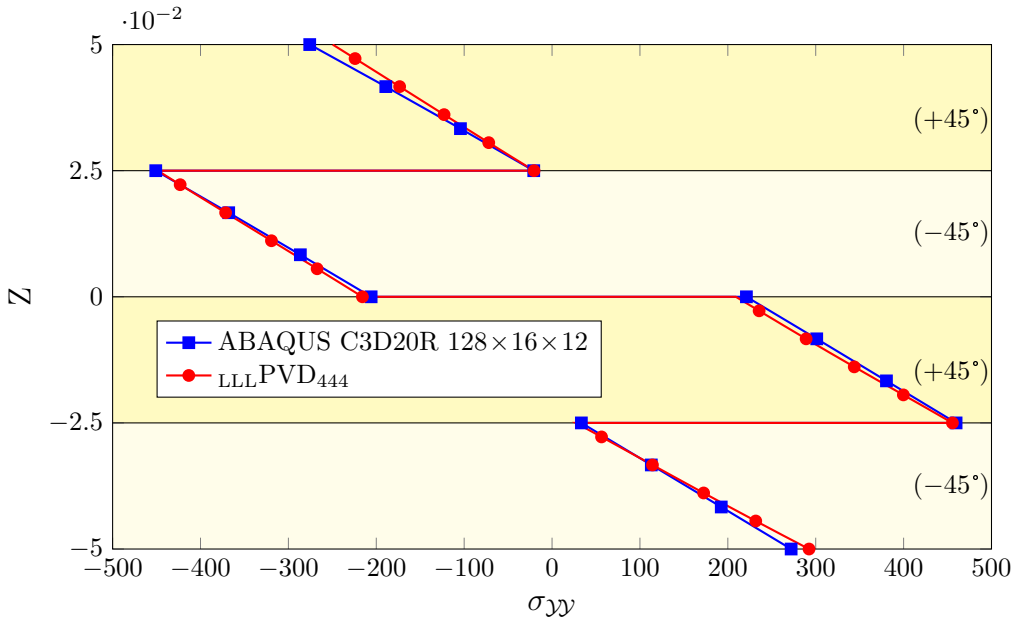

Figure 6.12: Cauchy stress component σ_{yy} at point C using the proposed stress recovery procedure for the transverse components of SPKST.

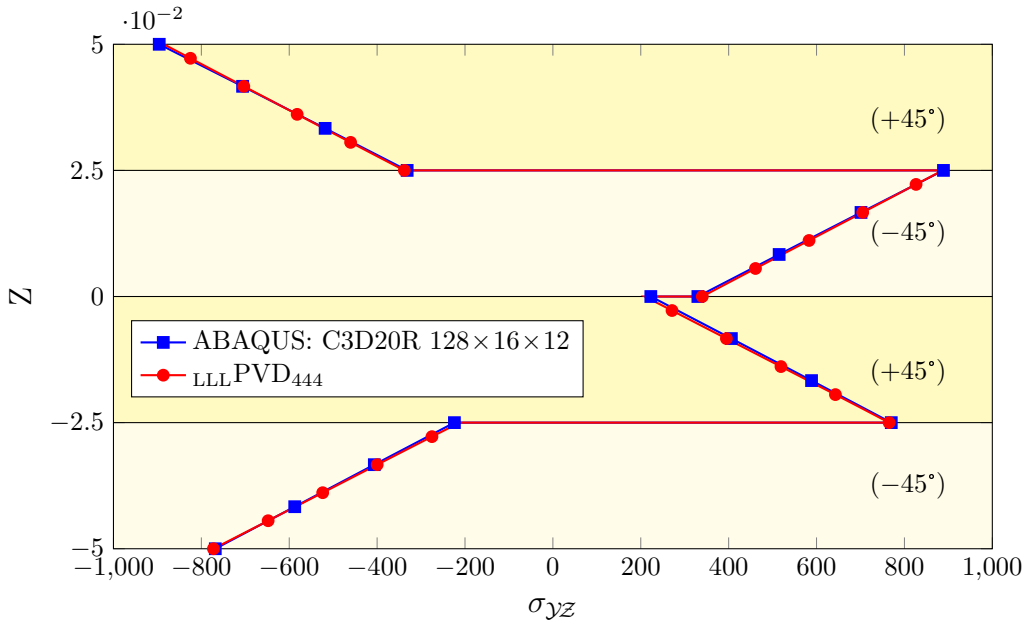

Figure 6.13: Cauchy stress component σ_{yz} at point C using the proposed stress recovery procedure for the transverse components of SPKST.

Stress field: ESL models The SPKST component S_{yz} calculated at point B (see Fig. 6.3) is calculated with both CFHL and the present integration of the equilibrium equations in Fig. 6.14. Qualitative behavior and quantitative values are incorrect when Hooke's approach is used to calculate the stresses, and this is particularly the case when low-order theories are adopted. On the other hand, the use of the proposed stress recovery procedure is quite effective. Similar conclusions can be deduced from an analogous result relative to SS2 (see Fig. 6.15). SPKST can be converted to CST to allow a comparison with the commercial software ABAQUS. Results (see Fig. 6.16) indicate the excellent correlation of Zig-Zag theories with respect to the reference solution obtained with ABAQUS. Cubic Zig-Zag theory is able to provide stress values comparable to the ones obtained with the high-order layerwise approach (see Figs. 6.17 and 6.18). It is also observed that the largest error occurs in correspondence of the first 2 layers (this finding is a case dependent property).

6.1.3 Thick three-layered simply supported plate with bottom surface pressure

The simply supported three-layered structure is presented in Fig. 6.19. Two lamination schemes,

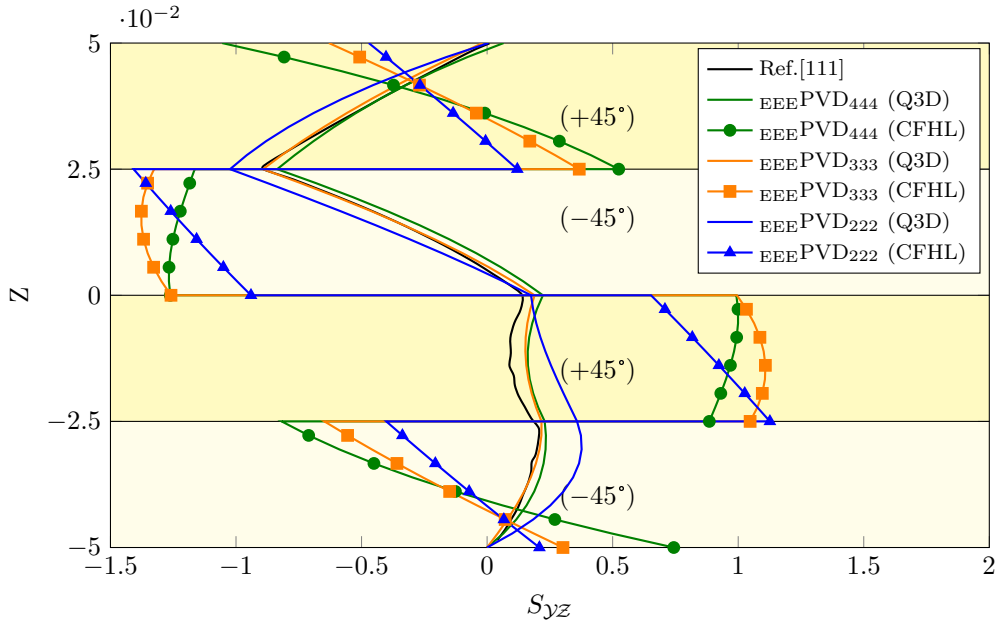

Figure 6.14: SPKST component S_{yz} at point B: case of SS1. Comparison of calculation of the stresses with constitutive laws and with the present stress recovery procedure.

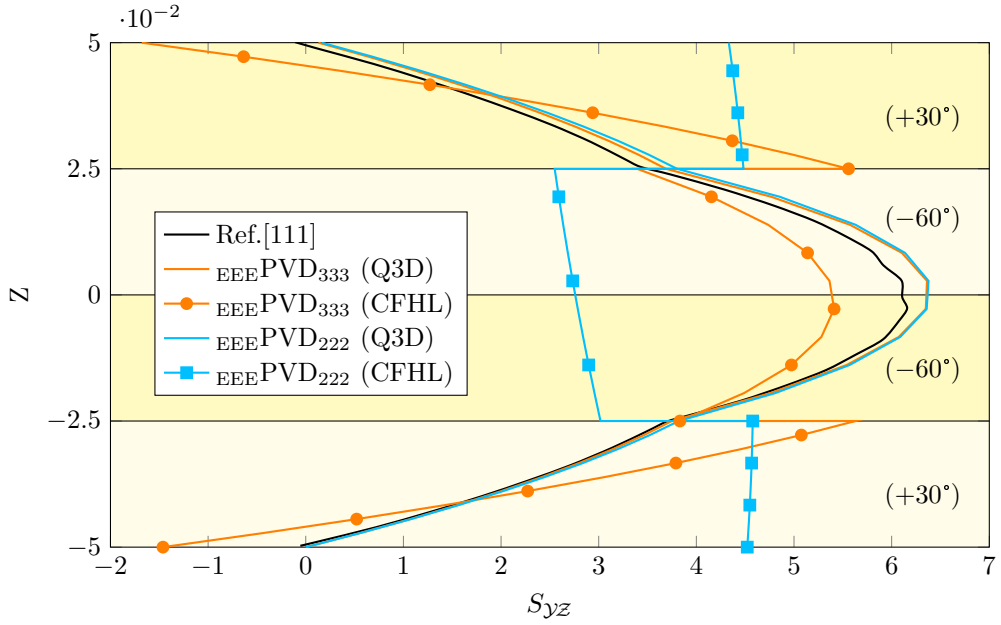

Figure 6.15: SPKST component S_{yz} at point B: case of SS2. Comparison of calculation of the stresses with constitutive laws and with the present stress recovery procedure.

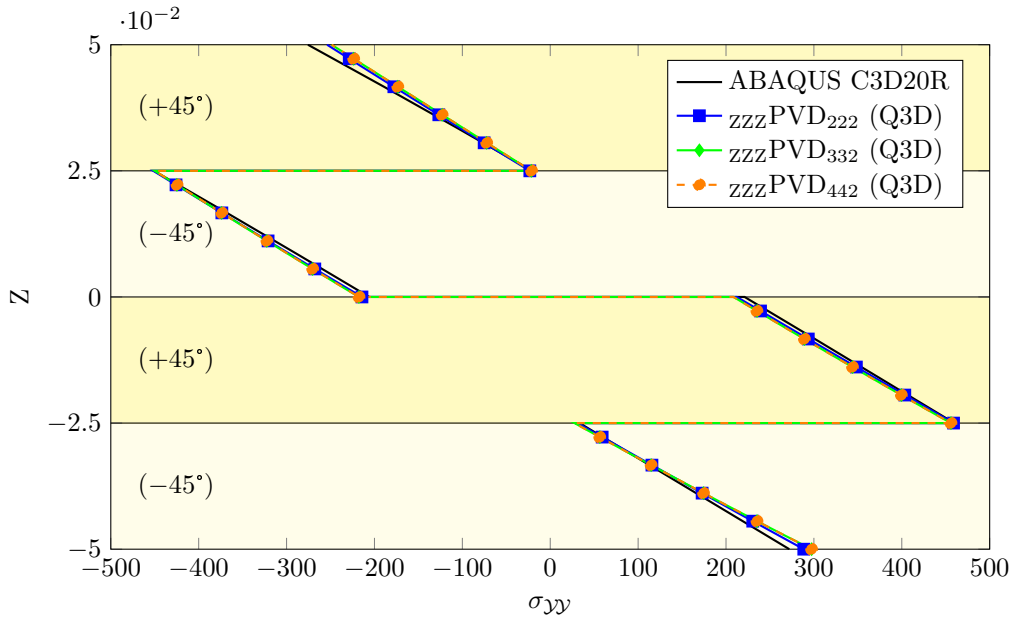

Figure 6.16: Cauchy stress component σ_{yy} at point C using the proposed stress recovery procedure for the transverse components of SPKST. SS1 is used.

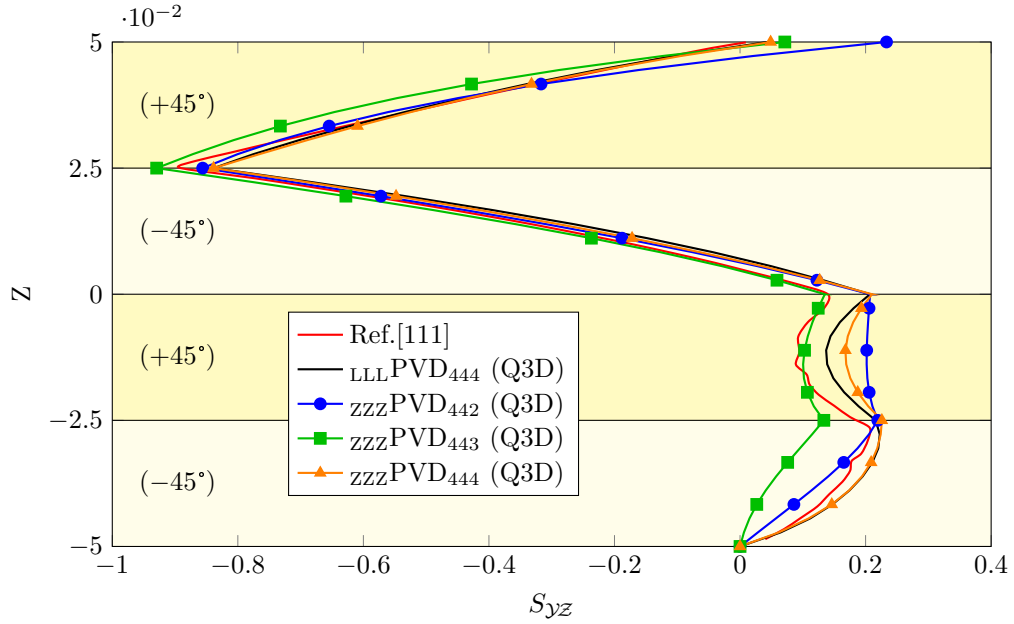

Figure 6.17: SPKST component S_{yz} at point B: case of SS1. Comparison of 5 Zig-Zag theories against literature and quasi-exact reference solution (Part I).

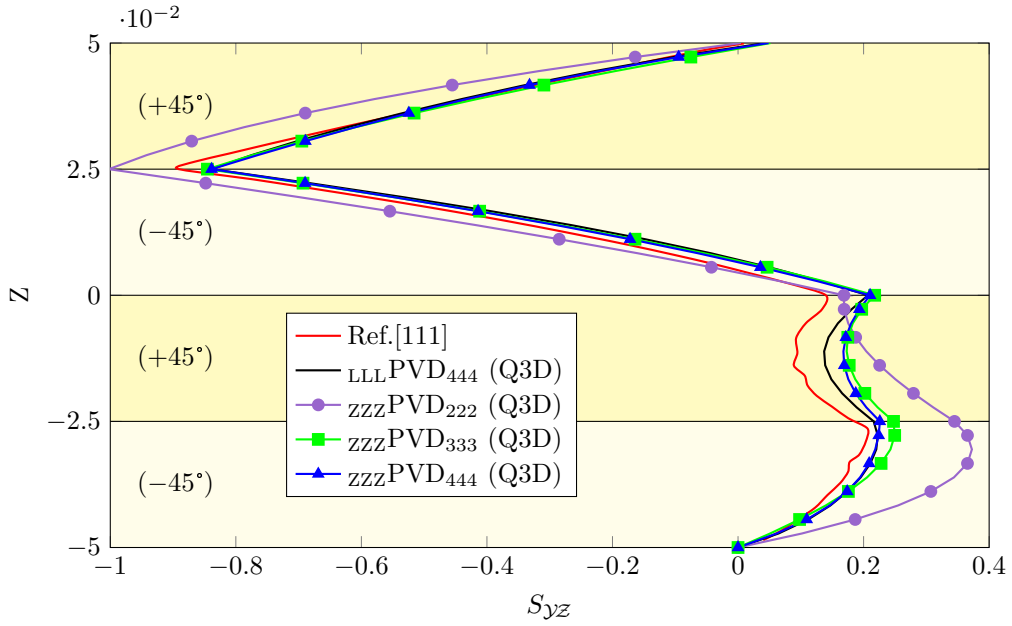

Figure 6.18: SPKST component S_{yz} at point B: case of SS1. Comparison of 5 Zig-Zag theories against literature and quasi-exact reference solution (Part II).

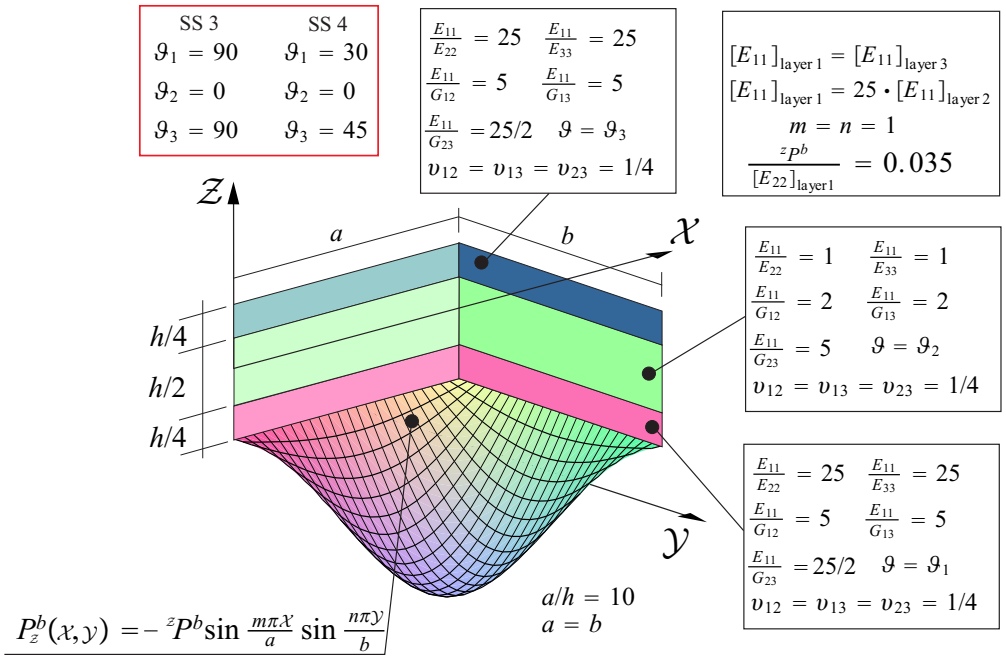

Figure 6.19: Multilayered plate subjected to a bottom surface conservative distributed load. Figure from [98]

.

named $SS3$ and $SS4$ are analyzed. All the results are written in dimensionless form as follows:

$$\begin{aligned}
&\widehat{u}_{\mathcal{X}} = u_{\mathcal{X}} \frac{E_{22}^{k=1}}{\mathcal{Z} P^b h \left(\frac{a}{h}\right)^3} \qquad \widehat{u}_{\mathcal{Y}} = u_{\mathcal{Y}} \frac{E_{22}^{k=1}}{\mathcal{Z} P^b h \left(\frac{a}{h}\right)^3} \qquad \widehat{u}_{\mathcal{Z}} = u_{\mathcal{Z}} \frac{100 E_{22}^{k=1}}{\mathcal{Z} P^b h \left(\frac{a}{h}\right)^4} \\
&\widehat{\sigma}_{\mathcal{Z}\mathcal{X}} = \frac{\sigma_{\mathcal{Z}\mathcal{X}}}{\mathcal{Z} P^b \left(\frac{a}{h}\right)} \qquad \widehat{\sigma}_{\mathcal{Z}\mathcal{Y}} = \frac{\sigma_{\mathcal{Z}\mathcal{Y}}}{\mathcal{Z} P^b \left(\frac{a}{h}\right)} \qquad \widehat{\sigma}_{\mathcal{Z}\mathcal{Z}} = \frac{\sigma_{\mathcal{Z}\mathcal{Z}}}{\mathcal{Z} P^b}; \\
&\widehat{\sigma}_{\mathcal{X}\mathcal{X}} = \frac{\sigma_{\mathcal{X}\mathcal{X}}}{\mathcal{Z} P^b \left(\frac{a}{h}\right)^2} \qquad \widehat{\sigma}_{\mathcal{Y}\mathcal{Y}} = \frac{\sigma_{\mathcal{Y}\mathcal{Y}}}{\mathcal{Z} P^b \left(\frac{a}{h}\right)^2} \qquad \widehat{\sigma}_{\mathcal{X}\mathcal{Y}} = \frac{\sigma_{\mathcal{X}\mathcal{Y}}}{\mathcal{Z} P^b \left(\frac{a}{h}\right)^2}
\end{aligned} \tag{6.2}$$

$k = 1$ identifies the bottom layer identity; $\widehat{u}_{\mathcal{Y}}$ is calculated at $\mathcal{X} = a/2, \mathcal{Y} = 0$; $\widehat{u}_{\mathcal{Z}}$, $\widehat{\sigma}_{\mathcal{X}\mathcal{X}}$, $\widehat{\sigma}_{\mathcal{Y}\mathcal{Y}}$ and $\widehat{\sigma}_{\mathcal{Z}\mathcal{Z}}$ are calculated at $\mathcal{X} = a/2, \mathcal{Y} = b/2$.

Lamination SS3 The reference solution is obtained by comparison with commercial codes ABAQUS and NASTRAN against the quasi-exact solution represented by a cubic layerwise theory (see Figs. 6.20, 6.21, 6.22). This is needed to create a benchmark reference case adopted later to compare various Zig-Zag theories. It can be noticed that the present quasi-exact is particularly correlated with the results obtained by NASTRAN.

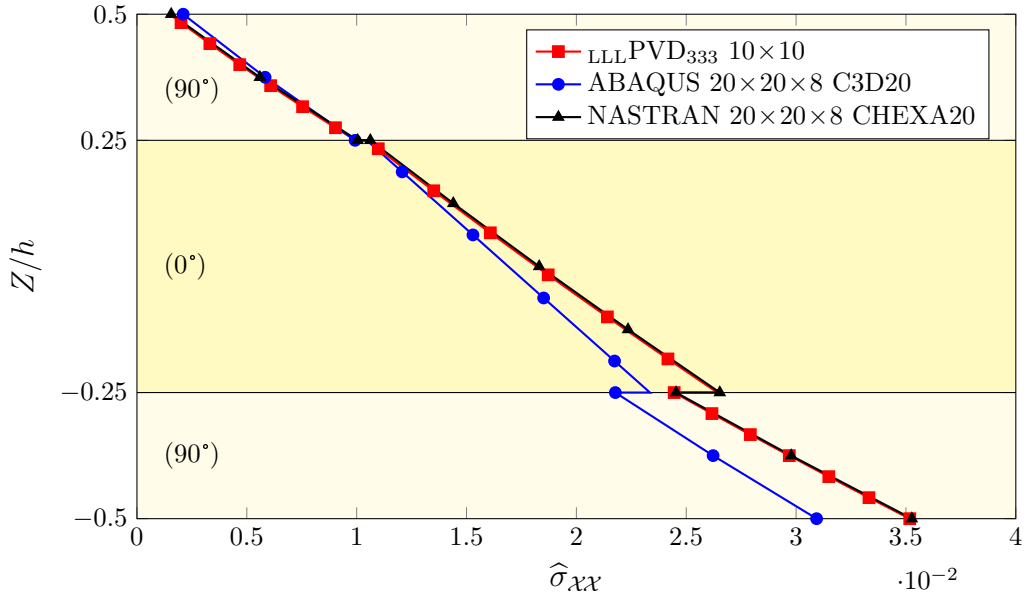

Figure 6.20: Case of SS3. In-plane normalized Cauchy stress $\widehat{\sigma}_{\mathcal{X}\mathcal{X}}$.

The Zig-Zag theories with different orders of expansions for the various displacement variables show an excellent agreement with the quasi-exact theory, as presented in Figs. 6.23, 6.24, and 6.25. The convenience of adding MZZF is obvious if theories with the same degrees of freedom are compared. The concept is shown in Figs. 6.26, 6.27, and 6.28 where a Zig-Zag theory with cubic expansion for all the

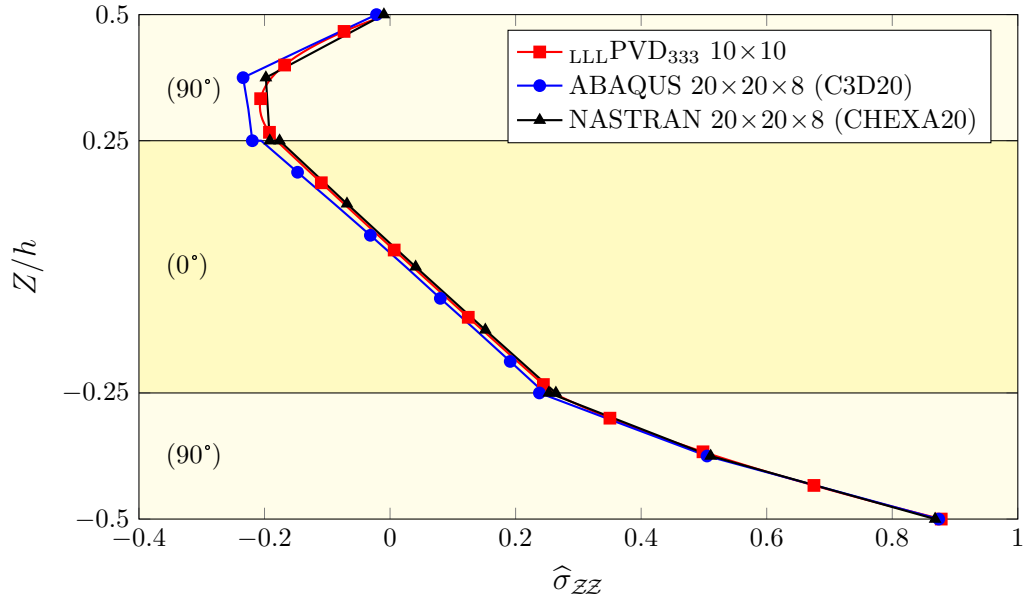

Figure 6.21: Case of SS3. Transverse normalized Cauchy stress $\widehat{\sigma}_{ZZ}$.

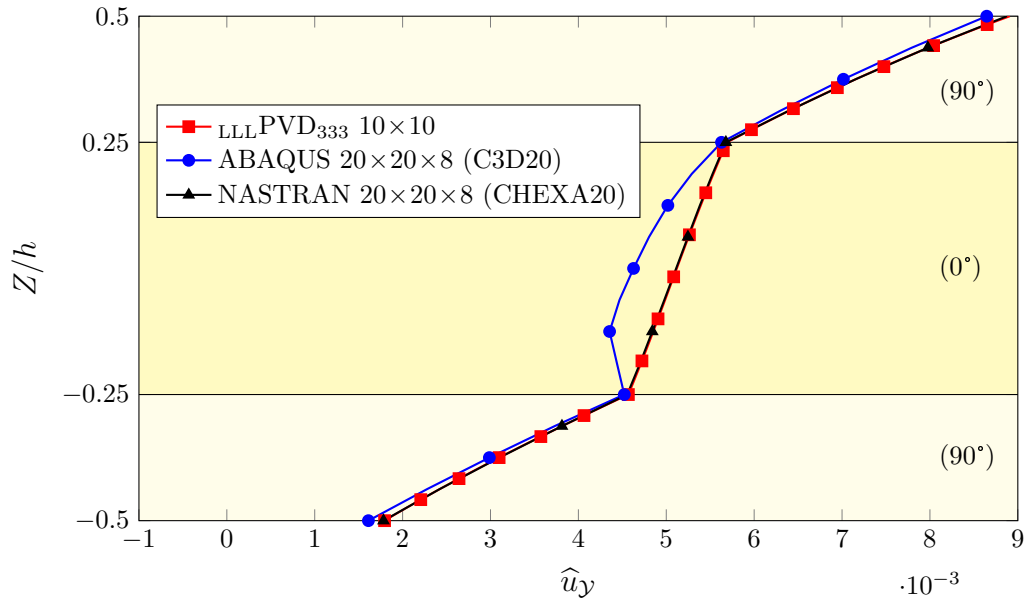

Figure 6.22: Case of SS3. In-plane normalized displacement $\widehat{u}_y$.

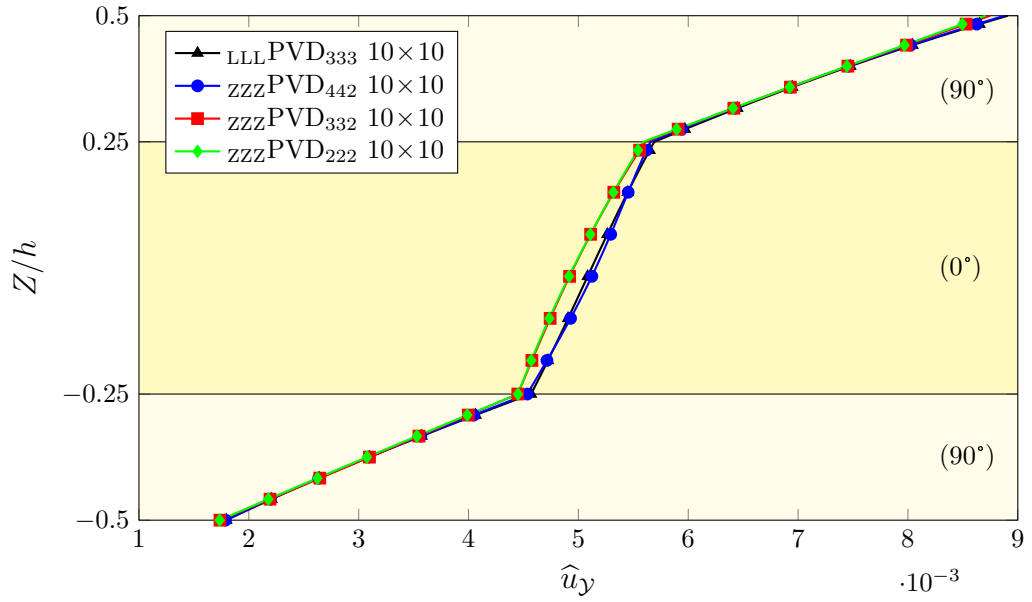

Figure 6.23: Case of SS3. In-plane normalized displacement $\widehat{u}_{\mathcal{Y}}$.

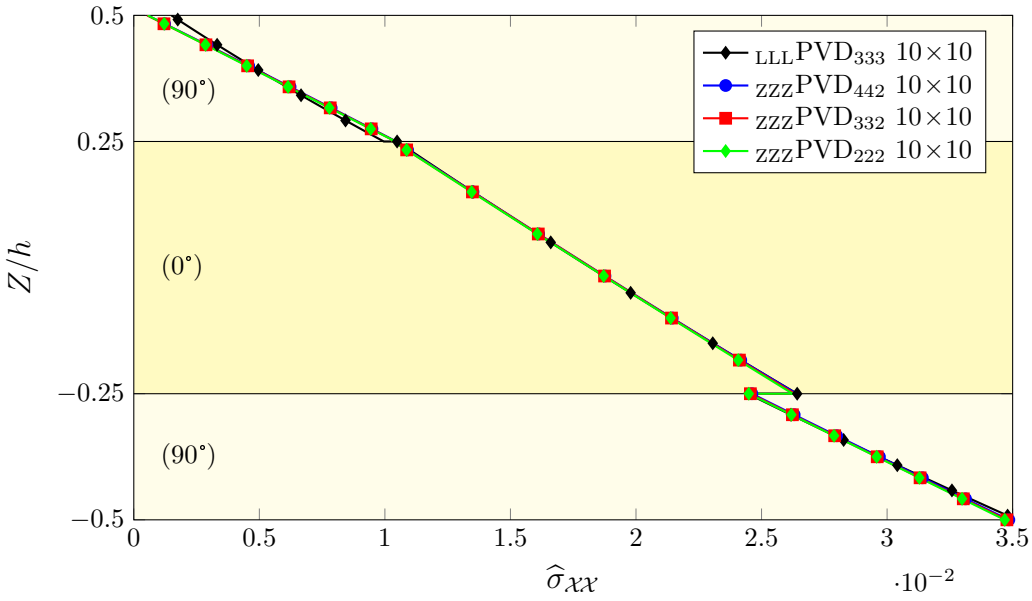

Figure 6.24: Case of SS3. In-plane normalized Cauchy stress $\widehat{\sigma}_{\mathcal{X}\mathcal{X}}$.

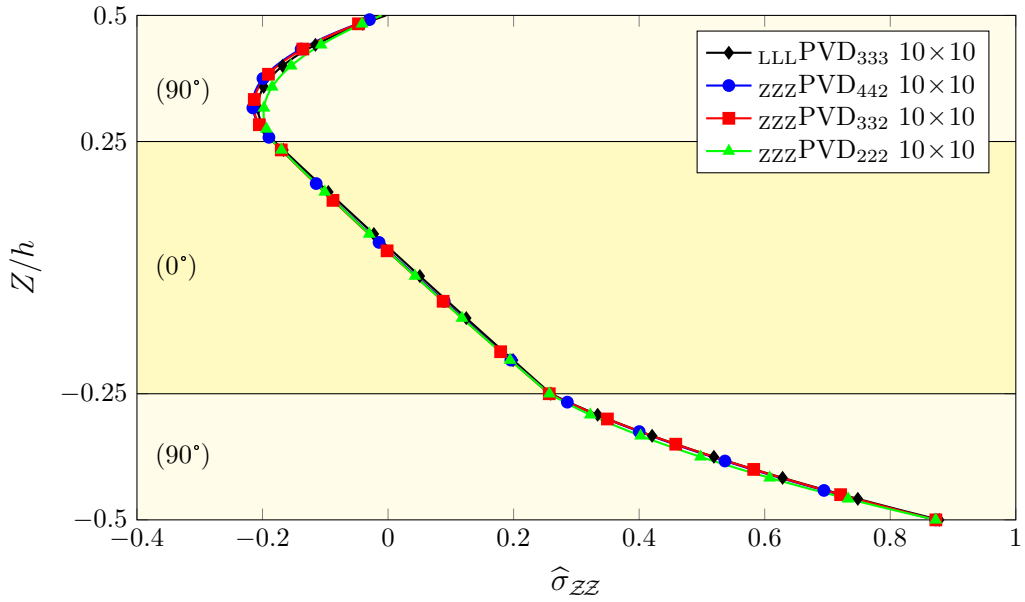

Figure 6.25: Case of SS3. Transverse normalized Cauchy stress $\widehat{\sigma}_{ZZ}$.

displacements (indicated with $_{\text{ZZZ}}\text{PVD}_{333}$) and a fourth-order ESL theory (indicated with $_{\text{EEE}}\text{PVD}_{444}$) are compared, indicating the undoubt advantage of adding MZZF also for the large displacement analysis case.

Lamination SS4 The results obtained including and discarding MZZF are also confirmed when generic lamination schemes are considered, like SS4 (see Figures 6.29, 6.30, and 6.31).

6.1.4 Thick three-layered VAT simply supported plate with bottom surface pressure

The capability of GUF for geometrical nonlinear VAT laminates is evaluated by the results with a model made of solid elements obtained with the commercial software NX NASTRAN.

Notation used for the fiber pattern The path of any fiber of layer k is defined by the angle between the fiber itself and the ${}^0\mathcal{X}$ axis

$$\vartheta^k({}^0\mathcal{X}) = \frac{2(T_1^k - T_0^k)}{a}\left|{}^0\mathcal{X} - \frac{a}{2}\right| + T_0^k \tag{6.3}$$

where T_0^k is the value of the angle in the middle of the plate and T_1^k its value on the edges (${}^0\mathcal{X} = 0$ and ${}^0\mathcal{X} = a$). Eq. (6.3) is equivalent to the expression available in the literature [27], but is formally different because here the origin of the global coordinate system is at the corner of the plate and not at its center. Since

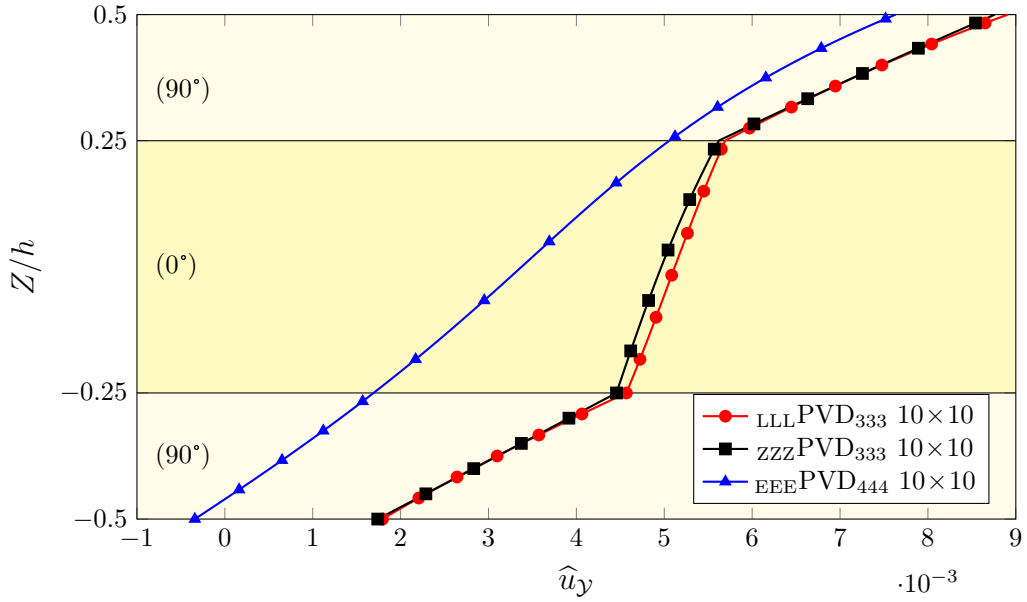

Figure 6.26: Case of SS3. In-plane normalized displacement $\widehat{u}_y$ including and discarding MZZF.

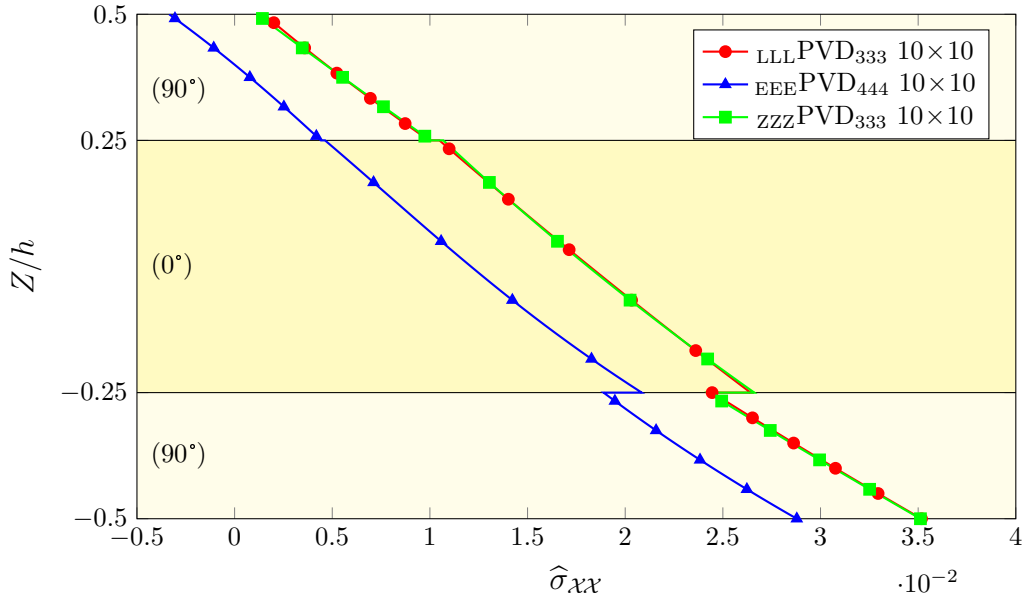

Figure 6.27: Case of SS3. In-plane normalized Cauchy stress $\widehat{\sigma}_{xx}$ including and discarding MZZF.

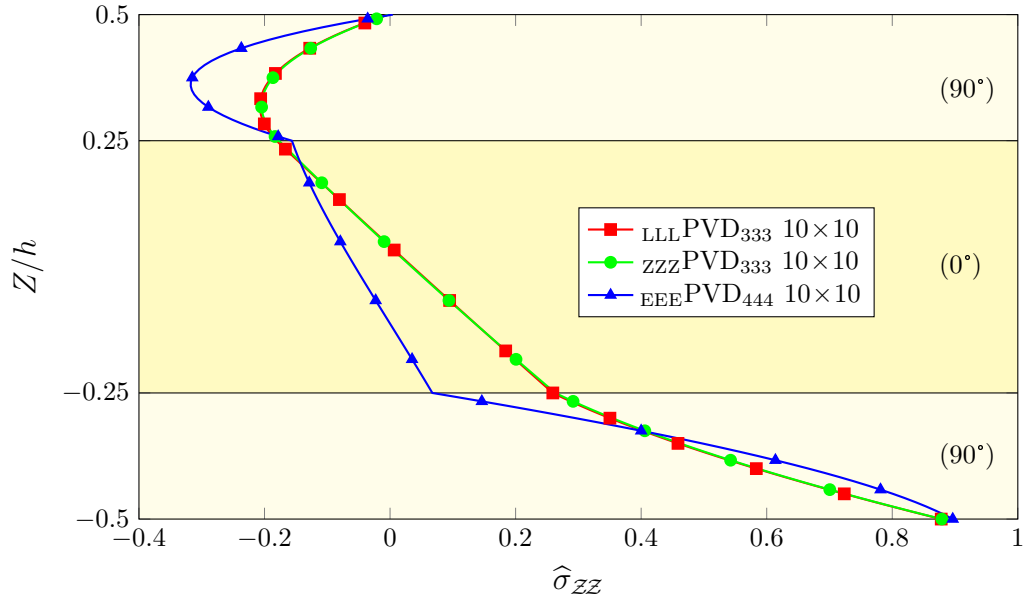

Figure 6.28: Case of SS3. Transverse normalized Cauchy stress $\widehat{\sigma}_{zz}$ including and discarding MZZF.

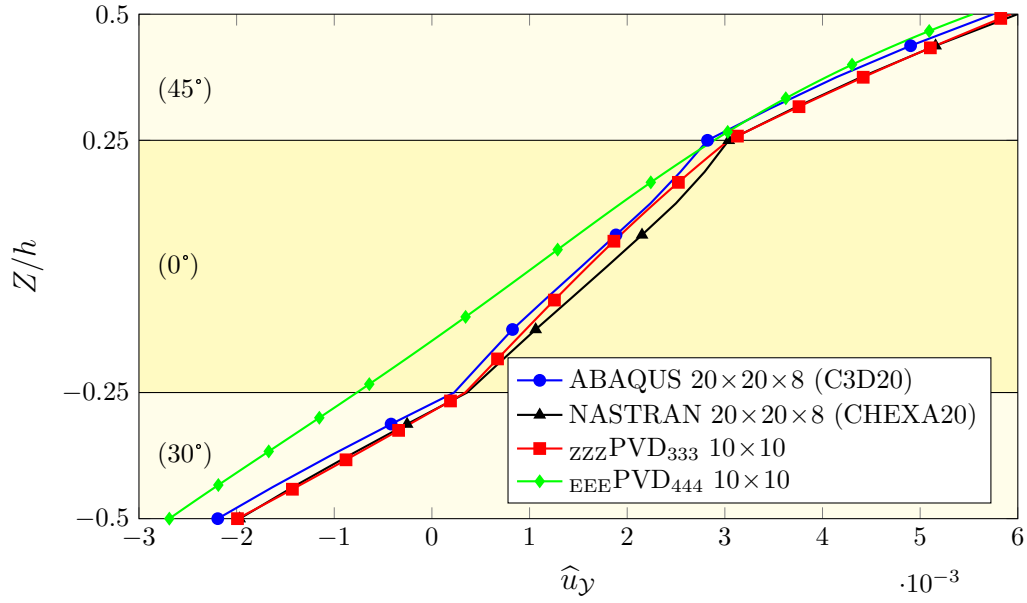

Figure 6.29: Case of SS4. In-plane normalized displacement $\widehat{u}_y$ including and discarding MZZF.

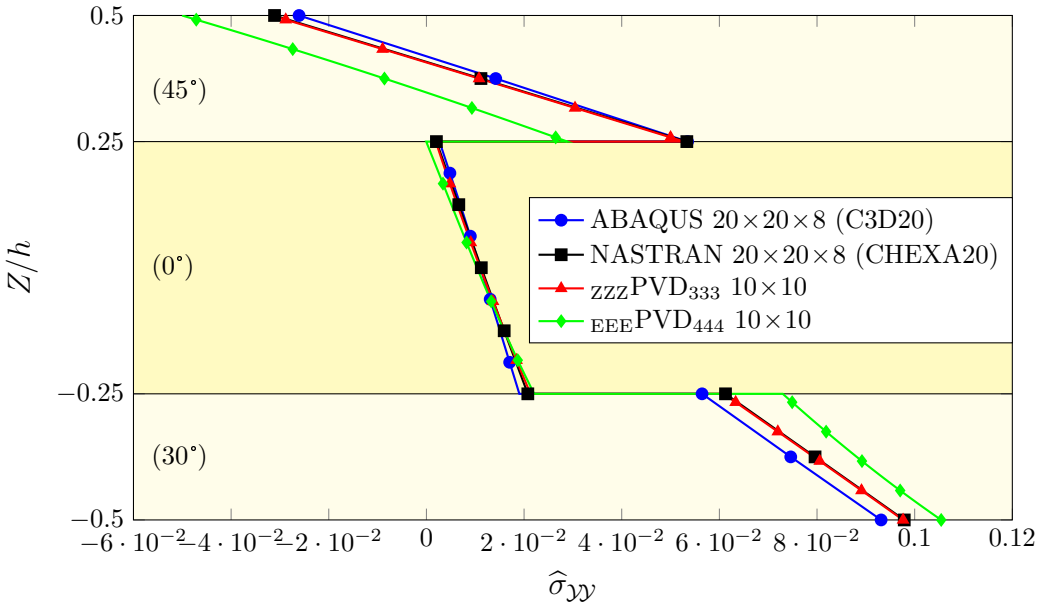

Figure 6.30: Case of SS4. In-plane normalized Cauchy stress $\widehat{\sigma}_{yy}$ including and discarding MZZF.

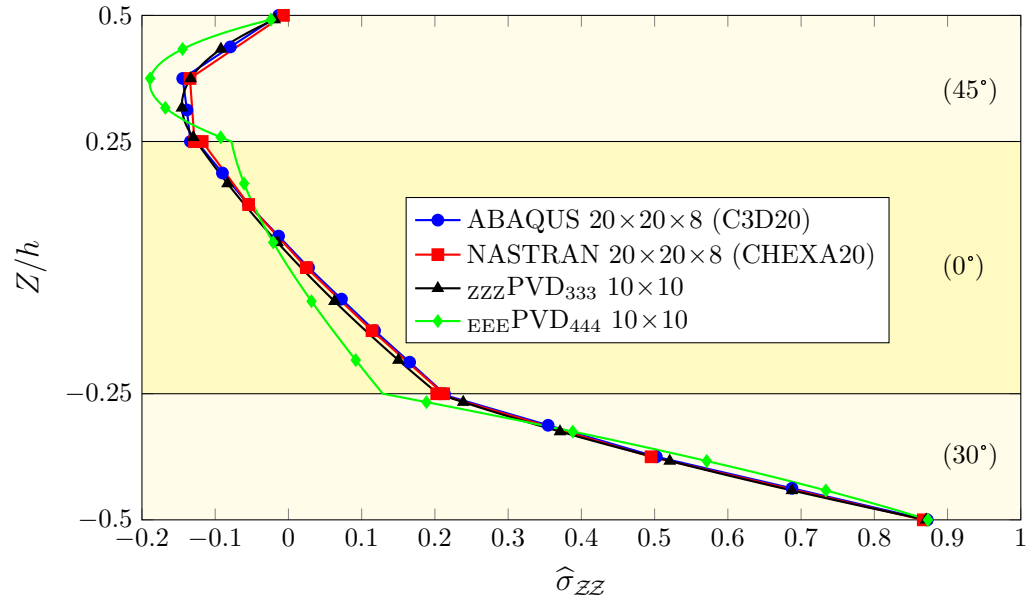

Figure 6.31: Case of SS4. Transverse normalized Cauchy stress $\widehat{\sigma}_{zz}$ including and discarding MZZF.

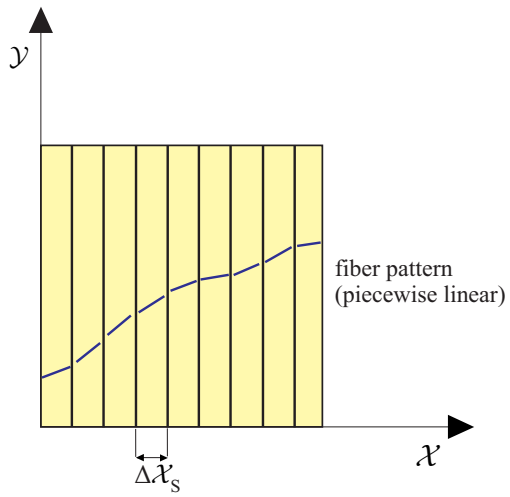

Figure 6.32: Subdivision of the solid geometry to create a piecewise linear approximation of the curvilinear fiber path within NX NASTRAN. Figure from Ref. [114].

it is assumed that the angle of the fibers is a function only of one coordinates, the fibers are parallel to each other along the ${}^0\mathcal{Y}$ axis. This simple fiber pattern can be reproduced with solid elements in a commercial software. Each layer of the 3D solid mesh is divided in vertical strips that extend from ${}^0\mathcal{X}_S - {}^0\Delta\mathcal{X}_S/2$ to ${}^0\mathcal{X}_S + {}^0\Delta\mathcal{X}_S/2$, where ${}^0\Delta\mathcal{X}_S$ is the strip width and ${}^0\mathcal{X}_S$ the position of the center of the strip on the ${}^0\mathcal{X}$ axis. Then all elements belonging to a specific strip (S) have a material reference system rotated by the angle $\vartheta^k({}^0\mathcal{X}_S)$ with respect the global reference system (see Fig. 6.32).

Test case description A simple supported square plate subject to bisinusoidal load on the bottom surface (see Fig. 6.33) has been used as a benchmark. The plate has a soft core and two skins made of orthotropic fibers. The core has a curvilinear fiber path $< (0|45) >$ and the skins have a pattern $< (30|10) >$ (see Fig. 6.34). The presence of a softer core with respect the skins will produce a significant Zig-Zag pattern of the displacements that can not be well approximated by the classical Equivalent Single Layer theories, as will be shown later.

The following dimensionless variables are introduced:

$$
\begin{aligned}
&\widehat{u}_{\mathcal{X}} = u_{\mathcal{X}} \frac{E_{22}^{k=1}}{{}^{\mathcal{Z}}P^b h \left(\frac{a}{h}\right)^3} \qquad \widehat{u}_{\mathcal{Y}} = u_{\mathcal{Y}} \frac{E_{22}^{k=1}}{{}^{\mathcal{Z}}P^b h \left(\frac{a}{h}\right)^3} \qquad \widehat{u}_{\mathcal{Z}} = u_{\mathcal{Z}} \frac{100 E_{22}^{k=1}}{{}^{\mathcal{Z}}P^b h \left(\frac{a}{h}\right)^4} \\
&\widehat{\sigma}_{\mathcal{Z}\mathcal{X}} = \frac{\sigma_{\mathcal{Z}\mathcal{X}}}{{}^{\mathcal{Z}}P^b \left(\frac{a}{h}\right)} \qquad \widehat{\sigma}_{\mathcal{Z}\mathcal{Y}} = \frac{\sigma_{\mathcal{Z}\mathcal{Y}}}{{}^{\mathcal{Z}}P^b \left(\frac{a}{h}\right)} \qquad \widehat{\sigma}_{\mathcal{Z}\mathcal{Z}} = \frac{\sigma_{\mathcal{Z}\mathcal{Z}}}{{}^{\mathcal{Z}}P^b}; \\
&\widehat{\sigma}_{\mathcal{X}\mathcal{X}} = \frac{\sigma_{\mathcal{X}\mathcal{X}}}{{}^{\mathcal{Z}}P^b \left(\frac{a}{h}\right)^2} \qquad \widehat{\sigma}_{\mathcal{Y}\mathcal{Y}} = \frac{\sigma_{\mathcal{Y}\mathcal{Y}}}{{}^{\mathcal{Z}}P^b \left(\frac{a}{h}\right)^2} \qquad \widehat{\sigma}_{\mathcal{X}\mathcal{Y}} = \frac{\sigma_{\mathcal{X}\mathcal{Y}}}{{}^{\mathcal{Z}}P^b \left(\frac{a}{h}\right)^2} \\
&\widehat{S}_{\mathcal{Z}\mathcal{X}} = \frac{S_{\mathcal{Z}\mathcal{X}}}{{}^{\mathcal{Z}}P^b \left(\frac{a}{h}\right)^2} \qquad \widehat{S}_{\mathcal{Z}\mathcal{Y}} = \frac{S_{\mathcal{Z}\mathcal{Y}}}{{}^{\mathcal{Z}}P^b \left(\frac{a}{h}\right)^2} \qquad \widehat{S}_{\mathcal{Z}\mathcal{Z}} = \frac{S_{\mathcal{Z}\mathcal{Z}}}{{}^{\mathcal{Z}}P^b \left(\frac{a}{h}\right)^2}
\end{aligned}
\tag{6.4}
$$

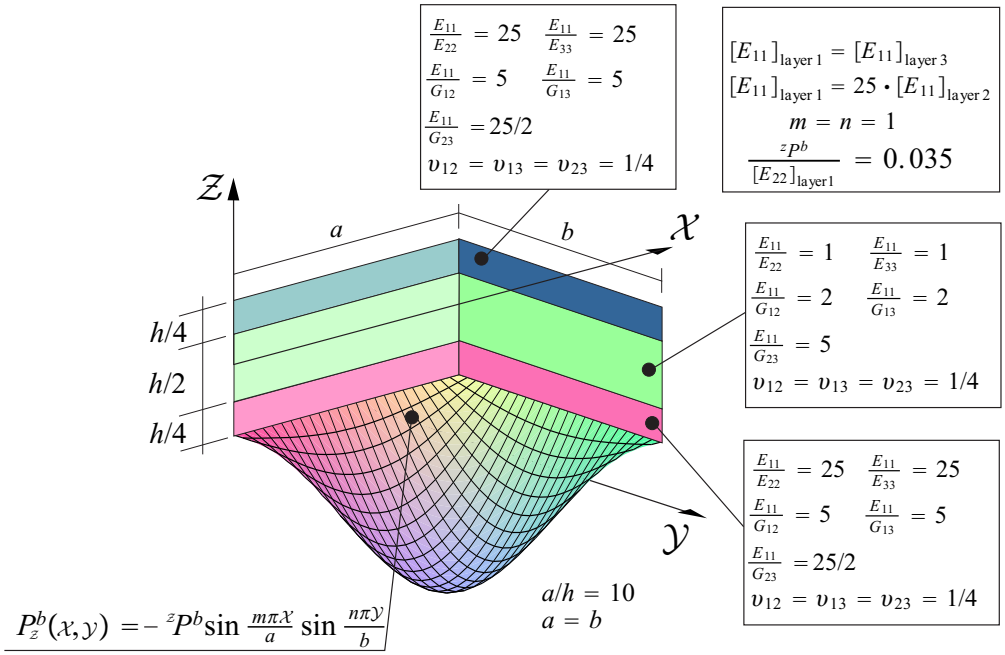

Figure 6.33: Test case geometry, materials and loads. Figure from Ref. [114].

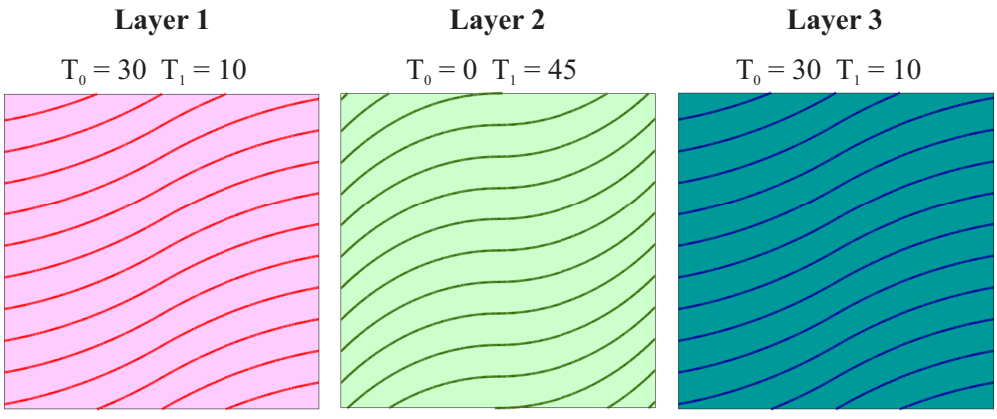

Figure 6.34: Fiber paths for all layers of the laminate. Figure from Ref. [114].

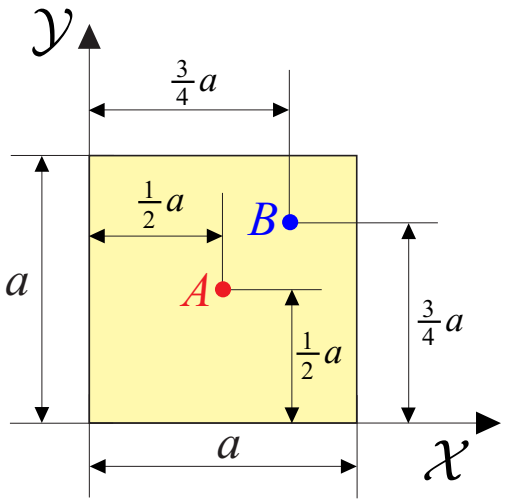

Figure 6.35: Anazlyzed points.Figure from Ref. [114].

The displacements and stresses of a point at (0.5a,0.5a) and (0.75a,0.75a) are chosen as shown in Fig. 6.35.

Finite element convergence The commercial software NX NASTRAN has been used to obtain a reference solution in order to validate and compare the axiomatic theories available in the GUF framework. Fig. 6.36 show the displacements and stress at point B along the thickness for two meshes made of parabolic solids element of size $20 \times 20 \times 12$ and $40 \times 40 \times 18$. A large number of elements has been used to improve the approximation of the curvilinear fiber path. In the following results the stress and displacement fields of the finer mesh have been considered.

Also a mesh convergence using a layerwise theory have been used (Fig. 6.37). Althoguh a 6×6 mesh reached convergence, the finer mesh has been used (10×10) for comparison with ESL theories.

Effect of including/discarding Murakami's Zig-Zag function The addition of MZZF is an effective method to improve the accuracy of the ESL theories. Fig. 6.38 shows the vertical displacements of point A as a function of the applied load. It can be seen that the addition of the Zig-Zag term allows ESL model to get an accuracy comparable with the more computational expensive and accurate cubic layerwise theory. Numerical values are reported in Table 6.3. Note that ESL theory discarding MZZF uses a higher order of expansion to keep the total number of degree of freedoms equal to the Zig-Zag model.

The presence of a softer core with respect to the skin produces a pronounced Zig-Zag form of the displacement along the thickness (Fig. 6.39). Although ESL theories discarding MZZF, also of higher order, can not reproduce this behavior, the addition of MZZF proved to solve this problem (Table 6.4).

Furthermore the stresses accuracy along the thickness significantly improves (Figs. 6.40-6.42). The

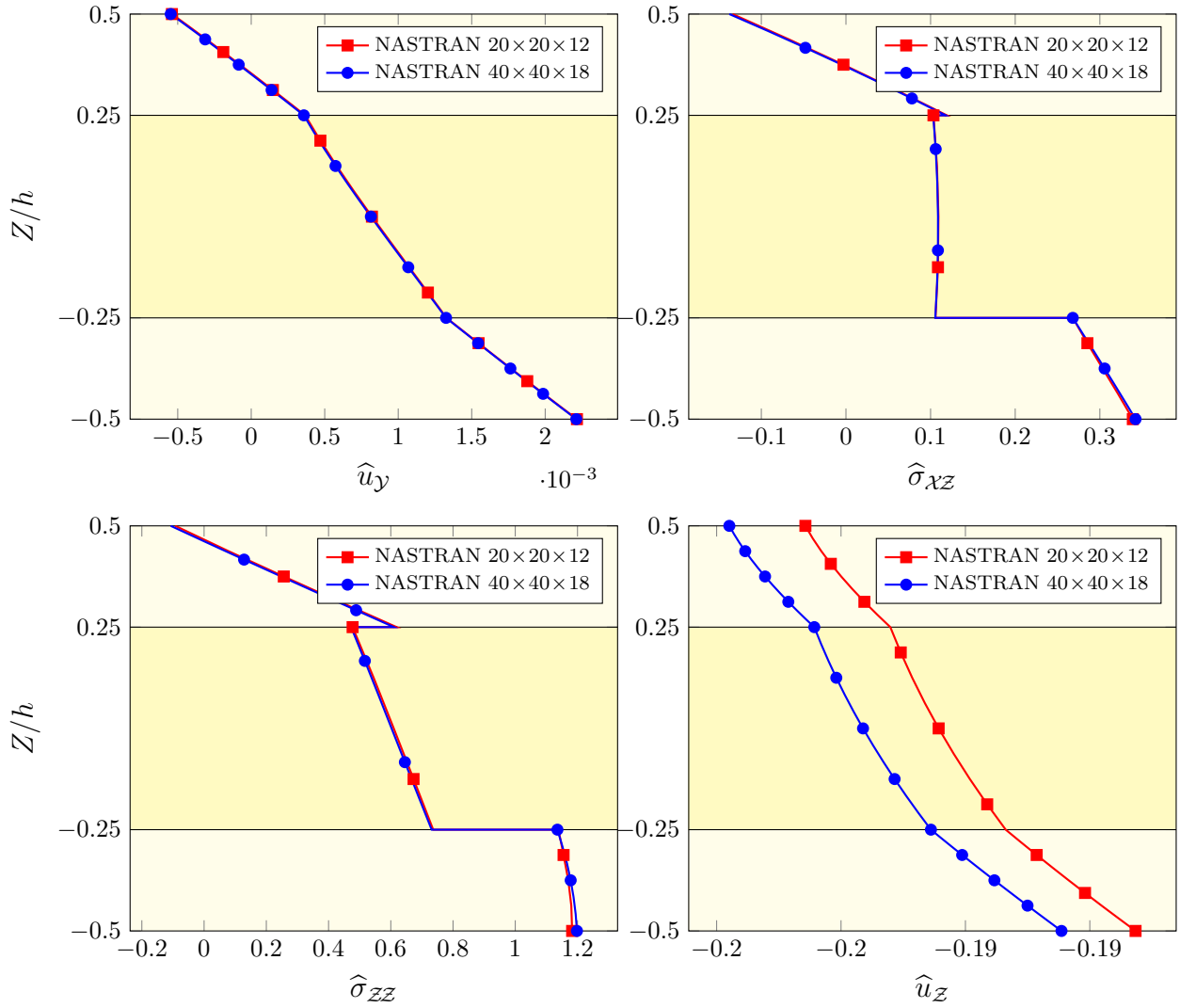

Figure 6.36: Displacements and stresses of NX NASTRAN 3D solid meshes at point B.

Table 6.3: Normalized transverse displacement u_z/h at point A. Values plotted in Fig. 6.38.

$\hat{P}$	NX NASTRAN $(40 \times 40 \times 18)$	EEEPVD$_{444}$ (10×10)	ZZZPVD$_{333}$ (10×10)	LLLPVD$_{333}$ (10×10)
35	−0.1694	−0.1457	−0.1693	−0.1689
70	−0.3278	−0.2845	−0.3275	−0.3269
140	−0.5999	−0.5323	−0.5989	−0.5981
210	−0.8187	−0.7400	−0.8165	−0.8161
280	−0.9991	−0.9148	−0.9950	−0.9955
350	−1.1521	−1.0641	−1.1457	−1.1471

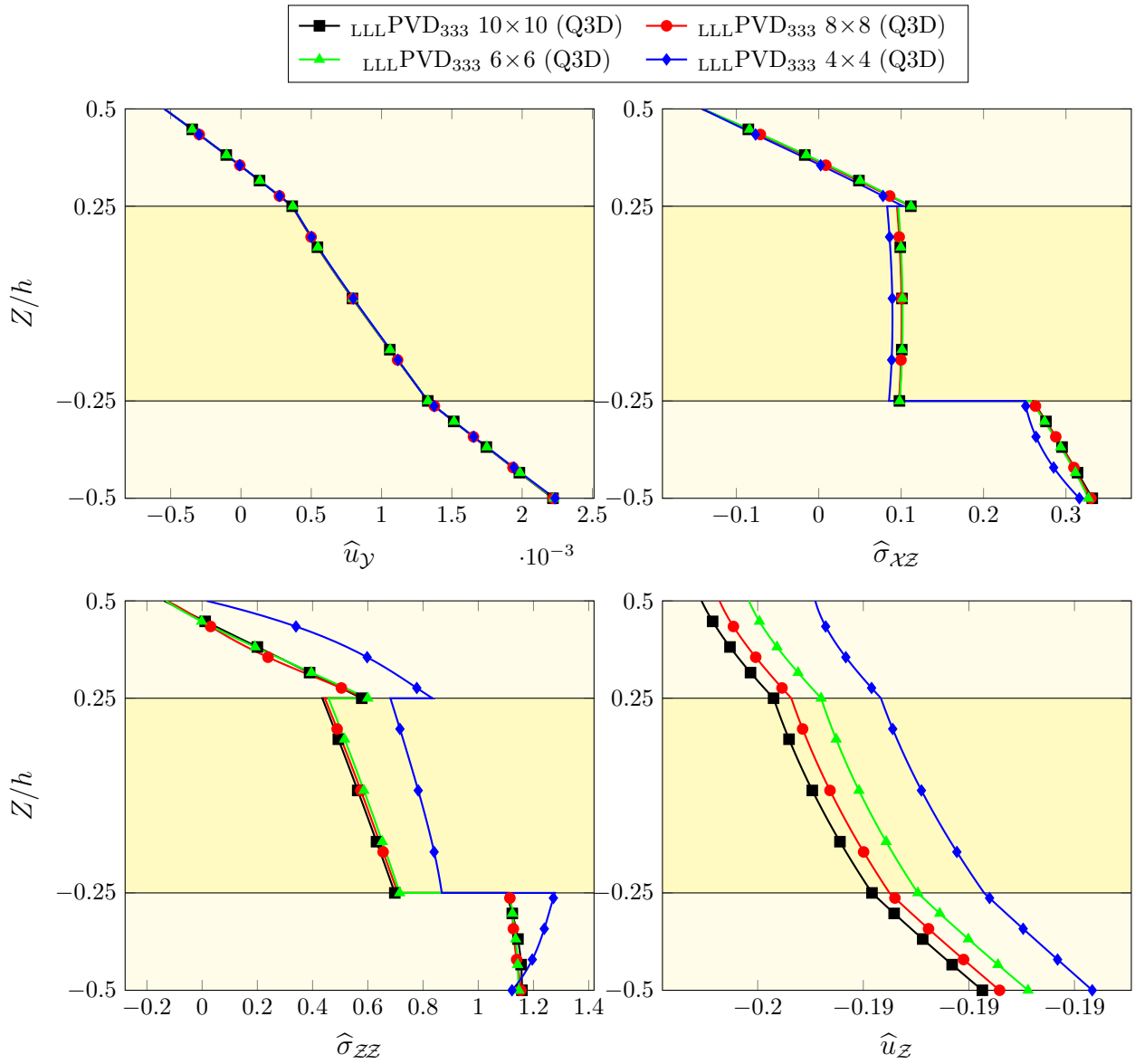

Figure 6.37: Mesh convergence using the present third-order layerwise theory LLLPVD333 at point B.

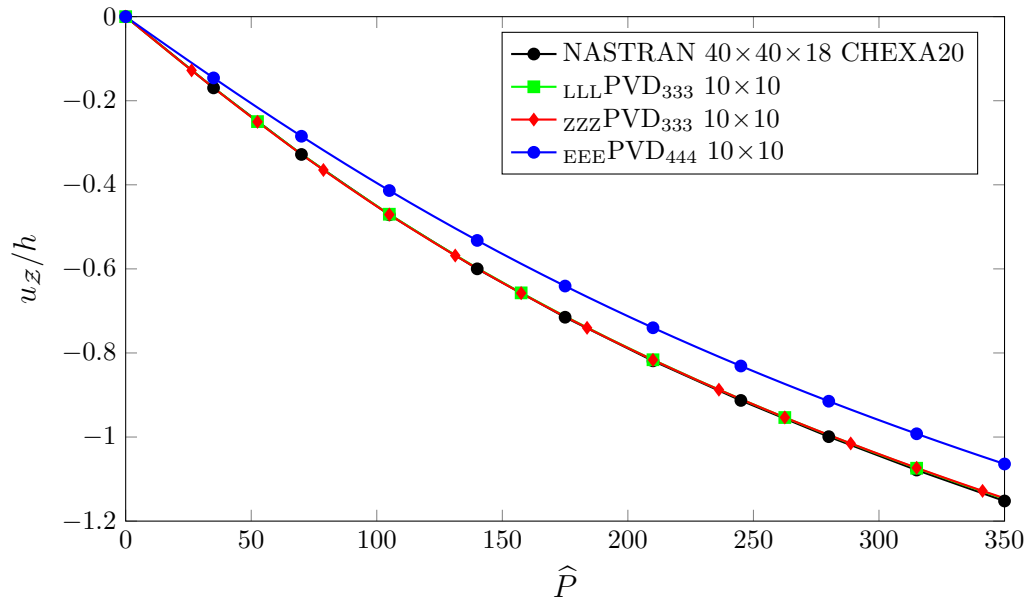

Figure 6.38: Transverse displacement u_Z/h as a function of adimensional load $\hat{P} = P \cdot (a/h)^4/E_{22}^{k=1}$

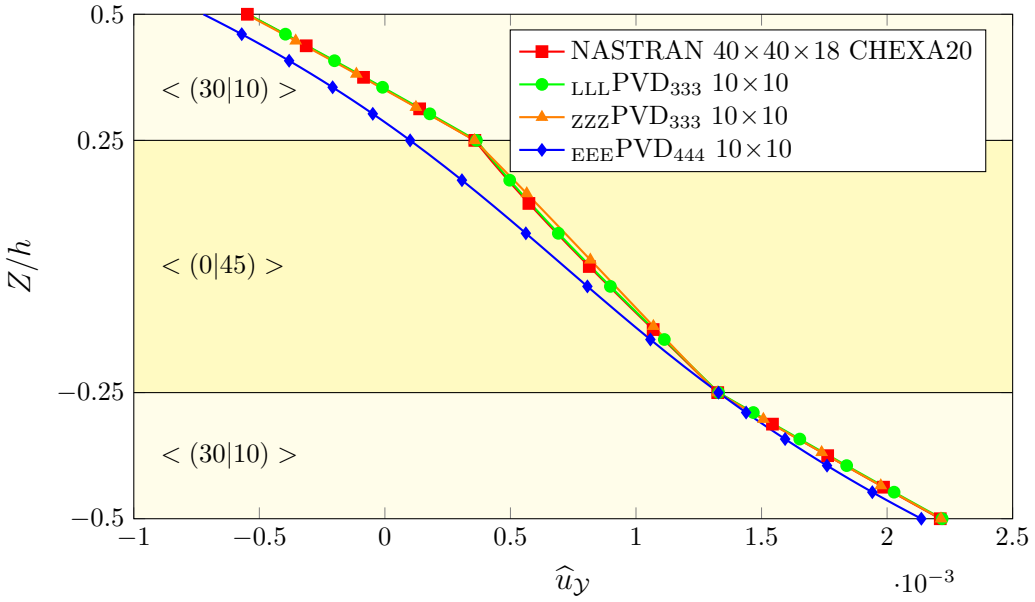

Figure 6.39: $\hat{u}_Y$ displacement at point B: effect of discarding (theory $_{\text{EEE}}\text{PVD}_{444}$) and including (theory $_{\text{ZZZ}}\text{PVD}_{333}$) MZZF.

Table 6.4: Normalized in-plane displacement $\hat{u}_y \cdot 1000$ along the laminate thickness at point B. Values plotted in Fig. 6.39.

Z/h	NX NASTRAN $(40 \times 40 \times 18)$	${}_{EEE}PVD_{444}$ (10×10)	${}_{ZZZ}PVD_{333}$ (10×10)	${}_{LLL}PVD_{333}$ (10×10)
-0.50	$+2.212$	$+2.136$	$+2.215$	$+2.219$
-0.25	$+1.326$	$+1.329$	$+1.324$	$+1.329$
$+0.00$	$+0.814$	$+0.715$	$+0.843$	$+0.819$
$+0.25$	$+0.358$	$+0.101$	$+0.357$	$+0.365$
$+0.50$	-0.548	-0.723	-0.552	-0.546

values of stresses at layer interfaces can be found in Tables 6.5-6.6. The transverse stress σ_{zz} at the center of the plate is continuous (as physically expected) along the thickness after application of the present stress recovery procedure.

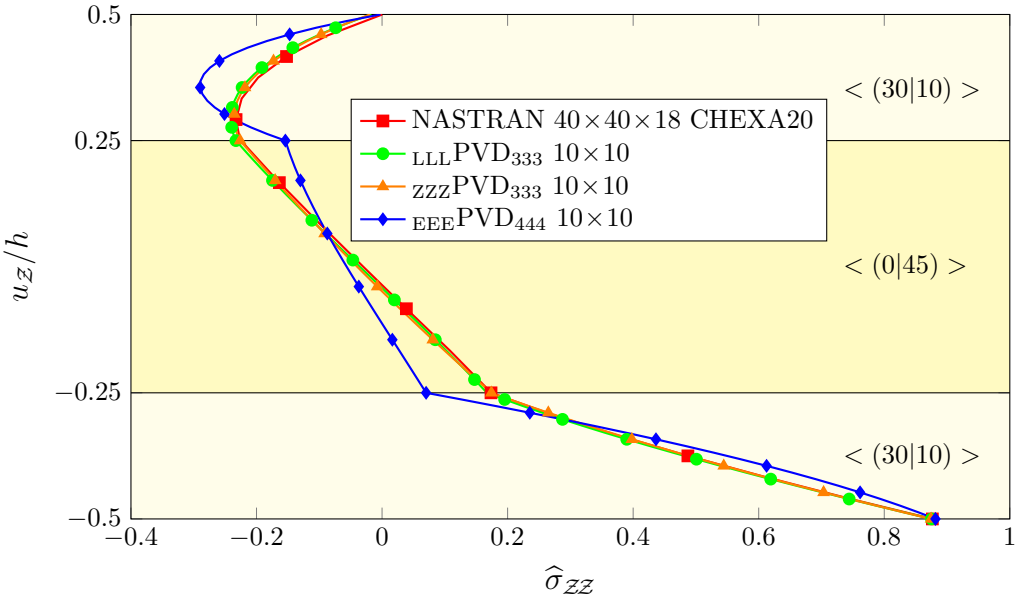

Figure 6.40: $\hat{\sigma}_{zz}$ at point A: effect of discarding (theory EEEPVD$_{444}$) and including (theory ZZZPVD$_{333}$) MZZF.

Assessment of the present stress recovery procedure Hooke's law provides accurate in-plane stresses, but does not impose the interlaminar continuity of the transverse stresses. Using the algorithm developed in section 5.3 the interlaminar continuity can be reestablished as seen in Figs. 6.43 and 6.44. Here the SPKST is shown. It can be seen that CFHL provides acceptable results for layerwise theories because the discontinuity is not much pronounced. It is of interest to note how the addition of MZZF improves the transverse stress S_{xz} predicted by ESL also in case where CFHL is used (Fig. 6.44).

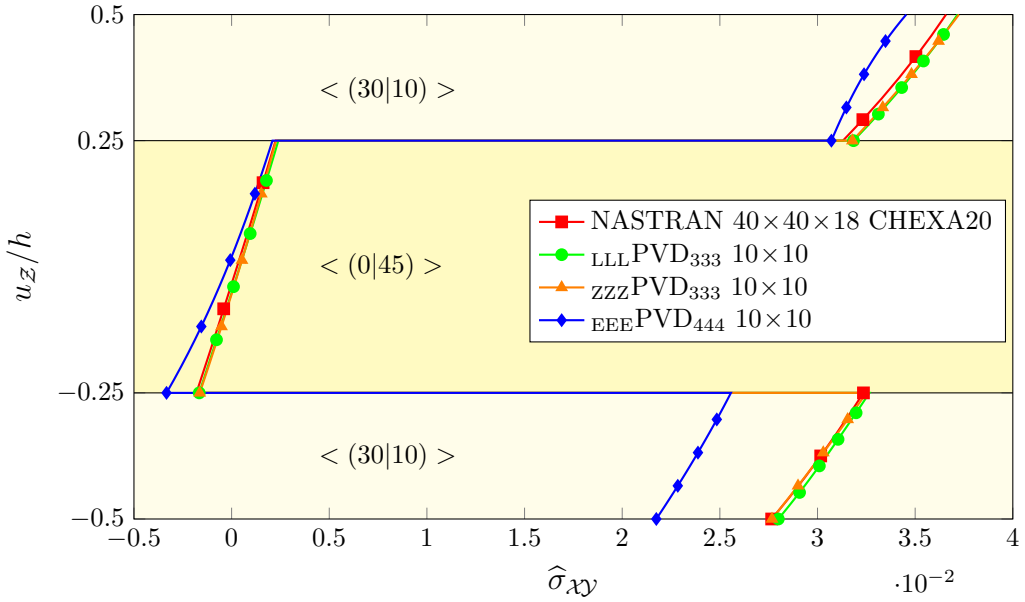

Figure 6.41: $\hat{\sigma}_{\mathcal{XY}}$ at point B: effect of discarding (theory $_{\text{EEE}}\text{PVD}_{444}$) and including (theory $_{\text{ZZZ}}\text{PVD}_{333}$) MZZF.

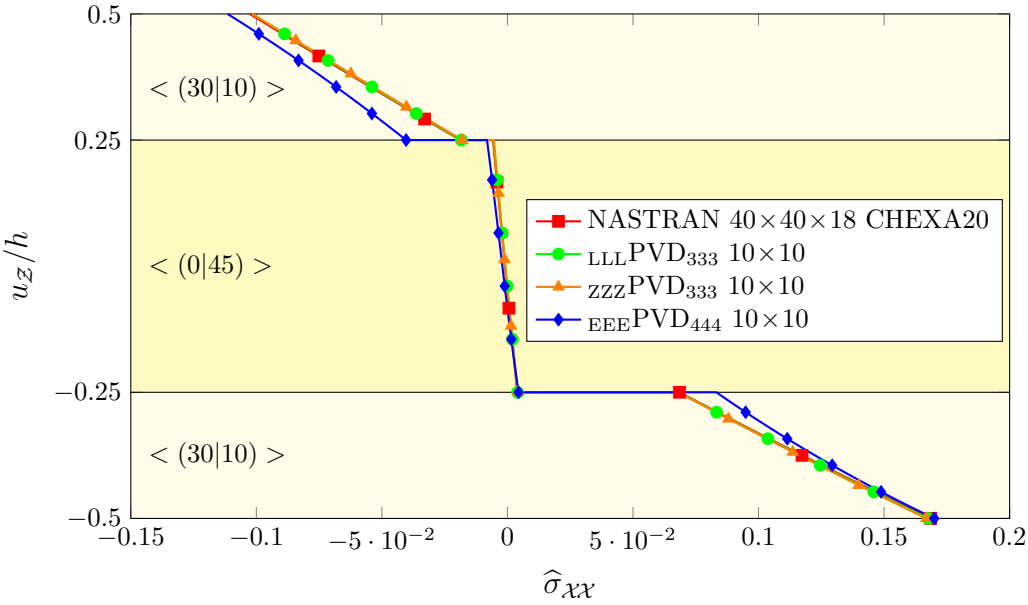

Figure 6.42: $\hat{\sigma}_{\mathcal{XX}}$ at point B: effect of discarding (theory $_{\text{EEE}}\text{PVD}_{444}$) and including (theory $_{\text{ZZZ}}\text{PVD}_{333}$) MZZF.

Table 6.5: Normalized in-plane Cauchy stress $\hat{\sigma}_{\mathcal{XY}} \cdot 1000$ along the laminate thickness at point B. Values plotted in Fig. 6.41.

Z/h	NX NASTRAN $(40 \times 40 \times 18)$	${}_{EEE}PVD_{444}$ (10×10)	${}_{ZZZ}PVD_{333}$ (10×10)	${}_{LLL}PVD_{333}$ (10×10)
-0.50	$+27.653$	$+21.746$	$+27.670$	$+27.992$
-0.25	$+32.352$	$+25.566$	$+32.505$	$+32.659$
-0.25	-1.8016	-3.3321	-1.6309	-1.6585
-0.00	$+0.2786$	-0.2062	$+0.4282$	$+0.4195$
$+0.25$	$+2.2538$	$+2.0909$	$+2.2779$	$+2.3921$
$+0.25$	$+31.301$	$+30.711$	$+31.786$	$+31.842$
$+0.50$	$+36.580$	$+34.543$	$+37.243$	$+37.170$

Table 6.6: Normalized transverse Cauchy stress $\hat{\sigma}_{\mathcal{ZZ}} \cdot 1000$ along the laminate thickness at point A. Values plotted in Fig. 6.40.

Z/h	NX NASTRAN $(40 \times 40 \times 18)$	${}_{EEE}PVD_{444}$ (10×10)	${}_{ZZZ}PVD_{333}$ (10×10)	${}_{LLL}PVD_{333}$ (10×10)
-0.50	$+876.6$	$+881.5$	$+874.6$	$+875.3$
-0.25	$+173.6$	$+70.19$	$+174.21$	$+167.16$
-0.25	$+174.1$	$+70.19$	$+174.21$	$+167.16$
-0.00	-29.99	-56.38	-39.61	-35.45
$+0.25$	-224.8	-154.0	-226.1	-232.8
$+0.25$	-226.2	-154.0	-226.1	-232.8
$+0.50$	$+0.351$	-2.517	-18.99	-16.97

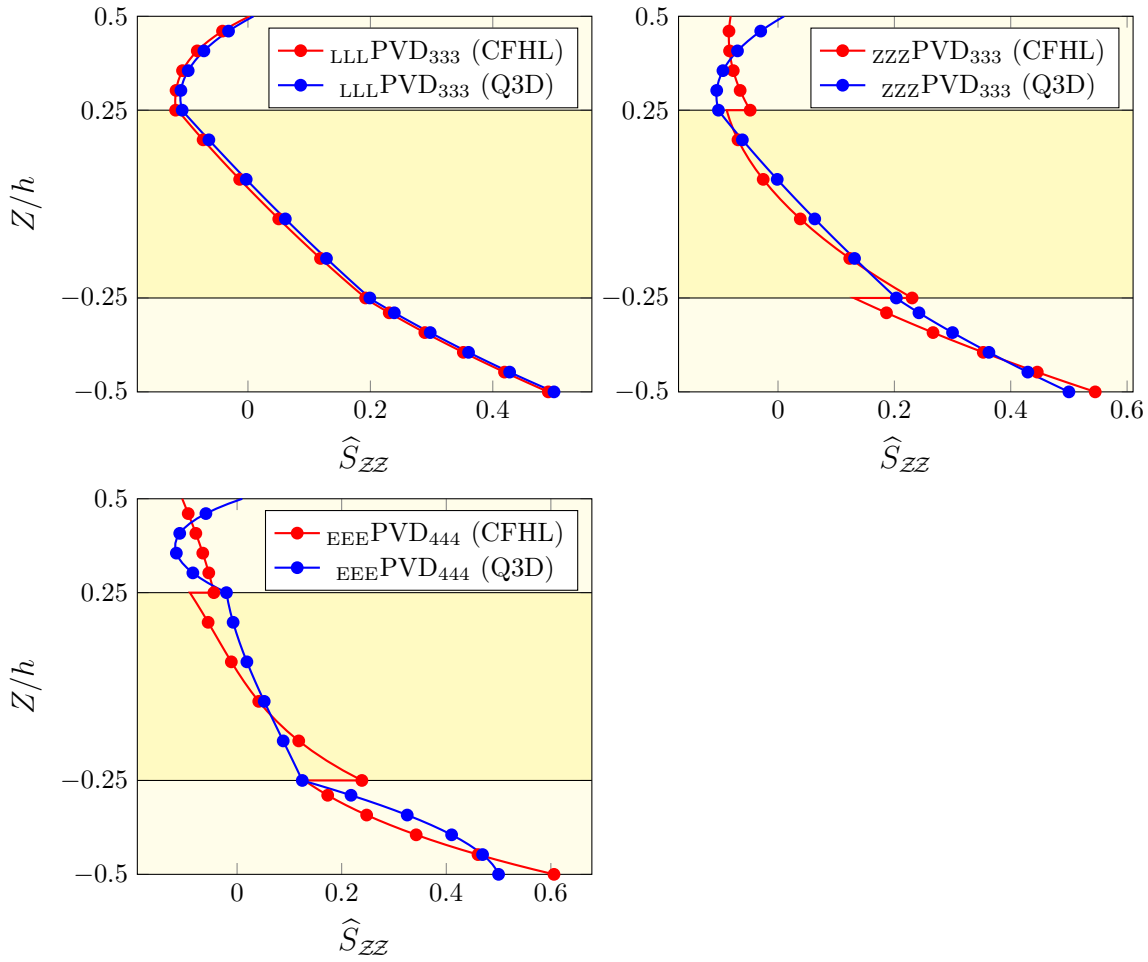

Figure 6.43: Stress $\hat{S}_{zz}$ obtained by CFHL and present recovery procedure at B.

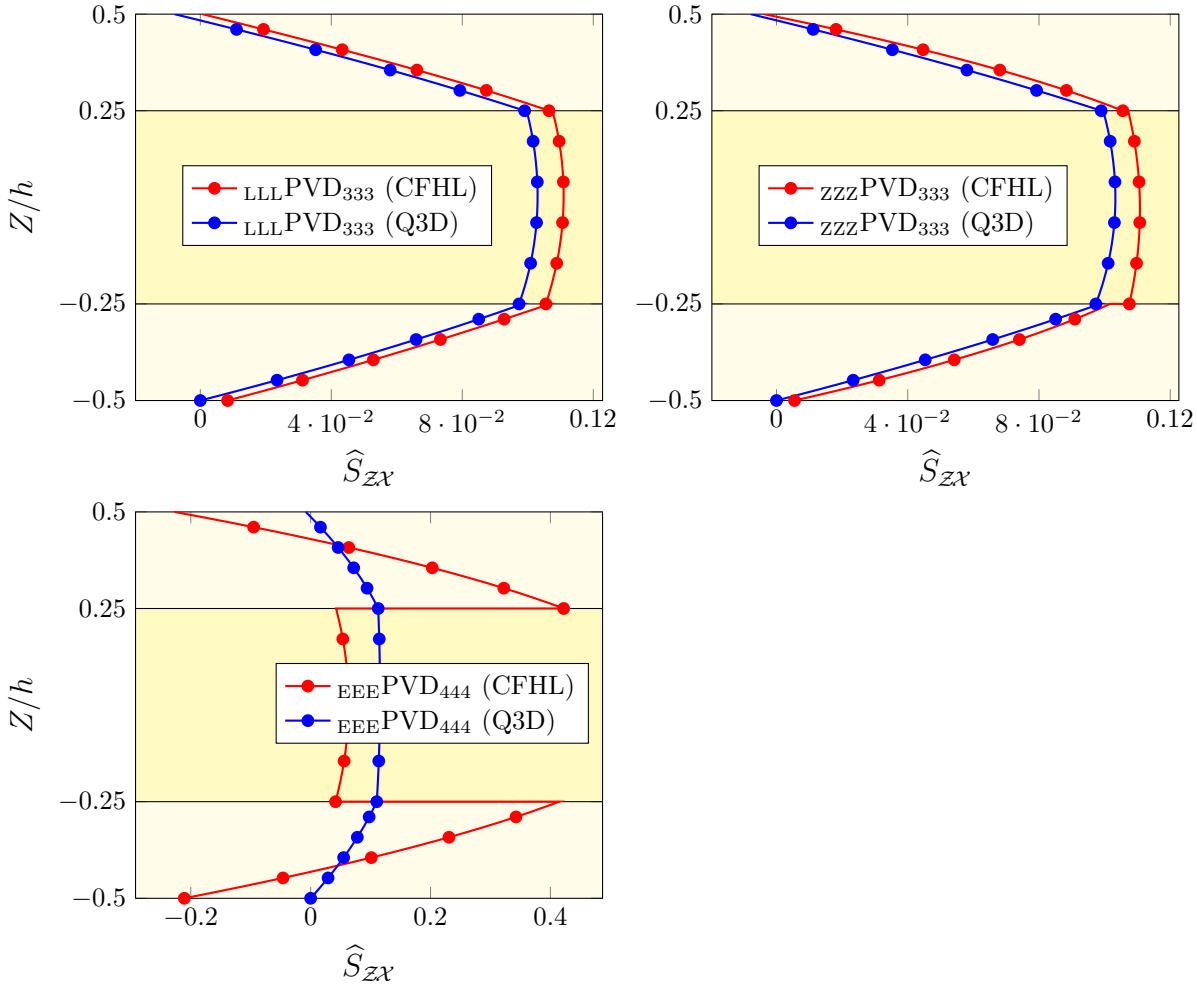

Figure 6.44: Stress $\hat{S}_{\mathcal{Z}\mathcal{X}}$ obtained by CFHL and present recovery procedure at B.

6.2 Dynamics

The following test cases are presented:

- *Plunging motion of a cantilever plate*: first benchmark problem to validate the implementation of FEM equations in a non-inertial reference frame.
- *Flap rotation of a rectangular plate*: second benchmark problem for validation of kinematically prescribed boundary condition in a non-inertial reference frame. In this case additional term are activated (e.g. gyroscopic damping and dynamic stiffness).
- *Clamped plate under uniform step function load*: the time variation of the transverse stresses obtained with different axiomatic theories are compared with data from literature. Successively, the solution of the ESL theories are improved by a multi-model analysis or the stress recovery procedure.

6.2.1 Plunging motion of a cantilever plate

This benchmark problem [105] is used to test the correct implementation of the dynamic algorithm in a moving reference frame. Due to a lack of rotation only the additional arrays coming from a rigid body translation (defined in paragraph 4.3.3) are considered. The model consists of a rectangular plate with an imposed sinusoidal motion at the root as shown in Fig. 6.45. The motion represent the only source of deformation, not external loads are applied. The plate is made of steel (Table 6.7) and it oscillates at a

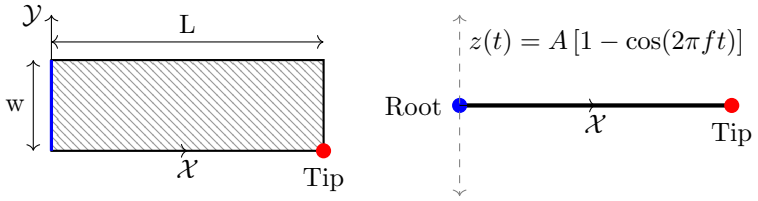

Figure 6.45: Geometry of plunging plate [105]. Nodes at root are kinematically constrained.

frequency f=1.78 Hz with a semi-amplitude A=0.0175 m. The plate has been discretized using six elements

Table 6.7: Dimensions and material property for plunging motion.

Data	Symbol	Value
length	L	0.3 m
width	w	0.1 m
thickness	h	0.001 m
Young's modulus	E	210 GPa
Poisson's ratio	ν	0.3
density	ρ	7800 kg/m^3

along the span and two along the chord (twenty-four triangular elements). The same time step size found in the reference has been used ($\Delta t = 0.001$ s).

The total vertical displacements, combination of the rigid motion and elastic deformation, is plotted against time (see Fig. 6.45). There is a perfect match with the reference data, also with a parabolic ESL theory. A low order theory was enough to capture the deformations because the plate analyzed is a thin isotropic lamina.

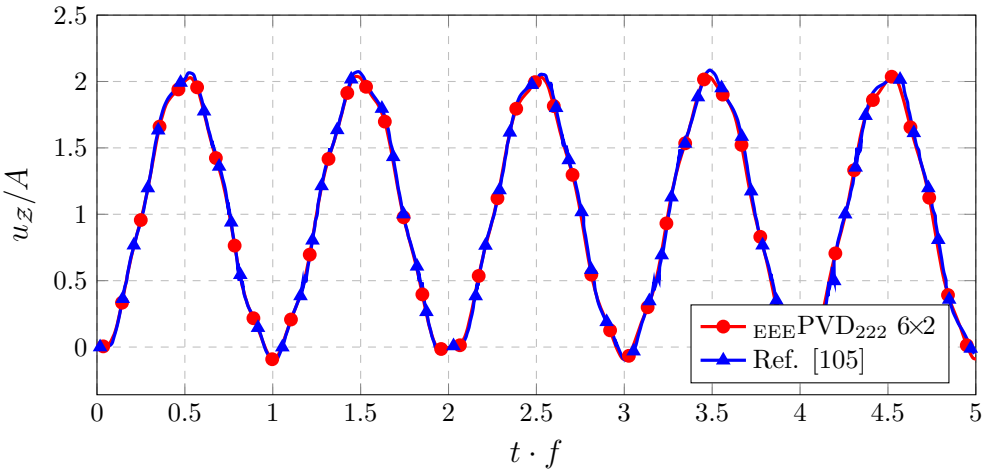

Figure 6.46: Time variation of transverse tip displacements of a pure plunging cantilever plate.

6.2.2 Flap rotation of a rectangular plate

This benchmark problem [105] has the objective to test the implementation of the remaining arrays linked to the rotational motion (e.g. centrifugal forces) that were not activated in the previous test. For this reason, the equations are solved in *a rotating reference frame*.

The model consists of a rectangular plate with an imposed sinusoidal rotation in a 5×5 mm square area at the root (blue square in Fig. 6.47). The motion represents the only source of deformation, no external loads are applied. The plate is made of aluminum (Table 6.8) and it oscillates at a frequency f=5 Hz with

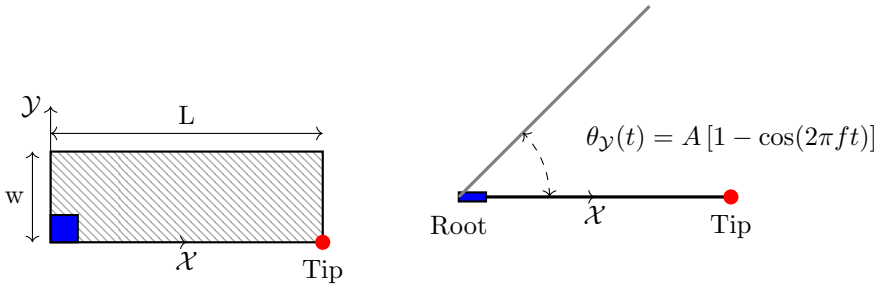

Figure 6.47: Geometry of flapping plate [105]. Nodes at root are kinematicaly constraint.

a semi-amplitude A=17 deg around the $\mathcal{Y}$ axis. The simulation have been performed with a mesh of sixteen

Table 6.8: Dimensions and material property for flap rotation.

Data	Symbol	Value
length	L	80 mm
width	w	27 mm
thickness	h	0.2 mm
Young's modulus	E	70 GPa
Poisson's ratio	ν	0.3
density	ρ	2700 kg/m^3

elements along the span and four along the chord and a the time step size $\Delta t = 0.00015$ s.

The total vertical displacement ($\mathcal{Z}$ direction) due to both rigid motion and elastic deformation is plotted against time (see Fig. 6.47). The results compare well with the available data.

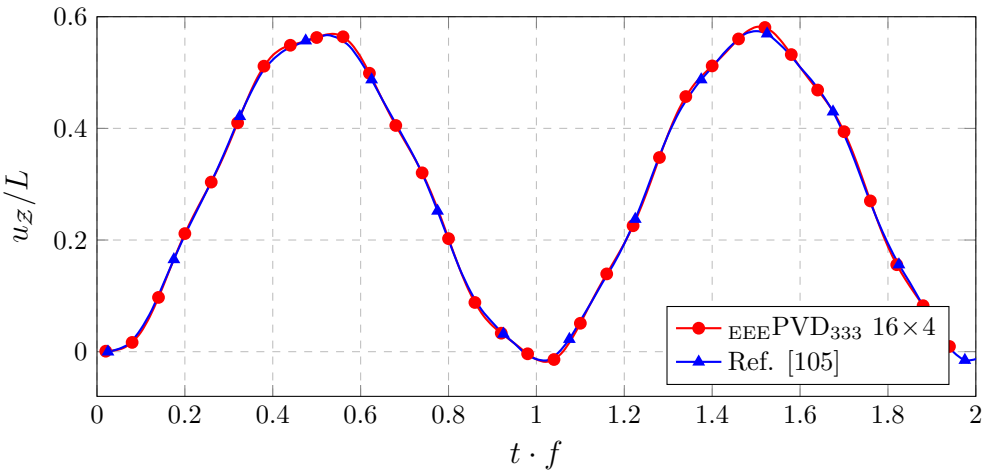

Figure 6.48: Time variation of transverse tip displacements for a flapping rectangular plate.

6.2.3 Clamped plate under uniform step function load

This problem, taken from literature [115], is used as a benchmark to test the capability of the *stress recovery procedure for dynamic loads and the effectiveness of GUF for global-local analysis*. Let's consider a square symmetric laminate $[0/90]_s$ with all four edges clamped with an applied pressure load on the top surface. This load is applied at the initial time t=0 instantaneously and kept constant during the duration of the simulation. Thanks to the symmetry present only a quarter of the plate is modeled (see Fig.6.49). The material properties and the plate dimensions are listed in Table 6.9.

A 5×5 mesh of quartic triangular elements have been used to model the quarter-plate laminate. It is of interest to compare the performance of the ESL, Zig-Zag and LW theories in term of displacement and

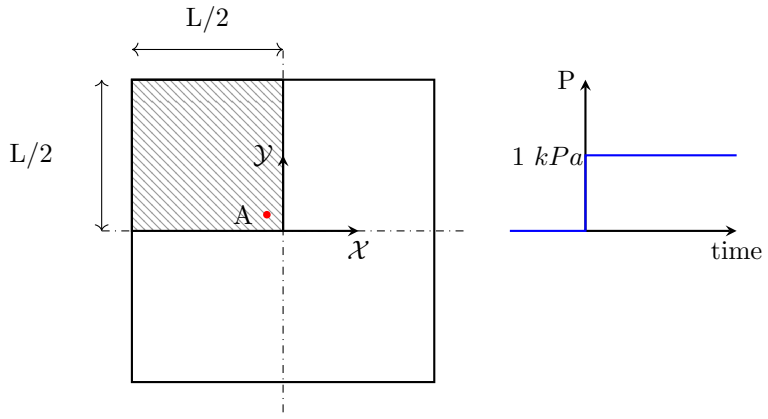

Figure 6.49: Geometry of plate and applied load.[115].

Table 6.9: Geometry and material property from Ref. [115].

Data	Symbol	Value
Length	L	220 mm
Thickness	h	3.43 mm
Young modulus	E_1	43.34 GPa
	E_2	12.73 GPa
	E_3	43.34 GPa
Shear modulus	G_{12}	4.46 GPa
	G_{13}	4.46 GPa
	G_{23}	4.46 GPa
Poisson's ratios	ν_{12}	0.3
	ν_{13}	0.3
	ν_{23}	0.3
density	ρ	1800 kg/m^3

stress field. For this purpose parabolic expansion have been chosen for all models.

Displacements The transverse displacement at the center of the plate (Fig.6.50) shows how the Zig-Zag theory outperform the ESL one; in fact it is capable to provide an accuracy comparable to the more computational expensive layerwise theory. The current ESL-based element is introducing a lag on the response. This error will amplify during the stress evaluation phase.

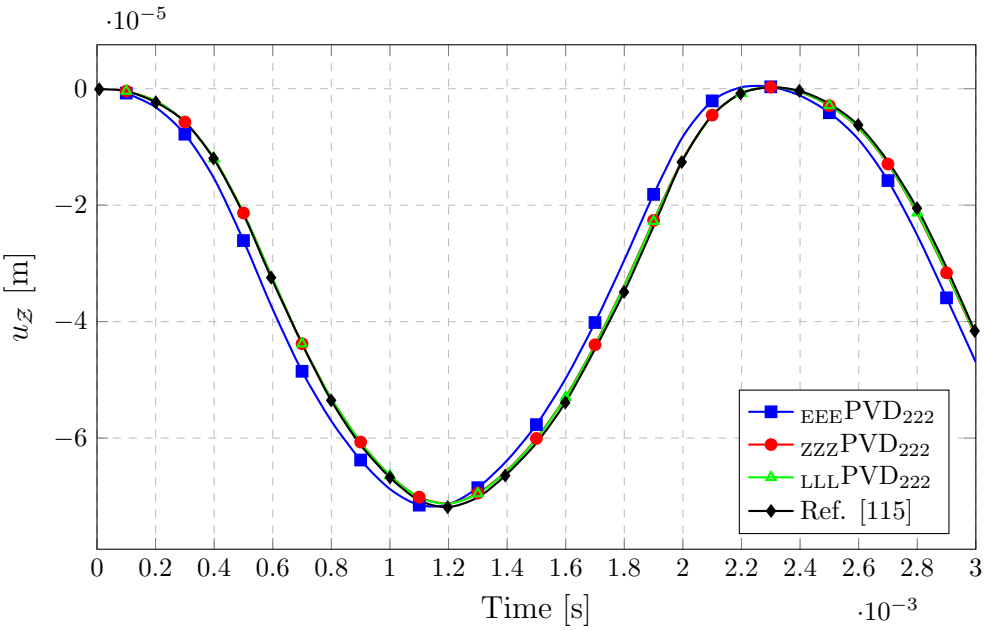

Figure 6.50: Time variation of transverse displacement $u_{\mathcal{Z}}$ at point (0,0).

Inplane stresses In Ref. [115] the stress tensor components are evaluated at point A of coordinate $(-3/56L, 3/56L, Z)$. Their values are compared with the stresses in correspondence of the closest node to that point.

All axiomatic theories provide an accurate estimate of the inplane stresses also with CFHL (Fig. 6.51). More specifically the Zig-Zag and LW theories perfectly match with the reference data. Instead the ESL presents a small lag, directly derived from the phase-lag in the displacement field.

Transverse Stresses: present stress recovery procedure and global-local analysis The time variation of the shear transverse stress $S_{\mathcal{Z}\mathcal{Y}}$ at thickness coordinate $\mathcal{Z}/h = 0.44$ is shown in Fig. 6.52, Fig. 6.53 and Fig. 6.55. If the stress is computed by means of CFHL (Fig. 6.52), expected results are obtained. ESL theory provides a wrong solution with stress peaks more then three time the reference value. The Zig-Zag correction with MZZF reduces drammatically the error, but it still inaccurate. On the contrary, the layerwise theory produces a reasonable good match with the reference data. However, if the stress recovery procedure

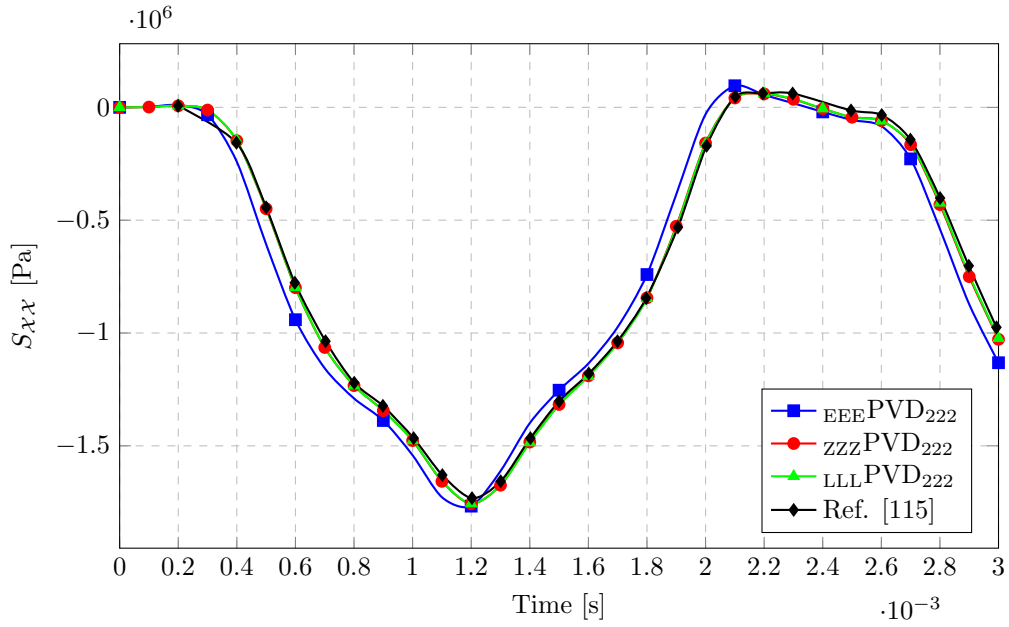

Figure 6.51: Time variation of transverse shear stress $S_{\mathcal{X}\mathcal{X}}$ at point A and thickness coordinate $Z/h = 0.4583$. A mesh 5x5 is used.

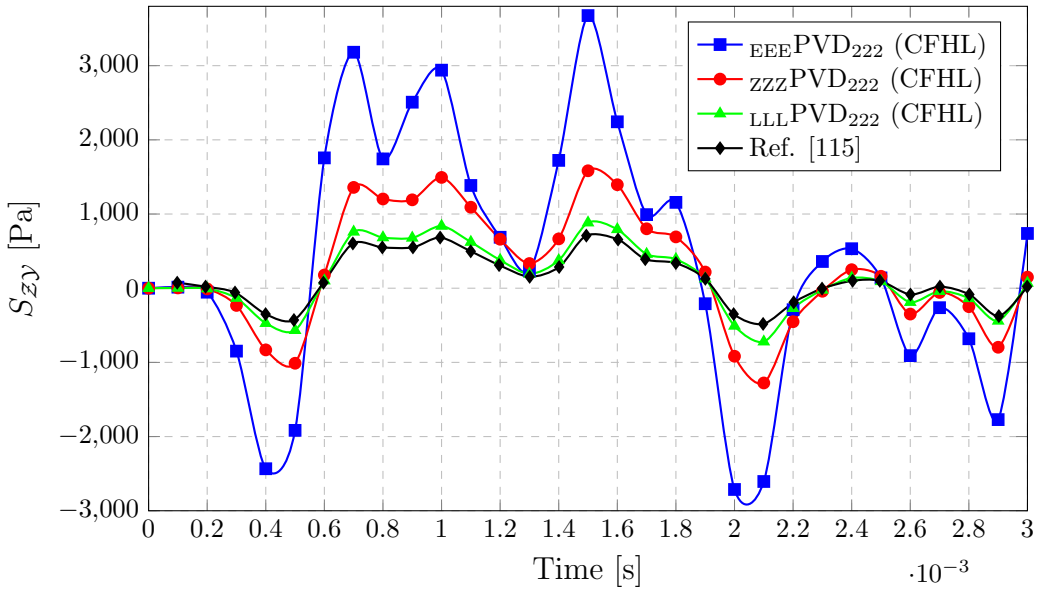

Figure 6.52: Time variation of transverse shear stress $S_{\mathcal{Z}\mathcal{Y}}$ at point A and thickness coordinate $Z/h = 0.44$. A mesh 5x5 is used. Stress obtained using Hooke's law.

is performed (Fig. 6.53), ESL, Zig-Zag and layerwise reach similar accuracy. In particular, the curve of the Zig-Zag model is indistinguishable from the layerwise one.

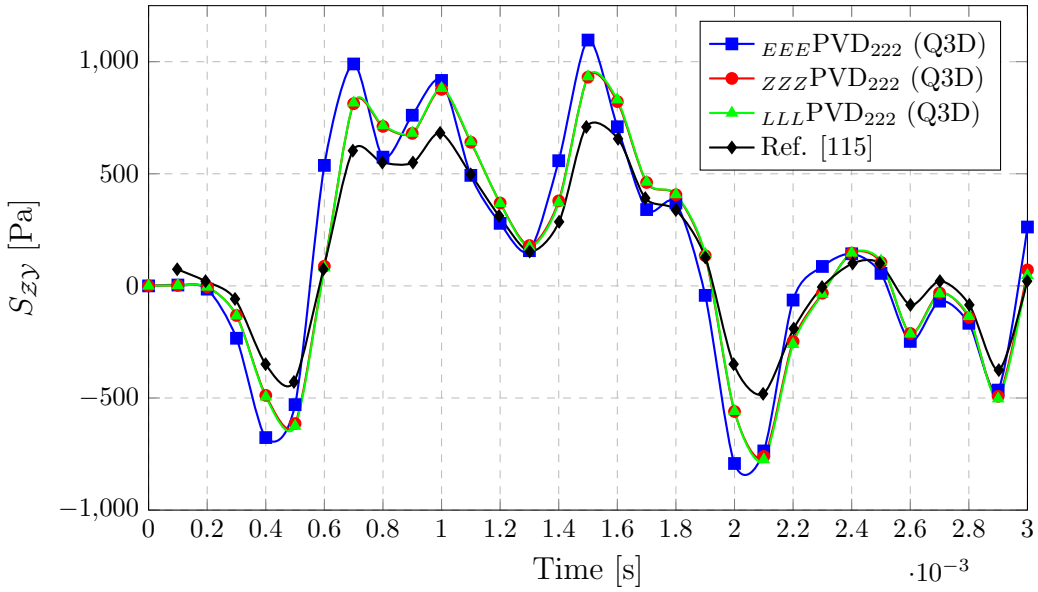

Figure 6.53: Time variation of transverse shear stress $S_{\mathcal{Z}\mathcal{Y}}$ at point A at thickness coordinate $Z/h = 0.44$. A mesh 5x5 is used. Stress computed through integration of equilibrium equations.

As an additional test, the ESL mesh is modified. The elements sharing the node analyzed are replaced with parabolic layerwise elements (Fig. 6.54 for mesh visualization). The outcome is a global-local analysis where the global response is still described by an ESL theory, and the local stress field in proximity of the center of the plate is modeled by a LW one. This alteration has a strong positive effect at the cost of very few additional degree of freedoms (Fig. 6.55). In fact, the global-local model reaches an accuracy in terms of stress comparable with the Zig-Zag model. The discrepancy with the full LW one could be explained with the fact that, as seen in Fig. 6.50, a full ESL element mesh is not able to capture the temporal variation of the displacement field. As a matter of fact, it introduces a lag. The substitution of few elements in a very limited area does not affect the deformation response. This initial error on the displacements can affect the final stress computation of the layerwise element used for local analysis.

A similar argument can be done also for the transverse normal stress $S_{\mathcal{Z}\mathcal{Z}}$ evaluated at the same thickness location (Figs. 6.56, 6.57, 6.58). Although, in this case, the Zig-Zag theory provides a poor estimation of the stress if CFHL is used (Fig. 6.56). As for $S_{\mathcal{Z}\mathcal{Y}}$ the proposed stress recovery procedure improves both ESL and Zig-Zag stress field. If the same multi-model used for $S_{\mathcal{Z}\mathcal{Y}}$ (Fig. 6.54) is also used for $S_{\mathcal{Z}\mathcal{Z}}$, a solution closer to the LW is achieved (Fig. 6.58). Although larger oscillations are present.

It is interesting to note that if the stress recovery procedure is applied to the multi-model mesh, the stress is not any better than the one obtained with the stress recovery applied on the full ESL mesh (Fig.

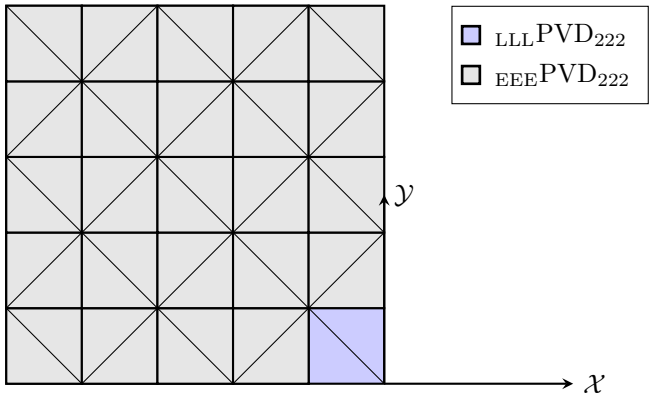

Figure 6.54: Application of GUF for global-local analysis. Elements sharing the node analyzed are modeled with a layerwise theory.

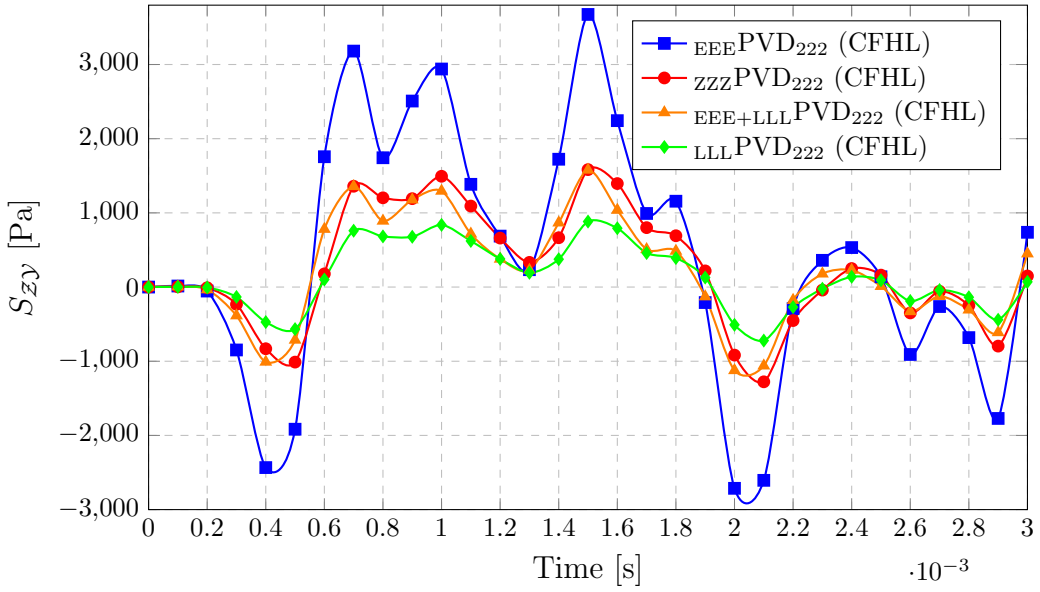

Figure 6.55: Time variation of transverse shear stress S_{zy} at point A and thickness coordinate $Z/h = 0.44$. A mesh 5x5 is used. Stress obtained using Hooke's law. Effect of using an layerwise theory in element of interest.

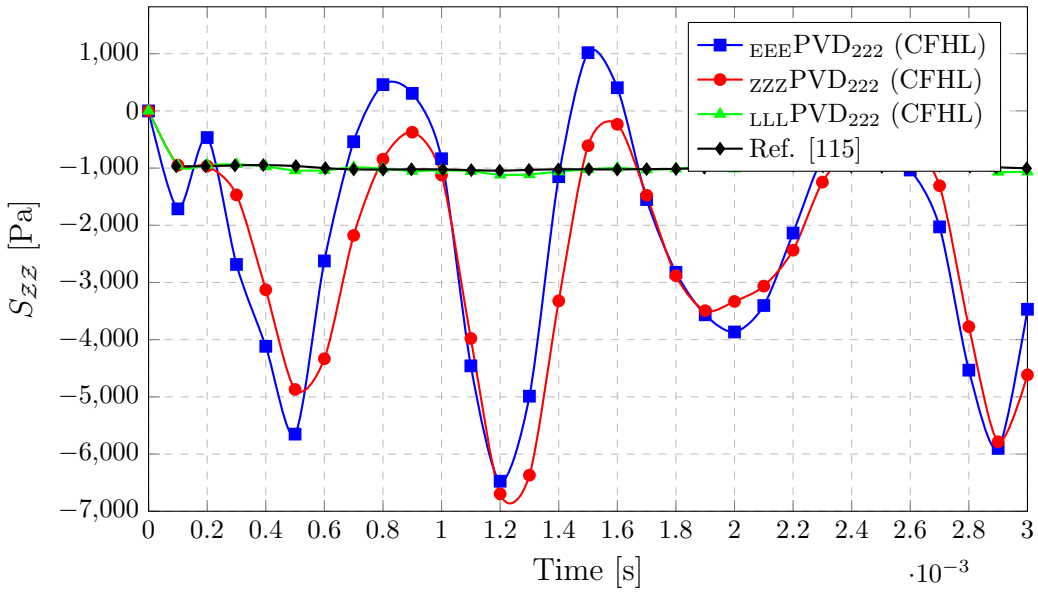

Figure 6.56: Time variation of transverse shear stress S_{ZZ} at point A and thickness coordinate $Z/h = 0.45946$. A mesh 5x5 is used. Stress obtained using Hooke's law.

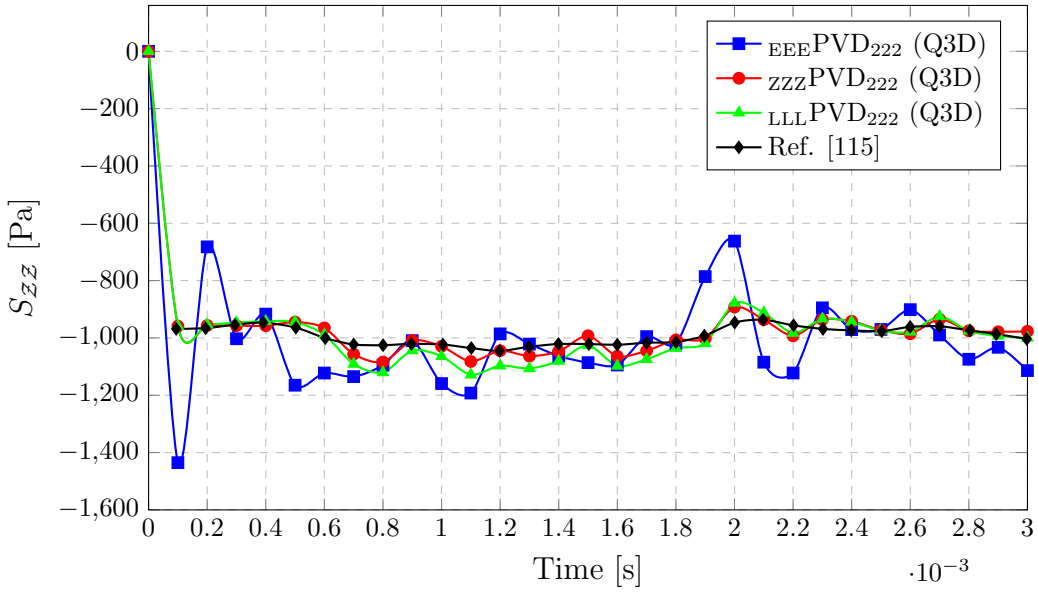

Figure 6.57: Time variation of transverse shear stress S_{ZZ} at point A and thickness coordinate $Z/h = 0.45946$. A mesh 5x5 is used. Stress computed through integration of equilibrium equations.

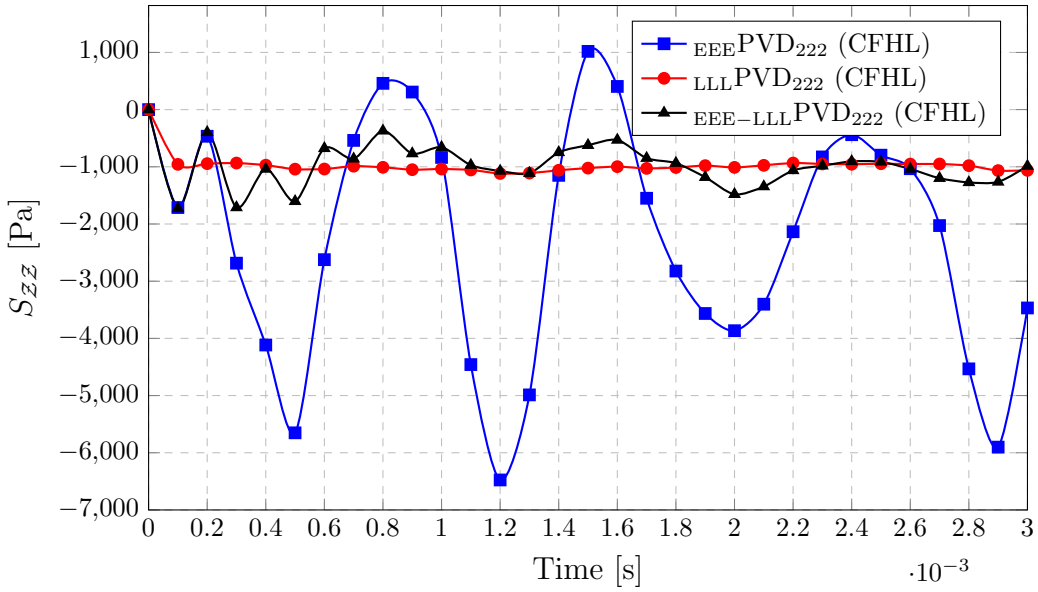

Figure 6.58: Time variation of transverse shear stress S_{zz} at point A and thickness coordinate $Z/h = 0.45946$. A mesh 5x5 is used. Stress obtained using Hooke's law. Multimodal.

6.59). On the other hand, if the thickness location is changed to a lower thickness coordinate $Z/h = -0.45946$ the multi-model combined with the stress recovery provide a normal transverse stress time history comparable with the full layerwise model (Fig. 6.60). This suggests a strong dependence on the local accuracy of the model along the thickness direction. An explanation could be represented by the presence of steeper gradients near the top surface, where the load is applied.

Indipendent displacement component modeling An unique feature of GUF is that it allows to indipendently model the displacement components in the element reference system. It becomes possible to perform studies decoupling the inplane and out-of-plane displacement modeling. Figs. 6.61, 6.62, 6.63 and 6.64 show the relative importance of displacement component for the evaluation of the transverse stresses. If CFHL is used, the transverse displacement axiomatic model seems to not have any effect on the transverse shear stress evaluation, whereas the inplane displacements do. The opposite situation occurs if the normal transverse stress is considered (Fig. 6.63), where the discrepancy seems to be all attributed to the transverse displacement. In case the stress recovery procedure is applied, all models provide a very similar solution (Figs. 6.62, 6.64).

Order of expansion effect A Zig-Zag theory seems to improves the shear transverse stress predicted by the ESL, but it does not affect the normal transverse stress that are still inaccurate (Fig. 6.65). This is somewhat expected: in certain situations a layerwise model represents the best options for accurate evaluation of the stress levels in the structure.

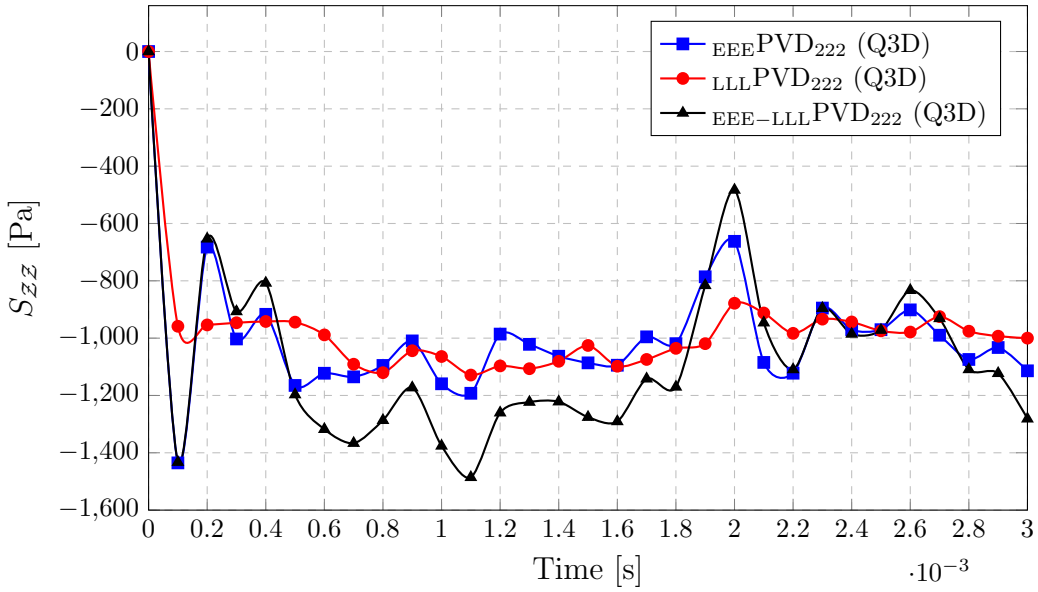

Figure 6.59: Time variation of transverse shear stress S_{zz} at point A and thickness coordinate $Z/h = 0.45946$. A mesh 5x5 is used. Stress computed through integration of equilibrium equations. Global-local effect.

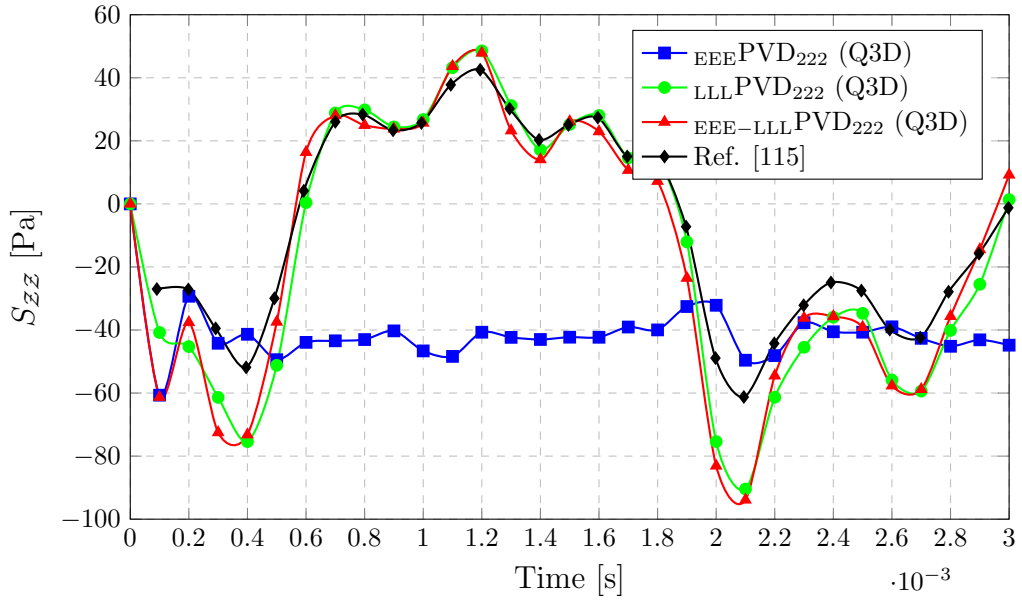

Figure 6.60: Time variation of transverse shear stress S_{zz} at point A and thickness coordinate $Z/h = -0.45946$. A mesh 5x5 is used. Stress computed through integration of equilibrium equations. Global-local effect.

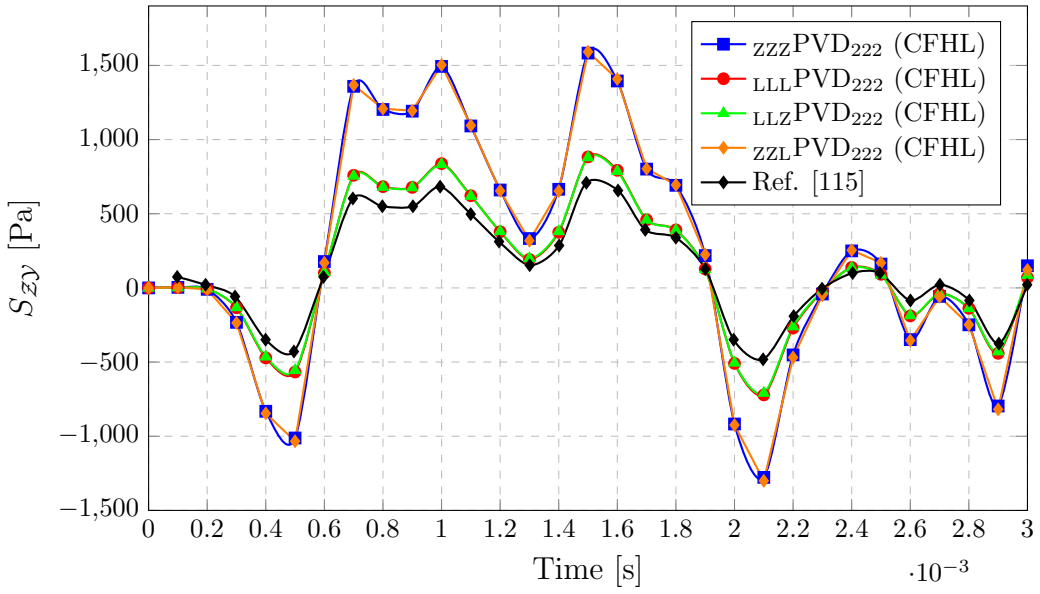

Figure 6.61: Time variation of transverse shear stress S_{zy} at point A and thickness coordinate $Z/h = 0.44$. A mesh 5×5 is used. Partial layerwise theories. Stress obtained using Hooke's law.

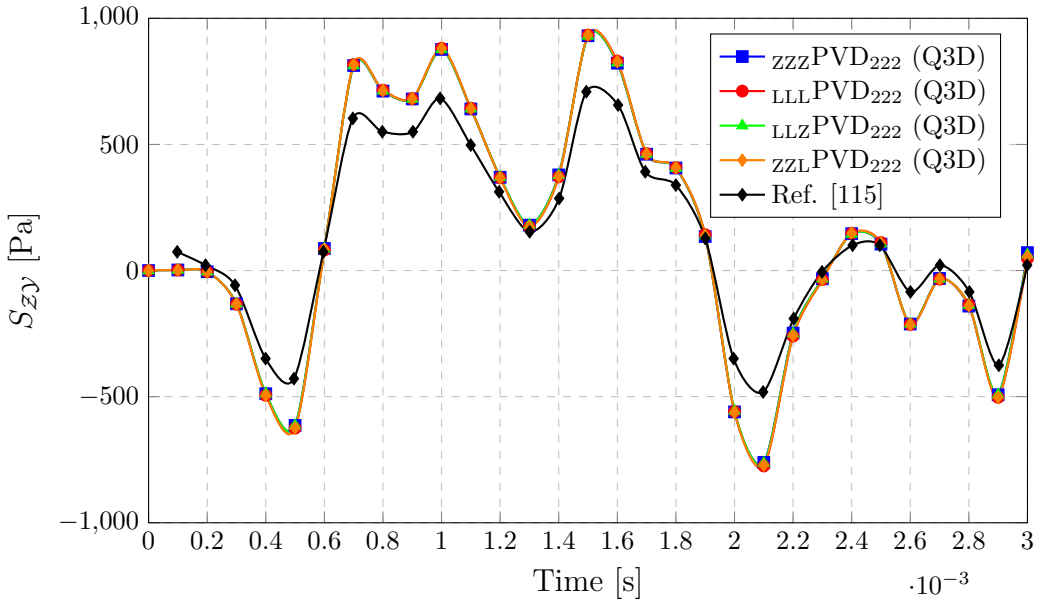

Figure 6.62: Time variation of transverse shear stress S_{zy} at point A and thickness coordinate $Z/h = 0.44$. Partial layerwise theories. Stress computed through integration of equilibrium equations.

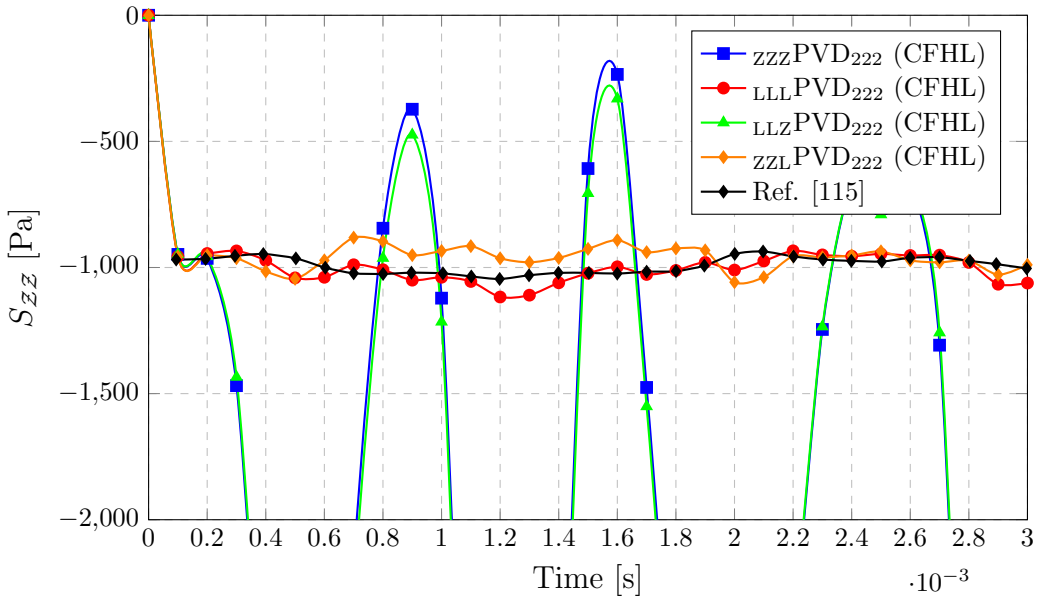

Figure 6.63: Time variation of transverse shear stress S_{zz} at point A and thickness coordinate $Z/h = 0.45946$. Partial layerwise theories. Stress obtained using Hooke's law.

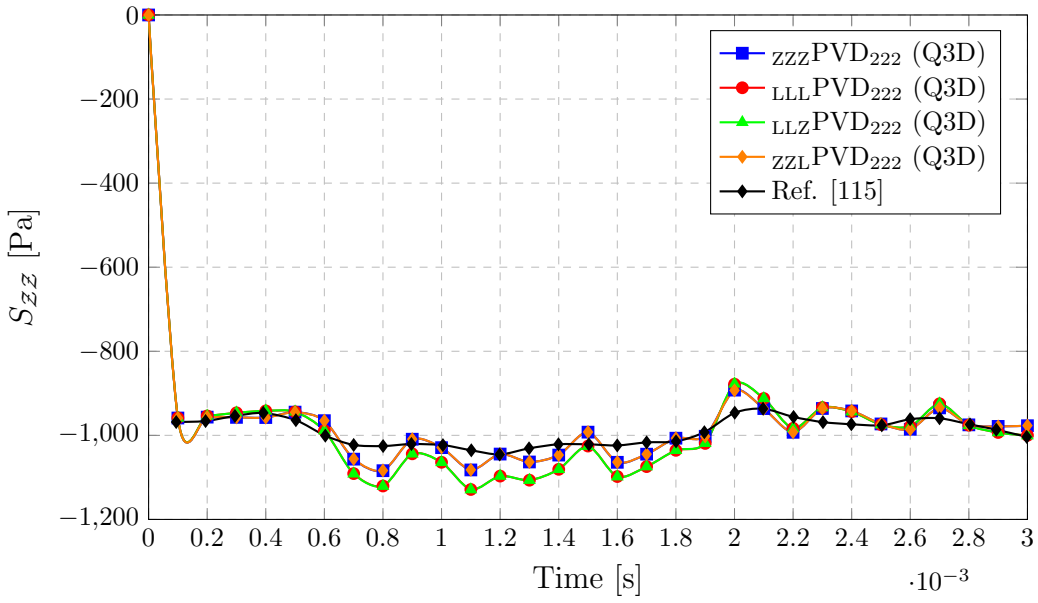

Figure 6.64: Time variation of transverse shear stress S_{zz} at point A and thickness coordinate $Z/h = 0.45946$. A mesh 5x5 is used. Partial layerwise theories. Stress computed through integration of equilibrium equations.

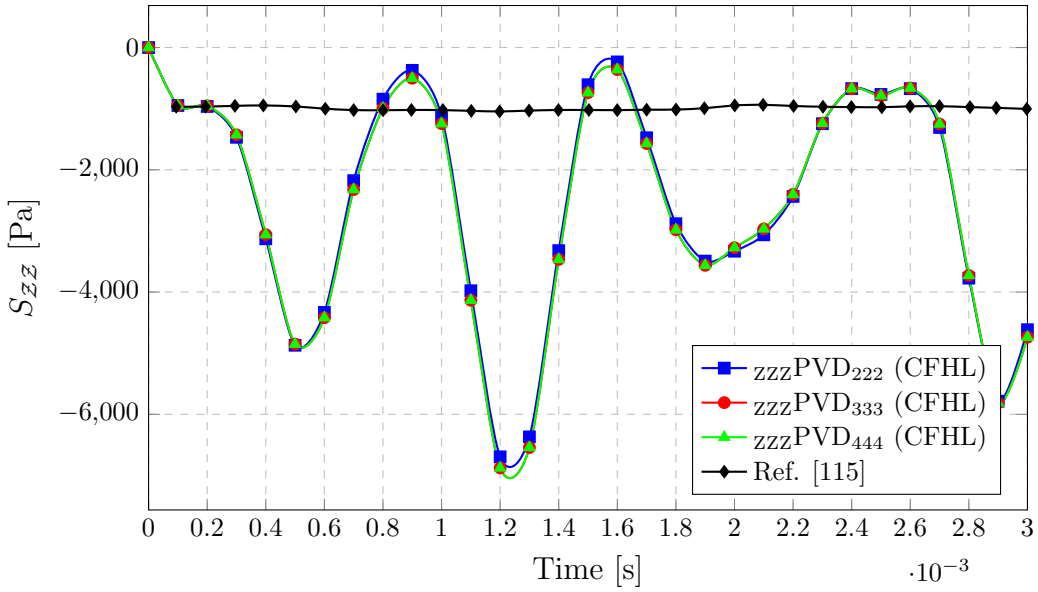

Figure 6.65: Time variation of transverse shear stress S_{zz} at point A and thickness coordinate $Z/h = 0.45946$. A mesh 5x5 is used. Effect of polynomial order of expansion. Stress obtained using Hooke's law.

6.3 Acknowledgments

Chapter 6 is in part a reprint of :

- "*Large displacement models for composites based on Murakami's Zig-Zag Function, Green-Lagrange Strain Tensor, and Generalized Unified Formulation*", published online in *Thin-Walled Structures* on February 27^{th}, 2020 and co-authored by Luciano Demasi. The author of this dissertation is the primary investigator and author of this paper.

- "*Computational Architecture Based on Murakami's Zig-Zag function for the Geometrically Nonlinear Analysis of Variable Angle Tow Laminates*", published online in *AIAA Scitech 2020 Forum, Orlando, Florida* on January 5^{th}, 2020 and co-authored by Luciano Demasi. The author of this dissertation is the primary investigator and author of this paper.

Chapter 7

Conclusions

This dissertation introduces a new framework for the study of multilayered Variable Angle Tow composite plates in the geometrically nonlinear regime for both static and dynamic analysis. It is based on a variable-kinematic finite element approach. This architecture can encompass several axiomatic theories under an invariant expression written by using an indicial notation. The present approach encompasses a great number of theories including Equivalent Single Layer, Zig-Zag and layerwise ones. Moreover it allows for an independent modeling of the displacement components in the element reference system extending the collection of axiomatic theories to mixed ones and partially-layerwise theories. The final results is a polymorphic element that in combination with a weak imposition of the inter-element compatibility via penalty method provides an additional alternative to the multi-model class of methods.

The proposed computational architecture presents the following features:

- It allows a simple comparison of different models for Variable Angle Tow composites and use them simultaneously for global-local analysis purpose.
- It can include Murakami's Zig-Zag function, and this is highly beneficial also for the geometrically nonlinear static and dynamic analyses, as proven in this study for the first time. This information can be used for aeroelastic applications, where the correct prediction of the aerodynamic load is tightly connected to the accuracy of the deformation. Using a Zig-Zag theory over a layerwise one can provide practically the same results in most of the applications, but with the advantage of taking a fraction of the computational resources.
- In aerospace industry VAT laminates are becoming more common thanks to the advancement of the manufacturing technology. Moreover, there is a push in both European and American aerospace agencies to introduce aerodynamically efficient new configurations (such as the Truss-Braced Wings)

which result in aircraft with more flexible wings, where both geometric nonlienarities and aeroelastic tailoring (i.e., high variability of stiffness properties) become crucial since the very beginning of the design phase. The proposed computational technology can be effectively applied in the early design process, by using the zig-zag models, but can also be useful later for more detailed studies, where a more refined investigation is pursued and layerwise models can be a valuable tool in the hands of engineers.

- CSCL and VAT laminates can provide an improved efficiency also in rotor design and flapping wing systems. For this purpose, the governing equation for dynamic analysis are expressed in a non-inertial reference frame to improve the robustness of the algorithm for moving body. The proposed FEM approach was tested with benchmark problems found in literature. The present approach, formulated for single body, can be easily extended to multi-body dynamics.

- It is of paramount importance to be able to accurately predict the stress field, in fact most of the failure criteria are based on it. This requirement should be satisfied with reasonable computational resources. Calculations based on the constitutive relations (Hooke's law) are usually ineffective in predicting the shear and normal transverse stresses, that are a main cause for laminate failure mechanism, especially if a lower order model is used e.g. ESL. The present framework satisfies this need of effectiveness through its capability for multi-model analysis and the application of Murakami's Zig-Zag function. A new stress recovery procedure tailored to improve the predictions of the second Piola-Kirchhoff stress tensor is proposed. This algorithm can be used to reconstruct the three-dimensional stress field from the displacement solution of two dimensional axiomatic theory. It can also be used for large displacements and rotations as opposed to typical stress recovery techniques that are restricted to moderate rotations. Several numerical tests proved the effectiveness of this post-processing technique.

Future work

In the near future the structural model is going to be used for multi-fidelity fluid-structure interaction simulation for aerospace and marine applications. In particular, for rotor blade analysis. For this purpose, the formulation will be extended to multi-body analysis.

Another line of research will be on VAT optimization. It will be necessary to compute the sensitivity matrix analytically from the expression of the nonlinear kernels.

Appendix A

Kernels for linear analysis

The internal virtual work of a layer has been shown in section 2.3 to be:

$$\begin{aligned}
\delta W_I^k = {} & \delta^x U^k_{\alpha_{u_x} i}\, K^{k\,\alpha_{u_x}\beta_{u_x} ij}_{u_x\, u_x}\, {}^x U^k_{\beta_{u_x} j} + \delta^x U^k_{\alpha_{u_x} i}\, K^{k\,\alpha_{u_x}\beta_{u_y} ij}_{u_x\, u_y}\, {}^y U^k_{\beta_{u_y} j} + \\
& + \delta^x U^k_{\alpha_{u_x} i}\, K^{k\,\alpha_{u_x}\beta_{u_z} ij}_{u_x\, u_z}\, {}^z U^k_{\beta_{u_z} j} + \delta^y U^k_{\alpha_{u_y} i}\, K^{k\,\alpha_{u_y}\beta_{u_x} ij}_{u_y\, u_x}\, {}^x U^k_{\beta_{u_x} j} + \\
& + \delta^y U^k_{\alpha_{u_y} i}\, K^{k\,\alpha_{u_y}\beta_{u_y} ij}_{u_y\, u_y}\, {}^z U^k_{\beta_{u_y} j} + \delta^y U^k_{\alpha_{u_y} i}\, K^{k\,\alpha_{u_y}\beta_{u_z} ij}_{u_y\, u_z}\, {}^z U^k_{\beta_{u_z} j} + \\
& + \delta^z U^k_{\alpha_{u_z} i}\, K^{k\,\alpha_{u_z}\beta_{u_x} ij}_{u_z\, u_x}\, {}^x U^k_{\beta_{u_x} j} + \delta^z U^k_{\alpha_{u_z} i} K^{k\,\alpha_{u_z}\beta_{u_y} ij}_{u_z\, u_y}\, {}^x U^k_{\beta_{u_y} j} + \\
& + \delta^z U^k_{\alpha_{u_z} i}\, K^{k\,\alpha_{u_z}\beta_{u_z} ij}_{u_z\, u_z}\, {}^y U^k_{\beta_{u_z} j}
\end{aligned} \tag{A.1}$$

$K^{k\,\alpha_{u_x}\beta_{u_x} ij}_{u_x\, u_x}$, $K^{k\,\alpha_{u_y}\beta_{u_y} ij}_{u_x\, u_y}$, $K^{k\,\alpha_{u_x}\beta_{u_z} ij}_{u_x\, u_z}$, $K^{k\,\alpha_{u_y}\beta_{u_x} ij}_{u_y\, u_x}$, $K^{k\,\alpha_{u_y}\beta_{u_y} ij}_{u_y\, u_y}$, $K^{k\,\alpha_{u_y}\beta_{u_z} ij}_{u_y\, u_z}$, $K^{k\,\alpha_{u_z}\beta_{u_x} ij}_{u_z\, u_x}$, $K^{k\,\alpha_{u_z}\beta_{u_y} ij}_{u_z\, u_y}$, and ${}^{\mathrm{loc}}K^{k\,\alpha_{u_z}\beta_{u_z} ij}_{u_z\, u_z}$ are the *kernels* of the Generalized Unified Formulation. These kernels are invariant with respect to the adopted theory. It should be noted that the kernel are obtained in the local (element) coordinate system. In fact, equation A.1 was written working in the local (element) coordinate system. Their explicit expression are:

$$\begin{aligned}
K^{k\,\alpha_{u_x}\beta_{u_x} ij}_{u_x\, u_x} = {} & \int_\Omega \overline{Z}^{k\,\alpha_{u_x}\beta_{u_x}}_{11\; u_x\, u_x}\, {}^x N_{i,_x}\, {}^x N_{j,_x} \mathrm{d}x\mathrm{d}y + \int_\Omega \overline{Z}^{k\,\alpha_{u_x}\beta_{u_x}}_{16\; u_x\, u_x}\, {}^x N_{i,_x}\, {}^x N_{j,_y} \mathrm{d}x\mathrm{d}y \\
+ {} & \int_\Omega \overline{Z}^{k\,\alpha_{u_x}\beta_{u_x}}_{16\; u_x\, u_x}\, {}^x N_{i,_y}\, {}^x N_{j,_x} \mathrm{d}x\mathrm{d}y + \int_\Omega \overline{Z}^{k\,\alpha_{u_x}\beta_{u_x}}_{66\; u_x\, u_x}\, {}^x N_{i,_y}\, {}^x N_{j,_y} \mathrm{d}x\mathrm{d}y \\
+ {} & \int_\Omega \overline{Z}^{k\,\alpha_{u_x,_z}\beta_{u_x,_z}}_{55\; u_x\, u_x}\, {}^x N_i\, {}^x N_j \mathrm{d}x\mathrm{d}y
\end{aligned} \tag{A.2}$$

$$
\begin{aligned}
K^{k\,\alpha_{u_x}\beta_{u_y}ij}_{u_x\,u_y} &= \int_\Omega \overline{Z}^{k\,\alpha_{u_x}\beta_{u_y}}_{12\,u_x\,u_y}\, {}^{x}N_{i,x}\, {}^{y}N_{j,y}\mathrm{d}x\mathrm{d}y + \int_\Omega \overline{Z}^{k\,\alpha_{u_x}\beta_{u_y}}_{16\,u_x\,u_y}\, {}^{x}N_{i,x}\, {}^{y}N_{j,x}\mathrm{d}x\mathrm{d}y \\
&+ \int_\Omega \overline{Z}^{k\,\alpha_{u_x}\beta_{u_y}}_{26\,u_x\,u_y}\, {}^{x}N_{i,y}\, {}^{y}N_{j,y}\mathrm{d}x\mathrm{d}y + \int_\Omega \overline{Z}^{k\,\alpha_{u_x}\beta_{u_y}}_{66\,u_x\,u_y}\, {}^{x}N_{i,y}\, {}^{y}N_{j,x}\mathrm{d}x\mathrm{d}y \\
&+ \int_\Omega \overline{Z}^{k\,\alpha_{u_{x,z}}\beta_{u_{y,z}}}_{45\,u_x\,u_y}\, {}^{x}N_i\, {}^{y}N_j\mathrm{d}x\mathrm{d}y
\end{aligned} \tag{A.3}
$$

$$
\begin{aligned}
K^{k\,\alpha_{u_x}\beta_{u_z}ij}_{u_x\,u_z} &= \int_\Omega \overline{Z}^{k\,\alpha_{u_x}\beta_{u_{z,z}}}_{13\,u_x\,u_z}\, {}^{x}N_{i,x}\, {}^{z}N_j\mathrm{d}x\mathrm{d}y + \int_\Omega \overline{Z}^{k\,\alpha_{u_x}\beta_{u_{z,z}}}_{36\,u_x\,u_z}\, {}^{x}N_{i,y}\, {}^{z}N_j\mathrm{d}x\mathrm{d}y \\
&+ \int_\Omega \overline{Z}^{k\,\alpha_{u_{x,z}}\beta_{u_z}}_{55\,u_x\,u_z}\, {}^{x}N_i\, {}^{z}N_{j,x}\mathrm{d}x\mathrm{d}y + \int_\Omega \overline{Z}^{k\,\alpha_{u_{x,z}}\beta_{u_z}}_{45\,u_x\,u_z}\, {}^{x}N_i\, {}^{z}N_{j,y}\mathrm{d}x\mathrm{d}y
\end{aligned} \tag{A.4}
$$

$$
\begin{aligned}
K^{k\,\alpha_{u_y}\beta_{u_x}ij}_{u_y\,u_x} &= \int_\Omega \overline{Z}^{k\,\alpha_{u_y}\beta_{u_x}}_{12\,u_y\,u_x}\, {}^{y}N_{i,y}\, {}^{x}N_{j,x}\mathrm{d}x\mathrm{d}y + \int_\Omega \overline{Z}^{k\,\alpha_{u_y}\beta_{u_x}}_{26\,u_y\,u_x}\, {}^{y}N_{i,y}\, {}^{x}N_{j,y}\mathrm{d}x\mathrm{d}y + \\
&+ \int_\Omega \overline{Z}^{k\,\alpha_{u_y}\beta_{u_x}}_{16\,u_y\,u_x}\, {}^{y}N_{i,x}\, {}^{x}N_{j,x}\mathrm{d}x\mathrm{d}y + \int_\Omega \overline{Z}^{k\,\alpha_{u_y}\beta_{u_x}}_{66\,u_y\,u_x}\, {}^{y}N_{i,x}\, {}^{x}N_{j,y}\mathrm{d}x\mathrm{d}y \\
&+ \int_\Omega \overline{Z}^{k\,\alpha_{u_{y,z}}\beta_{u_{x,z}}}_{45\,u_y\,u_x}\, {}^{y}N_i\, {}^{x}N_j\mathrm{d}x\mathrm{d}y
\end{aligned} \tag{A.5}
$$

$$
\begin{aligned}
K^{k\,\alpha_{u_y}\beta_{u_y}ij}_{u_y\,u_y} &= \int_\Omega \overline{Z}^{k\,\alpha_{u_y}\beta_{u_y}}_{22\,u_y\,u_y}\, {}^{y}N_{i,y}\, {}^{y}N_{j,y}\mathrm{d}x\mathrm{d}y + \int_{\mathcal{I}\Omega} \overline{Z}^{k\,\alpha_{u_y}\beta_{u_y}}_{26\,u_y\,u_y}\, {}^{y}N_{i,y}\, {}^{y}N_{j,x}\mathrm{d}x\mathrm{d}y \\
&+ \int_\Omega \overline{Z}^{k\,\alpha_{u_y}\beta_{u_y}}_{26\,u_y\,u_y}\, {}^{y}N_{i,x}\, {}^{y}N_{j,y}\mathrm{d}x\mathrm{d}y + \int_{\mathcal{I}\Omega} \overline{Z}^{k\,\alpha_{u_y}\beta_{u_y}}_{66\,u_y\,u_y}\, {}^{y}N_{i,x}\, {}^{y}N_{j,x}\mathrm{d}x\mathrm{d}y \\
&+ \int_\Omega \overline{Z}^{k\,\alpha_{u_{y,z}}\beta_{u_{y,z}}}_{44\,u_y\,u_y}\, {}^{y}N_i\, {}^{y}N_j\mathrm{d}x\mathrm{d}y
\end{aligned} \tag{A.6}
$$

$$
\begin{aligned}
K^{k\,\alpha_{u_y}\beta_{u_z}ij}_{u_y\,u_z} &= \int_\Omega \overline{Z}^{k\,\alpha_{u_y}\beta_{u_{z,z}}}_{23\,u_y\,u_z}\, {}^{y}N_{i,y}\, {}^{z}N_j\mathrm{d}x\mathrm{d}y + \int_\Omega \overline{Z}^{k\,\alpha_{u_y}\beta_{u_{z,z}}}_{36\,u_y\,u_z}\, {}^{y}N_{i,x}\, {}^{z}N_j\mathrm{d}x\mathrm{d}y \\
&+ \int_\Omega \overline{Z}^{k\,\alpha_{u_{y,z}}\beta_{u_z}}_{45\,u_y\,u_z}\, {}^{y}N_i\, {}^{z}N_{j,x}\mathrm{d}x\mathrm{d}y + \int_\Omega \overline{Z}^{k\,\alpha_{u_{y,z}}\beta_{u_z}}_{44\,u_y\,u_z}\, {}^{y}N_i\, {}^{z}N_{j,y}\mathrm{d}x\mathrm{d}y
\end{aligned} \tag{A.7}
$$

$$
\begin{aligned}
K^{k\,\alpha_{u_z}\beta_{u_x} ij}_{u_z\,u_x} &= \int_\Omega Z^{k\,\alpha_{u_z}\beta_{u_{x,z}}}_{55\;u_z\,u_x}\;{}^{z}N_{i,x}\;{}^{x}N_j \mathrm{d}x\mathrm{d}y + \int_\Omega Z^{k\,\alpha_{u_z}\beta_{u_{x,z}}}_{45\;u_z\,u_x}\;{}^{z}N_{i,y}\;{}^{x}N_j \mathrm{d}x\mathrm{d}y + \\
&+ \int_\Omega Z^{k\,\alpha_{u_{z,z}}\beta_{u_x}}_{13\;u_z\,u_x}\;{}^{z}N_i\;{}^{x}N_{j,x}\mathrm{d}x\mathrm{d}y + \int_\Omega Z^{k\,\alpha_{u_{z,z}}\beta_{u_x}}_{36\;u_z\,u_x}\;{}^{z}N_i\;{}^{x}N_{j,y}\mathrm{d}x\mathrm{d}y
\end{aligned} \tag{A.8}
$$

$$
\begin{aligned}
K^{k\,\alpha_{u_z}\beta_{u_y} ij}_{u_z\,u_y} &= \int_\Omega Z^{k\,\alpha_{u_z}\beta_{u_{y,z}}}_{45\;u_z\,u_y}\;{}^{z}N_{i,x}\;{}^{y}N_j \mathrm{d}x\mathrm{d}y + \int_\Omega Z^{k\,\alpha_{u_z}\beta_{u_{y,z}}}_{44\;u_z\,u_y}\;{}^{z}N_{i,y}\;{}^{y}N_j \mathrm{d}x\mathrm{d}y + \\
&+ \int_\Omega Z^{k\,\alpha_{u_{z,z}}\beta_{u_y}}_{23\;u_z\,u_y}\;{}^{z}N_i\;{}^{y}N_{j,y}\mathrm{d}x\mathrm{d}y + \int_\Omega Z^{k\,\alpha_{u_{z,z}}\beta_{u_y}}_{36\;u_z\,u_y}\;{}^{z}N_i\;{}^{y}N_{j,x}\mathrm{d}x\mathrm{d}y
\end{aligned} \tag{A.9}
$$

$$
\begin{aligned}
K^{k\,\alpha_{u_z}\beta_{u_z} ij}_{u_z\,u_z} &= \int_\Omega \overline{Z}^{k\,\alpha_{u_z}\beta_{u_z}}_{55\;u_z\,u_z}\;{}^{z}N_{i,x}\;{}^{z}N_{j,x}\mathrm{d}x\mathrm{d}y + \int_\Omega \overline{Z}^{k\,\alpha_{u_z}\beta_{u_z}}_{45\;u_z\,u_z}\;{}^{z}N_{i,x}\;{}^{z}N_{j,y}\mathrm{d}x\mathrm{d}y \\
&+ \int_\Omega \overline{Z}^{k\,\alpha_{u_z}\beta_{u_z}}_{45\;u_z\,u_z}\;{}^{z}N_{i,y}\;{}^{z}N_{j,x}\mathrm{d}x\mathrm{d}y + \int_\Omega \overline{Z}^{k\,\alpha_{u_z}\beta_{u_z}}_{44\;u_z\,u_z}\;{}^{z}N_{i,y}\;{}^{z}N_{j,y}\mathrm{d}x\mathrm{d}y \\
&+ \int_\Omega \overline{Z}^{k\,\alpha_{u_{z,z}}\beta_{u_{z,z}}}_{33\;u_z\,u_z}\;{}^{z}N_i\;{}^{z}N_j\mathrm{d}x\mathrm{d}y
\end{aligned} \tag{A.10}
$$

where the integration along the thickness is done separately and contained in the $\overline{Z}$ terms. Here some examples:

$$
\begin{aligned}
\overline{Z}^{k\,\alpha_{u_{z,z}}\beta_{u_{z,z}}}_{33\;u_z\,u_z} &= \int_{z_{bot_k}}^{z_{top_k}} \bar{C}^k_{33}\;{}^{z}F^k_{\alpha_{u_z},z}\;{}^{z}F^k_{\beta_{u_z},z}\mathrm{d}z^k \\
\overline{Z}^{k\,\alpha_{u_x}\beta_{u_y}}_{26\;u_x\,u_y} &= \int_{z_{bot_k}}^{z_{top_k}} \bar{C}^k_{26}\;{}^{x}F^k_{\alpha_{u_x}}\;{}^{y}F^k_{\beta_{u_y}}\mathrm{d}z^k \\
\overline{Z}^{k\,\alpha_{u_z}\beta_{u_y,z}}_{45\;u_z\,u_y} &= \int_{z_{bot_k}}^{z_{top_k}} \bar{C}^k_{45}\;{}^{z}F^k_{\alpha_{u_z}}\;{}^{y}F^k_{\beta_{u_y},z}\mathrm{d}z^k
\end{aligned} \tag{A.11}
$$

These integrals are solved numerically using Gauss quadrature and assembled to form the global stiffness matrix.

Appendix B

Strong forms

In this appendix it will be shown the derivation of the strong form of the governing equation in the undeformed configuration.

Let's start from the statement in the current configuration:

Strong form current configuration

Given $b_i : V \to \mathbb{R}$, $\rho : V \to \mathbb{R}$, $\hat{g}_i : \Gamma_{g_i} \to \mathbb{R}$, $\hat{h}_i : \Gamma_{h_i} \to \mathbb{R}$, $\bar{\bar{u}} : V \to \mathbb{R}$, $\bar{\sigma}_{ij} : V \to \mathbb{R}$, find $u_i : V \to \mathbb{R}$, such that

$$\begin{cases} \sigma_{ji,j}(X,t) + b_i(X,t) &= \rho(X)\ddot{u}_i(X,t) \quad \text{in} \quad \Omega \\ u_i(X,t) &= \hat{g}_i(X,t) \quad \text{on} \quad \Gamma_{g_i} \\ n_j(X,t)\sigma_{ji}(X,t) &= \hat{h}_i(X,t) \quad \text{on} \quad \Gamma_{h_i} \\ \dot{u}_i(X,0) &= \bar{\bar{u}} \quad \text{in} \quad \Omega \\ \sigma_{ij}(X,0) &= \bar{\sigma}_{ij} \quad \text{in} \quad \Omega \end{cases} \tag{B.1}$$

B.1 Equilibrium equation

The governing equations is

$$\frac{\partial \sigma_{ji}}{\partial x_j} + b_i = \rho \ddot{u}_i \quad i = 1,2,3 \tag{B.2}$$

where σ_{ji} are the components of the CST $\boldsymbol{\sigma}$. The coordinate x_j is considered in the *deformed* continuum.

The generic component σ_{ji} of CST can be related to SPKST as follows:

$$\sigma_{ji} = \mathcal{J}^{-1} G_{jl} S_{lm} G_{im} \qquad i,j,l,m = 1,2,3 \tag{B.3}$$

where G_{jl} and G_{im} are the components of the deformation gradient tensor, whereas $\mathcal{J}$ is its determinant. Substituting Eq. B.3 into Eq. B.2 and calculating the derivatives by using the chain rule, the following formula is obtained:

$$\frac{\partial \sigma_{ji}}{\partial x_j} = \frac{\partial}{\partial x_j}\left(\mathcal{J}^{-1} G_{jl} S_{lm} G_{im}\right) = S_{lm} G_{im} \frac{\partial\left(\mathcal{J}^{-1} G_{jl}\right)}{\partial x_j} + \mathcal{J}^{-1} G_{jl} \frac{\partial\left(S_{lm} G_{im}\right)}{\partial x_j} = -b_i + \rho \ddot{u}_i \tag{B.4}$$

Using the property [95] reported below,

$$\frac{\partial\left(\mathcal{J}^{-1} G_{jl}\right)}{\partial x_j} = 0 \tag{B.5}$$

Eq B.4 is simplified as follows:

$$\frac{\partial \sigma_{ji}}{\partial x_j} = \mathcal{J}^{-1} G_{jl} \frac{\partial\left(S_{lm} G_{im}\right)}{\partial x_j} = -b_i + \rho \ddot{u}_i \tag{B.6}$$

The definition of deformation gradient tensor and chain rule of differentiation implied the following relations:

$$G_{jl} = \frac{\partial x_j}{\partial X_l} \qquad \frac{\partial(\bullet)}{\partial X_l} = \frac{\partial(\bullet)}{\partial x_j} \frac{\partial x_j}{\partial X_l} \tag{B.7}$$

Equation B.7 can be used to rewrite Eq. B.6 as reported below:

$$\mathcal{J}^{-1} G_{jl} \frac{\partial\left(S_{lm} G_{im}\right)}{\partial x_j} = \mathcal{J}^{-1} \frac{\partial x_j}{\partial X_l} \frac{\partial\left(S_{lm} G_{im}\right)}{\partial x_j} = \mathcal{J}^{-1} \frac{\partial\left(G_{im} S_{lm}\right)}{\partial X_l} = -b_i + \rho \ddot{u}_i \tag{B.8}$$

Notice that X_l is referred to the element coordinate system in the *undeformed* continuum.

Using the fact that l is a repeated dummy index in RHS of Eq. B.8, it is possible to express Eq. B.8 in the following equivalent form:

$$\frac{\partial\left(G_{im} S_{jm}\right)}{\partial X_j} = -\mathcal{J} b_i + \mathcal{J} \rho \ddot{u}_i \tag{B.9}$$

Finally, using the symmetry properties of SPKST, Eq. B.9 is simplified as

$$\frac{\partial\left(G_{im} S_{mj}\right)}{\partial X_j} = -\mathcal{J} b_i + \mathcal{J} \rho \ddot{u}_i \quad i, j = 1, 2, 3 \tag{B.10}$$

Which represents the governing equations written in terms of SPKST.

B.2 Neumann boundary condition

The natural boundary condition is (Eq.B.1):

$$n_j \sigma_{ji} = \hat{h}_i \tag{B.11}$$

or in vector form:

$$\mathbf{n} \cdot \boldsymbol{\sigma} = \hat{\mathbf{h}} \tag{B.12}$$

Recall the relation between the Cauchy and SPKST:

$$\boldsymbol{\sigma} = \frac{1}{\det(\mathbf{G})} \mathbf{G} \cdot \mathbf{S} \cdot \mathbf{G}^T \tag{B.13}$$

and the relation that exist between the normals in the deformed ($\mathbf{n}$) and undeformed configuration ($\mathbf{N}$).

$$\mathbf{n} = \frac{\mathbf{G}^{-T} \cdot \mathbf{N}}{\sqrt{\mathbf{N} \cdot \left(\mathbf{G}^T \cdot \mathbf{G}\right)^{-1} \cdot \mathbf{N}}} \tag{B.14}$$

The mapping of the traction force is obtained as follow:

$$\mathbf{h} \mathrm{d}s = \mathbf{H} \mathrm{d}S \tag{B.15}$$

where $\mathbf{H}$ is the traction force mapped in the undeformed configuration, $\mathrm{d}s$ and $\mathrm{d}S$ are the surface area in the current and undeformed configuration respectively. Eq. B.15 can be rewritten as:

$$\mathbf{h} = \mathbf{H} \mathrm{d}S / \mathrm{d}s \tag{B.16}$$

The relations between the areas is given by Nelson's formula:

$$\mathbf{n} \mathrm{d}s = \det(\mathbf{G}) \mathbf{G}^{-T} \cdot \mathbf{N} \mathrm{d}S \tag{B.17}$$

Solving Eq.B.17 for the area ratio:

$$\frac{dS}{ds} = \frac{1}{\det(\mathbf{G}) \sqrt{\mathbf{N} \cdot \left(\mathbf{G}^T \cdot \mathbf{G}\right)^{-1} \cdot \mathbf{N}}} \tag{B.18}$$

Substituting Eq. B.18 in Eq. B.16:

$$\mathbf{h} = \mathbf{H}\frac{1}{\det(\mathbf{G})\sqrt{\mathbf{N}\cdot\left(\mathbf{G}^T\cdot\mathbf{G}\right)^{-1}\cdot\mathbf{N}}} \tag{B.19}$$

Putting everything together

$$\mathbf{n}\cdot\boldsymbol{\sigma} = \frac{\mathbf{G}^{-T}\cdot\mathbf{N}}{\sqrt{\mathbf{N}\cdot\left(\mathbf{G}^T\cdot\mathbf{G}\right)^{-1}\cdot\mathbf{N}}}\cdot\frac{1}{\det(\mathbf{G})}\mathbf{G}\cdot\mathbf{S}\cdot\mathbf{G}^T = \mathbf{H}\frac{1}{\det(\mathbf{G})\sqrt{\mathbf{N}\cdot\left(\mathbf{G}^T\cdot\mathbf{G}\right)^{-1}\cdot\mathbf{N}}} = \hat{\mathbf{h}} \tag{B.20}$$

Simplifying:

$$\mathbf{G}^{-T}\cdot\mathbf{N}\cdot\mathbf{G}\cdot\mathbf{S}\cdot\mathbf{G}^T = \mathbf{H} \tag{B.21}$$

Now it is convenient to rewrite this epression in indicial form

$$G^{-1}_{kj}N_kG_{jp}S_{pq}G_{iq} = H_i \tag{B.22}$$

$$N_kG^{-1}_{kj}G_{jp}S_{pq}G_{iq} = H_i \tag{B.23}$$

$$N_k\delta_{kp}S_{pq}G_{iq} = H_i \tag{B.24}$$

$$N_kS_{kq}G_{iq} = H_i \tag{B.25}$$

Finally using the symmetry of the SPKST, the expression of the Neumann boundary condition is found

$$G_{iq}S_{kq}N_k = H_i \tag{B.26}$$

$$\mathbf{G}\cdot\mathbf{S}\cdot\mathbf{N} = \mathbf{H} \tag{B.27}$$

Appendix C

Deformation gradient written with GUF notation

In the formulation it is necessary to compute the deformation gradient at the converged iteration:

$$ {}^{t}_{0}G_{ij} = \delta_{ij} + {}^{t}_{0}u_{i,j} \tag{C.1} $$

or

$$ {}^{t}_{0}\mathbf{G} = \mathbf{I} + {}^{t}_{0}\nabla\mathbf{u} \tag{C.2} $$

The displacement gradient is defined as

$$
\begin{aligned}
{}^{t}_{0}u_{X,X} &= {}^{X}_{0}F_{\alpha_{u_X}} \quad {}^{X}_{0}N_{I,X} \quad {}^{t}_{0}U_{X\alpha_{u_X}I} \\
{}^{t}_{0}u_{X,Y} &= {}^{X}_{0}F_{\alpha_{u_X}} \quad {}^{X}_{0}N_{I,Y} \quad {}^{t}_{0}U_{X\alpha_{u_X}I} \\
{}^{t}_{0}u_{X,Z} &= {}^{X}_{0}F_{\alpha_{u_{X,Z}}} \; {}^{X}_{0}N_{I} \quad {}^{t}_{0}U_{X\alpha_{u_X}I} \\
{}^{t}_{0}u_{Y,X} &= {}^{Y}_{0}F_{\alpha_{u_Y}} \quad {}^{Y}_{0}N_{I,X} \quad {}^{t}_{0}U_{Y\alpha_{u_Y}I} \\
{}^{t}_{0}u_{Y,Y} &= {}^{Y}_{0}F_{\alpha_{u_Y}} \quad {}^{Y}_{0}N_{I,Y} \quad {}^{t}_{0}U_{Y\alpha_{u_Y}I} \\
{}^{t}_{0}u_{Y,Z} &= {}^{Y}_{0}F_{\alpha_{u_{Y,Z}}} \; {}^{Y}_{0}N_{I} \quad {}^{t}_{0}U_{Y\alpha_{u_Y}I} \\
{}^{t}_{0}u_{Z,X} &= {}^{Z}_{0}F_{\alpha_{u_Z}} \quad {}^{Z}_{0}N_{I,X} \quad {}^{t}_{0}U_{Z\alpha_{u_Z}I} \\
{}^{t}_{0}u_{Z,Y} &= {}^{Z}_{0}F_{\alpha_{u_Z}} \quad {}^{Z}_{0}N_{I,Y} \quad {}^{t}_{0}U_{Z\alpha_{u_Z}I} \\
{}^{t}_{0}u_{Z,Z} &= {}^{Z}_{0}F_{\alpha_{u_{Z,Z}}} \; {}^{Z}_{0}N_{I} \quad {}^{t}_{0}U_{Z\alpha_{u_Z}I}
\end{aligned}
\tag{C.3}
$$

Substituting equation C.3 into equation C.1 the expression for the deformation gradient is obtained as reported below:

$$
\begin{aligned}
{}^{t}_{0}G_{XX} &= 1 + {}^{X}_{0}F_{\alpha_{u_X}} \; {}^{X}_{0}N_{I,X} \; {}^{t}_{0}U_{X\alpha_{u_X}I} \\
{}^{t}_{0}G_{XY} &= \quad\; {}^{X}_{0}F_{\alpha_{u_X}} \; {}^{X}_{0}N_{I,Y} \; {}^{t}_{0}U_{X\alpha_{u_X}I} \\
{}^{t}_{0}G_{XZ} &= \quad\; {}^{X}_{0}F_{\alpha_{u_{X,Z}}} \; {}^{X}_{0}N_{I} \; {}^{t}_{0}U_{X\alpha_{u_X}I} \\
{}^{t}_{0}G_{YX} &= \quad\; {}^{Y}_{0}F_{\alpha_{u_Y}} \; {}^{Y}_{0}N_{I,X} \; {}^{t}_{0}U_{Y\alpha_{u_Y}I} \\
{}^{t}_{0}G_{YY} &= 1 + {}^{Y}_{0}F_{\alpha_{u_Y}} \; {}^{Y}_{0}N_{I,Y} \; {}^{t}_{0}U_{Y\alpha_{u_Y}I} \\
{}^{t}_{0}G_{YZ} &= \quad\; {}^{Y}_{0}F_{\alpha_{u_{Y,Z}}} \; {}^{Y}_{0}N_{I} \; {}^{t}_{0}U_{Y\alpha_{u_Y}I} \\
{}^{t}_{0}G_{ZX} &= \quad\; {}^{Z}_{0}F_{\alpha_{u_Z}} \; {}^{Z}_{0}N_{I,X} \; {}^{t}_{0}U_{Z\alpha_{u_Z}I} \\
{}^{t}_{0}G_{ZY} &= \quad\; {}^{Z}_{0}F_{\alpha_{u_Z}} \; {}^{Z}_{0}N_{I,Y} \; {}^{t}_{0}U_{Z\alpha_{u_Z}I} \\
{}^{t}_{0}G_{ZZ} &= 1 + {}^{Z}_{0}F_{\alpha_{u_{Z,Z}}} \; {}^{Z}_{0}N_{I} \; {}^{t}_{0}U_{Z\alpha_{u_Z}I}
\end{aligned}
\tag{C.4}
$$

Appendix D

Strain-displacement matrix

The contribution to the linear strain displacement matrix due to node J is:

$$
\begin{aligned}
{}^{t}_{0}B_{L\,11}^{\beta_{u_X}\,J} &= {}^{t}_{0}G_{XX}\,{}^{X}_{0}F_{\beta_{u_X}}\,{}^{X}_{0}N_{J,X} \\
{}^{t}_{0}B_{L\,12}^{\beta_{u_Y}\,J} &= {}^{t}_{0}G_{YX}\,{}^{Y}_{0}F_{\beta_{u_Y}}\,{}^{Y}_{0}N_{J,X} \\
{}^{t}_{0}B_{L\,13}^{\beta_{u_Z}\,J} &= {}^{t}_{0}G_{ZX}\,{}^{Z}_{0}F_{\beta_{u_Z}}\,{}^{Z}_{0}N_{J,X} \\
{}^{t}_{0}B_{L\,21}^{\beta_{u_X}\,J} &= {}^{t}_{0}G_{XY}\,{}^{X}_{0}F_{\beta_{u_X}}\,{}^{X}_{0}N_{J,Y} \\
{}^{t}_{0}B_{L\,22}^{\beta_{u_Y}\,J} &= {}^{t}_{0}G_{YY}\,{}^{Y}_{0}F_{\beta_{u_Y}}\,{}^{Y}_{0}N_{J,Y} \\
{}^{t}_{0}B_{L\,23}^{\beta_{u_Z}\,J} &= {}^{t}_{0}G_{ZY}\,{}^{Z}_{0}F_{\beta_{u_Z}}\,{}^{Z}_{0}N_{J,Y}
\end{aligned}
\tag{D.1}
$$

$$
\begin{aligned}
{}^{t}_{0}B_{L\,31}^{\beta_{u_X}\,J} &= {}^{t}_{0}G_{XX}\,{}^{X}_{0}F_{\beta_{u_X}}\,{}^{X}_{0}N_{J,Y} + {}^{t}_{0}G_{XY}\,{}^{X}_{0}F_{\beta_{u_X}}\quad{}^{X}_{0}N_{J,X} \\
{}^{t}_{0}B_{L\,32}^{\beta_{u_Y}\,J} &= {}^{t}_{0}G_{YX}\,{}^{Y}_{0}F_{\beta_{u_Y}}\,{}^{Y}_{0}N_{J,Y} + {}^{t}_{0}G_{YY}\,{}^{Y}_{0}F_{\beta_{u_Y}}\quad{}^{Y}_{0}N_{J,X} \\
{}^{t}_{0}B_{L\,33}^{\beta_{u_Z}\,J} &= {}^{t}_{0}G_{ZX}\,{}^{Z}_{0}F_{\beta_{u_Z}}\,{}^{Z}_{0}N_{J,Y} + {}^{t}_{0}G_{ZY}\,{}^{Z}_{0}F_{\beta_{u_Z}}\quad{}^{Z}_{0}N_{J,X} \\
{}^{t}_{0}B_{L\,41}^{\beta_{u_X}\,J} &= {}^{t}_{0}G_{XZ}\,{}^{X}_{0}F_{\beta_{u_X}}\,{}^{X}_{0}N_{J,X} + {}^{t}_{0}G_{XX}\,{}^{X}_{0}F_{\beta_{u_{X,Z}}}\,{}^{X}_{0}N_{J} \\
{}^{t}_{0}B_{L\,42}^{\beta_{u_Y}\,J} &= {}^{t}_{0}G_{YZ}\,{}^{Y}_{0}F_{\beta_{u_Y}}\,{}^{Y}_{0}N_{J,X} + {}^{t}_{0}G_{YX}\,{}^{Y}_{0}F_{\beta_{u_{Y,Z}}}\,{}^{Y}_{0}N_{J} \\
{}^{t}_{0}B_{L\,43}^{\beta_{u_Z}\,J} &= {}^{t}_{0}G_{ZZ}\,{}^{Z}_{0}F_{\beta_{u_Z}}\,{}^{Z}_{0}N_{J,X} + {}^{t}_{0}G_{ZX}\,{}^{Z}_{0}F_{\beta_{u_{Z,Z}}}\,{}^{Z}_{0}N_{J}
\end{aligned}
\tag{D.2}
$$

$$
\begin{aligned}
{}^{t}_{0}B_{L\,51}^{{\beta_u}_X\,J} &= {}^{t}_{0}G_{XY}\,{}^{X}_{0}F_{{\beta_u}_{X,Z}}\,{}^{X}_{0}N_J + {}^{t}_{0}G_{XZ}\,{}^{X}_{0}F_{{\beta_u}_X}\,{}^{X}_{0}N_{J,Y} \\
{}^{t}_{0}B_{L\,52}^{{\beta_u}_Y\,J} &= {}^{t}_{0}G_{YY}\,{}^{Y}_{0}F_{{\beta_u}_{Y,Z}}\,{}^{Y}_{0}N_J + {}^{t}_{0}G_{YZ}\,{}^{Y}_{0}F_{{\beta_u}_Y}\,{}^{Y}_{0}N_{J,Y} \\
{}^{t}_{0}B_{L\,53}^{{\beta_u}_Z\,J} &= {}^{t}_{0}G_{ZY}\,{}^{Z}_{0}F_{{\beta_u}_{Z,Z}}\,{}^{Z}_{0}N_J + {}^{t}_{0}G_{ZZ}\,{}^{Z}_{0}F_{{\beta_u}_Z}\,{}^{Z}_{0}N_{J,Y} \\
{}^{t}_{0}B_{L\,61}^{{\beta_u}_X\,J} &= {}^{t}_{0}G_{XZ}\,{}^{X}_{0}F_{{\beta_u}_{X,Z}}\,{}^{X}_{0}N_J \\
{}^{t}_{0}B_{L\,62}^{{\beta_u}_Y\,J} &= {}^{t}_{0}G_{YZ}\,{}^{Y}_{0}F_{{\beta_u}_{Y,Z}}\,{}^{Y}_{0}N_J \\
{}^{t}_{0}B_{L\,63}^{{\beta_u}_Z\,J} &= {}^{t}_{0}G_{ZZ}\,{}^{Z}_{0}F_{{\beta_u}_{Z,Z}}\,{}^{Z}_{0}N_J
\end{aligned}
\tag{D.3}
$$

Appendix E

Kernels of the linear part of the elastic stiffness matrix

First, the following auxiliary quantity is defined:

$$\mathbf{g} = \left[{}^{t}_{0}G_{XX} \quad {}^{t}_{0}G_{XY} \quad {}^{t}_{0}G_{XZ} \quad {}^{t}_{0}G_{YX} \quad {}^{t}_{0}G_{YY} \quad {}^{t}_{0}G_{YZ} \quad {}^{t}_{0}G_{ZX} \quad {}^{t}_{0}G_{ZY} \quad {}^{t}_{0}G_{ZZ} \right] \tag{E.1}$$

Products of components of the array $\mathbf{g}$ are indicated with a compact notation as follows:

$$g_{rs} = g_r \cdot g_s \tag{E.2}$$

where, for example, it is

$$g_{25} = {}^{t}_{0}G_{XY} \cdot {}^{t}_{0}G_{YY} \tag{E.3}$$

Next, let's consider one of the thickness integrals involving the Hooke coefficients, thickness functions, and deformation gradients:

$${}^{t}_{0}\tilde{Z}^{\alpha_{u_X}\beta_{u_X}g_{11}}_{11u_Xu_X} = \int_Z \tilde{C}_{11}\, {}^{t}_{0}G_{XX}\, {}^{t}_{0}G_{XX}\, {}^{X}_{0}F_{\alpha_{u_X}}\, {}^{X}_{0}F_{\beta_{u_X}}\, \mathrm{d}Z \tag{E.4}$$

where Eq. E.2 has been used in the superscript appearing on the LHS.

To make the notation more compact, the left sub and superscript (t and 0, respectively) are omitted. An example of kernel is reported below:

$$
\begin{aligned}
K_{\mathrm{L}\ u_X u_Y}^{\alpha_{u_X}\beta_{u_Y} IJ} = \int_{{}_0A} \Big[& \tilde{Z}_{11 u_X u_Y}^{\alpha_{u_X}\beta_{u_Y} g_{14}} \ {}_0^X N_{I,X}\ {}_0^Y N_{J,X} + \tilde{Z}_{12 u_X u_Y}^{\alpha_{u_X}\beta_{u_Y} g_{14}} \ {}_0^X N_{I,Y}\ {}_0^Y N_{J,X} \\
+ & \tilde{Z}_{12 u_X u_Y}^{\alpha_{u_X}\beta_{u_Y} g_{15}} \ {}_0^X N_{I,X}\ {}_0^Y N_{J,Y} + \tilde{Z}_{13 u_X u_Y}^{\alpha_{u_X,Z}\beta_{u_Y} g_{34}} \ {}_0^X N_{I}\ {}_0^Y N_{J,X} \\
+ & \tilde{Z}_{13 u_X u_Y}^{\alpha_{u_X}\beta_{u_Y,Z} g_{16}} \ {}_0^X N_{I,X}\ {}_0^Y N_{J}\ + \tilde{Z}_{16 u_X u_Y}^{\alpha_{u_X}\beta_{u_Y} g_{41}} \ {}_0^X N_{I,Y}\ {}_0^Y N_{J,X} \\
+ & \tilde{Z}_{16 u_X u_Y}^{\alpha_{u_X}\beta_{u_Y} g_{42}} \ {}_0^X N_{I,X}\ {}_0^Y N_{J,X} + \tilde{Z}_{16 u_X u_Y}^{\alpha_{u_X}\beta_{u_Y} g_{14}} \ {}_0^X N_{I,X}\ {}_0^Y N_{J,Y} \\
+ & \tilde{Z}_{16 u_X u_Y}^{\alpha_{u_X}\beta_{u_Y} g_{15}} \ {}_0^X N_{I,X}\ {}_0^Y N_{J,X} + \tilde{Z}_{22 u_X u_Y}^{\alpha_{u_X}\beta_{u_Y} g_{25}} \ {}_0^X N_{I,Y}\ {}_0^Y N_{J,Y} \\
+ & \tilde{Z}_{23 u_X u_Y}^{\alpha_{u_X,Z}\beta_{u_Y} g_{35}} \ {}_0^X N_{I}\ {}_0^Y N_{J,Y} + \tilde{Z}_{23 u_X u_Y}^{\alpha_{u_X}\beta_{u_Y,Z} g_{26}} \ {}_0^X N_{I,Y}\ {}_0^Y N_{J} \\
+ & \tilde{Z}_{26 u_X u_Y}^{\alpha_{u_X}\beta_{u_Y} g_{15}} \ {}_0^X N_{I,Y}\ {}_0^Y N_{J,Y} + \tilde{Z}_{26 u_X u_Y}^{\alpha_{u_X}\beta_{u_Y} g_{25}} \ {}_0^X N_{I,X}\ {}_0^Y N_{J,Y} \\
+ & \tilde{Z}_{26 u_X u_Y}^{\alpha_{u_X}\beta_{u_Y} g_{24}} \ {}_0^X N_{I,Y}\ {}_0^Y N_{J,Y} + \tilde{Z}_{26 u_X u_Y}^{\alpha_{u_X}\beta_{u_Y} g_{25}} \ {}_0^X N_{I,Y}\ {}_0^Y N_{J,X} \\
+ & \tilde{Z}_{33 u_X u_Y}^{\alpha_{u_X,Z}\beta_{u_Y,Z} g_{36}} \ {}_0^X N_{I}\ {}_0^Y N_{J}\ + \tilde{Z}_{36 u_X u_Y}^{\alpha_{u_X}\beta_{u_Y,Z} g_{16}} \ {}_0^X N_{I,Y}\ {}_0^Y N_{J} \\
+ & \tilde{Z}_{36 u_X u_Y}^{\alpha_{u_X}\beta_{u_Y,Z} g_{16}} \ {}_0^X N_{I,X}\ {}_0^Y N_{J}\ + \tilde{Z}_{36 u_X u_Y}^{\alpha_{u_X,Z}\beta_{u_Y} g_{43}} \ {}_0^X N_{I}\ {}_0^Y N_{J,Y} \\
+ & \tilde{Z}_{36 u_X u_Y}^{\alpha_{u_X,Z}\beta_{u_Y} g_{53}} \ {}_0^X N_{I}\ {}_0^Y N_{J,X} + \tilde{Z}_{44 u_X u_Y}^{\alpha_{u_X,Z}\beta_{u_Y,Z} g_{25}} \ {}_0^X N_{I}\ {}_0^Y N_{J} \\
+ & \tilde{Z}_{44 u_X u_Y}^{\alpha_{u_X,Z}\beta_{u_Y} g_{26}} \ {}_0^X N_{I}\ {}_0^Y N_{J,Y} + \tilde{Z}_{44 u_X u_Y}^{\alpha_{u_X}\beta_{u_Y,Z} g_{35}} \ {}_0^X N_{I,Y}\ {}_0^Y N_{J} \\
+ & \tilde{Z}_{44 u_X u_Y}^{\alpha_{u_X}\beta_{u_Y} g_{36}} \ {}_0^X N_{I,Y}\ {}_0^Y N_{J,Y} + \tilde{Z}_{45 u_X u_Y}^{\alpha_{u_X}\beta_{u_Y,Z} g_{35}} \ {}_0^X N_{I,X}\ {}_0^Y N_{J} \\
+ & \tilde{Z}_{45 u_X u_Y}^{\alpha_{u_X}\beta_{u_Y} g_{36}} \ {}_0^X N_{I,X}\ {}_0^Y N_{J,Y} + \tilde{Z}_{45 u_X u_Y}^{\alpha_{u_X,Z}\beta_{u_Y,Z} g_{15}} \ {}_0^X N_{I}\ {}_0^Y N_{J} \\
+ & \tilde{Z}_{45 u_X u_Y}^{\alpha_{u_X,Z}\beta_{u_Y} g_{16}} \ {}_0^X N_{I}\ {}_0^Y N_{J,Y} + \tilde{Z}_{45 u_X u_Y}^{\alpha_{u_X,Z}\beta_{u_Y} g_{26}} \ {}_0^X N_{I}\ {}_0^Y N_{J,X} \\
+ & \tilde{Z}_{45 u_X u_Y}^{\alpha_{u_X,Z}\beta_{u_Y,Z} g_{24}} \ {}_0^X N_{I}\ {}_0^Y N_{J}\ + \tilde{Z}_{45 u_X u_Y}^{\alpha_{u_X}\beta_{u_Y} g_{36}} \ {}_0^X N_{I,Y}\ {}_0^Y N_{J,X} \\
+ & \tilde{Z}_{45 u_X u_Y}^{\alpha_{u_X}\beta_{u_Y,Z} g_{34}} \ {}_0^X N_{I,Y}\ {}_0^Y N_{J}\ + \tilde{Z}_{55 u_X u_Y}^{\alpha_{u_X}\beta_{u_Y} g_{36}} \ {}_0^X N_{I,X}\ {}_0^Y N_{J,X} \\
+ & \tilde{Z}_{55 u_X u_Y}^{\alpha_{u_X}\beta_{u_Y,Z} g_{34}} \ {}_0^X N_{I,X}\ {}_0^Y N_{J}\ + \tilde{Z}_{55 u_X u_Y}^{\alpha_{u_X,Z}\beta_{u_Y} g_{16}} \ {}_0^X N_{I}\ {}_0^Y N_{J,X} \\
+ & \tilde{Z}_{55 u_X u_Y}^{\alpha_{u_X,Z}\beta_{u_Y,Z} g_{14}} \ {}_0^X N_{I}\ {}_0^Y N_{J}\ + \tilde{Z}_{66 u_X u_Y}^{\alpha_{u_X}\beta_{u_Y} g_{14}} \ {}_0^X N_{I,Y}\ {}_0^Y N_{J,Y} \\
+ & \tilde{Z}_{66 u_X u_Y}^{\alpha_{u_X}\beta_{u_Y} g_{15}} \ {}_0^X N_{I,Y}\ {}_0^Y N_{J,X} + \tilde{Z}_{66 u_X u_Y}^{\alpha_{u_X}\beta_{u_Y} g_{24}} \ {}_0^X N_{I,X}\ {}_0^Y N_{J,Y} \\
+ & \tilde{Z}_{66 u_X u_Y}^{\alpha_{u_X}\beta_{u_Y} g_{25}} \ {}_0^X N_{I,X}\ {}_0^Y N_{J,X} \Big] \mathrm{d}\,{}_0A
\end{aligned}
\tag{E.5}
$$

For *linear static case* the deformation gradient is the identity matrix and equation E.5 becomes:

$$
\begin{aligned}
K_{\mathrm{L}\,u_X u_Y}^{\alpha_{u_X}\beta_{u_Y}\,IJ} = \int_{{}_0A} [\; & \tilde{Z}_{12u_X u_Y}^{\alpha_{u_X}\beta_{u_Y}}\ {}_0^X N_{I,X}\ {}_0^Y N_{J,Y} + \tilde{Z}_{16u_X u_Y}^{\alpha_{u_X}\beta_{u_Y}}\quad {}_0^X N_{I,X}\ {}_0^Y N_{J,X} + \\
+ \quad & \tilde{Z}_{26u_X u_Y}^{\alpha_{u_X}\beta_{u_Y}}\ {}_0^X N_{I,Y}\ {}_0^Y N_{J,Y} + \tilde{Z}_{45u_X u_Y}^{\alpha_{u_X,Z}\beta_{u_Y,Z}}\ {}_0^X N_I\quad {}_0^Y N_J \\
+ \quad & \tilde{Z}_{66u_X u_Y}^{\alpha_{u_X}\beta_{u_Y}}\ {}_0^X N_{I,Y}\ {}_0^Y N_{J,X} \Big]\ \mathrm{d}\,{}_0A
\end{aligned}
\tag{E.6}
$$

Similar derivations can be used for the other kernels.

Appendix F

Penalty method and kernels of the spring stiffness matrix

Equation 3.119 is explicitly written by assuming that the spring connects two points located within layer k. The first point is on element c node J and the second point is on the same layer and is on element d, node L. We have the following relation deduced from Eq. 3.119:

$$ {}^{t+\Delta t}_{0}\mathcal{V}^{k} = \frac{1}{2}\left({}^{t+\Delta t}_{0}\mathbf{u}_{J}^{k\,c} - {}^{t+\Delta t}_{0}\mathbf{u}_{L}^{k\,d}\right)^{T}\boldsymbol{\gamma}^{k}\left({}^{t+\Delta t}_{0}\mathbf{u}_{J}^{k\,c} - {}^{t+\Delta t}_{0}\mathbf{u}_{L}^{k\,d}\right) \tag{F.1} $$

or

$$ \begin{aligned} {}^{t+\Delta t}_{0}\mathcal{V}^{k} = &\frac{1}{2}\,{}^{t+\Delta t}_{0}\mathbf{u}_{J}^{k\,c\,T}\;\boldsymbol{\gamma}^{k}\;{}^{t+\Delta t}_{0}\mathbf{u}_{J}^{k\,c} - \frac{1}{2}\,{}^{t+\Delta t}_{0}\mathbf{u}_{J}^{k\,c\,T}\;\boldsymbol{\gamma}^{k}\;{}^{t+\Delta t}_{0}\mathbf{u}_{L}^{k\,d} \\ &- \frac{1}{2}\,{}^{t+\Delta t}_{0}\mathbf{u}_{L}^{k\,d\,T}\;\boldsymbol{\gamma}^{k}\;{}^{t+\Delta t}_{0}\mathbf{u}_{J}^{k\,c} + \frac{1}{2}\,{}^{t+\Delta t}_{0}\mathbf{u}_{L}^{k\,d\,T}\;\boldsymbol{\gamma}^{k}\;{}^{t+\Delta t}_{0}\mathbf{u}_{L}^{k\,d} \end{aligned} \tag{F.2} $$

which is simplified by taking into account the fact that $\boldsymbol{\gamma}^{k}$ is symmetric as follows:

$$ \begin{aligned} {}^{t+\Delta t}_{0}\mathcal{V}^{k} = &\frac{1}{2}\,{}^{t+\Delta t}_{0}\mathbf{u}_{J}^{k\,c\,T}\;\boldsymbol{\gamma}^{k}\;{}^{t+\Delta t}_{0}\mathbf{u}_{J}^{k\,c} - {}^{t+\Delta t}_{0}\mathbf{u}_{J}^{k\,c\,T}\;\boldsymbol{\gamma}^{k}\;{}^{t+\Delta t}_{0}\mathbf{u}_{L}^{k\,d} \\ &+ \frac{1}{2}\,{}^{t+\Delta t}_{0}\mathbf{u}_{L}^{k\,d\,T}\;\boldsymbol{\gamma}^{k}\;{}^{t+\Delta t}_{0}\mathbf{u}_{L}^{k\,d} \end{aligned} \tag{F.3} $$

Equation 3.120 is now substituted into equation F.3:

$$ \begin{aligned} {}^{t+\Delta t}_{0}\mathcal{V}^{k} = &\frac{1}{2}\left({}^{t}_{0}\mathbf{u}_{J}^{k\,c\,T} + {}_{0}\Delta\mathbf{u}_{J}^{k\,c\,T}\right)\boldsymbol{\gamma}^{k}\;\left({}^{t}_{0}\mathbf{u}_{J}^{k\,c} + {}_{0}\Delta\mathbf{u}_{J}^{k\,c}\right) \\ &- \left({}^{t}_{0}\mathbf{u}_{J}^{k\,c\,T} + {}_{0}\Delta\mathbf{u}_{J}^{k\,c\,T}\right)\boldsymbol{\gamma}^{k}\;\left({}^{t}_{0}\mathbf{u}_{L}^{k\,d} + {}_{0}\Delta\mathbf{u}_{L}^{k\,d}\right) \\ &+ \frac{1}{2}\left({}^{t}_{0}\mathbf{u}_{L}^{k\,d\,T} + {}_{0}\Delta\mathbf{u}_{L}^{k\,d\,T}\right)\boldsymbol{\gamma}^{k}\;\left({}^{t}_{0}\mathbf{u}_{L}^{k\,d} + {}_{0}\Delta\mathbf{u}_{L}^{k\,d}\right) \end{aligned} \tag{F.4} $$

or

$$ {}^{t+\Delta t}_{0}\mathcal{V}^{k} = {}^{t+\Delta t}_{0}\mathcal{V}^{k}_{\Delta t-\Delta t} + {}^{t+\Delta t}_{0}\mathcal{V}^{k}_{\Delta t-t} + {}^{t+\Delta t}_{0}\mathcal{V}^{k}_{t-t} \tag{F.5} $$

where the following definitions have been used:

$$ \begin{aligned}
{}^{t+\Delta t}_{0}\mathcal{V}^{k}_{\Delta t-\Delta t} &= \frac{1}{2}\ {}_{0}\Delta\mathbf{u}^{k\,c\,T}_{J}\ \boldsymbol{\gamma}^{k}\ {}_{0}\Delta\mathbf{u}^{k\,c}_{J} - {}_{0}\Delta\mathbf{u}^{k\,c\,T}_{J}\ \boldsymbol{\gamma}^{k}\ {}_{0}\Delta\mathbf{u}^{k\,d}_{L} \\
&\quad + \frac{1}{2}\ {}_{0}\Delta\mathbf{u}^{k\,d\,T}_{L}\ \boldsymbol{\gamma}^{k}\ {}_{0}\Delta\mathbf{u}^{k\,d}_{L} \\
{}^{t+\Delta t}_{0}\mathcal{V}^{k}_{\Delta t-t} &= {}_{0}\Delta\mathbf{u}^{k\,c\,T}_{J}\ \boldsymbol{\gamma}^{k}\ {}^{t}_{0}\mathbf{u}^{k\,c}_{J} - {}_{0}\Delta\mathbf{u}^{k\,d\,T}_{L}\ \boldsymbol{\gamma}^{k}\ {}^{t}_{0}\mathbf{u}^{k\,c}_{J} \\
&\quad - {}_{0}\Delta\mathbf{u}^{k\,c\,T}_{J}\ \boldsymbol{\gamma}^{k}\ {}^{t}_{0}\mathbf{u}^{k\,d}_{L} + {}_{0}\Delta\mathbf{u}^{k\,d\,T}_{L}\ \boldsymbol{\gamma}^{k}\ {}^{t}_{0}\mathbf{u}^{k\,d}_{L} \\
{}^{t+\Delta t}_{0}\mathcal{V}^{k}_{t-t} &= \frac{1}{2}\ {}^{t}_{0}\mathbf{u}^{k\,c\,T}_{J}\ \boldsymbol{\gamma}^{k}\ {}^{t}_{0}\mathbf{u}^{k\,c}_{J} - {}^{t}_{0}\mathbf{u}^{k\,c\,T}_{J}\ \boldsymbol{\gamma}^{k}\ {}^{t}_{0}\mathbf{u}^{k\,d}_{L} \\
&\quad + \frac{1}{2}\ {}^{t}_{0}\mathbf{u}^{k\,d\,T}_{L}\ \boldsymbol{\gamma}^{k}\ {}^{t}_{0}\mathbf{u}^{k\,d}_{L}
\end{aligned} \tag{F.6} $$

The spring contribution to the tangent stiffness matrix depends on the *second derivatives* of the potential energy expression (see Eq. F.6) with respect to the incremental nodal displacement unknowns (which need to be set equal to zero after the derivative is calculated, within the linearized approach). It is also observed that all the terms of the type similar to ${}_{0}\Delta\mathbf{u}^{k\,c\,T}_{J}$ have *linear* dependency on the incremental nodal displacements (actual finite element degree of freedom). This can be see for example from the explicit formula of ${}_{0}\Delta\mathbf{u}^{k\,c\,T}_{J}$ written in *global coordinate system*:

$$ {}_{0}\Delta\mathbf{u}^{k\,c\,T}_{J} = \left[\ {}_{0}\Delta u^{k\,c}_{\mathcal{X}J}\quad {}_{0}\Delta u^{k\,c}_{\mathcal{Y}J}\quad {}_{0}\Delta u^{k\,c}_{\mathcal{Z}J}\ \right]^{T} \tag{F.7} $$

where for example it is (see Eq. 3.123)

$$ \begin{aligned}
{}_{0}\Delta u^{k\,c}_{\mathcal{X}J} &= {}^{0}_{0}a^{k\,c}_{11}\ {}^{X}_{0}F^{k\,c}_{\alpha_{u_X}}\ {}_{0}\Delta U^{k\,c}_{X\alpha_{u_X}J} + {}^{0}_{0}a^{k\,c}_{21}\ {}^{Y}_{0}F^{k\,c}_{\alpha_{u_Y}}\ {}_{0}\Delta U^{k\,c}_{Y\alpha_{u_Y}J} \\
&\quad + {}^{0}_{0}a^{k\,c}_{31}\ {}^{Z}_{0}F^{k\,c}_{\alpha_{u_Z}}\ {}_{0}\Delta U^{k\,c}_{Z\alpha_{u_Z}J}
\end{aligned} \tag{F.8} $$

From all of this reasoning it is realized that the tangent stiffness matrix contribution due to the springs is generated only from ${}^{t+\Delta t}_{0}\mathcal{V}^{k}_{\Delta t-\Delta t}$ (see Eq. F.6). Of course, this term needs to be written explicitly as a function of the finite element unknowns following the procedure which led to Eq. F.8. It should also be observed that the transformation coefficients (for example ${}^{0}_{0}a^{k\,c}_{31}$) between coordinate systems does not depend on the finite element unknowns since everything is referred to the initial geometry (TLF).

To show how a generic contribution of the spring matrix (which needs to be added to the tangent

stiffness matrix) is obtained, let us consider term ${}^{t}_{0}K^{k\,c\,\alpha_{u_X}\beta_{u_Y}\,JJ}_{\mathrm{sp}\,u_X u_Y}$, which is the "self contribution" node J of element c generates. By definition, it is the derived as follows:

$${}^{t}_{0}K^{k\,c\,\alpha_{u_X}\beta_{u_Y}\,JJ}_{\mathrm{sp}\,u_X u_Y} = \left.\frac{\partial^2\left({}^{t+\Delta t}_{0}\mathcal{V}^{k}\right)}{\partial\,{}_{0}\Delta U^{k\,c}_{\beta_{u_X}J}\quad\partial\,{}_{0}\Delta U^{k\,c}_{\beta_{u_Y}J}}\right|_{{}_{0}\Delta\mathbf{U}=\mathbf{0}} \tag{F.9}$$

which is written, by taking into account the discussion previously made, as follows:

$${}^{t}_{0}K^{k\,c\,\alpha_{u_X}\beta_{u_Y}\,JJ}_{\mathrm{SP}\,u_X u_Y} = \left.\frac{\partial^2\left({}^{t+\Delta t}_{0}\mathcal{V}^{k}_{\Delta t-\Delta t}\right)}{\partial\,{}_{0}\Delta U^{k\,c}_{\beta_{u_X}J}\quad\partial\,{}_{0}\Delta U^{k\,c}_{\beta_{u_Y}J}}\right|_{{}_{0}\Delta\mathbf{U}=\mathbf{0}} \tag{F.10}$$

Similar methodology can be followed for the the "coupled" terms. It should also be noted that the tangent stiffness matrix is not written in the global coordinate system: the terms are obtained in the element coordinate system referred to the undeformed configuration.

In the present formulation actually a thickness distribution of springs is used to enforce the compatibility at layer level. The formulation of the related matrix is very similar. The only difference is that integrals of the products of thickness functions appear [27]. For example, in the case of a thickness distribution of springs, after the differentiation of the potential energy it is possible to show that

$${}^{t}_{0}K^{k\,c\,\alpha_{u_X}\beta_{u_X}\,JJ}_{\mathrm{SP}\,u_X u_X} = \left.\frac{\partial^2\left({}^{t+\Delta t}_{0}\mathcal{V}^{k}_{\Delta t-\Delta t}\right)}{\partial\,{}_{0}\Delta U^{k\,c}_{\beta_{u_X}J}\quad\partial\,{}_{0}\Delta U^{k\,c}_{\beta_{u_X}J}}\right|_{{}_{0}\Delta\mathbf{U}=\mathbf{0}} \tag{F.11}$$

$${}^{t}_{0}K^{k\,c\,\alpha_{u_X}\beta_{u_X}\,JJ}_{\mathrm{SP}\,u_X u_X} = \left[\left({}^{0}_{0}a^{k\,c}_{11}\right)^2\,\gamma^{k}_{\mathcal{X}} + \left({}^{0}_{0}a^{k\,c}_{12}\right)^2\,\gamma^{k}_{\mathcal{Y}} + \left({}^{0}_{0}a^{k\,c}_{13}\right)^2\,\gamma^{k}_{\mathcal{Z}}\right]\int_{Z} {}^{X}_{0}F^{k\,c}_{\alpha_{u_X}}\;{}^{X}_{0}F^{k\,c}_{\beta_{u_X}}\,\mathrm{d}Z \tag{F.12}$$

Notice that the spring stiffness matrix is actually independent of the time step. Thus, the following relationship holds:

$${}^{t}_{0}\mathbf{K}^{k}_{\mathrm{SP}} = {}^{0}_{0}\mathbf{K}^{k}_{\mathrm{SP}} \tag{F.13}$$

Similar formula holds also at multilayered element and structural levels.

Bibliography

[1] A. Lukaszewicz D.H.-J, C. Ward, and K. D. Potter. "The engineering aspects of automated prepreg layup: History, present and future". In: *Composites: Part B* (2012).

[2] B. C. Kim, P. M. Weaver, and K. Potter. "Computer aided modelling of variable angle tow composites manufactured by continuous tow shearing". In: *Composite Structures* 129 (2015), pp. 256–267.

[3] A. Capatano, M. Montemurro, J. A. Balcou, and E. Panettieri. "Rapid prototyping of variable angle-tow composites". In: *Aerotecnica Missili & Spazio* (2019).

[4] V. Olivieri, G. Zucco, D. Peeters, G. Clancy, R. Telford, M. Rouhi, C. McHale, R. M. O'Higgins, T. M. Young, and P. M. Weaver. "Design, Manufacture and Test of an In-Situ Consolidated Thermoplastic Variable-Stiffness Wingbox". In: *AIAA Journal* 57.4 (2019), pp. 1671–1683.

[5] M. Hyer and H. Lee. "The use of curvilinear fiber format to improve buckling resistance of composite plates with central circular holes". In: *Composites Structures* 18 (1991), pp. 239–261.

[6] B. H. Coburn, Z. Wu, and P. M. Weaver. "Buckling analysis of stiffened variable angle tow panels". In: *Composite Structures* 111 (2014), pp. 259–270.

[7] Z. Wu, P. M. Weaver, G. Raju, and B. C. Kim. "Buckling analysis and optimisation of variable angle tow composite plates". In: *Thin-Walled Structures* 60 (2012), pp. 163–172.

[8] Z. Wu, G. Raju, and Weaver. "Postbuckling analysis of variable angle tow composite plates". In: *International Journal of Solids and Structures* 50 (2013), pp. 1770–1780.

[9] Z. Wu, G. Raju, and P. M. Weaver. "Optimization of postbuckling behaviour of variable thickness composite panels with variable angle tows: Towards "Buckle-Free"design concept". In: *International Journal of Solids and Structures* 132 (2018), pp. 66–79.

[10] F. S. Liguori, G. Zucco, A. Madeo, D. Magisano, L. Leonetti, G. Garcea, and P. M. Weaver. "Postbuckling optimisation of a variable angle tow composite wingbox using a multi-modal Koiter approach". In: *Thin-Walled Structures* 138 (2019), pp. 183–198.

[11] A. Viglietti, E. Zappino, and E. Carrera. "Free vibration analysis of variable angle-tow composite wing structures". In: *Aerospace Science and Technology* 92 (2019), pp. 114–125.

[12] O. Stodieck, J. E. Cooper, P. M. Weaver, and P. Kealy. "Improved aeroelastic tailoring using tow-steered composites". In: *Composite Structures* 106 (2013), pp. 703–715.

[13] O. Stodieck, J. E. Cooper, P. M. Weaver, and P. Kealy. "Optimization of Tow-Steered Composite Wing Laminates for Aeroelastic Tailoring". In: *AIAA Journal* 53.8 (2015), pp. 2203–2215.

[14] T. A. M. Guimaraes, S. G. P. Castro, D. A. Rade, and C. E. S. Cesnik. "Panel Flutter Analysis and Optimization of Composite Tow Steered Plates". In: *AIAA SciTech Forum*. Grapevine, Texas, Jan. 2017.

[15] B. K. Stanford and C. V. Jutte. "Comparison of curvilinear stiffeners and tow steered composites for aeroelastic tailoring of aircraft wings". In: *Computer and Structures* 183 (2017), pp. 48–60.

[16] H. Akhavan and P. Riberio. "Aeroelasticity of composite plates with curvilinear fibres in supersonic flow". In: *Composite Structures* 194 (2018), pp. 335–344.

[17] B. Agarwal, L. Broutman, and K. Chandrashekhara. *Analysis and performance of fiber composites*. Wiley, 2006.

[18] H. Akhavan, P. Riberio, and M. F. S. F. de Moura. "Large deflection and stresses in variable stiffness composite laminates with curvilinear fibers". In: *International Journal of Mechanical Sciences* 73 (2013).

[19] K. Lee and S. W. Lee. "A postprocessing approach to determine transverse stresses in geometrically nonlinear composite and sandwich structures". In: *Journal of Composite Materials* (2003).

[20] B. C. Park, J. W. Park, and Y. H. Kim. "Stress recovery in laminated composite and sandwich panels undergoing finite rotation". In: *Composite Structures* 59 (2003), pp. 227–235.

[21] T. B. Hartman, M. W. Hyer, and S. W. Case. "Stress recovery in composite laminates including geometrically nonlinear and dynamic effects". In: *AIAA Journal* 54.8 (2016), pp. 2521–2529.

[22] L. Demasi. "inf3 Hierarchy plate theories for thick and thin composite plates: The Generalized Unified Formulation". In: *Composite Structures* 84 (2008), pp. 256, 270.

[23] L. Demasi. "∞^6 Mixed plate theories based on the Generalized Unified Formulation. Part II: Governing equations". In: *Composite Structures* (2009).

[24] L. Demasi. "∞^3 hierarchy plate theories for thick and thin composite plates". In: *Composite Structures* 84 (2008), pp. 256–270.

[25] L. Demasi. "∞^6 Mixed plate theories based on the generalized unified formulation. Part V: results". In: *Composite Structures* 87 (2009), pp. 195–205.

[26] L. Demasi. "Partially Layer Wise advanced Zig Zag and HSDT models based on the Generalized Unified Formulation". In: *Engineering Structures* 53 (2013), pp. 63–91.

[27] L. Demasi, Y. Ashenafi, R. Cavallaro, and E. Santarpia. "Generalized Unified Formulation Shell Elements for Functionally Graded Variable Stiffness Composite Laminates and Aeroelastic Applications". In: *Composite Structures* 131 (2015), pp. 501–515.

[28] L. Demasi, G. Biagini, F. Vannucci, E. Santarpia, and R. Cavallaro. "Equivalent single layer, zig-zag, and layer wise theories for variable angle tow composites based on the Generalized Unified Formulation". In: *Composite Structures* (2017).

[29] L. Demasi, G. Biagini, F. Vannucci, E. Santarpia, and R. Cavallaro. "Generalized Unified Formulation-Based Bending Analysis of Variable Angle Tow Panels in the Presence of Hole". In: *AIAA / ASCE / AHS / ASC Structures, Structural Dynamics, and Materials Conference*. Kissimmee, Florida, Jan. 2018.

[30] R. Averill and Y. Yip. "Thick Beam Theory and Finite Element Model with Zig-Zag Sublaminate Approximations". In: *AIAA Journal* 34 (1996), pp. 1627–1632.

[31] V. Aitharaju and R. Averill. "C^0 Zig-Zag Finite Element for Analysis of Laminated Composite Beams". In: *J Eng Mech ASCE* 125 (1999), pp. 323–330.

[32] S. Kapuria, P. Dumir, and A. Ahmed. "An Efficient Higher Order Zig-Zag Theory for Composite and Sandwich Beams Subjected to Thermal Loading". In: *Int J Solids Struct* 40 (2003), pp. 6613–6631.

[33] F. Tornabene, N. Fantuzzi, and M. Bacciocchi. "Refined shear deformation theories for laminated composite arches and beams with variable thickness: natural frequency analysis". In: *Engineering Analysis with Boundary Elements* 100 (2019), pp. 24–47.

[34] H. Murakami. "Laminated composite plate theory with improved in-plane response". In: *Journal of Applied Mechanics* 53 (1986), pp. 661–666.

[35] J. Reddy. *Mechanics of laminated composite plates and shells. Theory and analysis*. Ed. by C. Press. 2004.

[36] V. Hong, L. Demasi, and E. Santarpia. "Reissner's Mixed Variational Theorem and Energy Reconstitution for Triangular Elements". In: *AIAA Scitech Forum*. AIAA. Orlando, Florida, Jan. 2020.

[37] L. Demasi and E. Santarpia. "Functional reconstitution of Reissner's mixed variational theorem for finite element applications". In: *AIAA Journal* 57.1 (2019), pp. 1–14.

[38] W. Zhen and C. Wanji. "A global higher-order zig-zag model in terms of the HW variational theorem for multilayered composite beams". In: *Composite Structures* 158 (2016), pp. 128–136.

[39] E. Reissner. "On a Certain Mixed Variational Theory and a Proposed Application". In: *International Journal for Numerical Methods in Engineering* 20 (1984), pp. 1366–1368.

[40] E. Carrera. "Historical review of Zig-Zag theories for multilayered plates and shells". In: *App Mech Rev* 56 (2003).

[41] S. G. Lekhnitskii. "Strength calculation of composite beams". In: *Vestnik inzhen i tekhnikov* 9 (1935).

[42] S. A. Ambartsumian. "On a theory of bending of anisotropic plates". In: *Investiia Akad Nauk SSSR, Ot Tekh Nauk* 4 (1958).

[43] S. A. Ambartsumian. "On a general theory of anisotropic shells". In: *Prikl. Mat. Mekh.* 22 (1958), pp. 226–237.

[44] S. A. Ambartsumian. "Analysis of two-layer orthotropic shells". In: *Investiia Akad Nauk SSSR, Ot Tekh Nauk* 7 (1957).

[45] S. A. Ambartsumian. "Two analysis method for two-layer orthotropic shells". In: *Izv An Arm SSR Seiya Fiz-Matem nauk X(2)* (1957).

[46] M. Cho and R. R. Parmerter. "Efficient higher order composite plate theory for general lamination configurations". In: *AIAA Journal* 7 (1993), pp. 1299–1306.

[47] E. Reissner. "On a Mixed Variational Theorem and on Shear Deformable Plate Theory". In: *International Journal for Numerical Methods in Engineering* 23 (1986), pp. 193–198.

[48] E. Carrera and Kröplin. "Zig-Zag and interlaminar equlibra effects in large-deflection and postbuckling analysis of multilayered plates". In: *Mechanics of Composite Materials and Structures* 4 (1997), pp. 69–94.

[49] J. D. Rodrigues, C. Roque, A. J. M. Ferreira, E. Carrera, and M. Cinefra. "Radial basis functions-finite differences collocation and a Unified Formulation for bending, vibration abd buckling analysis of laminated plates, according to Murakami's zig-zag theory". In: *Composite Structures* 93 (2011), pp. 1613–1620.

[50] E. Carrera. "C^0 Reissner-Mindlin multilayered plate elements including zig-zag and interlaminar stress continuity". In: *Int. J. Numer. Methods Eng.* 39 (1996), pp. 1797–1820.

[51] L. Demasi. "∞^6 Mixed plate theories based on the generalized unified formulation. Part IV: zig-zag theories". In: *Composite Structures* 87 (2009), pp. 195–205.

[52] R. M. J. Groh and P. Weaver. "On displacement-based and mixed variational equivalent single layer theories for modelling highly heterogeneous laminated beams". In: *Int. J. Solids Structures* 59 (2015), pp. 147–170.

[53] M. Patni, S. Minera, R. M. J. Groh, A. Pirrera, and P. M. Weaver. "On the accuracy of localised 3D stress fields in tow-steered laminated composite structures". In: *Composite Structures* (Oct. 2019). in press.

[54] H. B. Coda. "Continuous inter-laminar stress for regulr and inverse geometrically nonlinear dynamic and static analyses of laminated plates and shells". In: *Composite Structures* 132 (2015), pp. 406–422.

[55] H. Coda, R. Paccola, and R. Carrazedo. "Zig-Zag effect without degrees of freedom in linear and non linear analysis of laminated plates and shells". In: *Composite Structures* (2017).

[56] A. Loredo, M. D'Ottavio, P. Vidal, and O. Polit. "A family of higher-order single layer plate models meetin C_z^0-requirements ofr arbitrary laminates". In: *Composite Structures* 225 (2019).

[57] J.N.Reddy. *Mechanics of laminated composite plates and shells. Theory and analysis.* CRC Press, 2004.

[58] A. T. Baranski and S. B. Biggers. "Postbucklig Analysis of Laminated Composite Plates sing a Higher-Order Zig-Zag Theory". In: *Mechanics of Advanced Materials and Structures* 7 (2000), pp. 285–314.

[59] D. Eby and R. C. Averill. "Zigzag Sublaminate Model for Nonlinear Analysis of Laminated Panels". In: *Journal of Aerospace Enringeering* 13 (2000), pp. 100–109.

[60] M. E. Fares and M. K. Elmarghany. "A refined zigzag nonlinear first-order shear deformation theory of composite laminated plates". In: *Composite Structures* 82 (2008), pp. 71–83.

[61] F. G. Flores. "Implementation of the refined zigzag theory in shell elements with large displacements and rotations". In: *Composite Structures* 118 (2014), pp. 560–570.

[62] F. Xie, Y. Qu, W. Zhang, Z. Png, and G. Meng. "Nonlinear aerothermoelastic analysis of composite laminated panels using a general higher-order shear deformation theory". In: *Int. J. of Mechanical Sciences* 150 (2019), pp. 226–237.

[63] N. F. J. Knight, J. Ransom, O. Griffin, and D. Thompson. "Global/local methods reseatch using a common structural analysis framework". In: *Finite Elements in Analysis and Design* 9 (1991), pp. 91, 112.

[64] S. Voleti, N. Chandra, and J. Miller. "Global-local analysis of large-scale composite structures using finite element methods". In: *Computers and Structures* 58.3 (1996), pp. 453, 464.

[65] A. Noor, W. Burton, and J. Peters. "Hierarchical adaptive modeling of structural sandwiches and multilayered composite panels". In: *Applied Numerical Mathematics* 14 (1994), pp. 69, 90.

[66] I. Babuska, W. Henshaw, J. Flaherty, J. Hopcroft, and T. Tezduyar. *Modeling, mesh generation, and adaptive numerical methods for partial differential equations*. Springer, 1995.

[67] I. Babuska, B. Szabo, and I. Katz. "The p-Version of the Finite Element Method". In: *Journal on Numerical Analysis* 18.3 (1981), pp. 515, 545.

[68] I. Babuska and M. Dorr. "Error estimates for the combined h and p versions of the finite element method". In: *Numerische Mathematik* 37 (1981), pp. 257, 277.

[69] D. Thompson and O. Griffin. "2D to 3D global/local finite element analysis of cross-ply composite laminates". In: *Journal of Reinforced Plastics and Composites* 9 (1990), pp. 492, 502.

[70] K. Mao and C. Sun. "A refined global-local finite element analysis method". In: *International Journal for Numerical Methods in Engineering* 32 (1991), pp. 29, 43.

[71] J. Whitcomb. "Iterative global/local finite element analysis". In: *Computers and Structures* 40.4 (1991), pp. 1027, 1031.

[72] J. Whitcomb and K. Woo. "Application of iterative global/local finite element analysis. Part 1: Linear analysis". In: *Communications in Numerical Methods in Engineering* 9 (1993), pp. 745, 756.

[73] J. Whitcomb and K. Woo. "Application of iterative global/local finite-element analysis. Part 2: geometrically non-linear analysis". In: *Communications in Numerical Methods in Engineering* 9 (1993), pp. 757, 766.

[74] A. Wang and F. Crossman. "Calculation of edge stresses in multi-layer laminates by sub-structuring". In: *Journal of Composite Materials* 12 (1978), pp. 76, 83.

[75] R. Jones, R. Callinan, K. Teh, and K. Brown. "Analysis of multi-layer laminates using three-dimensional super-elements". In: *International Journal for Numerical Methods in Engineering* 20 (1983), pp. 583, 587.

[76] N. Pagano and S. Soni. "Global-local laminate variational model". In: *International Journal of Solids Structures* 3 (1983), pp. 207, 228.

[77] C. Sun and W. Liao. "Analysis of thick section composite laminates using effective moduli". In: *Journal of Composite Materials* 24 (Sept. 1990), pp. 977, 993.

[78] K. Bathe and S. Bolourchi. "A geometric and material nonlinear plate and shell element". In: *Computers and Structures* 11 (1980), pp. 23, 48.

[79] K. Surana. "Transition finite elements for three-dimensional stress analysis". In: *International Journal for Numerical Methods in Engineering* 15 (1980), pp. 991–1020.

[80] K. Surana. "Geometrically non-linear formulation for the three dimensional solid-shell transition finite elements". In: *Computers and Structures* 15.5 (1982), pp. 549, 566.

[81] C. Davila. "Solid-to-shell transition elements for the computation of interlaminar stresses". In: *Computing Systems in Engineering* 5.2 (1994), pp. 193, 202.

[82] M. Aminpour, S. McCleary, and J. Ransom. "A global/local analysis method for treating details in structural design". In: *Third NASA Advanced Composites Technology Conference*. Vol. 1. 1993, pp. 967, 986.

[83] E. Carrera, A. Pagani, and M. Petrolo. "Use of Lagrange multipliers to combine 1D variable kinematic finite elements". In: *Computers and Structures* 129 (2013), pp. 194, 206.

[84] J. Fish. "The s-version of the finite element method". In: *Computers and Structures* 43.3 (1992), pp. 539, 547.

[85] J. Fish and S. Markolefas. "The s-version of the finite element method for multilayer laminates". In: *International Journal for Numerical Methods in Engineering* 33 (1992), pp. 1081, 1105.

[86] H. Ben Dhia. "Multiscale mechanical problems: the Arlequin method". In: *Comptes Rendus de l'academie des Sciences Series IIB Mechanics Physics Astronomy* 326 (1998), pp. 899–904.

[87] H. Ben Dhia and G. Rateau. "The Arlequin method as a flexible engineering tool". In: *International Jounral for Numerical Methods in Engineering* 62 (2005), pp. 1442–1462.

[88] F. Biscani, G. Giunta, S. Belouettar, E. Carrera, and H. Hu. "Variable kinematic beam elements coupled via Arlequin method". In: *Composite Structures* 93 (2011), pp. 697–708.

[89] E. Carrera and L. Demasi. "Classical and advanced multilayered plate elements based upon PVD and RMVT. Part 1: Derivation of finite element matrices". In: *International Journal for Numerical Methods in Engineering* 55 (2002), pp. 191, 231.

[90] E. Carrera and L. Demasi. "Classical and advanced multilayered plate elements based upon PVD and RMVT. Part 2: Numerical implementations". In: *International Journal for Numerical Methods in Engineering* 55 (2002), pp. 253, 291.

[91] E. Zappino, G. Li, A. Pagani, and E. Carrera. "Global-local analysis of laminated plates by node-dependent finite elements with variable ESL/LW capabilities". In: *Composites Structures* 172 (2017), pp. 1, 14.

[92] E. Carrera, A. Pagani, and S. Valvano. "Multilayered plate elements accounting for refined theories andnode-dependent kinematics". In: *Composites Part B* 114 (2017), pp. 189, 210.

[93] G. Li, E. Carrera, M. Cinefra, A. de Miguel, P. A., and E. Zappino. "An adaptable refinement approach for shell finite element models based onnode-dependent kinematics". In: *Composite Structures* 210 (2019), pp. 1, 19.

[94] E. Carrera, M. Cinefra, E. Zappino, and M. Petrolo. *Finite element analysis of structures through Unified Formulation*. John Wiley and Sons Ltd, 2014.

[95] T. Belytschko, W. K. Liu, B. Moran, and K. I. Elkhodary. *Nonlinear finite elements for continua and structures*. Wiley, 2014.

[96] L. E. Malvern. *Introduction to the mechanics of a continuous medium*. Prentice-Hall, 1969.

[97] J. K. Bathe, E. Ramm, and E. L. Wilson. "Finite element formulations for large deformation dynamic analysis". In: *International Journal for Numerical Methods in Engineering* 9 (1975), pp. 353–386.

[98] E. Santarpia and L. Demasi. "Large displacement models for composites based on Murakami's Zig-Zag Function, Green-Lagrange Strain Tensor, and Generalized Unified Formulation". In: *Thin-Walled Structures* 150 (May 2020), pp. 1, 18.

[99] G. Wempner. "Finite elements, finite rotations and small strains of flexible shells". In: *International Journal of Solid Structures* 5 (1969), pp. 117–153.

[100] T. Belytschko and B. J. Hsieh. "Non-linear transient finite element analysis with convected co-ordinates". In: *International Journal for Numerical Methods in Engineering* 7 (1973), pp. 255–271.

[101] C. Rankin and F. Brogan. "An element independent corotational procedure for the treatment of large rotations". In: *ASME J. Pressure Vessel Technology* 108 (1986), pp. 165–174.

[102] C. Felippa. "Error Analysis of Penalty Function Techniques for Constraint Definition in Linear Algebraic System". In: *International Journal for Numerical Methods in Engineering* 11 (1977), pp. 709–728.

[103] H. Ben Dhia. "Numerical modelling of multiscale problems: the Arlequin method". In: In: CD Proceedings ECCM'99, Munchen; 1999. 1995.

[104] A. Barut, M. Das, and E. Madenci. "Nonlinear deformations of flapping on a micro air vehicle". In: *47th AIAA/ASME/ASCE/AHS/ASC Structures, Structural Dynamics, and Materials Conference*. Newport, Rhode Island, 2006.

[105] S. Chimakurthi. "A computational aeroelasticity framework for analyzing flapping wings". PhD thesis. The University of Michigan, 2009.

[106] N. Newmark. "A method of computation for structural dynamics". In: *Journal of the Engineering Mechanics Division,ASCE* 85 (1959), pp. 67–94.

[107] T. Hilbert H.M. abd Hugher and R. Taylor. "Improved numerical dissipation for time integration algorithms in structural dynamics". In: *Earthquake Eng. and Struct. Dynamics* 5 (1977), pp. 283–292.

[108] W. Wood, M. Bossak, and O. Zienkiewicz. "An alpha modification of Newmark's method". In: *International Journal for Numerical Methods in Engineering* 15 (1980), pp. 1562–1566.

[109] J. Chung and G. Hulbert. "A time integration algorithm for structural dynamics with improved numerical dissipation: the generalized-alpha method". In: *Journal of Applied Mechanics* 60.2 (1993), pp. 371–375.

[110] J.N.Reddy. *Theory and Analysis of Elastic Plates and Shells*. CRC Press, 2007.

[111] S. V. P. Gennady M. Kulikov. "Finite rotation exact geometry solid-shell element for laminated composite structures through extended SaS formulation and 3D analytical integration". In: *International Journal of Numerical Methods in Engineering* (2019), pp. 1–27.

[112] M. Patni, S. Minera, C. Bisagni, P. M. Weaver, and A. Pirrera. "Geometrically nonlinear finite element model for predicting failure in composite structures". In: *Composite Structures* (Oct. 2019). in press.

[113] G. S. Payette and J. N. Reddy. "A new twelve-parameter spectral/hp shell finite element for large deformation analysis of composite shells". In: *Comput. Methods Appl. Mech. Engrg.* 278 (2014), pp. 664–704.

[114] E. Santarpia and L. Demasi. “Computational Architecture Based on Murakami’sZig-Zag function for the Geometrically NonlinearAnalysis of Variable Angle Tow Laminates”. In: *AIAA Scitech 2020 Forum*. AIAA. Orlando, FL, Jan. 2020.

[115] K. Lee, H. Park, and S. Lee. “A post-processing scheme to evaluate transverse stresses for composite panels under dynamic loads”. In: *Computer Modeling in Engineering and Sciences* 32.3 (2008), pp. 113–122.